Implication of anticoagulant heparan sulfate as protection against tumor invasion and angiogenesis: study in endometrial adenocarcinoma grade 1

Zouggari, Nawel

UNIVERSITÉ DE GENÈVE

Section de chimie et biochimie
Département de biochimie
Section de médecine fondamentale
Département de pathologie et immunologie

FACULTÉ DES SCIENCES
Professeur Marcos Gonzalez-Gaitan
FACULTÉ DE MÉDECINE
Professeure Laura Rubbia-Brandt
Docteure Ariane De Agostini

Implication Of Anticoagulant Heparan Sulfate As Protection Against Tumor Invasion And Angiogenesis: Study In Endometrial Adenocarcinoma Grade 1.

THÈSE

présentée à la Faculté des sciences de l'Université de Genève
pour obtenir le grade de Docteur ès sciences, mention biochimie

Par

Nawel ZOUGGARI

de

Sidi Bel Abbès (Algérie)

Thèse N° nnnn

GENÈVE

Nom de l'Atelier d'Impression

2020

Table of Contents

Résumé 1
Abstract 3
Acknowledgments 5
List of Figures 6
List of Tables 7
Abbreviations 8
1. PHYSIOLOGY OF THE ENDOMETRIUM 10
1.1. Architecture of the uterus 10
1.2. The Estrus cycle 11
1.3. Glandular remodeling 14
1.4. Endometrial angiogenesis 15
2. ENDOMETRIAL ADENOCARCINOMA 18
2.1. Endometrial cancer Grade 1 generalities and histopathology 18
2.2. What causes endometrial cancer? 21
2.3. Diagnosis state of knowledge 25
2.4. Targeted drug therapy: state of knowledge 26
3. HEPARAN SULFATE IN PHYSIOLOGY 28
3.1. Proteoglycans and Glycosaminoglycans 28
3.1.1. HS and Heparin 30
3.2. HS biosynthesis 31
3.3. HS post-biosynthetic modification and degradation 34
3.4. HSPGs in physiology 34
4. HS AND CANCER 37
4.1. HS in cancer cell proliferation 39
4.2. HS in tumor angiogenesis 40
4.3. HS in cancer invasion 42
5. AIMS OF THE STUDY 44
5.1. Evaluation of aHS expression as potential diagnosis and prognosis tool 45
5.2. Evaluation of treatment with HS mimetics as potential therapeutic tool. 45
5.3. Understanding the biosynthetic pathways implicated in aHS downregulation in invasive tumors. 46

Extensive Downregulation of AHS in Invasive forms of Endometrioid Carcinoma Grade 1 47
1. SUMMARY 47
2. INTRODUCTION 47
3. RESULTS 49
4. ADDITIONAL EXPERIMENTS 63
5. DISCUSSION 65
6. MATERIAL & METHODS 69
HS and its derivatives in EC therapy: the challenge of modulating tumor cell invasion and angiogenesis 73
1. SUMMARY 73
2. INTRODUCTION 73
3. RESULTS 75
4. ADDITIONAL EXPERIMENTS 91
5. DISCUSSION 92
6. MATERIAL & METHODS 95
Laser capture microdissection and RNA-Seq analysis: high sensitivity approaches to explore biosynthetic pathways implicated in aHSPG downregulation and tumor-microenvironment crosstalk in Endometrioid Carcinoma Grade 1 cases 103
1. SUMMARY 103
2. INTRODUCTION 104
3. RESULTS 105
4. DISCUSSION 114
5. MATERIAL AND METHODS 115
General Discussion 119
1. aHS SUPPRESSION ENHANCES TUMOR INVASION IN EC GRADE 1 119
2. aHS DELETION ENHANCES TUMOR ANGIOGENESIS IN EC GRADE 1 121
3. aHS AS DIAGNOSTIC AND PROGNOSTIC TOOL IN EC GRADE 1 122
4. aHS AS THERAPEUTIC TOOL IN EC GRADE 1 123
5. PERSPECTIVES 124
References 125
Paper in published format 139

Résumé

Le cancer de l'endomètre (CE) est un cancer oestrogène-dépendant de type « adéno-carcinome » et débouche dans certains cas au développement d'un cancer invasif. Il n'y a, à ce jour, aucun moyen efficace pour détecter précocement les patients qui évolueront vers une maladie métastatique. Pour envahir, les cellules tumorales doivent détruire leur membrane basale et perturber l'intégrité de la matrice extracellulaire (MEC), à savoir le remodelage tissulaire. De plus, les cellules tumorales favorisent l'angiogenèse, un processus crucial pour le développement tumoral et la métastatisation. Le remodelage tissulaire et l'angiogenèse constituent des cibles privilégiées pour développer de nouveaux outils diagnostiques et thérapeutiques, notamment dans le cancer de l'endomètre. Les Heparan Sulfate Protéoglyganes (HSPG) sont des glycoprotéines ubiquitaires trouvées à la surface des cellules animales et dans la MEC. Ils sont impliqués dans de nombreux processus biologiques tels que la prolifération, la migration et l'angiogenèse à travers une vaste gamme de liaisons protéiques. Dans l'utérus humain, les héparanes sulfate anticoagulant (aHS) sont retrouvées sur les parois des vaisseaux et également dans l'épithélium glandulaire mais disparaîssent lors du remodelage tissulaire survenant lors de la fenêtre d'implantation du cycle menstruel. Nous émettons donc l'hypothèse que la tumeur pourrait utiliser la même stratégie pour induire le remodelage pathologique requis pour sa propagation (invasion et l'angiogenèse). Cette hypothèse est appuyée par le fait que, dans la plupart des cancers, l'héparanase (HPSE) qui est l'enzyme catabolique des aHS, est élevée et relachée dans le milieu extracellulaire modulant ainsi la matrice extracellulaire et les voies de signalisation impliquant les HS.

Le premier objectif de cette thèse est d'évaluer si la suppression des aHS par l'HPSE pourrait être un outil de diagnostic pour identifier à un stade précoce le CE invasif. L'expression des aHS et HPSE ont été caractérisées sur des coupes de tissus de 102 cas de CE de grade 1 avec des intensités d'invasion variables. L'analyse a été effectuée à la fois dans le compartiment tumoral et dans le microenvironnement tumoral (MET). Il a été démontré que les glandes tumorales augmentent fortement l'expression de l'HPSE de 110,1% et réduisent les aHS de 45,5% comparées aux glandes normales. Il est intéressant de noter que la diminution des aHS est plus prononcée le pattern d'invasion le plus agressif, MELF, avec une diminution de 68,8%. Nous avons ensuite évalué l'expression des aHS dans les capillaires entourant la tumeur ainsi que la densité et la prolifération vasculaire. Les capillaires au front tumoral étaient également négatifs pour l'aHS. Nous observons une distance de plus de 400 µm entre le front tumoral et le premier capillaire marqué par rapport à une moyenne de 20 µm dans les cas normaux. Les cas MELF ayant la plus forte diminution de l'aHS dans les glandes présentent un halo négatif de l'aHS dans le TME le plus large. De plus, la prolifération des capillaires MELF atteint 11,1%, contre 4,5% dans les cas moins invasifs et 1,9% dans les cas contrôles suggérant une angiogenèse tumorale. Dans cette première analyse, nous avons démontré que la baisse des aHS est en corrélation avec la prolifération des vaisseaux et l'invasion glandulaire. Au fur et à mesure que la tumeur évolue, le stroma subit un remodelage tissulaire sous l'action d'enzymes capables de modifier les chaînes glycosidiques de la MEC, dont les glycosyltransférases, sulfotransférases, sulfatases (sulfs) et l'HPSE. L'aHS est ainsi un acteur majeur des communications entre tumeur et MET. Nous avons ensuite cherché à comprendre comment les

glandes tumorales induisent une baisse des aHS sur les vaisseaux sur une aussi longue distance. Pour ce faire, nous avons analysé l'expression génique du tissu épithélial endométrial invasif microdisséqué au laser et l'avons comparé aux cas d'invasivité moyenne et faible IG et BF, chacun avec son MET environnant. Nous avons constaté que les MELF présentent une signature oncogénique particulière dans les cellules tumorales et stromales et augmentent l'expression des gènes suivants: HPSE, Sulfs, MMP9, MMP2, MMP12, VGFA et FGF2. Sulf1 est particulièrement augmenté dans les cas MELF tandis que Sulf2 est observé parmi tous les modèles d'invasion myométriale. L'augmentation de ces gènes par les cellules tumorales et les cellules stromales activées induira à son tour un remodelage enzymatique des HS protéoglycanes dans l'EMT conduisant à l'activation des voies oncogéniques liées aux HS. Parmi les processus régulés à la hausse dans tous les MELF, nous trouvons la prolifération cellulaire (FGFR, STAT, MAPK, AKT), la transformation cellulaire (JAK-STAT), la survie cellulaire (AKT oncoprotéine), la migration cellulaire (MAPK) et l'angiogenèse (VEGF et signalisation d'activation plaquettaire). La signalisation par le VEGF est particulièrement exclusive au modèle MELF. La forte diminution des aHS est supposée participer à l'activation de la voie de signalisation du VEGF via l'activation plaquettaire. Ce résultat explique la forte augmentation de la prolifération cellulaire observée dans les capillaires du stroma négatif des MELF. Ensemble, ces résultats montrent que les MELF ont des caractéristiques moléculaires distinctes soutenant des caractéristiques plus agressives. La combinaison d'évaluations histologiques et des aHS pourrait être utile pour réévaluer les patients dont le pronostic est potentiellement mauvais.

Comme la dégradation des aHS est associée à des caractéristiques invasives et pro-angiogéniques du CE, nous avons ensuite cherché à inhiber, in vitro, l'activité catabolique de l'HPSE afin de restaurer les activités biologiques normales des cellules tumorales. Les effets anti-prolifératifs, anti-migratoires, anti-invasifs et anti-angiogéniques de l'héparine et des HS mimétiques synthétiques conçus pour entrer en compétition avec les HS endogènes et inhiber l'activité de l' HPSE, ont été évalués. Ces traitements ont remarquablement ralenti la vitesse migratoire avec un maximum de -52,62% à une concentration de 100 µg/ml par rapport aux cellules non traitées. Nous avons constaté les inhibitions plus élevées étaient attribuées aux composés ayant un fort pourcentage de sulfatation et n'était pas médiée par des interactions AT-aHS. L'invasion des cellules tumorales a diminué de 87% et nous observons une inhibition de -52,97% de la prolifération cellulaire. Les dérivés des HS ont également inhibé de 51,7% l'angiogenèse induite par la tumeur en diminuant le nombre de branches endothéliales induites par le milieu conditionné de la tumeur, suggérant que ces inhibiteurs neutralisent les molécules angiogéniques libérées par les cellules tumorales. Enfin, le test de liaison de l'AT de milieu conditionné a révélé que les glycanes sulfatés induisent un turnover dans lequel le les aHSPG endogènes sont excrétées des cellules vers la MEC pour piéger les molécules pro-tumorgéniques libres.

Pour conclure, la diminution de l'expression des aHS est corrélée à l'invasivité tumorale et l'inhibition in vitro des processus tumoraux par les dérivés HS soutiennent le potentiel pronostique et thérapeutique des aHS en tant que modulateur de l'invasion des cellules tumorales dans l'endomètre.

Abstract

Endometrial adenocarcinoma (EC) develops through an estrogen-driven “adenoma carcinoma” pathway and leads in some cases to the development of invasive adenocarcinoma. There is no effective screening test for early detection to distinguish which patients are going to evolve into a metastatic disease. Aggressive tumor cell invasion requires the disruption of the invaded tissue through the breakdown of its basement membranes and extracellular matrix (ECM), namely, tissue remodeling. In addition, tumor cells promote angiogenesis, a process crucial to tumor development and metastatization. Tissue remodeling and angiogenesis constitute privileged targets to develop new diagnostic and therapeutic tools, in particular in EC. Heparan Sulfate Proteoglycans (HSPG) are glycoproteins ubiquitously distributed on the surface of animal cells and in ECM. They are implicated in many biological processes such as cell proliferation, migration and angiogenesis through a vast array of protein binding. In human uterus, aHS (aHS) is present on vessel walls and the glandular epithelium but disappears during tissue remodeling occurring in the implantation window of the estrus cycle. We thus hypothesize that the tumor could use the same strategy to induce pathological tissue remodeling required for its propagation including invasion and angiogenesis. This assumption is supported by the fact that, in most cancers, aHS catabolic enzyme heparanase (HPSE) is elevated and shifted to an extracellular form modulating ECM HS and GF signaling.

We postulate that aHS serves as marker of tissue integrity and its post-biosynthetic enzymatic modifications facilitates tissue remodeling and invasion. The first aim of the present thesis is to evaluate if aHS downregulation through HPSE degradation could be a valuable diagnostic tool to identify at early stage highly invasive EC. aHS and HPSE expression were characterized on tissue sections of 102 neoplastic carcinoma grade 1 cases with variable intensity of invasion. The analysis was done in both tumor compartment and the TME [2]. Tumor glands were shown to strongly increase by 110.1% HPSE expression and reduce aHS by 45.5% compared to normal glands. Interestingly aHS showed extensive downregulation in the most aggressive pattern of myometrial invasion MELF with a decrease of 68.8%. We then assessed aHS expression in capillaries surrounding the tumor and micro vessel density and proliferation index were evaluated. Capillaries at tumor front were also negative for aHS. We observe a distance of more than 400µm between tumor front and the first labeled capillary compared to an average of 20 µm in normal cases. MELF cases with the highest decrease of aHS in glands at the tumor front had the largest aHS negative halo in the TME. Additionally, in invasive tumor fronts of MELF, capillaries proliferation was increased up to 11.1%, compared to 4.5% in less invasive cases and 1.9% in control cases suggesting a tumor-induced angiogenesis. In this first analysis we demonstrated that aHS downregulation correlates with vessels proliferation and glandular invasiveness. As the tumor evolves, the stroma undergoes tissue remodeling under the action of enzymes able to modify the glycosidic chains of the ECM, i.e., glycosyltransferases, sulfotransferases, sulfatases (Sulfs), and HPSE. aHS is thus a major player in tumor-TME crosstalk. We then aimed to understand how tumor glands downregulates aHS on blood vessels of the TME by such a long distance. To do so, we performed gene expression profiling of laser capture microdissected MELF invasive endometrial epithelial tissue and compared it to medium and less invasive IG and BF

endometrial epithelial tissues, each with its immediately surrounding TME. We found that MELF pattern exposes particular oncogene signature in both tumor and TME cells with upregulated HPSE, Sulfs, MMP9, MMP2, MMP12, VGFA and FGF2. Sulf1 is particularly upregulated in MELF cases while Sulf2 is seen among all the patterns of myometrial invasion. Upregulation of these genes by tumor cells and activated TME cells will in turn induce enzymatic remodeling of HS proteoglycans in the TME leading to activation of HS-related oncogenic pathways. Among processes upregulated in all MELF we find cell proliferation (FGFR, STAT, MAPK, AKT), cell transformation (JAK-STAT), cell survival (AKT oncoprotein), cell migration (MAPK) and angiogenesis (VEGF and platelet activation signaling). VEGF angiogenesis pathway is particularly exclusive to MELF pattern. Strong downregulation of aHS expression is believed to participate in VEGF pathway activation via platelet activation. This result explains the sharp rise of cell proliferation observed in MELF capillaries in aHS negative stroma. Together these results show that MELF patterns have distinct molecular characteristics supporting more aggressive features. Combination of histological and aHS evaluations could be useful to re-evaluate patients with potential worse prognosis.As aHS degradation is associated with invasive and pro-angiogenic features of EC, we next aimed to target *in vitro* HS-degrading activity of HPSE to restore normal biological activities of tumor cells. The anti-proliferative, anti-migratory, anti-invasive and anti-angiogenic effects of heparin and synthetic HS mimetics designed to compete with endogenous HS and inhibit HPSE activity was analysed. Drugs treatments remarkably slowed the cell front velocity with a maximum of -52.62% on a concentration 100µg/ml compared to non-treated cells. We have found that higher inhibition was attributed to compounds with high sulfation and was not mediated through AT-aHS interactions. Tumour cell invasion was decreased by 87% and we observe an inhibition of -52.97% of cell proliferation. HS derivatives also inhibited by 51.7% tumour-induced angiogenesis by decreasing the number of endothelial branches induced by tumour conditioned media suggesting that these inhibitors neutralize angiogenic molecules released by tumour cells. Finally, AT-ligand binding assay of conditioned media revealed that sulfated glycans, induce a turnover in which endogenous aHSPGs are released from the cells to the TME to trap free pro-tumorigenic molecules.

To conclude, decreased expression of aHS correlates with tumor invasiveness and in vitro inhibition of tumorigenesis-related processes under HS derivatives support the prognostic and therapeutical potential of aHS as modulator of tumor cell invasion in the endometrium.

Acknowledgments

Five years spent, five years during which I have searched a lot, found a little, but above all learned a lot. It was such an intellectual as well as a personal enrichment.

I would like to thank the Swiss Government for awarding me an excellence scholarship giving me the opportunity to come in Switzerland and participate in a wonderful research adventure. I am deeply grateful to the University of Geneva for its support and the Fondation Ernst et Lucie Schmidheiny for financial support.

Thank you, Ariane, for believing in me and for giving me a chance and accepting me in your lab allowing me to join this amazing team. Thank you for your increasing involvement after hard times, for your mentoring and, most importantly, for always being extremely helpful and positive when fostering this research. Thank you for always listening to what I had to say, thank you for all your advices and your help both on a professional and a personal level. I learned a lot from you. Thanks for being the cornerstone of this work.

I would like to thank the jury members, Marcos Gonzalez-Gaitan, Laura Rubbia-Brandt and Martin Götte for your feedback, and your time to read this thesis and to evaluate my work. Thanks to Karsten Kruse for agreeing to be the president of the jury and for chairing my PhD defence.

To Isabelle and Jennifer, I would like to thank you from the bottom of my heart. Thank you for putting a welcoming atmosphere when starting a life in the lab and in Geneva; it was much funnier with you in our side. To Isabelle thank you for all your implications and for accepting to help me at any time during all these years; you are a pillar of this lab.

To Noemi, my most sincere thanks. You have only been there for a year and yet you brought freshness to the lab and you were also a mentor for me by your experience and your positivity. Writing my first manuscript under your supervision was very enriching. I can't thank you enough for taking the time to review my work!

A special thanks to Lou. You are not only a co-worker but a dear friend for life. We went through so many things and we knew how to stick together. Thank you for your help and moral support!!!

Thank you Jean-Christophe for taking part in my thesis with great interest and involvement. Thank you for always being there for discussions despite your busy schedule. You have been invaluable help.

I could not make an exhaustive list so much this adventure was enriching in networking. Thank you to all the people who have directly or indirectly participated in this project and who have so kindly agreed to help me anytime; giving me technical and scientific advices and to make very enriching intellectual exchanges even if it meant spending hours listening to my updates and my questions each time. Thank you, Labidi-Galy Lab, Bochaton-Piallat Lab, Tsantoulis Lab, Mario Kreutzfeldt, the Genomics Platform of iGE3, Jean Gruenberg, Thierry Soldati, Vincent Braunersreuther, the histology platform and many more.

Et enfin merci à ma famille pour leur soutien et leur écoute et pour être toujours disponible si j'ai un problème et/ou besoin de parler. Maman, papa je vous admire et vous resterez toujours mes modèles dans la vie.

List of Figures

Figure 1. Regions of the uterus. 10
Figure 2. Structure and layers of the uterus. 11
Figure 3. Layers of the endometrium. 12
Figure 4. The menstrual cycle. 13
Figure 5. Glandular remodeling during the estrus cycle. 14
Figure 6. Schematic diagram of endometrial angiogenesis. 16
Figure 7. Histopathology of EC Grade 1. 19
Figure 8. The patterns of myometrial invasion. 21
Figure 9. Molecular changes during endometrial carcinogenesis. 23
Figure 10. Endometrial cancer pathway. 25
Figure 11. Schematic representation of the description which follows. 28
Figure 12. Structure of the different glycosaminoglycan chains. 29
Figure 13. Structures of AT-binding domain and anticoagulant activity of HS. 31
Figure 14. HS biosynthesis. 33
Figure 15. Functions of cell surface and ECM heparan sulfate proteoglycans. 37
Figure 16. Schematic model of HPSE trafficking. 38
Figure 17. Schematic model of HS pathways in cancer proliferation. 40
Figure 18. Schematic model of HS pathways in cancer angiogenesis. 41
Figure 19. Schematic model of HS pathways in cancer invasion. 43
Figure 20. The 3 main objectives of this PhD thesis. 44
Figure 21. aHS and HPSE expression analysis in glands during estrus cycle. 51
Figure 22. aHS and HPSE expression analysis in glands of EC grade 1. 52
Figure 23. aHSPG and HPSE expression analysis in tumor glands according to the different patterns of myometrial invasion. 54
Figure 24. Quantification of CD-31+ endothelial and C2-40+ lymphatic vessel density. 57
Figure 25. Microvessel proliferation (MVP) analysis. 58
Figure 26. aHSPG expression analysis in endometrial stroma and tumor micro-environment. 60
Figure 27. Correlation analysis of parameters used in the study to identify high invasive characteristics. 62
Figure 28. Specificity of AT-b to aHS (Competition test). 63
Figure 29. aHS and HPSE in pre-cancerous and cancerous phases. 64
Figure 30. SULF2 expression in the pattern of myometrial invasion. 64
Figure 31. Summary scheme of aHS expression analysis in gland and stroma of normal and cancer cases. 68
Figure 32. Schematic representing the steps for immunodetection and ligand binding of HPSE and aHS on human FFPE histological sections. 70
Figure 33. Illustration of algorythm optimization to detect Nestin+Mib-1+ vessels for MVP analysis. 72
Figure 34. Anti Sulf activity analysis on IFREMER HS mimetics. 78
Figure 35. Characterization of in vitro model cells lines for aHS and HPSE. 80
Figure 36. A6 inhibitor effect on aHSPG release on conditioned media. 81

Figure 37. A6 HS mimetic effect on tumor cell proliferation and cell viability. 82
Figure 38. Heparin and GAGs effects on Ishikawa cell migration......84
Figure 39. Heparin derivatives and HS mimetics effects on Ishikawa cell migration 85
Figure 40. Heparin derivatives effects on tumor cell invasion.....87
Figure 41. Tumor cells effects on endothelial cell tube formation 88
Figure 42. Effect of heparin and HPSE inhibitors on spontaneous and tumor-induced endothelial cell tube formation 89
Figure 43. HPSE expression is influenced by treatment with HS mimetics. 90
Figure 44. Effect of A6 on cell tube structure over time 91
Figure 45. Verification of migration rather than proliferation 92
Figure 46. Steps of the wound closure assay.....99
Figure 47. Schematic diagram of the Transwell. 100
Figure 48. Steps of the cell tube formation assay 101
Figure 49. Laser capture microdissection LCM procedure.....106
Figure 50. Quality control of extracted RNA 107
Figure 51. Correlation between heat map and Principal Component Analysis.....109
Figure 52. Heat maps of pathways upregulated in tumor and TME compartments in each myometrial invasion subtypes......111
Figure 53. Heat map of genes upregulated in pattern of myometrial invasion.....113

List of Tables

Table 1 Molecular characteristics of Grade 1 and 2 EC. 24
Table 2. Heparan sulfate binding proteins. 35
Table 3. Molecular characteristics of the glycans used in the study. 76
Table 4. Summary table of anti-HPSE activities of IFREMER HS mimetics......77
Table 5. Summary table of anti- arylsulfatase and 6-O-endosulfatase activity of IFREMER HS mimetics......79
Table 6. Summary table of samples used for LCM and RNA evaluation 108

Abbreviations

aHS: Anticoagulant Heparan Sulfate

aHSPG: Anticoagulant Heparan Sulfate Proteoglycan

AL: Adenomyose Like

AM: Adenoma malignum

AT-III: Antithrombin III

AT-b: Biotylinated Antithrombin

BF: Broad Front

BSA: Bovine Serum Albumin

CM: Conditioned Medium

CS: Chondroitin Sulfate

DMEM: Dulbecco's Modified Eagle's Medium

DR: Desmoplasic Reaction

DS: Dermatan Sulfate

DxS: Dextran Sulfate

EC: Endometrial Cancer

ECM: Extra Cellular Matrix

EGFR: Epidermal Growth Factor

EMT: Epithelial-Mesenchymal Transition

FIGO: International Federation of Obstetrics and Gynecology

FFPE: Formalin-Fixed Paraffin-Embedded

GAGs: Glycos-Amino-Glycans

GF: Growth Factor

H&E: Hematoxylin and Eosin

HMW: Hight Molecular Weight

HPSE: Heparanase

HS: Heparan Sulfate

HSPG: Heparan Sulfate Proteoglycan

IG: Infiltrating Gland

KO: Knock-out

LCM: Laser-Capture Microdissection

LH: Luteinizing Hormone

LMWH: Low Molecular Weight Heparin

MELF: Microcystic, Elongated and Fragmented

MMPs: Matrix metalloproteinases

MVD: Micro-Vascular Density

MVP: Micro-Vascular Proliferation

3OST: 3-O-Sulfotransferase

PBS: Phosphate-Buffered Saline

RIN: RNA Integrity Number

RNA-Seq: RNA sequencing

RPMI: Roswell Park Memorial Institute medium

RT: Room temperature

Sdc: Syndecan

SULF: Sulfatase

TME: Tumour micro-environment

UFH: Unfractionated heparin

VEGF: Vascular endothelial growth factor

Introduction

Like most great scientific advances, the discovery of heparin was the result of chance and a certain irony of fate [3]. Indeed, it all started in 1916, when Jay McLean, a second-year medical student, manages to isolate a very strong anticoagulant activity compound [4], while he was trying to identify pro-coagulating molecules! It was originally isolated from dog liver cells, hence its name (hepar or "ήπαρ" is Greek for "liver"; hepar + -in).

It will take nearly 15 years for heparin to finally be associated with glycosaminoglycans (GAG), a family of polysaccharides complexes (including chondroitin sulfate, dermatan sulfate, hyaluronic acid and keratan sulfate) recognized from the end of the 19th century as basic constituents of extracellular matrices and connective tissues [3, 5]. Heparan sulfate (HS) was identified later on during the purification of heparin and was initially called "heparin monosulfate", because considered as a by-product of heparin [3]. It was in 1958 that the concept of proteoglycan was born, thanks to Helen Muir works [6].

Due to their potent anticoagulant activity, a big interest in heparin and HS then emerges. From the 1930s to 1970s, several researchers were investigating heparin and HS structure. The culmination of all this work will lead to the identification of the specific pentasaccharide motif for the fixation and activation of antithrombin III (AT-III) [3, 7]. Purified heparin preparations extracted from tissues rich in mast cells remains today the ideal rapid anticoagulant and have been used clinically for over half a century [8]. Again, the emerging roles of heparin and HS in cancer result of a coincidence. As venous thromboembolism is a well-known cause of death in patients with cancer [9], heparin has been frequently used in the treatment of cancer-associated thromboembolism and it appeared that cancer patients treated with heparin survived longer than patients treated with other anticoagulants [10, 11].

Finally, during the late 1980s, identification of new ligand properties of HS proteoglycans (HSPG) paved the way for new biological functions. It first started with the discovery of the major role of HSPGs as a co-receptor essential for the activity of the growth factor FGF-2 [3]. Today, more than 300 proteins are known to interact with GAGs and these polysaccharides are clearly identified as essential players to regulate key cellular processes in both physiological and pathological conditions [3, 12].

Cancer is characterized by abnormal cell growth that involves a range of unique alterations in intracellular and intercellular space. Because HSPGs are the main mediators of communication (cell–cell and cell–ECM communication) in the intracellular space, they play a major role in malignant transformation and tumor metastasis [13]. Over the last 30 years of active research, there has been an explosion of information about the molecular biology of cancer. The challenge remains to translate this information into advances in drug therapy for patient care. How are anticoagulant HSPGs implicated in endometrial cancer and how can we manipulate them for our benefit? …will be the main problematics of the following work.

1. PHYSIOLOGY OF THE ENDOMETRIUM

1.1.Architecture of the uterus

The uterus belongs to the family of female hormone-responsive reproductive organs, including ovaries, breast, uterus, cervix, vagina and vulva in adult woman. These organs have the particularity to be in constant remodeling from puberty to menopause under the influence of the cycling release of sex hormones of the estrus cycle. This constant hormonal stimulation induces cyclic proliferations making them more prone to mutations increasing the risk of developing cancer [14].

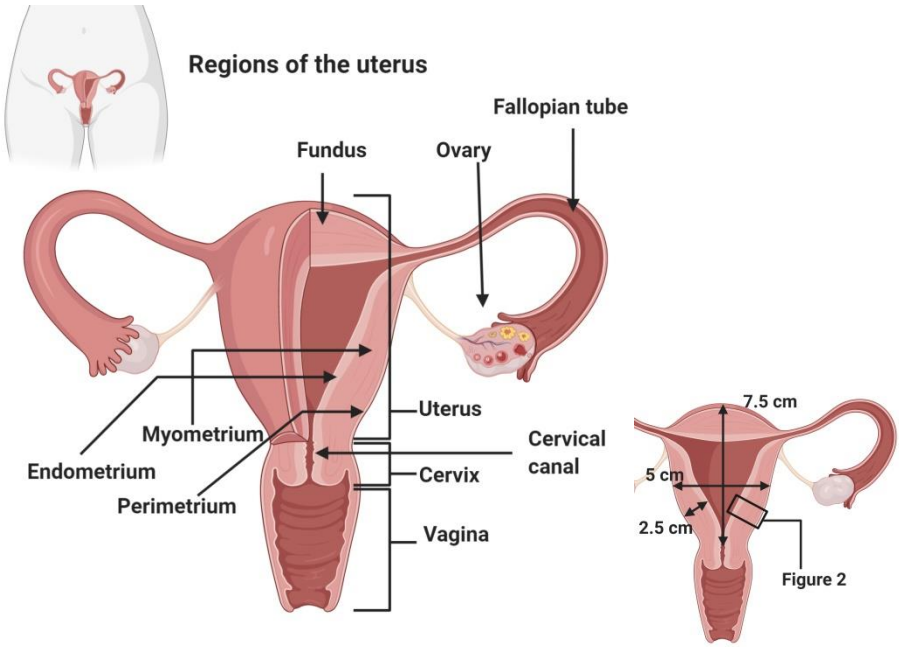

Figure 1. Regions of the uterus.
The uterus is located within the pelvic region immediately behind and almost overlying the bladder, and in front of the sigmoid colon. The uterus can be divided anatomically into four regions: the fundus – the uppermost rounded portion of the uterus in which the fallopian tubes connect to the uterus, the corpus (body), the cervix, and the cervical canal. The uterus has three layers, which together form the uterine wall. From innermost to outermost, these layers are the endometrium (light pink), myometrium (medium pink), and perimetrium (deep pink).

The uterus is a hollow, muscular organ with thick walls, and it has a glandular lining called the endometrium (Figure 1). In an adult the uterus is 7.5 cm long, 5 cm in width, and 2.5 cm thick [15]. The uterus is composed of three layers of tissue; from outermost to innermost, we find, the perimetrium, the myometrium and the endometrium (Figure 1). The outer layer is a serous coat, equivalent to peritoneum. Perimetrium consists of superficial mesothelium (simple squamous epithelium), and a thin layer of loose connective tissue beneath it containing blood vessels. The middle layer of tissue (myometrium) is muscular and comprises the greater part of the bulk of the organ. It is very firm and consists of densely packed smooth muscle fibers. Blood vessels, lymph vessels, and nerves are also present. The muscle is more or less arranged in three layers of fibers running in different directions. The outermost fibers are arranged longitudinally. Those of the middle layer run in all directions without any orderly arrangement;

this layer is the thickest. The innermost fibers are longitudinal and circular in their arrangement. The innermost layer of tissue in the uterus is the mucous membrane, or endometrium. It lines the uterine cavity as far as the isthmus of the uterus, where it becomes continuous with the lining of the cervical canal. The endometrium consists of a single layer of columnar epithelial followed by the endometrial stroma. The endometrial stroma is composed of simple tubular glands, blood vessels and connective tissue including fibroblasts, adipocytes, macrophages, mast cells and leucocytes. The glands secretions function to provide the initial nutritional support of the conceptus and may have a role in maintaining adhesion.

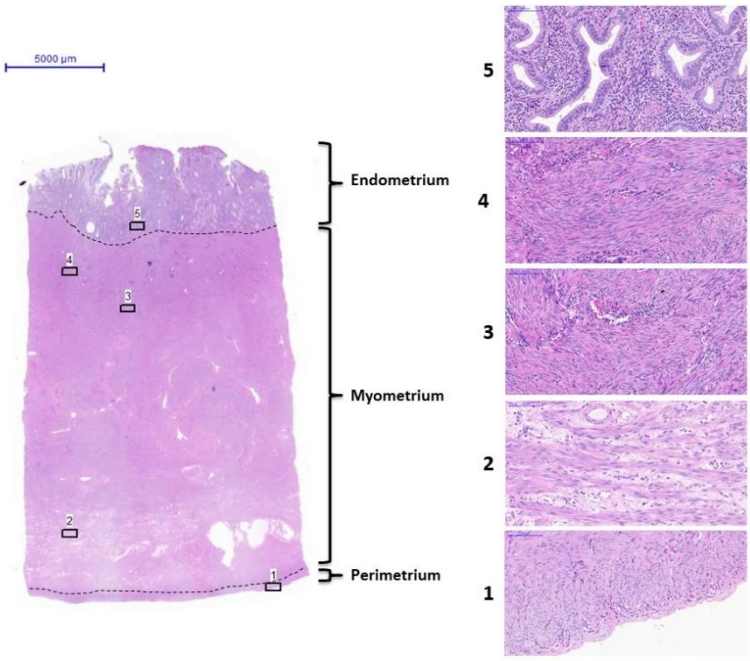

Figure 2. Structure and layers of the uterus.
Histological images showing the overall topographical organization of the uterus by hematoxylin-Eosin staining. This slide is actually at stage between proliferative and secretory (luteal phase). The perimetrium (1) is composed of superficial mesothelium and a thin layer of loose connective tissue. The myometrium is arranged in three layers of smooth muscle fibers running in different directions: longitudinally in the outer region (2), in all directions in the thickest middle region (3) and longitudinally and circular in the inner region (4). The myometrium is composed of lot of blood vessels with bigger arteries in the regions (2) and (3), lymphatic vessels, and nerves with connective tissue. The endometrium (5) contains numerous uterine glands that open into the uterine cavity and are embedded in the cellular framework or stroma of the endometrium.

The appearances of the endometrium vary considerably at the different stages in reproductive life. It begins to reach full development at puberty and thereafter exhibits dramatic changes during each menstrual cycle. It undergoes further changes before, during, and after pregnancy, during the menopause, and in old age. These changes are for the most part hormonally induced and controlled by the activity of the ovaries.

1.2.The Estrus cycle

The female reproductive tract is a highly dynamic organ system. It undergoes numerous sequential morphological changes over the course of estrous cycle. Knowledge of the normal histological appearance of the reproductive tract at each stage of the estrous cycle is essential

when evaluating female reproductive tissues remodeling of both physiological and pathological conditions.

To understand the nature of the changes in the endometrium during each menstrual cycle we will consider the endometrium to be composed of two layers or zones. They blend imperceptibly but are functionally distinct. The inner layer is shed at menstruation, and the outer layer remains in position against the innermost layer of the myometrium. The two layers are called, respectively, the functional endometrium and the basal endometrium (Figure 3).

The functional endometrium is adjacent to the uterine cavity and contains first a single layer of columnar epithelium facing the lumen, plus a layer of connective tissue, the stroma that varies in thickness according to hormonal influences. This layer contains the main portion of uterine glands called functional glands. They are simple tubular glands that reach from the endometrial and superficial blood vessels and lie beneath the lining cells of the stroma.

The basal endometrium stratum lies against the uterine muscle; it contains blood vessels and the bases of the uterine glands. Its stroma remains relatively unaltered during the menstrual cycle.

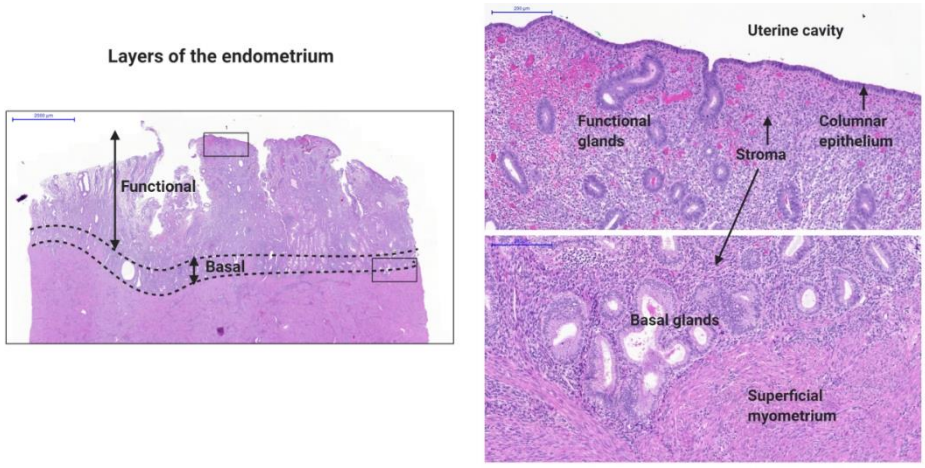

Figure 3. Layers of the endometrium.
Histological images showing the overall topographical organization of the endometrium by hematoxylin-Eosin staining. The endometrium consists of two layers, the functional and the basal. The functional layer is nearest to the uterine cavity and is composed of a single layer of columnar epithelium plus the stroma containing functional glands. This layer undergoes tissue remodeling during the cycle. The basal layer, adjacent to the superficial myometrium, is composed of stable stroma and basal parts of glands.

The menstrual cycle extends over a period of about 28 days (normal range 21–34 days), from the first day of one menstrual flow to the first day of the next. It reflects the cycle of changes occurring in the ovary, which is itself under the control of the anterior lobe of the pituitary gland. The menstrual cycle in the uterus can be divided into menstruation, proliferative phase, and secretory phase and is controlled by the endocrine system (Figure 4).

It is important to note that, in the endometrium, only the functional layer undergoes tissue remodeling during the estrus cycle.

In humans, the functional layer is completely shed during menstruation. Then, under complex hormonal interplay, follicles in the ovary start to develop. As they mature, the ovarian follicles secrete increasing amounts of estrogens which initiate the formation of a new layer of endometrium in the uterus. The functional layer is built up after the end of menstruation during the first part of the menstrual cycle. The basal layer, adjacent to the myometrium and below the functional layer, is not shed at any time during the menstrual cycle. The functional layer develops on top of it. Proliferation is induced by estrogen. The functional layer grows to a thick, blood vessel-rich, glandular tissue layer. When fully developed at the middle of the cycle, the dominant ovarian follicle releases an ovum (egg) initiating the secretory phase of the endometrial cycle.

During the secretory phase, pituitary hormones cause the remaining parts of the dominant follicle to transform into the corpus luteum, which produces progesterone. The functional endometrium again undergoes tissue remodeling engendered by the rise of progesterone levels by the corpus luteum. The functional endometrium prepares for implantation of the blastocyst (fertilized egg) and provides an optimum environment for the implantation and growth of the embryo. This time-lapse, in which the endometrium is receptive, constitutes the implantation window. If implantation does not occur within approximately two weeks, the levels of progesterone and estrogen drops causing the uterus to shed its lining and egg in menstruation.

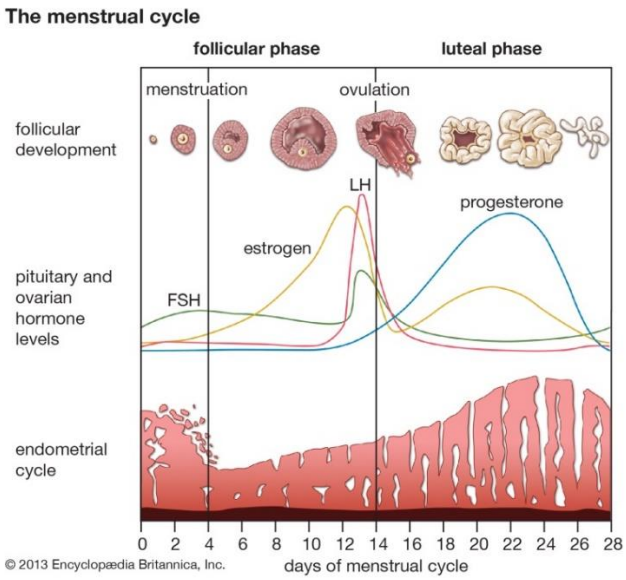

Figure 4. The menstrual cycle.
Figure showing the progression of the menstrual cycle and the different hormones contributing to it. Endometrial remodeling results from cyclic secretions of both pituitary gland and ovary. FSH pituitary hormone stimulates estrogens production by the ovary and follicles maturation. Estrogens in turn stimulate proliferation of endometrium. LH pic induces ovulation in the middle of the cycle. Corpus luteum produces increasing amount of progesterone that will further act on endometrium and triggers the lining to thicken to accept a fertilized egg. Corpus luteum breaks down at the end the cycle, lowering the progesterone levels. This change sparks menstruation [15].

1.3.Glandular remodeling

The hormonal changes influence both glandular component and the stroma of the functional endometrium (Figure 5).

During the menstruation, the endometrium is reduced in height and has an average thickness of 1.9 mm. The endometrium develops in the proliferative phase from 5 to 11 mm thickness [15]. Simple tubular glands appear round and oval shaped on histological sections and are relatively small. No morphological distinctions were noticed according the different layers.

In early secretory phase, right after the LH release, the endometrium increased by 2 folds as result of proliferation occurred in the previous phase. The endometrial glands have undergone dramatic changes. In the functional layer, they appear elongated and coiled with wide lumens and produce a glycogen-rich secretion. In the basal layer, they appear elongated but less coiled.

In the secretory phase, the endometrium shares a similar morphology to the early secretory indicating that physiological tissue remodeling occurs quickly after hormone stimulation with a thickness up to16 mm measured [15]. The glands appear more coiled with less stroma and clear secretions are visible inside the lumen. Glands of the basal layer are less subject to morphological changes and appear more stable during the cycling endometrium.

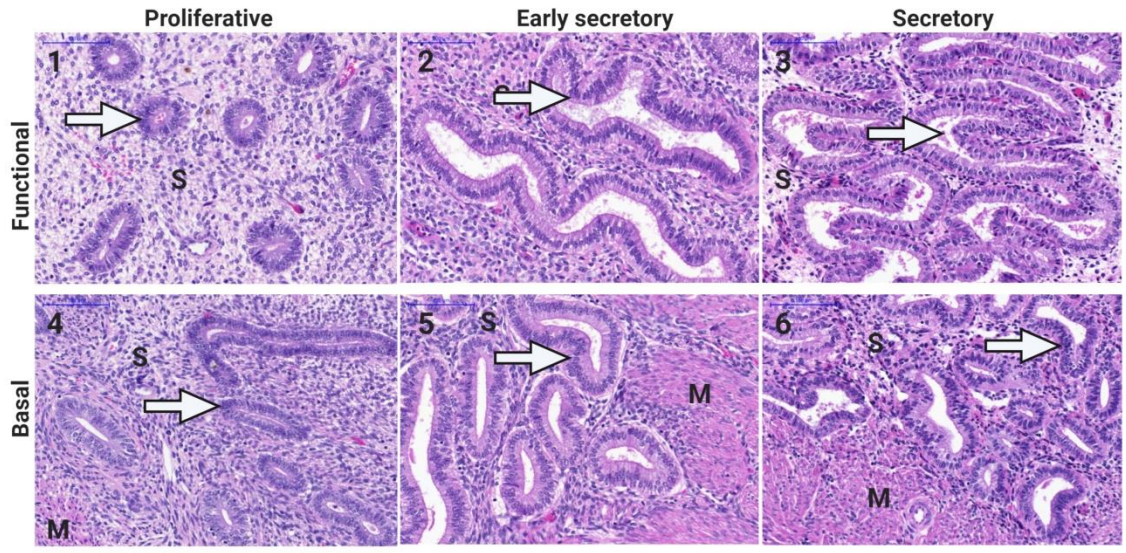

Figure 5. Glandular remodeling during the estrus cycle.
During the menstrual cycle, endometrial glands (→) undergo massive structural remodeling. Functional endometrium is the most to incur hormonal fluctuations. They go from small round/oval shaped during follicular stage **(1)** to coiled/elongated with wide lumen during luteal stage **(2, 3)** reducing stroma (S). We can observe a gradual change (from **1** to **3**). In mid-secretory phase, glands are fully functional and produce glycogen-rich secretion to produce a suitable environment for implantation. Basal glands adjacent to the myometrium (M) do not undergo big changes and appear constantly oval to slightly coiled **(4, 5, and 6)**.

As a result of hormonal stimulation, we can see in the Human Protein Atlas database that numerous proteins are overexpressed in the functional endometrium during the menstrual cycle [16]. Those proteins have an important role in the cyclic remodeling of the human endometrium. The corresponding specific proteins are expressed in the glandular and stromal cells of the endometrial mucosa [17]. The expression of many of these proteins vary depending on the menstrual cycle.

During menstruation, the expression of matrix metalloproteinases (MMPs) increases dramatically at the onset of the menstrual phase. MMP10 was shown to be overexpressed on epithelial cells of the glands and MMP11 on stroma cells [18]. They facilitate ECM breakdown and shedding of the endometrial superficial functional layer.

Proteins expressed during the proliferative phase include PGR, a progesterone receptor expressed in both glandular and stromal cells, which plays a central role in reproductive events regulating transcription [19]. Zieba et *al.* exposed on a remarkable analysis of the human endometrium-specific proteome defined by transcriptomics and antibody-based profiling. They have found that five genes (CPM, TXNRD3, UAP1, NUSAP1, and SLC9A3R1) showed a substantially higher level of expression in the glandular cells of proliferative phase compared to samples representing secretory phases [20]. These genes are regulated by estrogen and are known to play multiple roles in the cells including protection against oxidative stress and apoptosis, regulation of transcription factor activity, and regulation of cellular proliferation [21-25].

During the secretory phase, Progestogen-associated endometrial protein (PAEP) is overexpressed in glandular cells [26]. PAEP is a glycoprotein that inhibits cell immune function and plays an essential role in the pregnancy process [27].

Proteins expressed during both the proliferative and secretory phase include the transcription factor HOXA11, which is involved in the regulation of uterine development and is required for female fertility. It is interesting to note that the expression in glandular epithelium was dramatically decreased or disappeared in the mid-secretory phase at the time of implantation suggesting a role during receptivity of endometrium [28]. Also expressed in stroma cells, is HOXA11 while SFRP4, a modulators of Wnt signaling with a role in regulating cell growth and differentiation in specific cell types, is expressed both in stroma and glandular cells [29].

1.4.Endometrial angiogenesis

The uterus is supplied with blood by the two uterine arteries, which are branches of the internal iliac arteries, and by ovarian arteries, which connect with the ends of the uterine arteries and send branches to supply the uterus. In the healthy adult woman angiogenesis is rare and occurs only in the ovarian follicle, corpus luteum and uterine endometrium [30-32]. In this last one, angiogenesis participates in the three stages: during menstruation for repair of vasculature, during rapid endometrial growth of proliferative phase and during secretory phase [33]. As well as glandular component, the endometrial vasculature undergoes cyclic remodeling as it

grows and regresses during the menstrual cycle. Under these physiological circumstances angiogenesis is highly regulated, which means being turned on for brief periods and then completely inhibited [34].

There are two different types of angiogenesis: sprouting of capillaries from pre-existing vessels, and non-sprouting angiogenesis [35]. Sprouting angiogenesis is a multistep process involving degradation of the basement membrane, invasion in stroma, endothelial cell proliferation and migration, and tube formation. Non-sprouting angiogenesis can occur by proliferation of endothelial cells inside a vessel, producing a wide lumen that can be split by transcapillary pillars or fusion and splitting of capillaries [30, 35]. Sprouting was the first angiogenic mechanism to be described and occurs during neovascularization of avascular tissues, such as the rapidly growing corpus luteum, or vascular invasion of growing tumors [36]. These processes are controlled by an angiogenic switch mechanism, which is triggered by a change in the balance of inducers and inhibitors of angiogenesis [37].

Against all odds, giving an overview description of physiological angiogenesis in the endometrium during estrus cycle is challenging. Different points of view diverge, and the latest descriptions have been made few decades ago as the main interest nowadays remains on pathological processes. I will try to resume in a simplified way the main hallmarks of this topic.

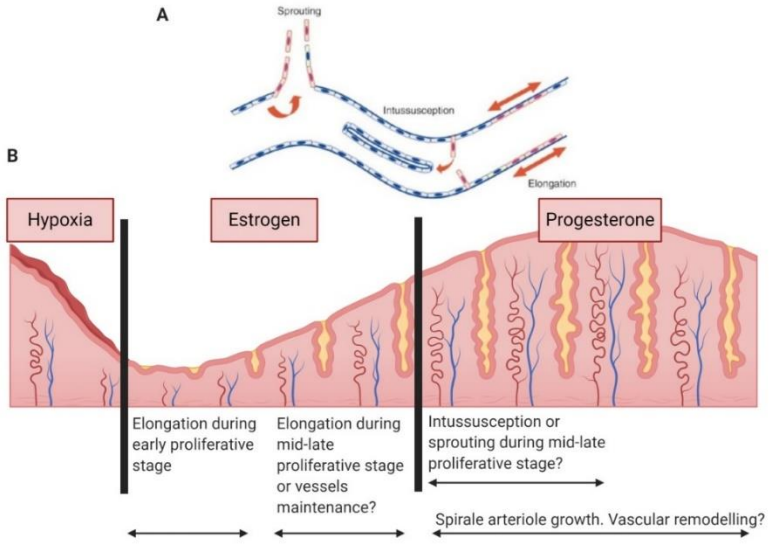

Figure 6. Schematic diagram of endometrial angiogenesis.
A. Schematic representation of the 3 mechanisms of angiogenesis: sprouting, intussusception and elongation. Quiescent endothelial cells are shown in blue and proliferating endothelial cells in red [33]. **B**. The proposed mechanisms of endometrial angiogenesis for each stage of the menstrual cycle stage is indicated.

The research community agrees that vessel elongation is the major endometrial angiogenic mechanism in the functional endometrium of the proliferative phase of the cycle (Figure 6). However, complexity is established while proliferative phase is often split into 3 periods; the early proliferative or post menstrual phase, the mid proliferative and finally the late proliferative phase. It has been shown that during early proliferative phase, post-menstrual

repair occurs from the remaining superficial layer of the basal endometrium. The mechanisms through which this repair occurs have not yet been determined. However, in a study published in 2002 Gambino et *al.* state that in early and mid-late proliferation phase, the vascular growth occurs by elongation of existing vessels under estrogen stimulation [38]. They also stipulate that between the early proliferative and mid–late proliferative phases another vessel growth occurs as the blood vessel length density is highest at the mid–late proliferative and early–mid secretory phases of the cycle and that patterns of vascular growth are similar in the functional and basal layers. In another study, it is described that in late proliferative phase, angiogenesis is slowed and a process of maintenance of vessels is then set up [30].

During secretory phase, spiral arterioles show significant growth and coiling in the functional layer. A sub epithelial capillary plexus, which is supplied by the arterioles, develops and reaches its maximum in mid secretory phase in the implantation window [33]. It has been found that during this stage there is an increase in the vessel branch point density, which may occur by sprouting or intussusceptive angiogenesis [39]. Again, Gambino et *al* affirm a decrease in vessel segment length in early-mid secretory phase while vessel length density remains elevated suggesting that this angiogenic remodeling results in more vessel junctions, rather than vascular regression [38]. At the end of the cycle, in the absence of progesterone, the arteries supplying blood to the functional layer constrict, so that cells in that layer become ischemic and die, leading to menstruation.

I think it is fair to say that vessel growth in the human endometrium occurs by broadly non-sprouting mechanisms (elongation or intussusception). The molecular mechanism is as well, complex and incomplete as sprouting mechanism is the most analyzed. While vascular endothelial growth factor (VEGF) is fundamental to endometrial angiogenesis, details of how and when different endometrial cell types produce VEGF, and how production and activity is controlled by estrogen and progesterone, remains to be elucidated [40]. A very good review made by Gargett and Rogers in 2001 highlighted the association of inflammatory conditions and endometrial angiogenesis. In this review we can read that correlation between foci of VEGF staining in the endometrial stroma component and proliferation of endothelial cells has successfully being proven. However, neither total glandular nor total stromal fibroblasts VEGF production was related to angiogenesis [33]. These observations suggest that the source of angiogenic factors for non-sprouting endometrial angiogenesis derived from circulating leucocytes such as neutrophils which are released in endometrial stroma when the cells become activated. Intravascular neutrophils containing VEGF have thus been identified as having a role in stimulating endometrial angiogenesis, although other currently unidentified mechanisms must also exist [40].

Despite accumulations of scientific data from pertinent publications, the analysis of human endometrial angiogenesis during the cycle is incomplete and it is still not clear which mechanisms control vascular growth in the endometrium and at which stage of the menstrual cycle new blood vessel formation occurs [41]. This thesis work will provide a modest complement to this analysis.

2. ENDOMETRIAL ADENOCARCINOMA

2.1.Endometrial cancer Grade 1 generalities and histopathology

Endometrial cancer (EC) is the most common cancer of the female reproductive system. In Europe, 1 to 2 in every 100 women will develop EC at some point in their life (based on the ESMO Clinical Practice Guidelines). In the European Union, over 88,000 women are diagnosed with an EA each year. This number is increasing in the majority of European countries. EC usually occurs in women over the age of 50 and thus after menopause, but up to 25% of cases may occur before the menopause [42]. The incidence of EC and the numbers of young women suffering from this disease are increasing globally [43]. It is estimated to increase by 50% to 100% in the next 20 years [44, 45].

Most of EAs are adenocarcinomas. The term “adenocarcinoma” designs a glandular origin as it is composed of “adeno” for glands and “carcinoma” for epithelial cancer. It results of the abnormal growth of epithelial cells from endometrial glands that have the ability to invade or spread firstly the endometrial compartment, then the myometrium and later other parts of the body. Staging is a way of describing where the cancer is located, if or where it has spread, and whether it is affecting other parts of the body in order to adapt treatments.

Doctors assign the stage of EC using the International Federation of Obstetrics and Gynecology (FIGO) system. In stage I, 80% of total EC, the cancer is found only in the uterus compartment, and it has not spread to the cervical stroma or beyond the pelvic area. In this first stage, two distinct sub categories are described: Stage IA and IB. In stage IA, the cancer is found only in the endometrium or less than one-half of the myometrium while in stage IB, the tumor has spread to one-half or more of the myometrium. Doctors also describe EA by its grade to evaluate how much EC cells resemble healthy cells. It is a three-tiered system for histologically classifying ECs, ranging from cancers with well-differentiated cells (grade I), to very poorly-differentiated cells (grade III) [46]. If tumor cells appear similar to healthy tissue and has different cell groupings, it is called "differentiated" or a "low-grade tumor." If the cancerous tissue looks very different from healthy tissue, it is called "poorly differentiated" or a "high-grade tumor." The cancer’s grade may help the doctor predict how quickly the cancer will spread and is used as prognosis.

In this thesis work, only EC Grade 1 Stage 1A and 1B with myometrial invasion was analyzed as our subject of interest is the evaluation of pathological tissue remodeling (invasion and angiogenesis) occurring in early stage EA. Grade I cancers are the least aggressive and have the best prognosis.

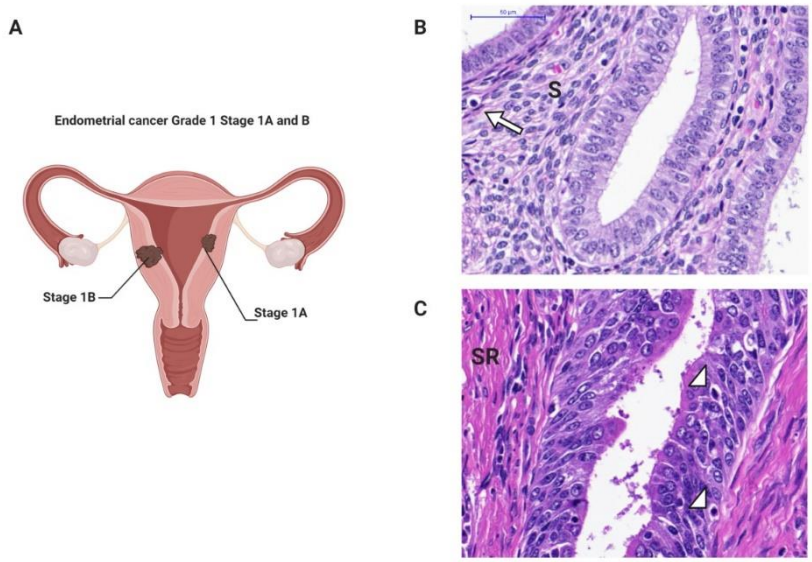

Figure 7. Histopathology of EC Grade 1.

A. In stage 1A, tumor is confined to the uterus with less than half myometrial invasion while in stage 1B, tumor involves more than half of the myometrium. **B.** In physiological circumstances, we observe a single columnar glandular epithelium inside the stroma (S). **C.** Tumor gland of EC grade 1 is characterized by an epithelial proliferation leading to a stratified epithelium and generates a stromal reaction (SR) in the myometrium. However, tumor epithelial cells are still well differentiated with a slight pleomorphism. In cancer, lymphocytes (arrow) are visible inside the epithelium and are called tumor-infiltrating lymphocytes (arrow head). H&E stain.

The histopathology of ECs is highly diverse but not less essential as it is the principal method for diagnosis. EC is composed of numerous, small, crowded glands with varying degrees of stratification and slight atypia (Figure 7). Nuclear polymorphism is variable but is usually only mild to moderate. We commonly observe large round nuclei with variable prominent nucleoli and a coarse clumped chromatin visible at high magnification, signs of an increase of the mitotic activity. A visible inflammation is often visible.

These glands invade the myometrium in different manners. Five patterns of invasion were recorded in EC grade 1: Infiltrating Glands (IG), Microcystic Elongated and Fragmented Glands (MELF) which is a distinctive histologic variant of the infiltrative gland pattern, broad front (BF), Adenomyosis Like (AL), and Adenoma Malignum (AM). Since all this patterns was present in my cohort study, a description of their histological characteristics will be done on the introduction in order to have a better comprehension and overview (Figure 8).

The IG pattern is the most common pattern of myometrial invasion in EC. This pattern is characterized by individual glands to small cluster of glands with irregular contour that infiltrate the myometrium with and without stromal response. The infiltrative gland pattern was also found in higher stage, (Stage IB and Stage II), and was associated with lymphovascular invasion and recurrence, suggesting that this growth pattern may be associated with tumors having other histologic features typically associated with more aggressive behavior [47]. The second most common pattern is the BF pattern. As indicated by his name, it is characterized by cluster of tight glands without stroma or myometrium space between glands that infiltrate

the myometrium with a pushing and undulated border, indicative of an irregular endometrial interface. When the myometrial invasion is superficial, the stromal response is often absent. The MELF pattern is composed of small, fragmented clusters of tumor cells set (or microcystic glands) in a fibromyxoid, desmoplastic stroma. Accompanying inflammatory cells, notably neutrophils, are typically seen. This pattern is believed to be the result of a stromal response to the IG pattern due to the fact that numerous IG glands are still observable between MELF areas. However, the microcystic glands could also result from an epithelial to mesenchymal transition (EMT) [48] where the tumor cells detach from the original tumor gland in order to metastasize. This hypothesis is supported by an immunohistological study in which MELF pattern shows an altered immunophenotype compared with conventional glandular tumor areas. MELF pattern was characterized by reduced E-cadherin expression. Another epithelial marker, cytokeratin CK7, was shown to be partially expressed as some glands gave strong expression while in contrast adjacent unstained tumor glands was observable [49]. This phenomenon can be explained by the fact that MELF pattern in broadly heterogeneous with a mix of MELF glands and IG glands suggesting an intermediate phenotype between epithelial and mesenchymal with a progressive loss of epithelial markers. MELF pattern have been correlated with lymph node metastasis or extra uterine Disease [50, 51]. Nevertheless, pathologists today consider IG and MELF as similar patterns. In the adenomyosis-like pattern, there are too many groups of closely packed neoplastic glands to represent the normal distribution of adenomyosis. This pattern is characterized by a nest of malignant glands that infiltrate the myometrium in irregular islands and connected lumens. And finally AM, a rare pattern of myometrial invasion comprised of histologically unremarkable glands that infiltrate the myometrium with no surrounding tissue response. Glands are described as little regular and round glands often widely spaced and deeply colonizing the myometrium.

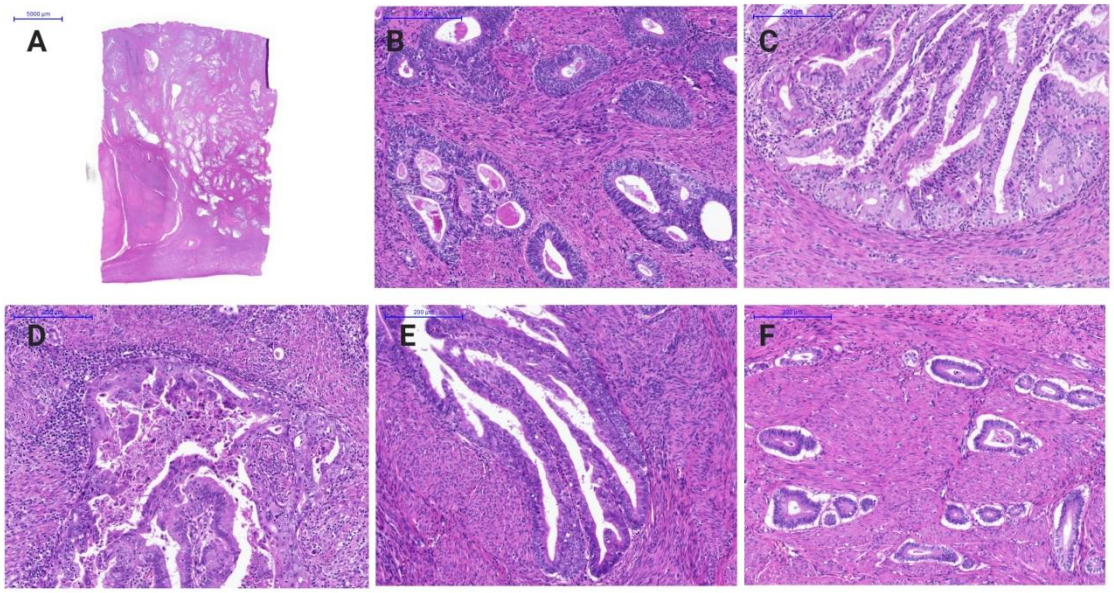

Figure 8. The patterns of myometrial invasion.
A. Histological section of an EC grade 1 stage 1B showing the extent of myometrial invasion. **B.** IGs are composed of single or small groups of glands with irregular contours scattered in the myometrium. **C.** BF, which has a linear limit between the tumor and the stroma beneath. **D.** MELF identified at the leading edge of the tumor associated with neutrophils infiltration and microcystic glands. **E.** Adenomyosis-like, composed of groups larger than five glands simulating adenomyosis. **E.** AM is composed of low cytological grade, regular, rounded, and widely spaced glands with no stromal response.

2.2. What causes endometrial cancer?

Today, it is not clear why EC occurs. Some risk factors have been identified. A risk factor increases the risk that cancer occurs, but is neither necessary nor sufficient to cause cancer. A risk factor is not a cause in itself.

The most common stage 1 EC is estrogen-related. Low grade EC is associated with atypical endometrial hyperplasia and is generally expressing estrogen and/or progesterone receptors (ER/PR positive). This is why, with a few exceptions, the factors increasing the risk of EC are linked to estrogens-induced proliferation and are therefore either endogenous (obesity, anovulatory cycles, estrogen secreting tumors…) or exogenous estrogen exposure (unopposed hormone replacement therapy, Tamoxifen…). In addition, numerous genomic alterations and activation pathways have also been demonstrated.

Estrogens-induced proliferation

Women with a personal history of breast or ovarian cancer outweigh the risk of developing EC as Tamoxifen is commonly given as treatment for its anti-estrogen activity. Decrease in the risk should be expected, but tamoxifen also has a stimulating effect on the endometrium that can support the development of EC.

An estimated 40% of cases are thought to be related to obesity. In obesity, the excess of adipose tissue increases conversion of androstenedione into estrone, an estrogen. Higher levels of estrone in the blood cause less or no ovulation and expose the endometrium to continuously high levels of estrogens. Polycystic ovary syndrome (PCOS), which also causes irregular or no ovulation, is associated with higher rates of EC for the same reasons as obesity. Specifically, obesity, type II diabetes, and insulin resistance are risk factors for Type I EC [52]. Obesity increases the risk for EC by 300–400%.

Estrogen replacement therapy during menopause when not balanced (or "opposed") with progestin is another risk factor. Higher doses or longer periods of estrogen therapy have higher risks of EC. Unopposed estrogen raises an individual's risk of EC by 2–10 fold, depending on weight and length of therapy. However, taking contraceptive pills containing both estrogen and progesterone lower the risk of developing EC.

Having more menstrual cycles in a lifetime increases the risk of developing EC, again for hormonal reasons. A longer period of fertility, either from an early first menstrual period or late menopause, is also a risk factor.

Lynch syndrome or HNPCC, an autosomal dominant genetic disorder that mainly causes colorectal cancer, also causes EC, especially before menopause. Women with Lynch syndrome have a 40–60% risk of developing EC, higher than their risk of developing colorectal (bowel) or ovarian cancer. Carcinogenesis in Lynch syndrome comes from a mutation in MLH1 or MLH2: genes that participate in the process of mismatch repair, which allows a cell to correct mistakes in the DNA. Other genes mutated in Lynch syndrome include MSH2, MSH6, and PMS2, which are also mismatch repair genes. Women with Lynch syndrome represent 5% of EC cases [53]. Depending on the gene mutation, women with Lynch syndrome have different risks of EC. With MLH1 mutations, the risk is 54%; with MSH2, 21%; and with MSH6, 16% [54].

Genomic alterations

Estrogen-related grade 1 EC is typified by high frequency genomic alterations and several genes signature can be identified (Figure 9). Studies using cDNA microarrays confirm that endometrioid cancer grade 1 and serous EC grade 2 and 3 have distinctively different gene expression profiles.

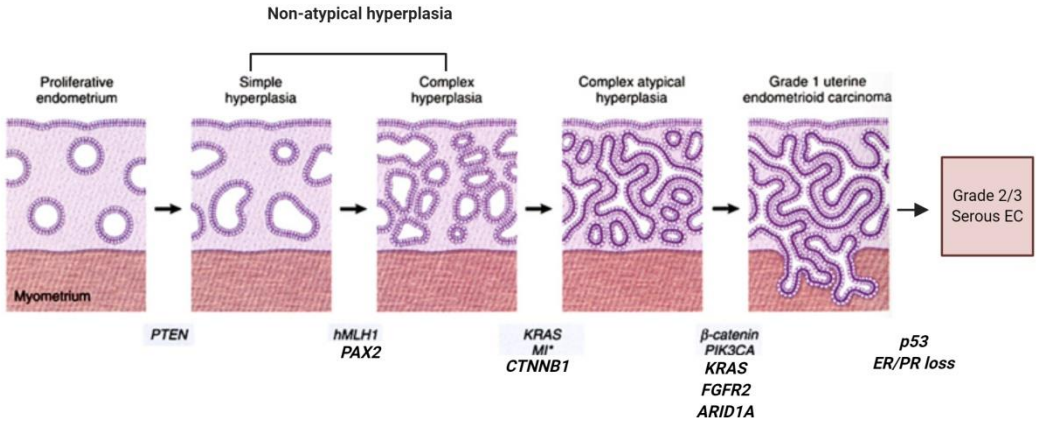

Figure 9. Molecular changes during endometrial carcinogenesis.

Scheme representing the estrogenic pathway leading to EC grade 1 from normal proliferating endometrium adapted from https://www.memorangapp.com/. It is well characterized that PTEN mutation is the first modification leading to non-atypical hyperplasia which is an excessive thickening of the endometrium with normal glandular epithelium. Several other modification of KRAS mutation and β-catenin activation leads to a precancerous atypical hyperplasia with accumulation of aberrant cells. Further mutations leading to AKT activation trigger endometrial tumorigenesis.

Increasing genetic damage can be seen in precursor lesions within the endometrioid pathway, beginning with PTEN tumor suppressor gene or PAX2 inactivation in normal-appearing glands (latent precancers), followed by positive hormonal selection and clonal outgrowth as non-atypical hyperplasia. PIK3CA mutations play an active role for transition to atypical endometrial hyperplasia. This stage is characterized by FGFR2, ARID1A (BAF250a), KRAS mutations, and activation of the β-catenin gene (CTNNB1), as well as epigenetic silencing of MLH1 and microsatellite instability to finally result in development of low grade EC.

Although this model is applicable to a high proportion of endometrial carcinomas, not all tumors fit in. In fact, a grey zone exists between the two broad grades, with a significant number of tumors showing overlapping clinical, morphologic, and molecular features (Table 1). Indeed, the estrogen-independent Grade 2 tumors show loss of heterozygosity at different loci, altered p53, and abnormalities in genes regulating mitotic checkpoints. However, p53 mutations are found in 14 to 20% of endometrioid carcinomas grade 1. This finding suggests that p53 is involved in the progression, but not the initiation, of endometrioid carcinoma. Moreover, there is an ongoing debate about whether a histologic subset of endometrioid carcinomas (those that are poorly differentiated or have high nuclear grade) should be assigned to the grade 2 group. A supporting study also revealed that MELF glands were usually negative for estrogen and progesterone receptor [49]. The MELF pattern of invasion is histologically very heterogeneous with a majority of IG type glands inside the tumor and toward the uterine cavity while MELF glands is mostly observable in the tumor front at the tumor-myometrium interface and thus are the pattern of invasion. We have previously seen that these MELF glands displayed more transformation compared to other types of invasions. A question then remains:

MELF glands should thus be associated to estrogen-related grade 1 endometrioid cancer or estrogen-independent grade 2 serous cancers?

	Grade 1	Grade 2
Incidence	≥80%	≤20%
Age	Varied	Postmenopause
Histology	Endometrioid	Serous, clear
Grade	Low	High
Clinical behavior	Less aggressive	More aggressive
Estrogen relation	Much evidence	Less evidence
BMI	High	Low
Parity	Low or null	Varied
Presence of precursor lesion	EIN or hyperplasia with/without atypia	Uncertain EIC
IHC	50–80% *PTEN* mutation	0–5% *PTEN* mutation
	14–20% p53 Mutation	90% p53 Mutation
	10–20% E-cadherin	80–90% E-cadherin
	20–45% MSI	0% MSI
	14–44% β-Catenin	0–5% β-Catenin
	10–18% Aneuploidy	85–95% Aneuploidy
	10–30% K-ras mutation	45–80% Her/neu overexpression P16 mutation
	Often with ER, PR, or AR positivity	

AR = androgen receptor; BMI = body mass index; EIC = endometrial intraepithelial carcinoma; EIN = endometrial intraepithelial neoplasia; ER = estrogen receptor; IHC = immunohistochemical staining; MSI = microsatellite instability; PR = progesterone receptor; *PTEN* = phosphatase and tensin homolog.

Table 1 Molecular characteristics of Grade 1 and 2 EC.

This table has been published in a pertinent paper from Lee et *al.* and shows the incidence of the principal mutations in both estrogen-related grade 1 and estrogen-independent grade 2 EC [1]. As we can see, several genes signatures are found in both highlighting the histologically complexity of EC.

Pathways activation

Our understanding of synergies between multiple independent genetic events that produce EC grade 1 centers upon the PI3K pathway, and its ability when perturbed to activate AKT/PKB signaling pathway, promoting survival and growth in response to extracellular signals. It is estimated that more than 80% of EC have an abnormality in the PI3K pathway. This pathway is initiated by multiple processes including genomic alterations described before. PTEN inactivation (50-80% of cases), or constitutive activation of KRAS (10–30%) (Table 1) or PIK3CA (30%) act in concert to accumulate PIP3, which in turn activates AKT by phosphorylation (Figure 10). Once activated, pAKT initiates a cascade of tumorigenic events that includes stimulation of the mTOR pathway, deregulation of cell cycle control, blocking of apoptosis, and prolonged cell survival [1].

Recently, it has been demonstrated that increased signal transducer and activator of transcription (STAT3) pathway, increased expression of midkine (MK) and decreased E-cadherin levels in EC cells may also play important roles in EC tumor transformation/dedifferentiation from latent to invasive cancer [55].

The activated Ras protein interacts with RAF to promote RAF phosphorylation and activate MEK. The activated MEK phosphorylates MAPK, which is also known as ERK. This pathway regulates cell proliferation and differentiation in EC. The signaling cascade is activated by several upstream signaling sources, which include genetic alterations (K-Ras mutation), GFs, cytokines, interleukin, and mitogen [56].

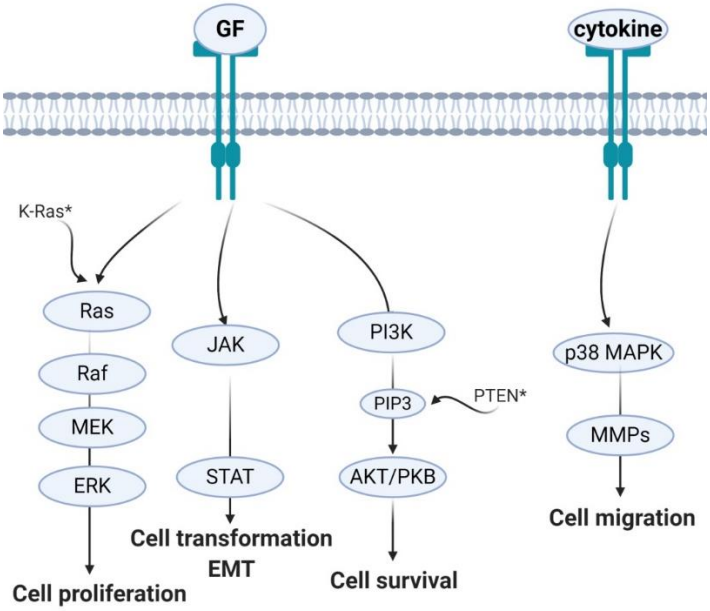

Figure 10. Endometrial cancer pathway.

Scheme representing the tumorigenic pathways from GFs and cytokines receptors activation leading to EC grade 1. This is not an exhaustive representation. Further pathways are implicated and a single pathway may impact more tumorigenic process at the same time with other pathways interactions.

Following activation of PI3K/AKT and p38 MAPK pathways, the PI3K/AKT and p38 MAPK pathways activates and recruits ETS-1 to the promoters of MMP-9 and MMP-13 to induce these genes. These MMPs in turn promote cell migration and invasion followed by metastasis [57].

2.3.Diagnosis state of knowledge

The first sign is most often vaginal bleeding not associated with a menstrual period. The EC is usually diagnosed early enough due to the fact that the majority of EC affect post-menopausal women. Other symptoms include pain with urination, pain during sexual intercourse, or pelvic pain. EC is first diagnosed with an ultrasound examination of the uterus. During this examination, the thickness of the endometrium is measured. When exceeding 3 to 4 mm, a uterine endoscopy in which tissue samples are taken is usually carried out and the final diagnosis is based on histological features recognition.

However, EC causes very few symptoms in its early stages as the tumor size is not consistent enough to cause visible disturbances. In addition, due to the rise of obesity, we observe an increase in the incidence in young women during the last decades where little bleeding outside of menstruation is often overlooked due to cycle irregularities induced by contraceptive pills [58, 59]. This is why a substantial percentage remains silent long enough to evolve. At diagnosis, only 75% of women have a cancer confined to the uterus (FIGO stage 1) [60]. For these women, the prognosis is good and the 5-year survival rate is 97% [60]. Due to the fact that grades 1 and 2 tumors usually do not spread to other parts of the body, they are

usually treated as low-risk. However, a subset will demonstrate an unexpected and aggressive course and will develop recurrence after initial treatment of the primary tumor. To this date, there is no effective screening test to identify these patients. The prognosis for recurrent disease is poor; the median survival hardly exceeds 12 months [61]. Currently, the absolute and proportional number of patients with recurrent EC increases [62]. It is thus important to identify prognostic factors that may predict the development of recurrent disease, better diagnose these patients early enough to improve the choice of adjuvant therapy subsequently. Research of these markers has been the subject of much interest in the scientific field lately. On a retrospective study of a total cohort of 209 EC, the factors that were highlighted to be associated with the development of recurrent disease include age, histology, grade, histological type, ER and PR expression and the depth of myometrial invasion [61]. However, the importance of these factors remains controversial [63]. The degree of myometrial invasion continues to be a consistent indication of tumor virulence. As the depth of myometrial invasion increases, the chance of having extra uterine disease is greater. As noted above, grade and depth of invasion, as a generalization, are interrelated. As the grade of the tumor increases, an increase usually occurs in the depth of myometrial invasion; however, exceptions exist in that a grade 1 lesion can have deep myometrial invasion and a grade 3 lesion can be limited to the endometrium. When grade and depth of invasion are evaluated separately, the depth of invasion appears to be a more important prognostic factor than the grade of the tumor (Medsccape). A further challenge is whether or not to include desmoplasia with evident MELF neoplastic cells in tumors higher risk tumor.

MELF pattern of myometrial invasion has been proposed as a prognostic marker in patients with EC. In a study within the category of low-grade endometrioid ECs, univariate analysis showed deep myoinvasion, MELF pattern of invasion and pelvic/paraaortic lymph node metastasis to be more common in patients whose tumors recurred at extravaginal sites [64]. Another study stipulates that MELF positive patients were more likely to present with higher grade tumors, lymph node metastasis, lymphovascular invasion and >50% myometrial invasion [65]. MELF pattern of myometrial invasion plays thus a critical role in lymphovascular space invasion and lymph node metastasis in patients with EC [50]. However, here, no difference was reported in global disease survival as well as local recurrence rates. Regardless, its implication in survival and recurrences still remains elusive [65]. A MELF pattern of invasion is reported to be associated with a higher “likelihood” of nodal involvement and distant recurrence but its significance as an independent risk factor remains unclear [66, 67].

Therefore, the presence of MELF-pattern invasion does not currently influence patient management but together with other invasive features remains the focus of research studies [68]. The challenge remains on finding the right complementary diagnosis/prognosis factor.

2.4.Targeted drug therapy: state of knowledge

Choice of EC treatment is closely dependent to the extent of stage diagnosed. Surgical procedures are still the most effective first-line treatments for this disease, which negatively affect future fertility that is important for young patients [44, 69]. Additionally, patients with recurrent EC have a poor prognosis, and are not usually cured by surgery, conventional

chemotherapy and radiation. Therefore, it seems imperative to develop new, effective, non-surgical and conservative treatments strategies for patients with EC [70]. Targeted drug treatments focus on specific weaknesses present within cancer cells. Taking advantage of these weaknesses, targeted drug treatments can cause cancer cells to die or limit tumorigenesis processes such as tumor cell proliferation, spread and angiogenesis. Targeted drug therapy is usually combined with chemotherapy for treating advanced EC. There are several experimental therapies for EC under research, including immunologic, hormonal, and chemotherapeutic treatments.

Cancers can be analyzed using genetic techniques (including RNA/DNA sequencing and immunohistochemistry) to determine if certain therapies specific to mutated genes can be used. Poly (ADP-ribose) polymerase inhibitor rucaparib is used to treat EC with PTEN mutations [71]. The PARP inhibitor shown to be active against EC is olaparib. Research is ongoing in this area as of the 2010s [71].

Recently, metformin, a widely used drug for the treatment of type II diabetes mellitus, is also a therapeutic candidate for EC treatment [72]. Metformin may exert its anticancer effects by inhibiting hyper proliferative processes, which trigger carcinogenesis [73]. Metformin decreases systemic insulin, and IGF-1 levels, which are strongly mitogenic and induce cancer cell proliferation and metastasis through activation of the PI3K/AKT/mTOR pathway, which is called insulin-dependent (indirect) effects. Additionally, metformin also inhibits activation of the PI3K/AKT/mTOR and MAPK/mTOR pathways through AMP-activated kinase (AMPK)-dependent and AMPK-independent pathways, which is also known as its direct effects. This leads to decreased protein synthesis and cell growth and increased autophagy and apoptosis. On a study published in 2020, short-term treatment with an oral metformin significantly reduced a proliferative marker Ki-67 index in women with endometrioid EC awaiting surgical staging [73]. On another recent study, metformin was shown to promote anti-tumor biomarkers in Ishikawa human EC cells [74]. Early research has shown that metformin administration can reduce expression of tumor markers by altering EMT protein expression and MAPK signaling components [75]. Long-term use of metformin has not been shown to have a preventative effect against developing cancer [52].

Temsirolimus, another mTOR inhibitor, is under investigation as a potential treatment [76]. Research shows that mTOR inhibitors may be particularly effective for cancers with mutations in PTEN. Ridaforolimus (deforolimus) is also being researched as a treatment for people who have previously had chemotherapy. Preliminary research has been promising, and a stage II trial for ridaforolimus was completed by 2013 [77]. Bevacizumab and tyrosine kinase inhibitors, which inhibit angiogenesis, are being researched as potential treatments for ECs with high levels of vascular endothelial GF [2]. Ixabepilone is being researched as a possible chemotherapy for advanced or recurrent EC [78].

These systemic treatment options are often accompanied by high toxicity and effective increase of survival rate is not yet proved but researches are still underway and there is no established standard of care yet for this disease. There is thus an urgent need to find modalities to developed more adequate treatment for patients with high risk of recurrence.

However, the research approach in blocking the activation of pathways implicated in tumorigenesis processes is interesting. This study contributes to this effort as modest complement by relying on an unexpected but no less essential element present in cancer cells and their microenvironment also both on the cells and the extra cellular matrix. Without raising more suspense, these elements are, as formulated in the title, heparan sulfates proteoglycans.

3. HEPARAN SULFATE IN PHYSIOLOGY

For the following part, I will introduce HSs in the context of EC by describing their characteristics from the widest to the detail as shown in the Figure 11.

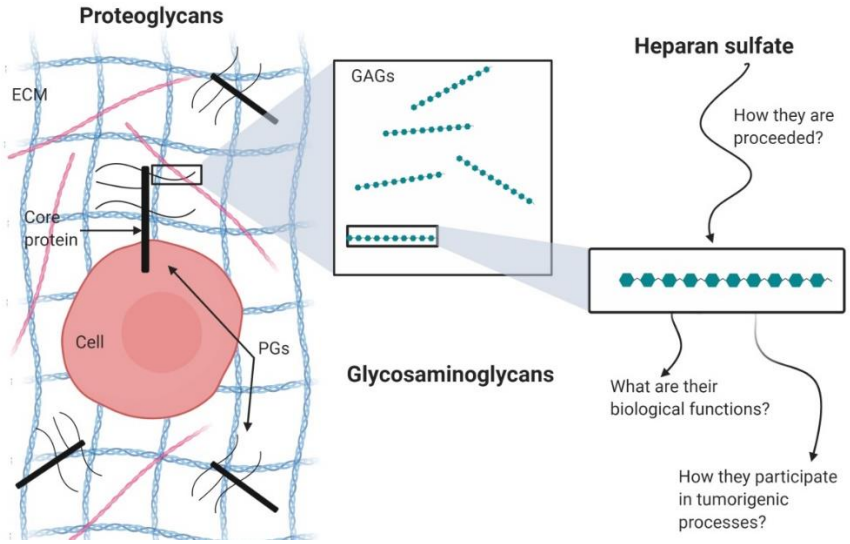

Figure 11. Schematic representation of the description which follows.

From widest to the detail, we will first describe proteoglycans to which several glycosaminoglycans are attached and among them there are HSs.

3.1.Proteoglycans and Glycosaminoglycans

Proteoglycans (PGs) are ubiquitous glycoproteins found in most mammalian tissues and characterized by a core protein to which one or more chains of glycosaminoglycans (GAGs) are covalently associated. The functional properties of PGs and their classification depend on the polypeptide sequence of their core protein (defining different subfamilies of PGs), on the nature of their GAG chains and on their location. For example, syndecans (Sdc) and glypicans (Gpc), which are among the main classes of core proteins are mostly associated with HS [79, 80]. They are anchored to the cell surface by a transmembrane domain or a glycosylphosphatidylinositol anchor. Some PGs are released in the extra cellular matrix (ECM) where they constitute major structural molecules [81, 82].

Glycosaminoglycans, also known as mucopolysaccharides, are a family of long linear negatively-charged polysaccharides that are present in every mammalian tissue [83]. They are composed of repeating disaccharide units of hexosamine (*N*-acetylglucosamine or *N*-acetylgalactosamine) and uronic (glucuronic/iduronic) acid or, in the case of keratan sulfate, galactose. On the basis of the aminosugar present in their chains, GAGs can be classified in two major categories: galactosaminoglycans, including chondroitin sulfate (CS) [84] and dermatan sulfate (DS); glucosaminoglycans, including hyaluronic acid (HA), heparin (HEP), HS and keratan sulfate (KS) (Figure 12).

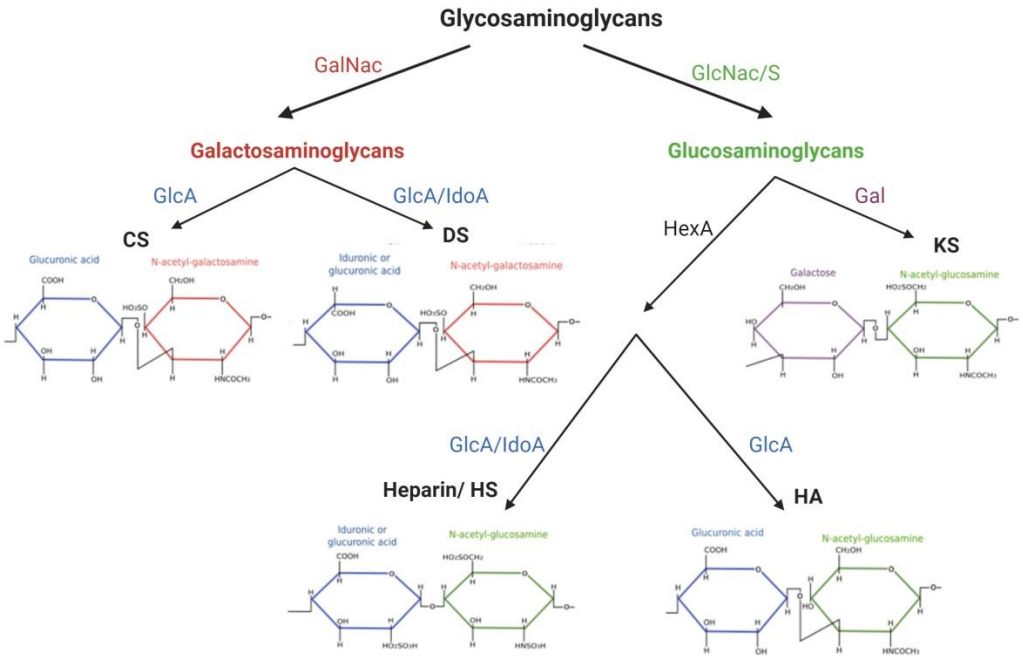

Figure 12. Structure of the different glycosaminoglycan chains.

A. Family of glycoaminoglycans. GalNAc : N-acetyl galactosamine ; GlcNAc/S : N-acetyl/N-sulfo glucosamine ; HexA : hexuronic acid ; Gal: galactose ; GlcA : glucuronic acid ; IdoA : iduronic acid. Adapted from [3] and https://mmegias.webs.uvigo.es/.

Each singe chain contains differently sulfated and acetylated disaccharide units which contribute to the structural variation of GAGs and allow to easily interact with a plethora of proteins, including GFs, morphogens, cytokines, enzymes and adhesion molecules. GAGs also vary in the geometry of the glycosidic linkage (α or β) and in aqueous solutions are surrounded by a shell of water molecules which makes them occupy an enormous hydrodynamic volume.

Hyaluronic acid (HA) has the simplest structure of all GAGs and is the only member of the family which is not attached to a core protein. It consists of sequential repetitions of GlcA-GlcNAc disaccharides up 10^7 Da [85]. The monosaccharide building blocks are synthesized in

the cell cytoplasm and are recruited to the inner plasma membrane where HA is assembled and then secreted unmodified into the extracellular space [86]. HA is an important component of skin, connective tissue, cartilage, synovial fluid, umbilical cord and the vitreous of the eye. It plays an essential role in maintaining hydration, particularly through interactions with its cell receptor CD44 which is expressed on the surface of virtually all stem cells including cancer stem cells [87].

CS [88] and DS [89] are constituted by N-acetylgalactosamine and an hexuronic acid: glucuronic acid in CS and both iduronic and glucuronic acid in DS, with a prevalence of IdoA. The sulfation pattern of CS/DS determines the biological activity of the resulting compound. CS can be O-sulfated on C-4 or C-6 of the galactosamine residue (CS type A and C, respectively) but also the double sulfated galactosamine has been found. DS can present additional sulfation on position 2 of the iduronic acid and has been called CS type B for a long time, due to the fact that it can also present glucuronic acid. CS chains are made up of 10-200 disaccharide units and are found both on cell surfaces and in the ECM, particularly in cartilage where they participate to the elastic and compressive properties of the connective tissue.

Keratan sulfate (KS) [90] is a β-1,3-linked poly-N-acetyl-lactosamine, the only GAG which contains galactose instead of a hexuronic acid. O-sulfation on C-6 may be present on both sugars, with increased frequency on the glucosamine, and give rise to differently sulfated regions. There are 3 types of KS, depending on how KS chains are attached to the core protein: KS I (N-linked to Asn) mainly found in cornea, skeletal KS-II (O-linked to Ser/Thr) typical of cartilage and KS III (mannose-Ser linkage) found in brain tissue. Another feature of KS is the presence of branches on the polysaccharide chain and the presence of fucose on the glucosamine and sialic acid at the end of chains (phenomenon known as "capping").

3.1.1. HS and Heparin

Heparin (HEP) is the GAG with the highest degree of sulfation and is constituted by repeating disaccharide units of N-sulfated- or N-acetylglucosamine linked to either glucuronic or iduronic acids, the main disaccharide being GlcNS,6S-IdoA2S. Heparin is mainly found in mast cell secretory granules, where several chains are bound to a core protein to form the proteoglycan serglycin.

HS is ubiquitously found in all cell types and is constituted by mainly GlcNAc linked to GlcA which are differently substituted to generate domains with mostly GlcNAc and absent/low sulfation (NA-domain), sulfated regions containing consecutive GlcNS (NS-domain) or mixed sequences with N-acetylated/N-sulfated glucosamine (NA/NS-domain). However, HS chains with high sulfation degree have been described in specific tissues and in pathologic conditions [91, 92].

Both HS and Heparin are linked to a core protein by O-serine linkage and follow the same biosynthetic pathway. While heparin is mostly known for its anticoagulant activity thanks to the ability to bind and activate AT-III, an anticoagulant activity of HS has also been found on endothelial cells basement membranes. The specific sequence responsible for binding to AT is a pentasaccharide bearing a rare 3-O-sulfated glucosamine (abbreviated as GlcN*) which is present in nearly 30% of pharmaceutical heparin. Additional residues flanking the

pentasaccharide can modulate the affinity of heparin chains towards AT. Only 1–10% of HS isolated from tissues was found to bind to AT, suggesting that AT recognizes a unique structure of HS [93] and this subset of chains is called anticoagulant HS (aHS) (Figure 13).

AT is a member of the serine protease inhibitor family capable of inhibiting all blood clotting factors, in particular factor Xa and IIa. The activity of AT is strongly dependent on its attachment to the specific pentasaccharide motif. This interaction induces a conformational change in AT, resulting in the exposure of the reactive loop of the protein, which will then allow the recognition of target proteases and stabilize irreversibly the AT / protease complex [94].

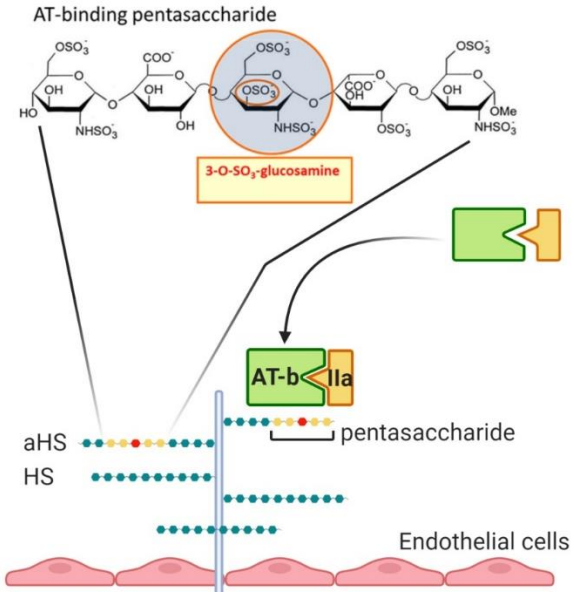

Figure 13. Structures of AT-binding domain and anticoagulant activity of HS.

HS anticoagulant pathway. Anchored by a proteoglycan core to the vessel wall, HS binds antithrombin (AT) via a unique pentasaccharide sequence (diamonds) found on 1 to 10% of the glycosaminoglycan side-chains. Key to the high-affinity binding of AT to the pentasaccharide is the 3-O-sulfated glucosamine residue in the middle of the pentasaccharide sequence (red diamond). Once bound, AT undergoes a conformational change at its reactive center loop that enhances its reactivity with thrombin (IIa), thereby promoting the formation of AT/IIa complexes. Adapted from [95].

3.2.HS biosynthesis

The biosynthesis of HS, is a complex and multi-step non-template driven process which begins in the Golgi apparatus and involves the coordinate action of several enzymes [96]. The process can be divided into 3 main steps: initiation, elongation and modification (Figure 14).

The first step is the formation of a glucuronic acid-galactose-galactose-xylose tetrasaccharide (GlcA-Gal$_2$-Xyl) also known as linkage region (LR) which allows the attachment of the polysaccharide chain to the core protein. The xylose residue is attached to a serine in the core protein by the action of one of two xylosyltransferases, XYLT1 or XYLT2 [97, 98]. Then, two galactose residues are added in sequence by the galactosyltransferases

GalT-1 and GalT-2, respectively. The formation of the linkage region is finally completed by the addition of a glucuronic acid unit by the GlcAT-1 transferase.

The members of the EXT family of glycosyltransferases are responsible for the polymerization and elongation of the newly formed polysaccharide which can become either HS or CS/DS depending on the addition of the first hexosamine to the non-reducing end of the acceptor linkage region by EXTL enzymes (EXT-like). If GlcNAc is added, the polysaccharide will follow the HS biosynthetic path, while GalNAc is added for a CS/DS path. Once the first hexosamine has been added, the assembly of the HS chains continues by sequential addition of GlcA and GlcNAc by the enzymes EXT1 and EXT2 to form a precursor polysaccharide.

The resultant polymer undergoes a series of sequential modification reactions, including N-deacetylation / N-sulfation of glucosamine residues, C-5 epimerization of GlcA to IdoA, 2-O sulfation of hexuronic acids, and 6-O- and possibly 3-O- sulfation of glucosamines.

The modification of HS chain is initiated by N-deacetylation/N-sulfation of GlcNAc residues by the N-deacetylase/N-sulfotransferase-1 (NDST) enzymes. The NDSTs play a key role in the formation of domains with different sulfation/acetylation degree which are responsible for different affinity towards ligand proteins [99]. Most modifications of the HS chain depend upon the presence of GlcNS residues and are therefore determined by the action of NDSTs. Indeed, proteins may interact with single NS domains rich in O-sulfate groups (e.g., growth factors of the fibroblast growth factor [FGF] family) or with two NS-domains separated by NA disaccharide residues [100] as shown for the angiogenic growth factor VEGFA165 [101], interleukin-8 [102] and interferon-γ [103]. Heparin exhibits a much higher degree of modification (i.e., epimerization and sulfation) than HS, with NDST2 being the rate limiting enzyme in heparin biosynthesis [104].

A single C5-epimerase converts many but not all GlcA units adjacent to GlcNS into IdoA [105], therefore IdoA residues are not present in NA-domains. Epimerization is followed by 2-O-sulfation on the majority of the IdoA units by a 2-O-sulfotransferase (2OST). The enzyme is also active on GlcA and indeed, rare GlcA2S-GlcNS disaccharide units have been described in adult human brain [106] and rat hepatocytes [107].

Following 2-O-sulfation, HS chains are then O-sulfated at C6 of glucosamine by enzymes of the 6-O-sulfotranferases (6OST) family, comprising 3 isoforms that show different preference on the target glucosamine but can 6-O-sulfate both GlcNS and GlcNAc residues [108].

Finally, the last family of enzymes, the 3-O-sulfotranferases (3OSTs), catalyzes the relatively rare 3-O-sulfation of glucosamine. Six isoforms and a splice variant have been identified in vertebrates that can introduce the GlcN* residue crucial for the formation of the antithrombin-binding pentasaccharide motif in heparin/aHS [109] but also in other sequences. Indeed, 3-O-sulfation was found in the epitope of HS interacting with Herpes simplex [110].

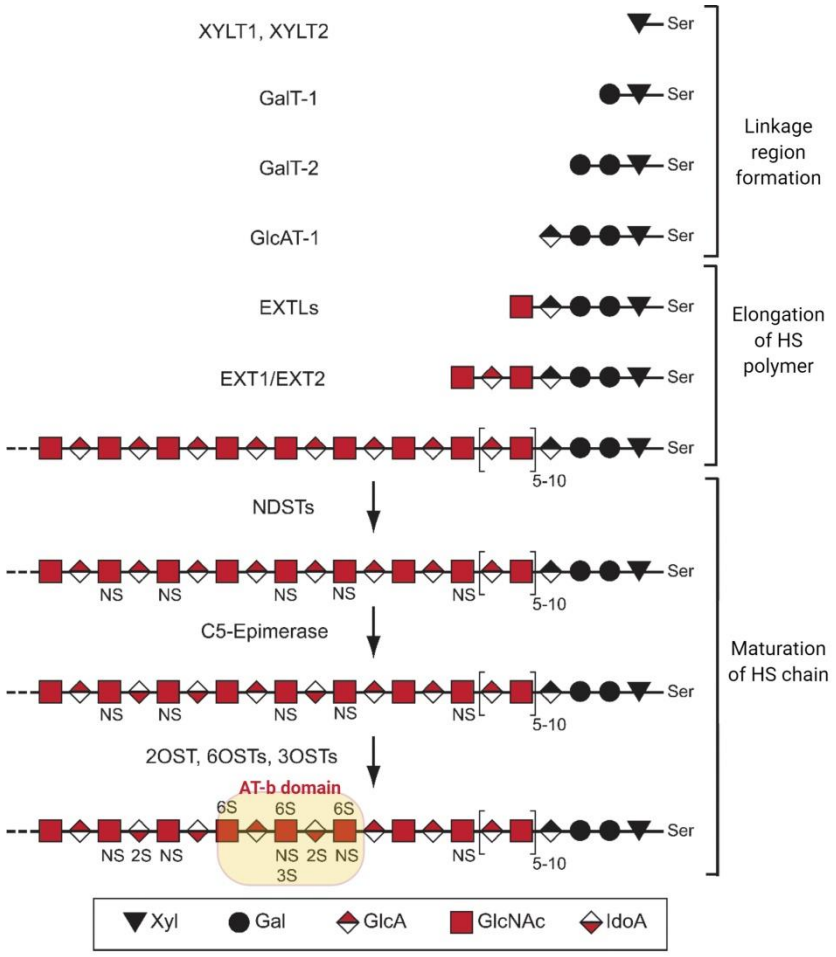

Figure 14. HS biosynthesis.

HS chains are linked by the linkage region to a specific serine residue of a core protein. Addition of the first N-acetylglucosamine catalyzed by the EXTL enzymes directs toward HS biosynthesis. Elongation of the chains is achieved through the alternative addition of glucuronic acid and N-acetylglucosamine by the transferases EXT1 and EXT2. During polymerization, chains undergo several modifications including epimerization of glucuronic acid and sulfation at different positions. These modifications occur in different clusters and generate N-acetylated, N-sulfated and mixed domains differently involved in interactions with ligands. Ser, serine; NS, N-sulfate group on glucosamine residues; 2S, 2-O-sulfate group on glucuronic or iduronic acid residues; 3S, 3-O-sulfate group on glucosamine residues; 6S, 6-O-sulfate group on glucosamine residues. Adapted from [98].

Combined together, all of these modifications generate 48 different disaccharide units with highly heterogeneous pattern of sulfation along HS chains especially due to the hyper variable NS domain[111]. The overall pattern of HS modification is not random but, on the contrary, quite conserved within a specific cell type or organ, showing that the biosynthesis must be strictly regulated [99]. Not unexpectedly, altered levels of HSPGs or altered expression of genes coding for HS biosynthetic enzymes have been associated with the development of many diseases [112-114], and due to the hundredth of possible HS-protein interactions, research interest is growing in the last decades.

3.3.HS post-biosynthetic modification and degradation

The last modification step in HS biosynthesis occurs on the cell surface by the action of SULF1 and SULF2 which catalyze the removal of sulfate groups in 6-O-position of glucosamine within highly sulfated regions [115]. Interestingly, SULFs act exclusively on the tri-sulfated disaccharides UA(2S) - GlcNS (6S) [116, 117] while no 6-O-desulfation is observed on other types of 6-O-sulfated disaccharides. This last step is crucial for the modulation of HS interaction with ligand proteins and overexpression/downregulation of SULFs is often described in pathologic conditions [117] [118].

In order to allow rapid adaptation of the cell to changes in its environment, HSPGs can be subjected to limited proteolysis and be released in the medium or they can be rapidly recycled (half-life of ~ 3-4 hours) and renewed on the cell surface.

Conventionally, HS catabolism pathway is a multistep process terminating in lysosomes that involves internalization by endocytosis, followed by degradation under the action of endoenzymes that will produce HS fragments which depolymerize HS chains into oligosaccharides. Exoenzymes are then responsible for depolymerization of large HS fragments into monosaccharides and inorganic sulfate to facilitate exit from the lysosome. This exo-degradative process requires a multienzyme complex composed of three glycosidases, potentially four sulfatases and an acetyl-transferase. Since theses exoenzymes can act only at the non-reducing end, the process is done sequentially [119].

The only known mammalian endoglycosidase able to cleave HS is heparanase (HPSE) that is secreted as a latent 65-kDa enzyme able to bind to HSPGs and the complex is then internalized by endocytosis [79]. HPSE uptake is a prerequisite for the delivery to lysosomes where it is activated by cathepsin L and cuts HS at a limited number of sites, specifically the β-(1,4) glycosidic linkage between GlcA and GlcNS, producing fragments that are 10–20 saccharide units in length and still able to interact with protein ligands [120, 121].

Although numerous studies have accumulated regarding HS turnover especially in the last years, there is still debate on certain aspects which remain unclear. For example, the exact location and moment of activation of HPSE, whether in late endosomes or lysosomes, is still not precisely defined, together with the mechanism of HSPGs trafficking.

3.4.HSPGs in physiology

The network of interactions of HS, called “HS-interactome”, seems endless and the whole complexity of this interactome has yet to be revealed. In table 2 a non-exhaustive list of the main examples of HS binding proteins is reported.

Receptor	Cytokines	Growth Factors
Unspecified HSPG	IL-5,6,8,10, CXCL12/SDF-1, TNF-α, and PF-4	**FGF-1, -2, -4, -7, -8, -10 and -18, HGF, PDGF, HBEGF, Neuregulin-1, VEGF, BMP-7, Noggin, Hh**
SDC1-4	CXCL12/SDF-1	**FGF-2, HGF, VEGF, HBEGF, Hh,** Midkine, Pleiotrophin, TGF-β, Wnt
GPC1-8		**FGF-1, -2, HGF, VEGF, BMP-7, Hh,** Wnt, TGFβ, Midkine, IGF
Agrin		**FGF-2**
Perlecan		**FGF-2, -7**
TβRIII		**FGF2**, TGFβ-1, -2, -3, inhibin, **BMP-7**, -2, -4, GDF-5
CD44	MCP-1	**FGF-2, VEGF, HBEGF, HGF**
NRP1-2		**FGF-2, -4, VEGF**, PIGF, PDGFB, semaphorins, TGFβ

Table 2. Heparan sulfate binding proteins.

Here a list of major GFs and cytokines that bind to HS chain according to core protein.

Abbreviations: BMP: bone morphogenetic protein, CXCL12: chemokine C-X-C motif ligand, FGF: fibroblast growth factor, GDF: growth and differentiation factor, HBEGF: heparin-binding epidermal growth factor, HGF: hepatocyte growth factor, Hh: Hedgehog, HS: heparan sulfate, TGF: transforming growth factor, IGF: insulin growth factor, IL: interleukin, MCP: monocyte chemoattractant protein, PDGF: platelet derived growth factor, PF: platelet factor, PIGF: placental growth factor, SDF: stroma cell-derived factor, TNF: tumor necrosis factor, VEGF: vascular endothelial growth factor. Table from [122].

HSPGs can interact with proteins through various mechanisms (for reviews, see [123] [124]) and while binding is generally mediated by HS chains, some factors such as Hedgehog [125] have been shown to directly interact with core proteins [126]. Some interactions require specific structural motifs along the HS chains [127], while others are non-selective in terms of motifs but require a certain type of sulfation or a certain negative charge density. It is the case of FGF2 in which 2-O-sulfation is essential for binding [128].

Cell membrane HSPGs act as co-receptors for various tyrosine kinase-type GF receptors, lowering their activation threshold or changing the duration of signaling reactions (Figure 15). They also regulate receptor trafficking to and from plasma membrane and control secretion of ligands at the cell surface. HSPGs are present in basement membranes (perlecan, agrin, and collagen XVIII), where they collaborate with other matrix components to define basement membrane structure and to provide a matrix for cell migration [82].

HS protects FGFs from denaturation and proteolytic degradation and increases FGF affinity for their receptors facilitating and stabilizing the formation of properly oriented FGF oligomers [129]. Similarly, HS localizes other GFs at the cell surface or in the ECM and promotes their biological activities, such as vascular endothelial growth factors (VEGFs),

hepatocyte growth factors (HGFs), transforming growth factor-β1 (TGF-β1); platelet derived growth factors (PDGFs).

HS was also observed to promote the activity of different chemokines, such as interleukin 8 (IL-8), platelet-derived factor 4 (PF4) and stromal cell derived factor-1α (SDF-1α or CXCL12), by sequestering these molecules at the cell surface, thereby increasing their effective concentration in the vicinity of their receptor sites. The interaction is mediated by quite extensive GAG sequences (12-20 saccharide moieties), as a result of chemokine oligomerization. Conversely, soluble GAGs can complex with chemokines in solution and prevent their binding with receptors, inhibiting their activities [130].

L-, E- and P-selectins are a family of transmembrane glycoproteins found on leukocyte endothelium and platelets. L-selectin binds highly sulfated, particularly O-sulfated, HS chains enriched in glucosamine residues whose amino groups are unsubstituted, whereas the presence of IdoA residues seems to inhibit this interaction [131].

HSPGs are used by many viruses as receptors to bind to and gain access into target cells, for example HIV-1, herpes simplex virus (HSV), and dengue virus. Plasmodium falciparum, the parasite causing malaria, bears at its surface circumsporozite protein that shows the ability to interact with liver cell HS proteoglycans, promoting pathogen attachment and subsequent cell invasion [132]

Recent unpublished data (pre-print version) suggest an interaction between the SARS-CoV- 2 Spike S1 protein receptor binding domain (SARS-CoV-2 S1 RBD) and heparin (which is often used instead of HSPG in laboratory experiments due to high availability). This has implications for the rapid development of a first-line therapeutic by repurposing heparin and for next-generation, tailor-made, GAG-based antivirals (doi: https://doi.org/10.1101/2020.02.29.971093).

HSPGs are also found in secretory vesicles, most notably serglycin, which plays a role in packaging granular contents and regulate various biological activities after secretion such as host defense, and wound repair [82].

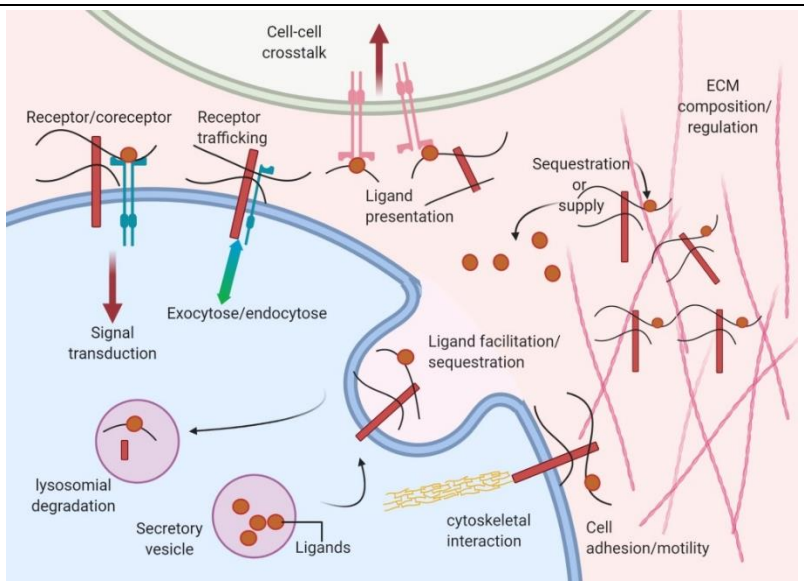

Figure 15. Functions of cell surface and ECM heparan sulfate proteoglycans.

HSPGs regulate signaling pathways in many different ways, both at the intracellular level and in the extracellular matrix (ECM). HSPGs have been shown to mediate signal transduction by acting as receptors or co-receptors; they regulate receptor trafficking to and from the plasma membrane and control the secretion of ligands [133]. HSPGs are present in basement membranes (perlecan, agrin, and collagen XVIII), where they collaborate with other matrix components to define basement membrane structure and to provide a matrix for cell migration [82]. They can also mediate signal to other cells by presenting ligands to their receptors, or by controlling the distribution of signaling gradients. Sequestration and release of GFs, chemokines, cytokines and morphogens can be achieved by selective degradation of the HS chains. Membrane proteoglycans cooperate with integrins and other cell adhesion receptors to facilitate cell-ECM attachment, cell–cell interactions, and cell motility. HSPGs are also found in secretory vesicles, most notably serglycin, which plays a role in packaging granular contents and regulate various biological activities after secretion such as host defense, and wound repair [82].

4. HS AND CANCER

As mentioned previously, HSPGs modulate fundamental biological processes including inflammation, angiogenesis, cell migration, cell proliferation, cell adhesion, endocytosis, cellular matrix assembly and many more [120]. These processes are essential for tumor initiation and progression and alteration of the normal expression levels of HSPGs has often been described in tumors. The fast turnover of HS could be a strategy used by cells to have a rapid control over signaling not only in physiologic but also in pathologic conditions [134].

Cancer cells uniquely reprogram their cellular activities to support their rapid proliferation and migration and to counteract metabolic stress by increasing the levels of several glycolytic enzymes during cancer progression [135, 136]. One of the most studied, yet still not completely understood mechanisms involves remodeling of the ECM by HPSE.

HPSE is overexpressed in many tumors and the active form of the enzyme is released extracellularly (Figure 16) [137-139] where it cuts HS chains promoting the release of numerous bioactive molecules that were sequestered on HSPGs. Consequently, induced

peripheral angiogenesis activation and disruption of ECM and basement membrane homeostasis facilitate invasion [140]. Furthermore, elevated HPSE expression in myeloma cells stimulates sustained ERK phosphorylation that in turn drives matrix metalloproteinase 9 (MMP-9) expression [141] [142]. MMP-9 and other MMPs are thought to mediate Sdc-1 shedding increasing soluble HSPGs in the tumor micro-environment [2]. Indeed, experiments in HPSE-KO and -overexpressing mice showed co-regulation between HPSE and MMPs [143].

This strategy adopted by tumor cells ensures rapid tissue response as a fast-acting mechanism independent from *de novo* protein synthesis that meets their needs to promote tumor growth, angiogenesis, peripheral immune tolerance and formation of a metastatic niche [134]. Briefly, tumor cells can change the nature of the microenvironment and *vice versa* the microenvironment can affect how a tumor grows and spreads [134].

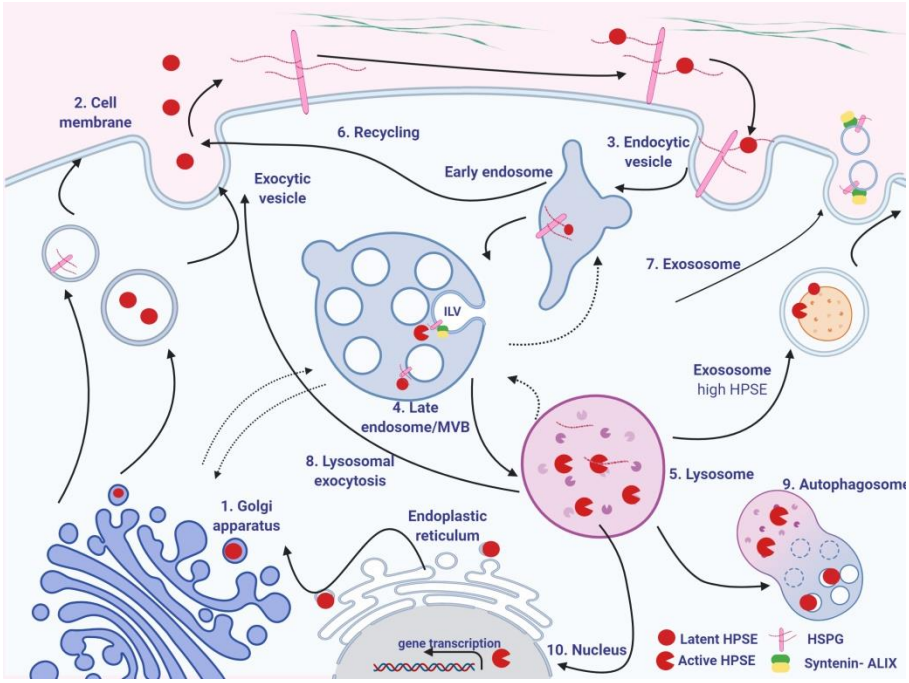

Figure 16. Schematic model of HPSE trafficking.

(1) In the Golgi apparatus HS chains are polymerized and preHPSE is processed to produce proHPSE by the elimination of the N-terminal signal peptide. (2) The newly biosynthesized HSPGs are then shifted to the cell membrane where they can interact with the proHPSE and the complex is rapidly internalized by endocytosis and then (4) accumulated in the late endosome. (5) Upon fusion of the late endosome with lysosome, proHPSE is activated and cleaves HS chains that are completely degraded by lysosomal hydrolases. (6) HPSE and HSPGs can be recycled to the cell surface from endosomes. It appears that active HPSE pursues other paths in the cells. (7) Trimming of HS from Sdcs by active HPSE present in late endosomes leads to formation of the Sdc-syntenin-ALIX complex [50]. Intraluminal vesicles (ILV) are then formed by the invagination of endosomal membranes, resulting in the formation of multivesicular bodies (MVBs). MVBs release ILVs as exosomes upon fusion with the cell membrane and deliver their cargo to recipient cells. In the presence of high levels of HPSE, the enzyme can be found on the surface of exosomes and modulates TME. (8) Lysosomal exocytosis has been observed in malignant cells. (9) HPSE also regulates autophagy by driving fusion of lysosomes with autophagosomes which degrade macromolecules into monomeric units. (10) Perinuclear lysosomal HPSE can also translocate into the nucleus and regulate gene transcription and cell differentiation. Taken from [134].

Given the extent of the biological processes involving HS, it would be impossible to draw up an exhaustive list of their functions in cancer. However, a number of examples will be reported with a focus on the three main tumorigenic processes: proliferation, angiogenesis and invasion. It should be noted that some GFs (e.g. FGF2) are upstream a variety of different cellular responses in that a clear distinction between their role in the three processes may be difficult.

4.1.HS in cancer cell proliferation

The binding interactions between HS and mitogenic GFs make HS an important player in proliferation. As summarized in figure 17, HSPGs bind both FGF2 and FGF receptors (FGFR1) forming a ternary complex to enhance downstream signaling via Janus kinase/ signal transducers and activators of transcription (JAK/STAT), phosphoinositide 3-kinase/ protein kinase B (PI3K/AKT), mitogen-activated protein kinases (MAPK), Ras homology (RhoA), or diacylglycerol/protein kinase C/calcium (DAG/PKC/Ca2+) [122].

A strategy that tumor cells adopt to increase proliferation is the upregulation of the normal expression levels of HSPGs [144]. For example, increasing expression level of glypican-1 and syndecan-2 (Sdc-2) was detected in colorectal cancer [145], while breast cancer was found to upregulate glypican-1 and Sdc-1 and 4 [146, 147].

HSPGs cleaved from the stromal cell surface and released in soluble form- for example, following the action of HPSE- can bind adjacent growth factors (FGFs) and increase extracellular signal-regulated kinase (ERK 1/2) phosphorylation, translocation to the nucleus and activation of transcription factors in breast cancer [148]. Soluble HSPGs and heparin promote differentiation and decrease proliferation through FGFR1 and ERK phosphorylation [149].

Moreover, HPSE can be found in the nuclear compartment where it would augment cell proliferation via its modulation of DNA topoisomerase I activity, an enzyme essential for DNA replication and gene transcription.

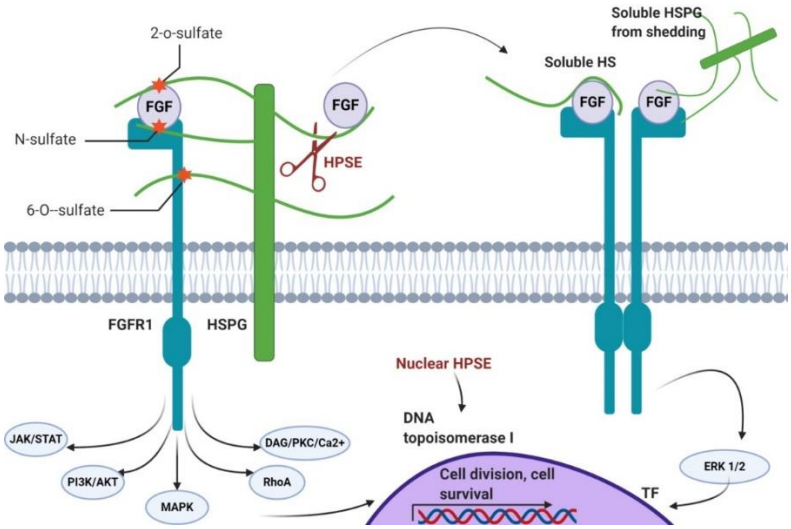

Figure 17. Schematic model of HS pathways in cancer proliferation.

HS cleaved from the stromal cell surface and released in soluble form can bind ligands including FGF via 2-O-sulfate on glucuronic acid and N-sulfate on glucosamine; and receptors including FGFR1 via 6-O-sulfate on glucosamine to enhance cancer cell signaling JAK/STAT, PI3K/AKT, MAPK, RhoA, or DAG/PKC/Ca2+; all converging into cellular activation and proliferation. Adapted from [122].

4.2. HS in tumor angiogenesis

In addition to HS implication on tumor initiation and proliferation, HS is also involved in ECM modifications priming the tumor micro-environment [2] for tumor spread and blood supply. Thus, as the tumor evolves, the stroma undergoes tissue remodeling under the action of enzymes able to modify the glycosidic chains of the ECM, i.e., glycosyltransferases, sulfotransferases, sulfatases, and HPSE [150].

HS also binds GFs with demonstrated roles in angiogenesis, including VEGF, FGF2, HGF (produced by stromal cells and tumor cells), PDGF-B (primarily produced by endothelial cells), TGF-b (often produced by tumor cells), TSP1, PF4 and endostatin [151-153]. Given that this section is only an overview of the implication of HS on the mechanism of angiogenesis, all the factors will not be listed below and I suggest the following review for further information [153].

The most abundant and best characterized isoforms of VEGF are VEGF121, VEGF165 and VEGF189 [154]. VEGF165, the predominant isoform, is the best studied in relation to heparin/HS binding [153] and its binding to endothelial cells is virtually completely dependent on HS. Indeed, digestion of HS with heparinases, that are bacterial HS-degrading enzymes, completely eliminates binding [155].

Binding of VEGF165, normally present as a homodimer, depends on both the domain organization of HS and specific sulfation. In fact, VEGF165 binding depends on all charged groups (carboxylate groups, N-, 2O- and 6O-sulfation), but N-sulfation and in particular 6O-sulfation are of most importance. Moreover, it has been suggested that a VEGF165 dimer

interacts simultaneously with two NS domains of the HS chain, which can be separated by a NA/NS domain [101] (Figure 18).

VEGFR2 is known to directly interact with heparin/HS, suggesting ternary complex formation between VEGF165, VEGFR2 and HS (Figure 18) [156], although one more component, neuropilin-1, is known to bind to VEGF165 and heparin, and could form a 4-component complex together with VEGFR2 [157].

Bioavailability of soluble VEGF is an important factor. For example, desulfation of HS by extracellular SULFs results in decreased interaction between HS and VEGF and consequent increase of bioavailable ligand. Indeed, SULFs are overexpressed in many tumors [158, 159]. On the contrary, aHS and heparin are known to suppress platelet activation through the AT domain activation which results in decreased release of VEGF [160]. Alteration of aHS distribution is therefore also involved in tumoral angiogenesis.

Other angiogenic factors have been described to be modulated by HS. FGF2 is a pleiotropic GF also implicated in angiogenesis [153]. We have seen previously that HS catalyzes the FGF2–FGFR1 interaction, but in the presence of high concentrations of released FGF2, dimerization and signaling can take place in the absence of cellular HS that is altered in tumors with high HPSE level [161]. Furthermore, it has been shown that perlecan at the surface of tumor cells and secreted into the ECM can bind ligand and adaptor proteins via its three HS chains located at the N-terminal and one C-terminal to enhance FGF signaling and tumor angiogenesis [162].

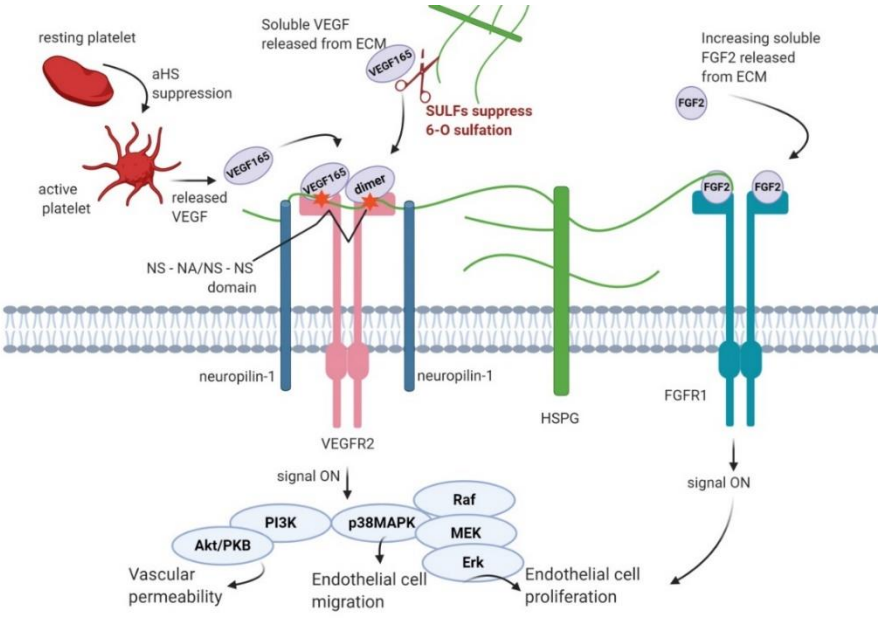

Figure 18. Schematic model of HS pathways in cancer angiogenesis.

HS interacts with both pro-angiogenic factors such as FGF2 and VEGF 165. HS binds to VEGF 165 dimer through two NS domains leading to signal activation. Elevated extracellular SULFs reduce HS sulfation and increases soluble VEGF ligands in the TME that will interact with adjacent receptors. aHS mediated platelet activation also increases available VEGF.

4.3.HS in cancer invasion

Aggressive tumor cell invasion requires the disruption of the invaded tissue through the breakdown of its basement membranes and ECM, namely, tissue remodeling. Upregulation of HPSE occurs in essentially all human tumors and is closely correlated with an invasive phenotype in experimental models and has been linked to worse outcomes in cancer patients [163]. Together HPSE, SULFs and MMPs activities disrupt the integrity of ECM by destructuring HS chains and their protein core thus increasing permeability for cell invasion and increasing soluble tumorigenic agents [164]. Thus, accumulating evidence indicates HPSE as a putative target for anticancer drug development. Indeed, HPSE silencing was shown to inhibit proliferation and invasion of ovarian cancer cells [165] while HPSE-neutralizing monoclonal antibodies block myeloma and lymphoma tumor growth [166].

Through GF binding, HSPGs also influence cell polarity, changes in morphology, namely cancer cell differentiation, during cancer progression. In this regard, the role of HS in regulating epithelial-to-mesenchymal transition (EMT) is noteworthy (Figure 19). Earlier in the introduction we have seen that EMT defines an indispensable process in metastatic progression in which epithelial cells lose cell-cell junctions and adhesions, undergo rearrangement of the cytoskeleton, and manifest a migratory phenotype. EMT has been implicated in the conversion of early-stage tumors to invasive malignancy, and its characteristic features include loss of E-cadherin expression, the translocation of β-catenin, and an increase in vimentin and Snail expression. EMT is triggered by the alterations in the components of ECM including HSPGs. For example, it has been shown in leukemia cells that 3-O sulfotransferase 3A is significantly downregulated and HS expression on cell-surface was also reduced in an EMT model [167]. Prostate cancer cells overexpressing SULF2 present increased EMT markers and Wnt signaling [168].

It is known that HS chains on Sdcs can bind matrix proteins to promote adhesion, maintenance of cell polarity and reduced cell invasiveness [169]. For example, Sdc-1 is implicated in the regulation of skin homeostasis and it is lost in squamous malignancies [170, 171]. Decreased expression or loss of Sdc-1 is also reported in colon, lung, liver, ovarian, cervical, head and neck cancers, as well as mesothelioma and myeloma where it disrupts HS signaling and promotes disease progression. This is not surprising given that HS binds GFs implicated in EMT, including HGF, VEGF and TGF-β [172].

Surface and soluble Sdc-1 have opposing actions on EMT signaling. It has been shown that Sdc-1 expression shifts from the tumor to the stroma during breast, lung, colon, and bladder cancer progression [173]. Both HSPGs, HPSE and SULFs can be upregulated during EMT, leading to enhanced HSPGs in the ECM that serve as a depot for EMT-promoting GFs [173].

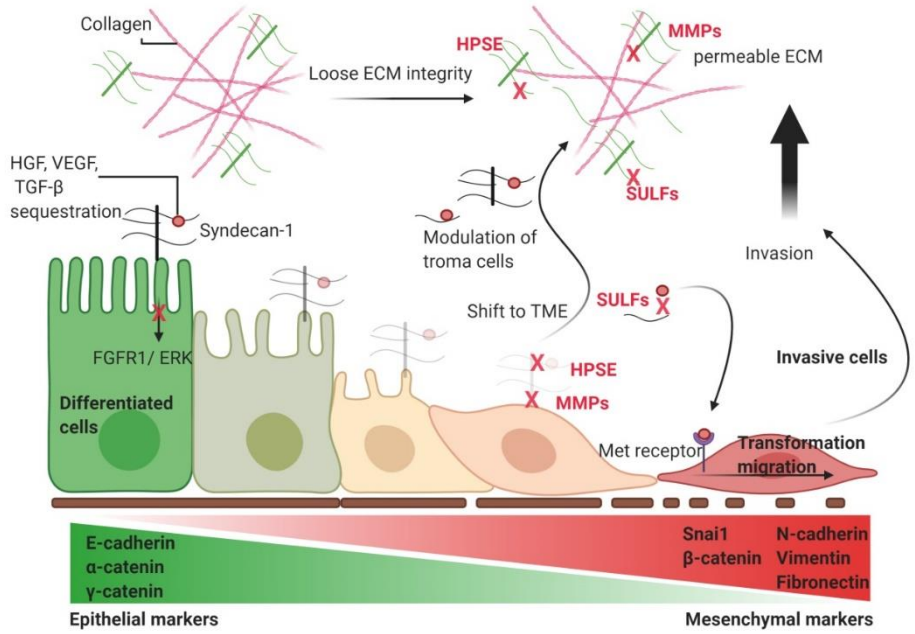

Figure 19. Schematic model of HS pathways in cancer invasion.

Sdc-1 is expressed on well differentiated cells, modulating GFs signaling. In normal conditions, intact ECM acts as a barrier to limit tissue remodeling. Upon HPSE, MMPs and SULFs upregulation- and shift to the ECM, basement membrane and ECM are degraded, increasing permeability to cells. As the tumor evolves, the stroma undergoes tissue remodeling: Sdc-1 is suppressed and available ligands modulate cell signaling by activating Met receptor and downstream RAS-RAF-MEK-ERK and STAT pathways. Consequent cellular proliferation, migration and transformation initiate the invasion process which is indeed the result of a complementary action of the tumor cell on TME and vice-versa.

Sdc-1 mediates HGF binding to its receptor MET that undergoes autophosphorylation and activation, resulting in the recruitment of various intracellular signaling proteins. For example, HGF-MET signaling leads to cell survival through PI3K-AKT while results in cellular migration through focal adhesion kinase. Moreover, MET activation also stimulates guanine nucleotide exchange factor Son of Sevenless via binding with SHC and GRB2, leading to the activation of RAS-RAF-MEK-ERK pathway, resulting in cell proliferation, cell motility and cell cycle progression. Finally, STAT-mediated MET signaling also results in the transformation and tubulogenesis [174].

Activation of HGF induced by Sdc-1was reported to enhance CD44 variant 6 expression that displays an additional sulfation site that could further promote GF signaling suggesting that HS modifications could be responsible for CD44 effects on cancer progression [175, 176]. However, contradictory CD44 involvement in progression and simultaneous loss of expression in certain cancer types- including endometrial and squamous cell cancers, was reported and illustrate the complex roles of this HSPG in tumor metastasis, many functions of which remains undefined. Nevertheless, all these studies are of high significance as they underline two major

points: first, the differentiation state of the cancer cells predicts survival; second, HS and HSPGs are among the key regulators of cancer differentiation states.

Tumor cell proliferation, tissue remodeling and angiogenesis thus constitute privileged targets to develop new diagnostic and therapeutic tools, in particular in EC.

5. AIM OF THE STUDY

So far, endometrial cancer (EC) is the 4th most common cancer in women in Switzerland with + 900 new cases/year and about +50 women/year in Geneva (data from HUG). To this date, the lack of early diagnosis of the invasive form of this disease results in recurrence in some patients. Due to the pleiotropic effect of aHS in many biological and pathological processes including early tumor initiation and metastatization, we thought that it would be interesting to explore HS in early grade EC.

We hypothesize that aHS expression is governed by tight physiological regulation to provide stability to mature, differentiated tissues and that its modifications allows limited physiological tissue remodeling. Cancer cells acquire the ability to bypass physiological checkpoints and invade tissues. We postulate that one of these checkpoints could be aHSPG expression and that suppression of aHSPG could render target tissues permissive to tumor invasion and tumor angiogenesis.

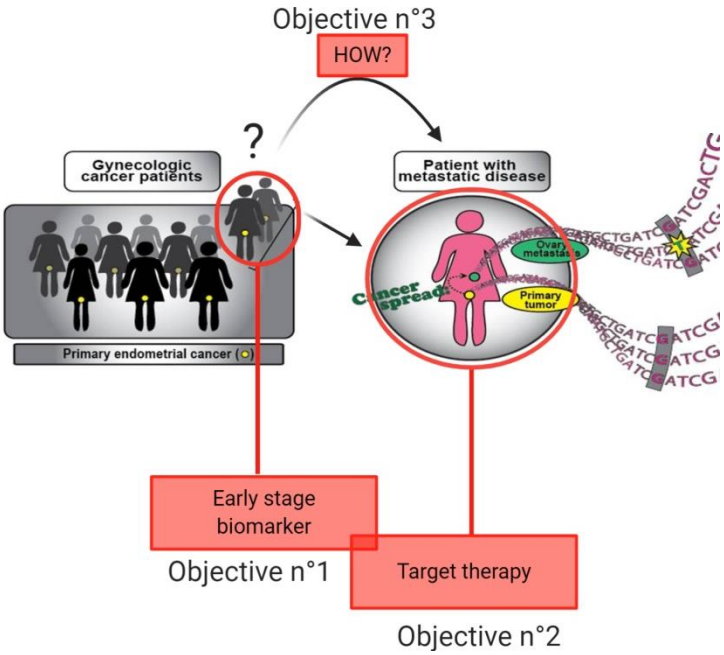

Figure 20. The 3 main objectives of this PhD thesis.

5.1.Evaluation of aHS expression as potential diagnosis and prognosis tool

The first aim of my PhD was to investigate if alteration of aHS expression could be a valuable signature of high-risk patients and a diagnostic tool to identify invasive form of EC at an early stage. To do so, we analyzed the presence of aHS in a series of histological sections from patients with EC Grade 1 with variable invasive characteristics to see if a particular pattern of expression could be attributed to invasiveness of the cancer.

The analysis was done into two different scenarios. We first analyzed aHS during physiological tissue remodeling- occurring during the estrus cycle, *vs* pathological tissue remodeling- in cancer. In parallel we evaluated aHS on both glandular and stromal compartments: separately, to investigate invasion and angiogenesis processes; together, to highlight the tumor-TME crosstalk. This analysis will permit to answer to these questions:

- Is aHS expression associated with pathological tissue remodeling in EC?
- Is aHS expression in tumor glands proportional to the degree of invasion in EC?
- Is aHS expression in capillaries of TME associated to angiogenesis in EC?

We then assessed if aHS suppression could be attributed to post-synthetic modifications by analyzing both HPSE and SULFs expression. Finally, the prognostic prediction from this cumulative analysis was confirmed with the clinical follow-up of the patients.

5.2.Evaluation of treatment with HS mimetics as potential therapeutic tool.

Today, cancer research focuses on inhibition of the main tumorigenic process that contributes to the initiation, growth, survival and spread of the tumor. In the first analysis on histological samples we observed that HS degradation was associated with invasive and pro-angiogenic features of EC. Thus, the second aim of my PhD was to target *in vitro* HS-degrading activity of HPSE to restore normal biological activities of tumor cells. In other words, if we manage to preserve endogenous aHS from degradation, could we reduce tumoral invasion and tumor-induced angiogenesis?

In this second part, I analyzed the anti-proliferative, anti-migratory, anti-invasive and anti-angiogenic effects of heparin and synthetic HS mimetics designed to compete with endogenous HS and inhibit HPSE activity. This analysis was performed in collaboration with IFREMER and Ronzoni Institute that provided us a panel of different HS mimetics with variable sulfation profile and structural modification in order to evaluate the best profile for anti-tumorigenic activity. Some of these HS mimetics are currently on clinical trials for other types of cancer and some are in patent proposal and could hereby be proposed as potential cancer treatment also for EC.

The purpose of this analysis was also to confirm the statement in the first analysis in which aHS reduction implicated in EC invasion and angiogenesis is mediated through post-synthetic modification of HS chains by HPSE.

5.3. Understanding the biosynthetic pathways implicated in aHS downregulation in invasive tumors.

The last aim of my PhD was to better characterize at mRNA level what makes the most invasive patients different from patients that will have a better prognosis and a milder invasion pattern. This analysis will highlight if a particular biosynthetic pathway is activated upon HS/HPSE/SULFs mediation and if other enzymatic modifications during biosynthesis of aHS of post synthetic cleavage of core proteins is responsible of aHS reduction in invasive tumor cases. We also aim at understanding how tumor signals reach over a thousand μm in distance to induce distant capillary proliferation on TME.

As well as for the first aim, we acted on two fronts. We first analyzed tumor compartments and TME independently and together case per case to highlight tumor-TME ligand/receptor crosstalk.

Finally, this analysis aimed to highlight differences between IG, BF and MELF patterns to characterize more this type of cancer.

Extensive Downregulation of AHS in Invasive forms of Endometrioid Carcinoma Grade 1

1. Summary

Endometrioid adenocarcinoma is the most frequent gynecologic cancer with a 5-year survival rate stagnant since 30 years despite active research. This cancer is characterized by 5 histological patterns of myometrial invasion: IG, BF, MELF, AL and AM, all categorized into grade 1. Patients with low grade EC have an overall good survival rate; however, 2.5 to 10% will demonstrate a more aggressive form of the tumor and will relapse. To this date, the diagnosis is not sufficient to early identify the patients with higher risks within Grade 1. In human uterus, aHS is present in vessel walls and the glandular epithelium but disappears during the implantation window allowing physiological tissue remodeling and leading to a permissive endometrium. We thus hypothesize that the tumor could use the same strategy to induce pathological tissue remodeling required for its propagation including invasion and angiogenesis. This assumption is supported by the fact that, in most cancers, aHS catabolic enzyme HPSE is elevated and shifted to an extracellular form modulating ECM HS and factor signaling. In this paper, we set out to evaluate the potential of aHS as early stage biomarker to identify aggressive endometrioid carcinoma. aHS and HPSE expression were analysed on 102 grade 1 endometrioid carcinoma cases tissue sections. Microvessel density and proliferation index were evaluated respectively with CD-31 and dual immunohistochemical staining of Nestin and Ki-67. Tumour glands were shown to strongly increase by 110.1% HPSE expression and reduce aHS by 45.5%. This downregulation interestingly correlates with more invasive histological phenotypes, IG and MELF. Capillaries at tumour front were also negative for aHS. In invasive tumor fronts of MELF, capillary proliferation was increased up to 11.1%, compared to 1.9% in control cases. The vessel density also increased by 8.33% suggesting a tumour-induced angiogenesis. Here we demonstrated that aHS down regulation correlates with vessels proliferation and glandular invasiveness. IG and MELF patterns have distinct molecular characteristics supporting more aggressive features. Combination of histological and aHS evaluations could be useful to re-evaluate patients with potential worse prognosis.

2. Introduction

Endometrial adenocarcinoma is mostly a disease of postmenopausal women with a sharp rise in incidence during the last decade, attributable to increased rates of obesity which may lead to a rise in the proportion of premenopausal cases [177, 178]. Type 1 adenocarcinoma develops through an estrogen-driven “adenoma carcinoma” pathway from atypical endometrial hyperplasia/endometrioid intraepithelial neoplasia and leads in some cases to the development of invasive adenocarcinoma [179]. The majority of low-stage Grade 1 endometrial

adenocarcinoma have a favorable prognosis [180]. However, a minority will demonstrate a more aggressive clinical course despite combined treatments of chemotherapy and total hysterectomy [67]. At the moment, there is no effective screening test for early detection to distinguish which patients are going to evolve into a metastatic disease [181].

Aggressive tumor cell invasion requires the disruption of the invaded tissue through the breakdown of its basement membranes and ECM, namely tissue remodeling of stroma, under the action of enzymes that modify the glycosidic chains of the ECM [139, 182]. In addition, tumor cells promote angiogenesis, a process crucial to tumor development and metastasization [183]. Tissue remodelling and angiogenesis constitute privileged targets to develop new diagnostic and therapeutic tools, particularly in EC.

As already explained in the introduction, Heparan sulfate proteoglycans (HSPG) are ubiquitously distributed on the surface of animal cells and in the ECM [184]. HS has thus numerous important biological activities including inflammation, tissue remodeling, angiogenesis and cell migration through interaction with a vast array of HS- binding proteins [185]. Anticoagulant HS (aHS) is a subset of HS chains that specifically binds and activates the serine protease inhibitor AT-III [186], containing a 3-O-sulfated glucosamine within a pentasaccharide motif that constitutes the AT binding site in both heparin and aHS. aHS is present in the basement membranes of endothelial cells where it is thought to confer an antithrombotic tone to vascular walls [187, 188]. However, aHS has also been found in various compartments of the genital tract with variable intensity during the cycle. It has been found that aHS in ovarian granulosa cells is at its maximum shortly before ovulation then it is downregulated at the onset of follicular development to reappear in luteal cells and in capillary endothelial cells of the mature corpus luteum [187, 189].

Modulation of extracellular aHS can occur by modification of its biosynthesis or by selective enzymatic inactivation. At the biosynthetic level, HS-3-O-sulfotransferases (3-OSTs) are the key enzymes responsible for 3-O-sulfation of HS and 3-OST-1 catalyses the rate-limiting step in the synthesis of aHS [190]. Alternatively, post-synthetic alteration of HS in the extracellular environment is catalyzed by two sets of enzymes, heparanase (HPSE) and sulfatases [191].. In cancer, HPSE level is increased, especially the extracellular form, thus modulating several cancer-related functions, including GF signaling and ECM remodeling [139]. The activity of HPSE has a triple effect: it destabilizes matrix cohesion and thus facilitates cell migration, invasion and the formation of new blood vessels; it releases cytokines and GFs (VEGF, FGFs, etc.) associated with the matrix, which will then induce numerous biological processes such as cell proliferation and neovascularization [3]; it catalyzes the release of fragments of HS having a structure of the NS domain type, biologically active, capable of promoting the activity of these GFs[192, 193].

We postulate that aHS downregulation through HPSE's degradation facilitates tissue remodeling and invasion in EC. The aim of this study is to evaluate if downregulation of aHS expression could be a valuable biomarker to identify aggressive endometrioid carcinoma at early stage, in order to diagnose patients with high risk of recurrence and death.

We have evaluated how aHS and HPSE contribute to the invasiveness of endometrial adenocarcinoma of grade 1 in a group of 102 cases subdivided in 4 histotypes. We have first determined the physiological aHS and HPSE expression pattern in the normal uterus in groups of 20 cases at each stage of the oestrus cycle. We made a full characterization of aHS and HPSE in endometrial glands and in blood and lymphatic vessels of the endometrium. Using the normal pattern as reference, we have then characterized aHS and HPSE expression in the total group of endometrioid carcinoma grade 1, showing markedly different patterns for both aHS and HPSE in the tumor and in its microenvironment in the myometrium. This study is supported by a deep analysis of endometrial vascular density and proliferation during oestrus cycle and cancer. Classification of the cases according to their histotypes allowed to distinguish cases with maximum differences in aHS in the TME in the two histotypes described as most invasive. Identification of such cases could allow offering additional treatment and surveillance. The data obtained in this study will enable us to evaluate the prognostic potential of aHS as modulator of tumor cell invasion and angiogenesis at the endometrium-myometrium interface.

3. RESULTS

The data obtained for the groups with normal uterus constitute the reference values for the parameters measured in the cancer groups, they are presented first and show the effects of the estrous cycle on uterine aHS and HPSE in endometrial glands and in endometrial stromal vessels.

The tumor cases have been analyzed for aHS and HPSE in the tumor glands and in the adjacent myometrium, constituting the TME [2]. The microvessel density (MVD) and proliferation (MVP) were recorded in the TME and the aHS signal in microvessels evaluated in the different tumor histotypes. The results are presented in parallel for the normal uterus and for the uterus with endometrioid adenocarcinoma Grade 1.

1. Characterization of aHS and HPSE in the glandular endometrial epithelium during physiological and pathological tissue remodeling.

1.1. aHS and HPSE expression in normal glands of the cycling endometrium.

The normal uterus is formed by the endometrium and the myometrium. The endometrium is composed of endometrial epithelial glands and of vascularized stroma with an upper layer close to the lumen of the uterus constituting the functional zone while the lower layer, in contact with the myometrium is called the basal zone. The functional zone of the endometrium is renewed at each estrous cycle and matures to be ready to support embryo implantation and development, while the basal zone constitutes the feeder layer that contains dividing cells that will produce the functional layer at each cycle. The myometrium is formed of smooth muscle cells with an abundant vasculature of blood and lymphatic capillaries, the section adjacent to the endometrium is called the superficial myometrium and the lower part the basal myometrium that contains large arteries. The different zones analyzed during the cycling endometrium are represented in the Figure 21A.

In endometrium, aHS and HPSE are present in the basal membrane and the luminal part of glands, respectively with variable intensity during the cycle. aHS is present during the proliferative phase at high intensity but shortly after the LH peak, in secretory phase, aHS is downregulated in epithelial cells of the functional zone of the endometrium (Figure 21 B). Indeed, functional glands have an average intensity for aHS of 298.6 (±6.5), 253.3 (±54.2) and 166.3 (±58.1) in proliferative cases (n=21), early secretory cases (n=15) and secretory cases (n=20), respectively (Figure 21C). The distribution of intensity labelling was also analyzed in functional glands of each estrus phase (Figure 21D). Our results show that 100% of proliferative cases (n=21) displayed high aHS intensity labelling (score 200≤300). This percentage decreases to 60% in early secretory cases and reaches only 10% in secretory cases where we observe a majority of medium intensity labelling for aHS (67% of 100≤200 score). These result suggest that, immediately after LH release, glands of the functional layer of the endometrium repress aHS while the endometrium undergo physiological tissue remodeling leading to the implantation window, a receptive time frame. Changes in aHS expression occur immediately after LH release, upstream of the receptive phase and therefore suggest a causal link with tissue receptiveness and tissue remodeling.

However, our results show that all basal endometrial glands at the myometrium interface are positive to aHS and display permanent high intensity of labelling when there is no physiological tissue remodeling (Figure 21B, C). Furthermore, 100% of all physiological cases display high aHS intensity labelling (score 200≤300) without distinction of the estrus phase (Figure 21 D). The basal layer of the endometrium is known to display stable phenotype across the cycle suggesting very few or no response to fluctuating hormones.

On the other hand, the signal intensity of HPSE is higher in the proliferative endometrium and lower in secretory phase of the functional endometrium (Figure 21B). Indeed, functional glands have an average intensity for HPSE of 208.3 (±73.9), 112.0 (±41.6) and 120.0 (±87.9) in proliferative cases (n=21), early secretory cases (n=15) and secretory cases (n=20), respectively (Figure 21C). In addition, the analysis of HPSE intensity distribution in functional glands revealed a majority of week intensity within the total physiological cases (n=56). HPSE expression exhibits a marked decrease from proliferative to secretory phase, quickly after LH release with low signal (0<100) representing 14% in proliferative phase, 73% in early secretory phase and 60% in secretory phase (Figure 21D).

In the basal layer however, glands exhibit a majority of week HPSE intensity labelling (Figure 21D) without significant modification during the cycle (Figure 21C) confirming the stable nature of the tissue.

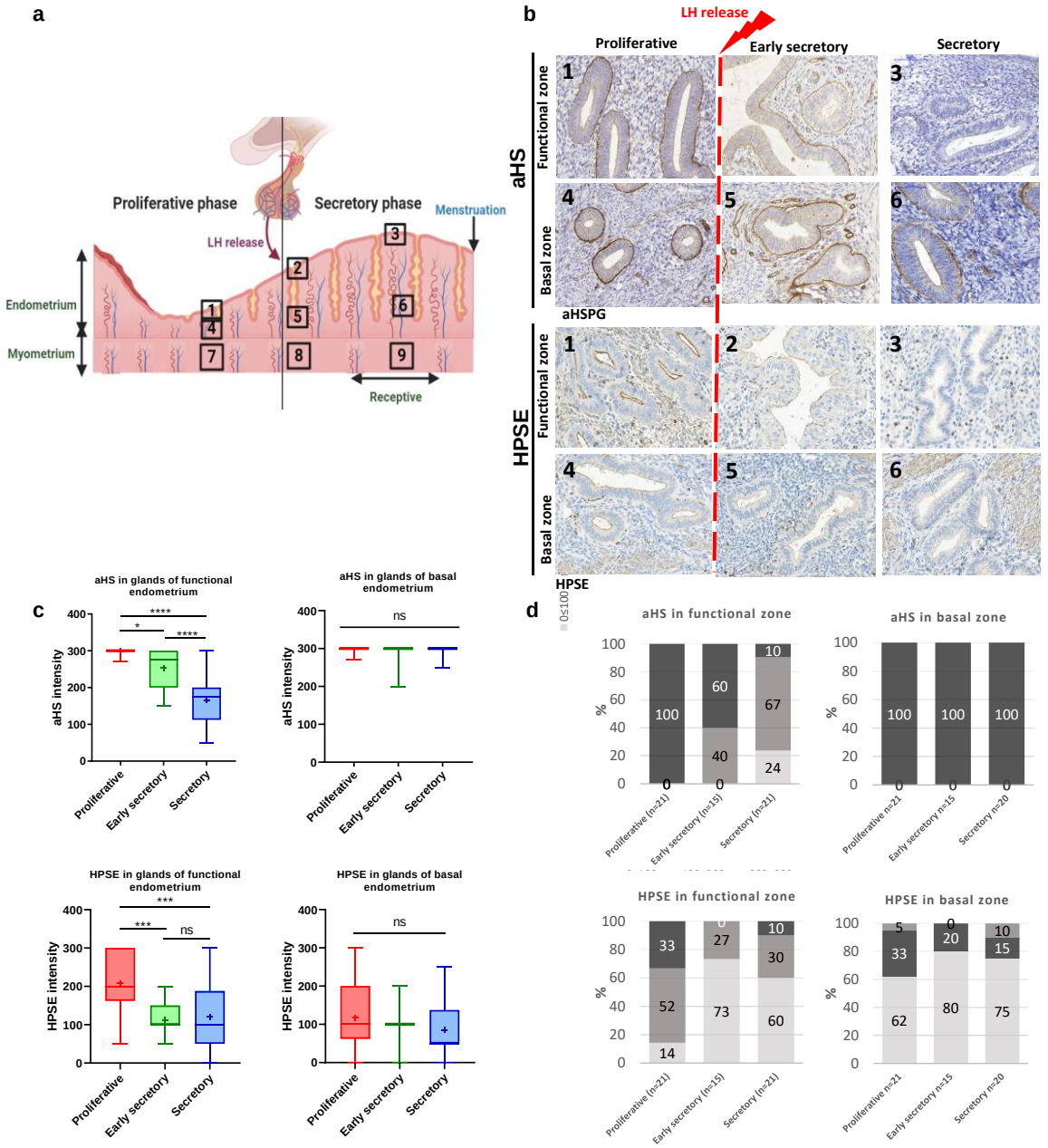

Figure 21. aHS and HPSE expression analysis in glands during estrus cycle.

a: Schematic representation of the different layers of the endometrium during the estrus cycle with 1,2,3 representing the functional zone; 4,5,6 representing basal zone and 7,8,9 representing the superficial myometrium of proliferative, early secretory and secretory respectively. **b:** Images showing the labeling for aHS expression (top) and the immunostaining for HPSE expression ((bottom) in the functional and basal layers of human endometrium during the three phases of the cycle. **c:** Quantification of aHS and HPSE intensity labeling. aHS and HPSE both decrease in the endometrial glands of the functional zone during the estrous cycle. In the basal zone of the endometrium, aHS is elevated and HPSE is low and they remain stable during the cycle *, p-value≤0.05; ***, p-value≤0.001; ****, p-value≤0.0001. **d:** aHS and HPSE intensity distribution analysis.

1.1. aHS and HPSE expression in tumor glands of endometrioid adenocarcinoma Grade 1.

In endometrioid adenocarcinoma grade 1, tumor glands constitute most of the tumor, with little stroma in between. They invade the adjacent myometrium that forms, the TME. aHS labelling analysis was restricted to the tumor glands at the invasive tumor front and was compared to the respective region of the basal layer in physiological cases. Our results show a highly significant decrease of aHS intensity in cancer compared to controls (Figure 22 A, B). We measured an average intensity of 159.7 (±92.6) in cancer cases (n=72) compared to 293.2 (±20.6) in physiological cases (n=56) (Figure 22B). There is an average decrease of 45.5 % aHS labelling intensity in tumor glands compared to controls. Only 28.5% of endometrioid adenocarcinoma cases (n=72) displayed high aHS labelling intensity in the glands (score 200≤300) to the benefit of other classes: 100≤200 (29.1%) and 0≤100 (42.4%) (Figure 22C). The intensity of aHS is lower with a majority of weak intensity reflecting a decline in expression within tumor cases. During pathological tissue remodeling occurring at the tumor front aHS is repressed and could be thus implicated in tissue permissiveness to tumor gland invasion.

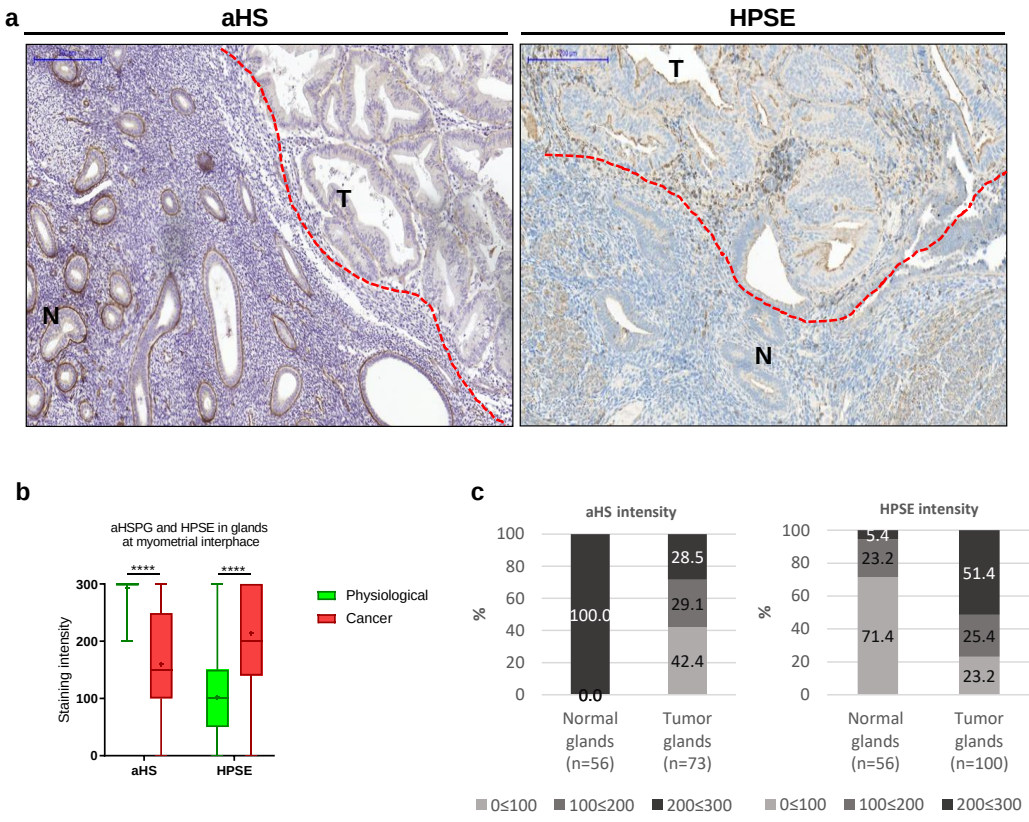

Figure 22. aHS and HPSE expression analysis in glands of EC grade 1.

A: Images showing the labeling for aHS expression (left) with AT-b and the immunostaining for HPSE expression (right) of non-cancerous glands (N) and tumor glands (T) in human endometrium sections. B: Quantification of aHS and HPSE intensity labelling in physiological (n=56) and cancer cases (n=100). In endometrioid cancer, the tumor glands have decreased aHS and increased HPSE labelling, a pattern distinct from that of normal endometrium. ****, p-value≤0.0001. C: aHS and HPSE intensity distribution analysis in physiological and cancer cases.

In contrast to aHS, HPSE increased significantly in cancer glands by 110.1% compared to normal glands (Figure 22A, B). We measured an average intensity of 214.1 (±83.8) in total cancer cases (n=100) compared to 101.9 (±70.6) in total physiological cases (n=56) (Figure 22B). HPSE analysis revealed in tumor cases a majority of tumor glands labeling intensity of 51.4% high (200<300), 25.4% medium (100<200) and 23.2% low (0<100) signal (Figure 22C). These data showed that the decrease of aHS at glands of the tumor front coincides with the increase of its catabolic enzyme HPSE expressed by tumor cells and thus HPSE might be involved in modulation of aHS in cancer.

1.2.Correlation of glandular HPSE and aHS expressions with subtypes of myometrial invasion in endometrioid adenocarcinoma Grade 1.

At the first stage of the endometrioid adenocarcinoma gathered in grade 1, different patterns of myometrial invasion are already distinguishable according to histology (Figure 23A). These patterns reflect the different approaches used by the glands to invade the surrounding tissue and are considered to have different invasive potency. We thus are interested in further analyzing the expression of our markers individually, according to the subtypes of myometrial invasion in order to see if aHS downregulation is associated with highest invasive patterns.

The analysis shows that the majority of adenocarcinoma cases of our cohort had an infiltrating gland pattern, n=37 (36.27% of cases) followed by the broad front pattern, n=36 (35.29%), MELF, n=17 (16.67%) and finally (11.76%) of adenomyosis like n=12 in a total of 102 cases.

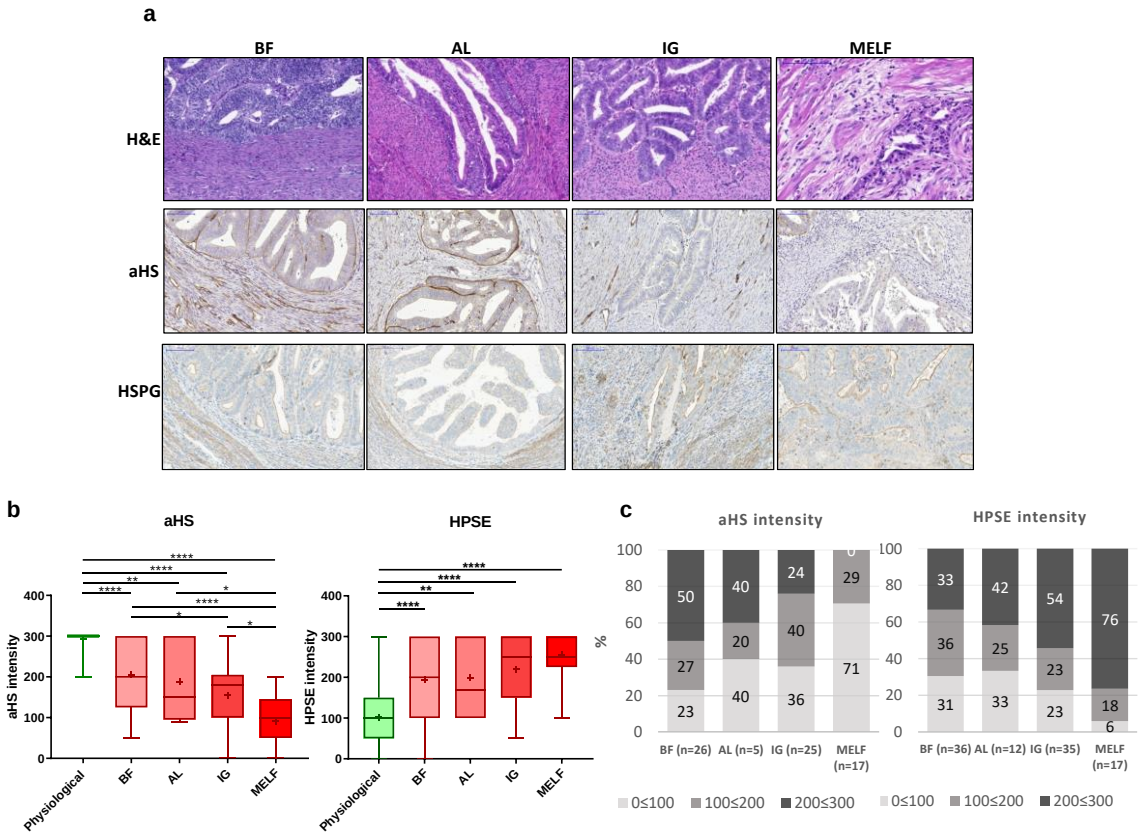

Figure 23. aHSPG and HPSE expression analysis in tumor glands according to the different patterns of myometrial invasion.

A: Histological structure of the different patterns of myometrial invasion (top) of aHS expression (middle) and HPSE expression ((bottom) of tumor glands. B: Quantification of aHS and HPSE intensity labeling in physiological (n=56) and BF (n=36), AL (n=12), IG (n=35) and MELF (n=17) patterns. In endometrioid cancer subtypes, aHS is decreased and HPSE is increased in function of the invasiveness of the subtypes, the most invasive MELF type has the biggest decrease in aHS and the biggest increase in HPSE compared to normal glands.*, p-value≤0.05; **, p-value≤0.01; ***, p-value≤0.001; ****, p-value≤0.0001. C: aHS and HPSE intensity distribution analysis in the different patterns of myometrial invasion.

aHS labeling intensity analysis revealed that all subtypes of myometrial invasion show significant downregulation of expression compared to physiological cases (Figure 23B). Comparison between subtypes shows significant differences between less invasive forms BF and AL and the most invasive IG and MELF (Figures 23A, B). We measured an average intensity labelling of 205.1 (±87.9), 188.0 (±104.7), 155.0 (±90.1) and 91.5 (±55.7) in BF (n=25), AL (n=5), IG (n=25) and MELF (n=17) cases (Figure 3B), respectively. The “bulky pushing” types (BF and AL) displayed a predominance of high intensity labeling level (200≤300): 50% in BF, 40% in AL while “widely dispersed” types, IG and MELF, displayed a majority of medium and weak intensity labeling, decreasing the high score (200≤300) to 24% in IG and 0% in MELF (Figure 23C). These data show that in the two most severe subtypes of myometrial invasion (IG and MELF) where the glands invade more easily the myometrium

with a permissive stromal reaction, downregulation of aHS within tumor epithelial cells is more relevant. Decrease of aHS correlates thus with tissue permissiveness and tumor invasion.

aHS catabolic enzyme HPSE showed a mirror intensity labelling compared to aHS in the different myometrial invasion types. We measured an average intensity labelling of 194.2 (±86.9), 198.3 (±93.9), 219.7 (±83.2) and 255.9 (±55.6) in BF cases (n=36), AL cases (n=12), IG cases (n=35) and MELF cases (n=17) respectively (Figure 3B). No significant difference of average intensity labelling was observable between the subtypes (Figure 23A). A significant increase of HPSE intensity labelling was noticed in all invasive patterns compared to physiological cases (Figure 23B). HPSE labeling intensity displayed the same pattern of expression in all subtypes of myometrial invasion (Figure 23A, B), and HPSE is thus overexpressed in all tumor subtypes. The distribution of labelling intensity, however, allows us to analyze more deeply the differences between the subtypes (Figure 23C). Graduate changes occur from the histologically less invasive BF and AL patterns to the most invasive IG and MELF patterns. Indeed, while BF has equal proportions of week, medium and strong intensity, AL shows slight predominance of strong intensity with 42% of 200≤300. The gap is widening with IG and MELF with a majority of high intensity labeling level of 54% and 76%, respectively (Figure 23C). HPSE is thus mostly overexpressed in invasive tumor cases where the lowest intensity of its aHS substrate is seen.

2. Characterization of endometrial vascularization during physiological and pathological tissue remodeling.

2.1.Quantification of blood and lymphatic vessel density.

2.1.1. Blood and lymphatic vessel density during the estrus cycle

Physiological tissue remodeling of the endometrial stroma was then explored. As labelling we used platelet endothelial cell adhesion molecule-1 (PECAM-1), also known as CD31, that will highlight both vascular and lymphatic vessels. It is the most sensitive and specific endothelial marker in paraffin sections and stains small as well as large vessels. To discriminate blood from lymphatic vessels, we used a second labelling, D2-40 which stains only lymphatic vessels. Blood and lymphatic vessels were counted in proliferative phase, early secretory and secretory phases of the estrus cycle.

The functional endometrium is a layer where physiological tissue remodeling occurs during the estrous cycle. However, the number of blood (CD31+) and lymphatic (D2-40+) vessels do not vary significantly during the cycle. The vessels were counted in functional endometrium with a mean of 40.39 (±21.09) CD31+ and 4.78 (± 3.14) D2-40+ vessels in proliferative stage, 29.28 (±14.76) CD31+ and 3.98 (± 3.11) D2-40+ vessels in early secretory stage and 35.91 (±12.79) CD31+ and 3.28 (± 2.98) D2-40+ vessels in secretory stage (Figure 24A).

In the basal endometrium, the stability of the stroma during the cycle also translates with stable number of vessels, with a mean of 50.24 (±23.06) CD31+ and 8.21 (±4.68) D2-40+ vessels in proliferative stage, 41.33 (±22.83) CD31+ and 7.46 (±3.01) D2-40+ vessels in early secretory stage and 44.76 (±15.38) CD31+ and 8.44 (±3.89) D2-40+ vessels in secretory stage (Figure 24A).

The superficial myometrium adjacent to the basal layer of the endometrium was also analyzed for comparison with the myometrium adjacent to the tumor. We noticed a little decrease of CD31+ vessels during the secretory phase. A mean of 75.8 (±43.12) CD31+ and 5.07 (±2.89) D2-40+ cells in proliferative stage, 55.99 (±19.47) CD31+ and 4.76 (±2.14) D2-40+ cells in early secretory stage and 52.37 (±23.91) CD31+ and 5.63 (±3.39) D2-40+ cells in secretory stage were counted in the basal layer (Figure 24A).

The stability in the number of blood and lymphatic vessels in the functional zone of the endometrium that develops from the basal layer during the cycle suggests that elongation of existing vessels is the major mechanism by which endometrial angiogenesis occurs in proliferative phase during the cycle.

2.1.2. Blood and lymphatic vessel density in TME of endometrioid adenocarcinoma Grade 1

Tissue remodeling in the TME such as angiogenesis and lymph angiogenesis has an essential role in the formation of a new vascular network to supply tumor cells with nutrients, oxygen, immune cells, and also to remove waste products [194]. Analysis of cancer cases gave interesting outputs. The numbers of blood and lymphatic vessels in the tumor's invasive front were increased by 8.33% and 122.05%, respectively, due to tumor neo-vasculogenesis compared to the normal cases, in which capillary and lymphatic vessels density remain stable during the cycle. Indeed, mean values of 66.22 (±24.33) CD31+ and 11.50 (±8.76) D2-40+ vessels at the tumor front were counted compared to 61.13 (±31.67) CD31+ and 5.17 (±2.85) D2-40+ vessels in superficial myometrium of physiological cases (Figure 24B).

The number of blood and lymphatic vessels did not significantly vary between the different patterns of myometrial invasion (Figure 24C), with CD31+ vessels counts of 69.09 (±21.3), 60.13 (±27.24) and 72.30 (±23.58) in the myometrium adjacent to the tumor, the TME, for BF, IG and MELF cases, respectively (Figure 4C). D2-40+ vessels were also counted as 15.04 (±11.97), 7.85 (±4.13) and 12.08 (±5.49) in the TME of BF, IG and MELF cases, respectively and significant increase in the number of lymphatic vessels in the TME was observed in BF and MELF histotypes, as compared to normal superficial myometrium (Figure 24C).

The number of blood and lymphatic vessels inside the tumor is significantly lower compared to the tumor front, with a mean of D2-40+ vessels of 4.31 (±9.82) inside the tumor compared to 11.50 (±8.76) at tumor front, respectively, corresponding to a decrease of 63.87% (Figure 24C). Also, a mean of CD31+ vessels of 12.35 (±6.19) inside the tumor compared to 66.22 (±24.34) at tumor front was detected corresponding to an 81.35% decrease. This phenomenon can be explained by the lack of stroma between glands in the tumor compartment due to very tight packaging of tumor glands leaving little stroma space for vessels.

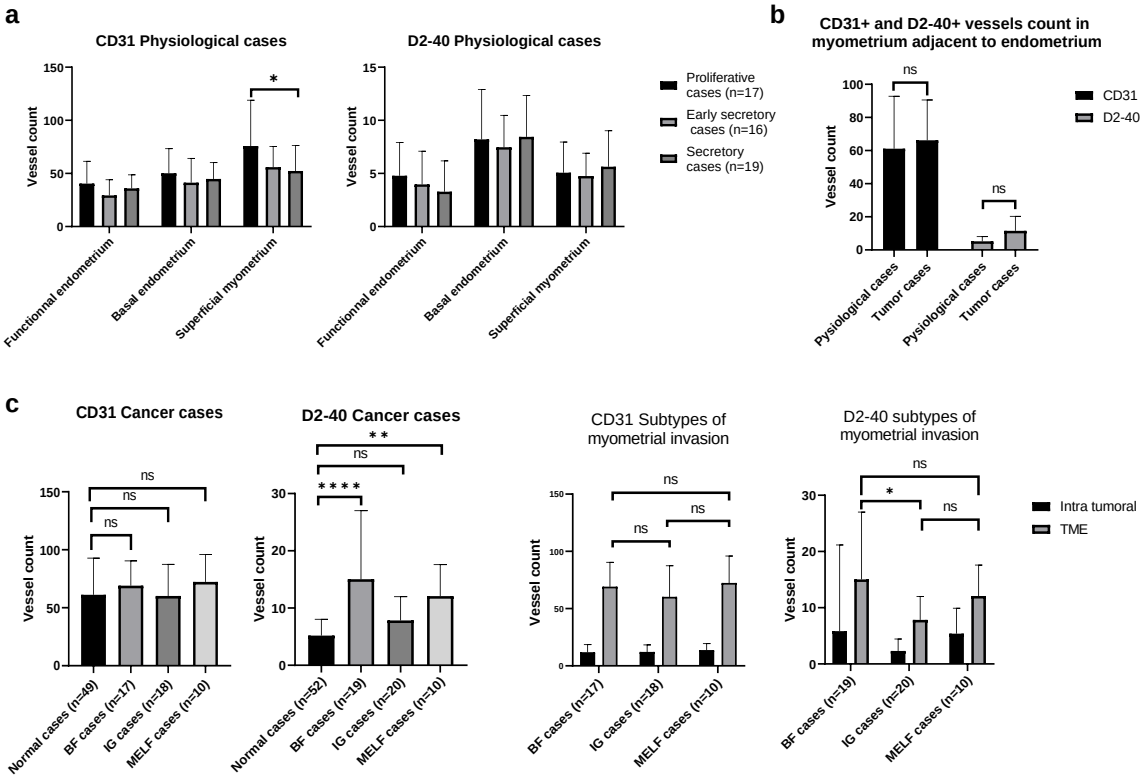

Figure 24. Quantification of CD-31+ endothelial and C2-40+ lymphatic vessel density.

A: In the normal uterus, blood and lymphatic vessels form a stable vasculature in the myometrium and the endometrium, with no variation in number during the estrus cycle. *, p-value≤0.05. B: In endometrioid cancer, in the superficial myometrium, constituting the tumor microenvironment TME, the microvessel density is similar between cancer and normal endometrium, for blood and lymphatic vessels with only a slight increase. C: In the TME of endometrioid cancer subtypes, the microvessel density is similar in the different subtypes for blood vessels while lymphatic vessels density was increased in BF and MELF cases. *, p-value≤0.05; **, p-value≤0.01; ****, p-value≤0.0001.

1.1.Quantification of blood and lymphatic vessel proliferation.

1.1.1. Blood and lymphatic vessels proliferation during estrus cycle

Angiogenesis in the human uterus is required to support the reconstruction and growth of endometrium after the menstrual period and to provide a vascularized, receptive endometrium for implantation and placentation three weeks later [195]. Physiological angiogenesis was further characterized and we measured a second parameter: endothelial cell proliferation within capillaries at the superficial myometrium. MIB-1 is a cell proliferation marker that recognizes the Ki-67 nuclear protein, which is associated with cell proliferation and is found throughout the cell cycle (G1, S, G2, and M phases) but not in resting (G0) cells. Nestin, on the other hand, is a type-IV intermediate filament (IF) expressed in endothelial cells. Only Nestin+ vessel with at least one MIB-1+ nucleus was considered as proliferating (Figure 25A). We have counted 2.07% (±1.7) of capillaries that are in proliferation among total capillaries in the proliferative phase. Positive Nestin/Mib1 signal was seen in 1.24% (±1.2) capillaries of the early secretory and in 2.37% (±2.1) capillaries of the secretory stages (Figure 25B). These results show that

there is no significant change of blood vessels proliferation between phases of the estrus cycle and the proliferation rate inside the vessel of physiological endometrium is low.

1.1.2. Blood and lymphatic vessels proliferation in TME of endometrioid adenocarcinoma Grade 1

Analysis of cancer cases showed that proliferating capillaries are significantly increased in the tumor compared to control cases. 6.46% (±8.1) of total capillaries in superficial myometrium adjacent to tumor front were found to be proliferating compared to 1.95% (±2.3) in normal endometrium (Figure 25C).

Blood vessels proliferation doubled in BF and IG patterns with an average of Nestin+/Mib1+ capillaries of 4.46% (±3.4) in BF and 4.46% (±5.2) in IG compared to an average of 1.95% (±2.3) in physiological cases (Figure 25D). In MELF pattern, a 6-fold increase in capillaries proliferation with an average of 11.09% (±12.3) was observed compared to control cases (Figure 25D). It can be derived that pathological tissue remodeling in the TME is characterized by an increase in endothelial cell proliferation inside the vessels. This proliferation is more relevant in the most aggressive histological myometrial invasion MELF were a desmoplastic reaction and an EMT is observable, conditions favorable to metastatization.

Increased MVP was significantly correlated with negative aHS status and with higher histological invasiveness. At early grade, EC has deregulated endothelial cell proliferation, but not increased MVP suggesting that in tumor cases, the angiogenesis by elongation is enhanced could support later sprouting angiogenesis which corresponds to the growth of new capillary vessels out of preexisting ones.

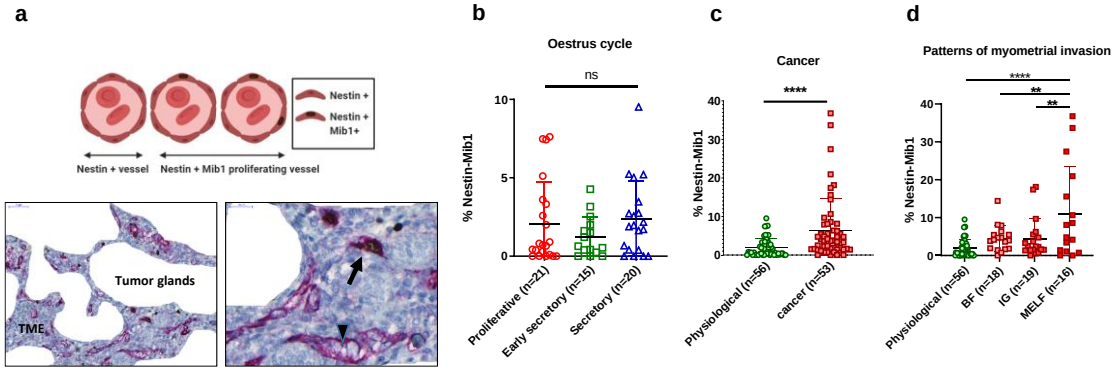

Figure 25. Microvessel proliferation (MVP) analysis.

A: Immunostaining of capillaries with Nestin (in pink) and endothelial cell proliferation with Ki-67 (in brown with arrow). Only Nestin+Mib1+ vessels are considered as proliferating capillaries ((arrow) and Nestin+ vessels (arrow head) was quantified as total number of capillaries. B: Quantification of Nestin+Mib1+ vessels in superficial myometrium during the three phases of the cycle. In the normal endometrium, microvessel proliferation in the endometrial stroma is stable during the cycle for blood and lymphatic vessels. C: MVP analysis in superficial myometrium of physiological and tumor cases. In the TME, the MVP is increased with distinct cases showing highly increased percentage of proliferating vessels. ****, p-value≤0.0001. D: Quantification of proliferating vessels in superficial myometrium of physiological (green) and each pattern of cancer invasion (red). Microvessel proliferation is increased mostly in the highly invasive subtype MELF with a 5-fold increase in percentage of proliferative vessels. **, p-value≤0.01; ****, p-value≤0.0001.

1.1.aHS expression analysis in vessels of superficial myometrium and TME during physiological and pathological tissue remodeling.

1.1.1. aHS expression in superficial myometrium and distance between glands front and the 1rst labelled capillary

In normal endometrium, capillaries are labelled for aHS in the functional and basal zone as well as inside the underlying myometrium. This labelling does not vary during the estrous cycle as shown for secretory endometrium (Fig 26). aHS is present in endothelial cells basement membranes where it displays an antithrombotic function [187]. aHS labelling with fluorescent AT-488 revealed that in 100% of the normal endometrium cases, capillaries in basal zone stroma of the endometrium and at the myometrium interface were strongly positive (Figure 26B) andthis labeling is constant during the cycle. The distance between normal glands at the myometrial interface and the first capillary labelled in the adjacent myometrium was almost imperceptible, ±10 to 30µm in all physiological cases without significant differences (Figure 26A). We have measured an average of 17.5 (±5.7) µm, 17.9 (±3.8) µm and 19.2 (±4.6) µm in total proliferative cases (n=22), early secretory cases (n=15) and secretory cases (n=20), respectively. We can conclude that the physiological tissue remodeling occurring during the estrus cycle does not affect the strong expression of aHS in capillaries in the myometrium, and the number of these vessels remains stable with low proliferation rate.

1.1.2. Pattern of aHS expression on myometrial vessels at the tumor front according to histological subtypes

The previous results show that labeling of aHS in capillaries is constant during physiological tissue remodeling, and the number of vessels remains constant during the estrus cycle. This suggests that aHS expression could be a marker of tissue integrity. Interestingly, in human adenocarcinoma cases, results show that aHS downregulation was not limited to the tumor but occurred also in the TME. Capillaries coming into the tumor did not express aHS as well as capillaries in the invasive tumor front in most of the cases (Figure 26B).

The distance from gland at the tumor front to the first labeled capillary in the adjacent TME revealed interesting output to understand the behavior of the tumor in its environment. In cancer, the distance between the first labelled capillary and the endometrial glands of tumor front increased from tens of micrometers with an average of 18.2 (±4.8) µm in normal cases to hundreds of um in tumor cases with an average of 388.3 (±384.8) µm (Figure 26B). By observing the distribution of distances, only 53% of cancer cases exhibited a short distance (0≤200), 18% of 200≤400 and 29% 400≤ (Figure 26B).

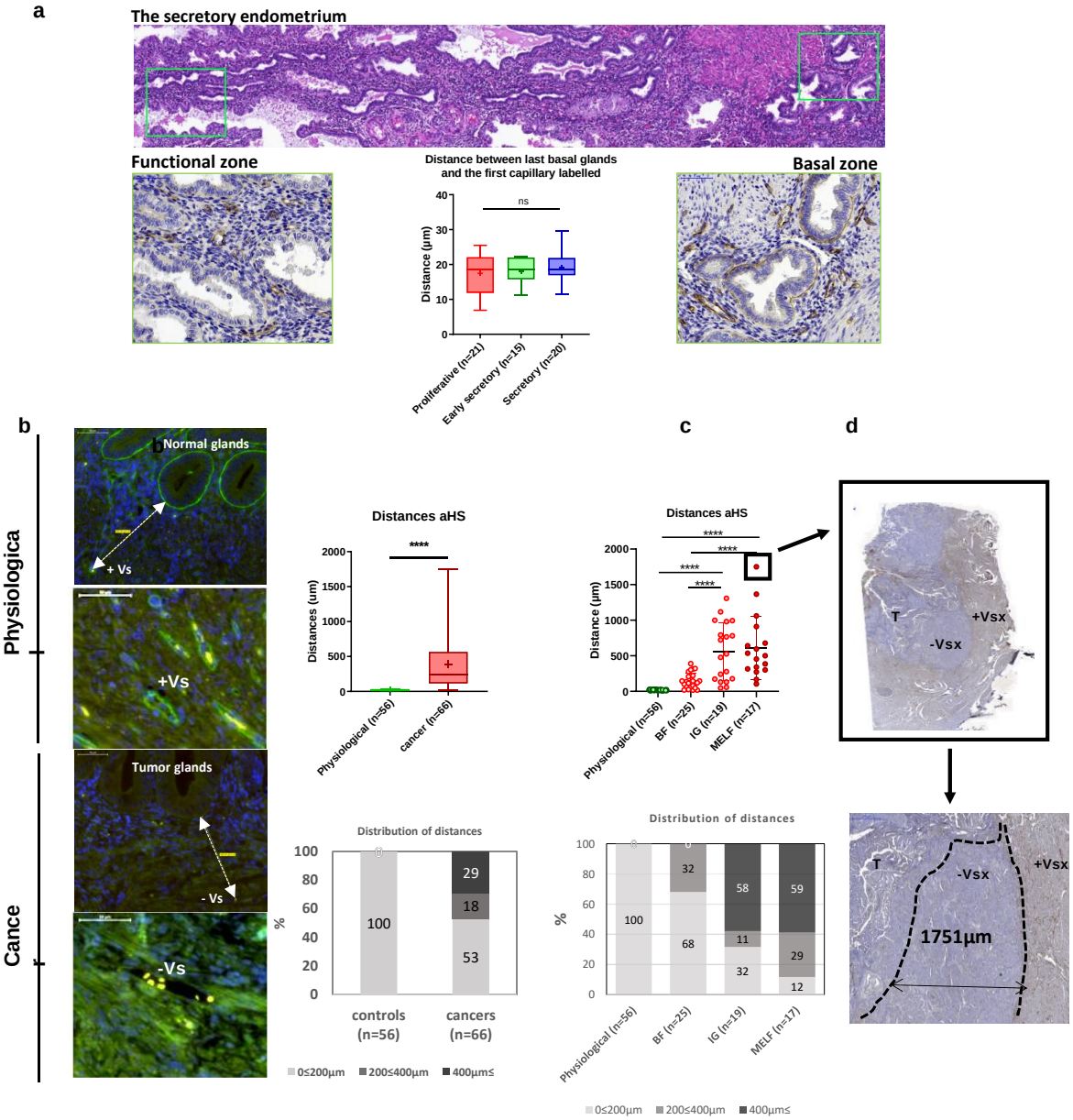

Figure 26. aHSPG expression analysis in endometrial stroma and tumor micro-environment.
A: Pattern of aHS expression on vessels of physiological cases. A1: Labelling of aHS expression on capillaries with AT-b labelling of a secretory endometrium, showing constant labelling on basal and functional layers in physiological cases. In healthy endometrium, the microvasculature present in the superficial myometrium is positive for aHS at short distance from the tumor front with a median of around 20µm., this labelling does not vary during the estrous. B: Labelling of aHS expression on capillaries at the superficial myometrium of physiological and tumor cases, with fluorescent AT-b labelling showing disappearance of aHS labelling in capillaries of the tumor micro-environment. The distance measured between the tumor front and the first aHS-labelled capillary in the TME is significantly higher than in normal endometrium, for all cancer cases. ****, p-value≤0.0001. C: Quantification of distance between tumor front the first capillary labelled and distribution analysis in each pattern of myometrial invasion in comparison with physiological cases. In the most invasive cancer subtypes, IG and MELF, this distance is considerably longer, suggesting that aHS downregulation in TME capillaries renders them permissive to cancer invasion and metastasis.****, p-value≤0.0001. D: Images showing the labelling for aHS expression on a MELF cases displaying a large halo of negative aHS labelling on capillaries with a distance of 1751µm.

We were then interested to see if a particular distance distribution could be found in the early stage of each invasion type. Interestingly, the extent of the suppression in aHS in capillaries of the TME corresponds to the decrease in aHS in tumor glands at the tumor front (Fig 23B, C). The distance is proportional to the ability of the tumor to manipulate its environment in order to remodel the tissue to its advantages and to invade. Thus, we observed that positive aHS tumor front is most of the time related to a short distance and conversely a negative front to a longer distance. The largest distances were observed in IG and MELF types, with a mean of 58% and 59% of cases exhibiting a distance greater than 400µm (Figure 26C), corresponding to an average value of 563.0 (±405.9) µm of distance in IG and an average value of 610.3 (±438.9) µm in MELF cases (Figure 26C) and a maximal distance of 1751µm observed in a MELF case (Figure 26 C, D). In BF and AL patterns, the distance between tumor front and the first labeled capillary was significantly shorter. BF and AL displayed a majority of 0 to 200µm distances, corresponding to 68% of the cases for BF and 100% of the cases in AL (Figure 6C), respectively and an average value of 149.3 (±106.2) µm in BF which is remarkably inferior compared to the two other patterns but still significantly bigger than the distance found on normal endometrium cases (Figure 26C).

3. Use of common prognostic factors from case series and cohort studies to identify potentially highest invasive cases with metastatic output cases.

Previous analyses were done between each parameter (aHS, HPSE, MVP, MVD, distances) with the histological characteristics. In the following section we will perform a dual analysis.

3.1. Identification of cases showing an extensive aHS downregulation in invasive glands and TME.

To further emphasize the causal relationship between the tumor and the TME, aHS expression in glands of the tumor front and on capillaries of the TME was analyzed in correlation together with the patterns (Figure 27A). A particular distribution was observable in each subtypes. BF cases present heterogeneous aHS labelling in tumor glands with short distances of aHS in TME. IG cases present heterogeneous aHS labelling in tumor glands with long distances of aHS in TME. And MELF cases present week aHS labelling in tumor glands with long distances of aHS in TME. MELF cases that have the most extensive decrease index of aHS in glands are the ones with the largest zones of aHS downregulation in capillaries with distances greater than 400µm. A gradual HS disappearance is thus observable with the intensity of invasion starting in the TME (Figure 27C). This result highlights a strong tumor-TME crosstalk.

3.2. Identification of cases showing an extensive aHS downregulation and vessel proliferation in TME.

To further emphasize the causal relationship between aHS expression in capillaries and tumor angiogenesis we have analyzed in correlation both parameters (Figure 27B). Again, we find a particular distribution in each subtypes with gradual intensity according to invasion. BF cases present the smallest index of capillary proliferation with short distances of aHS in TME. IG cases present small index of capillary proliferation with long distances of aHS in TME. Finally, we find that MELF cases that have the highest index of capillaries proliferation are the

ones with the largest zones of aHS downregulation with distances greater than 400µm. On capillaries, modifications start with aHS decrease followed by endothelial cell proliferation supporting the causal-link of aHS decrease in angiogenic activation (Figure 27C).

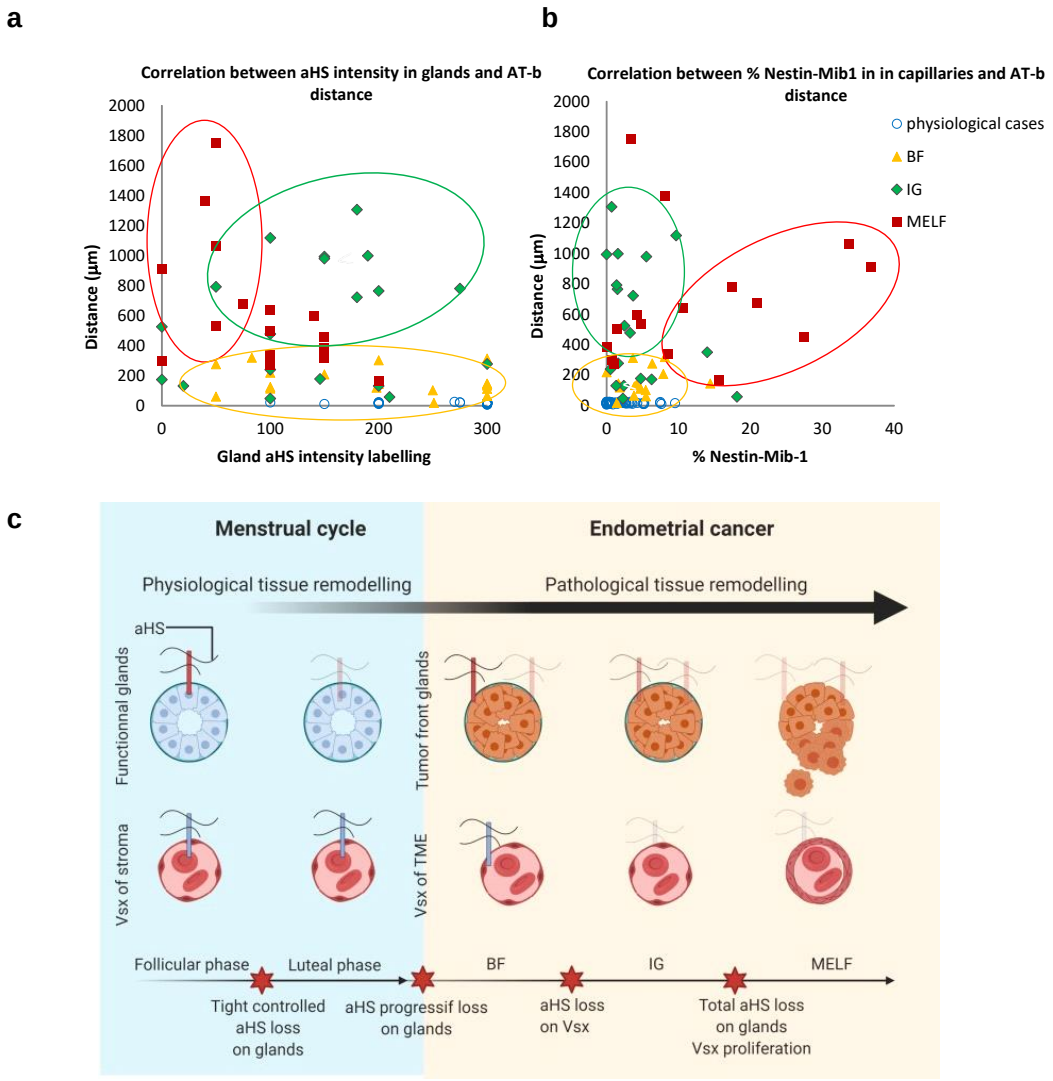

Figure 27. Correlation analysis of parameters used in the study to identify high invasive characteristics.

A: Correlation analysis between gland aHS intensity labelling and aHS distance shows a gradual decrease of aHS expression in the TME and glands from BF to MELF. B: Correlation analysis between blood vessels proliferation and aHS distance in the TME shows a gradual decrease of aHS expression in the TME followed by vessel proliferation from BF to MELF. C: Schematic model of aHS changes in the gland and the stroma from physiological to pathological tissue remodeling. Physiological tissue remodeling affects only endometrial glands in the secretory phase. In Cancer, both glands and vessels are affected leading to invasive glands and proliferating vessels.

3.3.Prognostic validation with clinical follow-up of the cancer cases.

Our analysis support that MELF pattern present molecular characteristics of invasive and pro-angiogenic features and suggest that those cases must be taken more carefully compared

to other grade 1 cases. It is possible to select within MELF cohort cases with severe aHS downregulation and vessels proliferation. We are currently planning to do a clinical follow-up of the cohort study to evaluate the prognostic value of aHS expression in MELF cases.

4. ADDITIONAL EXPERIMENTS

4.1. Verification of AT-binding assay specificity.

aHS, on the other hand, was detected in a ligand binding assay using biotinylated antithrombin (AT-b) developed by us following the protocol previously described [196]. To control the specificity of aHS-AT binding a competition assay was done by co-incubation of AT-b with UFH heparin (UFH liquemin, Drossapharm AG). aHS chains contain a 3-O-sulfated glucosamine within a pentasaccharide constituting the AT binding site in both heparin and aHS. Dextran sulfate (DxS), another glycan that does not contain the specific pentasaccharide within the chain, was used as negative control. A second control setting to ensure the specificity of the streptavidin protein conjugated to horseradish peroxidase (HRP) enzyme was used with BSA buffer incubation instead of AT-b (Figure 28).

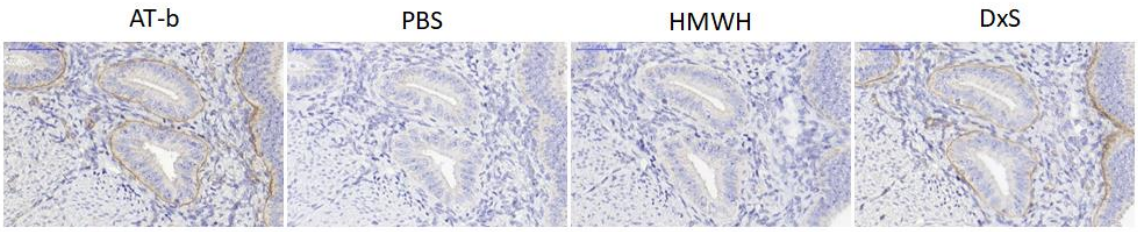

Figure 28. Specificity of AT-b to aHS (Competition test).
Histological staining of aHS with AT-b binding assay with and without competition. Suppression of signal in histological sections on the binding assay upon competition of AT-b with co-incubation with unfractionated heparin (UFH), but not with DxS, ensures the specificity of the AT-b to endogenous aHS.

4.2. aHS and HPSE evaluation in tumoral processes of latent EC Grade 1.

EC is an overwhelming cancer mostly affecting postmenopausal women. EC cancer derives from progressive transformation from normal postmenopausal atrophic endometrium, to latent precancer hyperplasia glandular cystic endometrium to finally endometrioid adenocarcinoma grade 1. To ensure the specificity of aHS and HPSE expression changes to cancer, labelling of these two parameters was also performed into these stages (Figure 29). aHS expression analysis revealed that postmenopausal and latent endometrium gave positive signals on glands and stromal capillaries unlike already established cancer. HPSE expression analysis also revealed an increasing expression labelling from hyperplasia with a maximum in EC grade 1. These results suggest that HPSE increase arrives upstream aHS decrease and that aHS downregulation labelling is specific for cancerous endometrium.

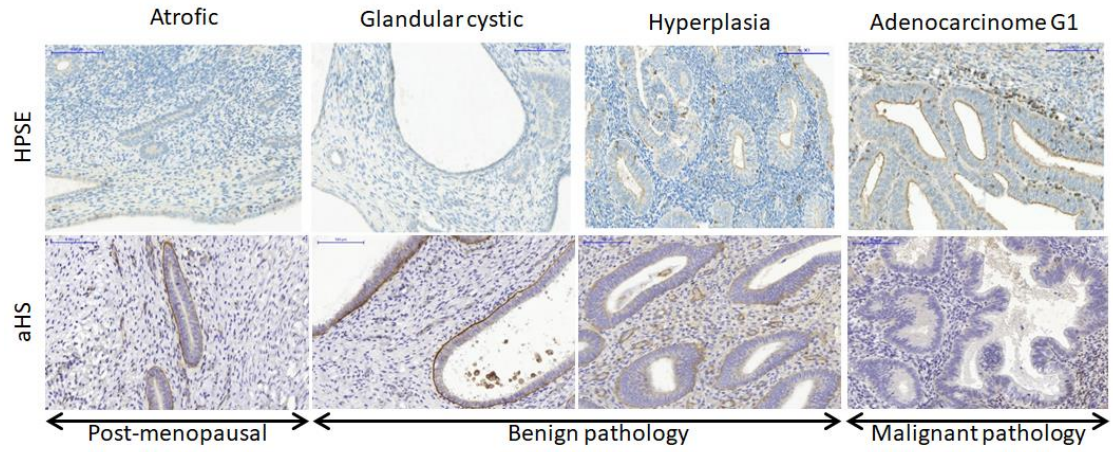

Figure 29. aHS and HPSE in pre-cancerous and cancerous phases.
Histological staining of HPSE (top) and aHS (bottom) in atrophic, benign and malignant pathology of endometrium. Upregulation of HPSE expression starts from latent hyperplasia and reaches its maximum in EC. aHS labelling decrease is attributed only to EC.

4.3. Sulfs expression analysis in EC Grade 1.

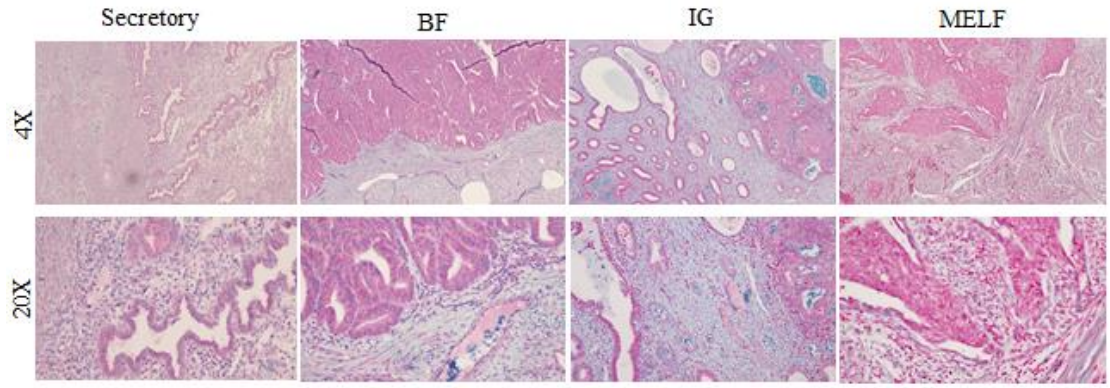

Figure 30. SULF2 expression in the pattern of myometrial invasion.
Strong SULF2 labelling was observed in glands of all tumor cases without distinction within the patterns of myometrial invasion. Strong signal was seen in lymphocytes in TME of MELF with desmoplasia.

In physiological endometrium, proliferative and secretory phases, the endometrial glands staining was homogenous in the basal and functional zone, with a moderated cytoplasmic intensity. There were no polarization to the basal nor apical border (Figure 30).

In EC of different pattern of myometrial invasion (IG, MEFL and BF) the distribution of the staining was homogenous across all the tumor surface such as the center and the invasive front. The staining intensity was strong and moderate in ¾ of the cases with no difference between the pattern of infiltration as well as HPSE. In the remaining cases the intensity was low and any cases were negatives. These results suggest that Sulf2 expression dos not directly impact the distribution of Ahs in tumor glands and other mechanisms implicated are involved.

However, we noticed MELF TME present recruitment of immune cells that display strong intensity labeling of Sulf2 suggesting that they could participate in aHS remodeling on the tumor front.

5. DISCUSSION

Tumor stroma is composed of the ECM including HSPGs, fibronectin, collagen, cytokines, and GFs [182]. As the tumor evolves, the stroma undergoes tissue remodeling under the action of enzymes able to modify the glycosidic chains of the ECM, i.e., glycosyltransferases, glycosidases, sulfotransferases, SULFs, and HPSE [150]. The presence and amount of these GAG-related enzymes help to identify high-risk patients and to develop personalized therapeutics [198]. Indeed, Barkeer and collaborators demonstrated that elevated expression of the O-glycosyltransferases GALNT3 and B3GNT3 regulates cancer stem cell markers in pancreatic cancer and their knockdown leads to decreased clonogenicity and migratory capacity [199]. Increased HPSE expression is also often described to promote an aggressive tumor behavior via multiple mechanisms [134]. It has been demonstrated that tumors are more aggressive when developed in transgenic mice overexpressing HPSE (Hpa-Tg and MMTV-heparanase), whereas smaller tumors develop in Hpa-KO mice [200, 201]. However, our analysis revealed that evaluation of HPSE alone was not sufficient to discriminate higher aggressive patterns of myometrial invasion in early stage EC. All EC gave strong positive signals for HPSE without distinction between the patterns when analyzed in the cohort. We thus analyzed aHSPG as potential candidate.

Remodeling of HSPGs through enzymatic modification of HS chains is associated with malignant transformation of cells and can potentially serve as molecular biomarker to aid in the diagnosis and prognosis of cancer [144, 202]. In this study we focused particularly on aHS expression during physiological and pathological tissue remodeling occurring in the basal membrane of the glandular endometrial epithelium and its stroma and TME. We hypothesize that the decrease of aHS by enzymatic degradation through HPSE post-synthetic modification through Sulfs could allow tumor glands to invade at the tumor front and allow ECM remodeling such as desmoplastic reaction, tumor angiogenesis and tumor cell metastatization. We analyzed aHS and HPSE on these aspects in a cohort on endometrioid adenocarcinoma cases at first grade and firsts stages of the disease in order to evaluate their implication in the first steps of tumorigenesis. To evaluate if they could be a valuable prognostic tool to identify at early stage aggressive endometrial carcinoma, a clinical follow-up of the cases will be done in order to confirm if aHS marker could predict at early stage the patients that are going to evolve into the disease.

We have found that aHS expression on glands of the functional layer of endometrium had cycling expression pattern accompanying the tissue remodeling occurring under the action of sexual hormones during the estrus cycle. Normal glands repress aHS in their basal lamina when the glands elongate during the secretory phase in the endometrial region undergoing tissue remodeling. HPSE exhibits medium to low level of expression in normal glands. Decreasing level of aHS during secretory phase is also accompanied with reduction of HPSE expression, a safety mechanism by which normal cells could contain the overshoot of tissue remodeling.

The basal zone of the endometrium, however, is not affected by the cycling tissue remodeling and aHS and HPSE expression remain stable on those glands. Physiological tissue remodeling in the endometrium is thus characterized by aHS downregulation in a tight delimited region during a precise time-lapse coinciding with the implantation window, a very controlled mechanism to allow normal glands to elongate. We hypothesized that in the same way, downregulation of aHS could also be implicated in tissue permissiveness to tumor invasion, angiogenesis and tumor progression. In cancer cases, the glands at the tumor front that invade the myometrium repress aHS and this downregulation is more extensive in the most aggressive pattern of myometrial invasion such as MELF glands. The expression of HPSE was found to be elevated in all cancer cases compared to controls without distinction of invasion histotypes. This result suggests that HPSE is implicated at the very beginning in the initiation of tumorigenesis. HPSE participates in numerous cancer related functions such as cancer motility, invasion, metastasis and nuclear activity mainly due to its HS degrading activity [139]. HPSE can translocate in the nucleus where it degrades nuclear HS and regulates genes associated with tumorigenesis [139]. A recent study demonstrated that knockdown of HPSE resulted in decreased cell proliferation by downregulating MMP1 expression via p38 MAPK signaling pathway *in vitro*, whereas overexpression of HPSE resulted in the opposite phenomenon [203]. Upregulation of HPSE in all cancer glands is observed in parallel with a dense and stratified epithelium in cancer glands as well as the increase of number of tumor glands. In cancer, HPSE catalyzes the cutting of the side chains of HS and contributes to the remodeling of the basal membrane of tumor glands and of the ECM of the tumor micro-environment [139]. HPSE promotes the release of various HS-linked molecules like grow factors, cytokines and enzymes that could diffuse in the TME and act at distance from the tumor front. Indeed, we observed in our tumor cases that capillaries from the TME were negative for aHS and the negative halo extended several hundred micrometers suggesting a distant action of the tumor glands on its micro-environment. It is known that HPSE also stimulates the expression of matrix metalloproteases [141] that degrade the core proteins of HSPG in the ECM favoring tissue remodeling such as desmoplastic reaction and tumor glands invasion which are relatable of histological characteristics of MELF pattern. aHS expressed on the cell surface is normally subjected to limited degradation and proteolysis resulting in its release in ECM or it can be internalized by endocytosis and degraded by a multi-step process terminating in the lysosomes [134]. In cancer, this degradation is enhanced increasing the bioavailability of molecules that were before sequestered by HS chains such as HS-bound growth factors (i.e., bFGF, VEGF, HB-EGF and KGF) which sustain neovascularization and wound healing [139].

We thus evaluated the relation between aHS downregulation in blood and lymphatic vessels with tumor-induced angiogenesis. We found that blood vessels during the normal estrus cycle had constant labelling for aHS no matter if they were in the stable basal zone or the functional zone of the endometrium where tissue remodeling occurs. Those vessels elongate as the endometrium acquires thickness during the proliferative stage of the cycle but the number of capillaries and lymphatic vessels does not increase. Those vessels are also characterized by a low proliferation rate, stable during the cycle. aHS expression is stable as well during this angiogenesis by vessel elongation which accompanies the thickening of functional endometrium during the proliferative phase, without requirement of tissue remodeling.

Furthermore, the permanence of aHS in the vessels of the functional endometrium during the implantation window and the secretory phase suggests that the physiologic adaptation of epithelial glands in preparation to the embryo implantation occurs without involvement of the neighboring vessels responsible of the blood supply [38]. However, during pathological tissue remodeling occurring in the TME of tumor cases, capillaries at the myometrium adjacent to the tumor were negative for aHS and those vessels had a strong index of endothelial cell proliferation suggesting an active angiogenesis. Nestin and Ki-67 is an independent prognostic marker and associated with several features of aggressive tumors [204], supporting a more aggressive phenotype of aHS negative MELF. Count of blood vessels at the myometrium adjacent to the tumor was made to ensure that the decrease of aHS labelling was not the consequence of a decreased amount of vessels. However, we were unable to detect a difference in blood and lymphatic vessel counts. On a previous immunostaining analysis of vessels during angiogenesis, it was shown that the four important basement membrane components- laminin, type IV collagen, HSPG (perlecan) and entactin, do not differ qualitatively between invading capillary sprouts from that of the established vasculature [205]. However, here we observe that capillary of the invasive TME strongly differ quantitatively for aHS suggesting their shedding from the perlecan core protein or degradation through HPSE thus increasing the GF gradients required for angiogenesis [206] that were previously sequestered by the perlecan on the N-terminus domain of HS [207]. Basement membranes are active participants in the regulation of cell functions including blood filtration, storing GFs and cytokines and control angiogenesis and tumor growth, and their integrity is essential for the maintenance of vascular homeostasis [206, 208].

We also interestingly observed that the tumor cases with the most aggressive histological pattern of myometrial invasion had the largest halo of aHS negative capillaries around the tumor with the biggest index of capillary proliferation. This is an important outcome suggesting an interesting tumor-microenvironment crosstalk. A possible candidate of this long-distance interaction could be the Sonic hedgehog (Shh) signaling in which cancer cells produce soluble a Shh that signals to distant stromal cells that express the receptor Patched (Ptc) [209]. Treatment with heparin or HS was shown to interfere with Shh release and reception [209], suggesting that when suppressed, Shh is free to act on distal vessels. The tumor has the ability to manipulate its environment in order to remodel the tissue to its advantages by supplementing blood and lymphatic vessels to prepare the mechanism of metastatization leading to a Grade 2 cancer. Indeed, MELF pattern that is characterized by an EMT [49] and thus by a metastatic leading process, had the biggest endothelial proliferation index and the strongest aHS downregulation. In addition, MELF pattern is characterized by strong inflammatory response in the TME and it has been demonstrated that circulating neutrophils release angiogenic factors in endometrial stroma when the cells becomes activated [33]. The implication of HS proteoglycan Sdc-1 in the mediation of leukocytes adhesion and activities during inflammation is well established as richly explained in the following article and review [112, 210].

Low-risk EC (grade 1 stage 1A,) develops recurrence of their EC in a medium time of 23 months after initially being diagnosed and treated for low-risk EC [211]. Micro anatomical variations of MELF pattern within grade 1 should thus be considered as they may be relevant to tumor invasion and progression. Euscher et *al.* suggested that the presence of single cell

invasion pattern in MELF is a potential predictor of advanced stage disease as it was associated with lymphovascular invasion and lymph node metastatic or extra uterine disease in low grade endometrial carcinoma [65, 212, 213]. During the last past years, MELF pattern has aroused much interests but its prognostic and predictive effect still remains elusive [65]. The clinical follow-up of MELF cases could confirm their higher risk of developing Grade 2 cancer and recurrence.

Collectively, these results confirm our working hypothesis that aHS is downregulated in pathologically permissive conditions allowing cell invasion and tumor angiogenesis and that HPSE might be involved in modulation of aHS in cancer invasion. In tumors with most aggressive invasiveness and with metastatic output, MELF cases, the downregulation of aHS expression within the tumor and tumor environment is more relevant and is associated with the highest angiogenesis and lymphangiogenesis index.

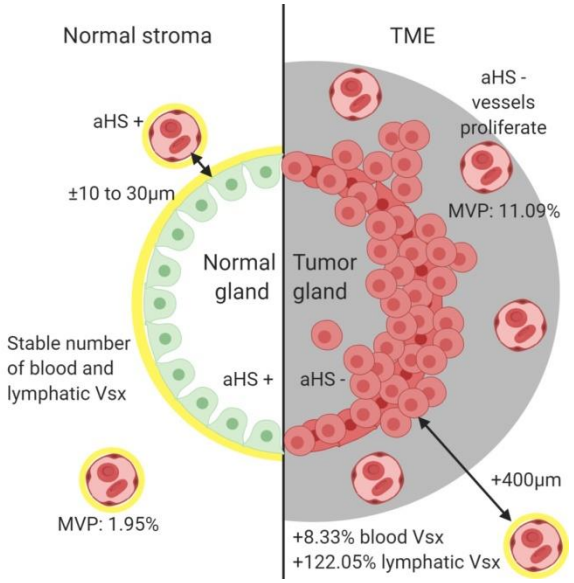

Figure 31. Summary scheme of aHS expression analysis in gland and stroma of normal and cancer cases.

Tumor progression is characterized by the decrease of aHS in glands of tumor front with a most extensive downregulation in the most invasive histotypes with an EMT process. Blood vessels in the TME also reduce aHS resulting in the increase of proliferation. The halo of perturbed TME reaches more than 400µm while normally positive vessels are found at a negligible distance from the gland.

To conclude, we suggest that a histological analysis together with aHS analysis made with a simple biding-assay could be a valuable tool to distinguish higher risks patients within MELF or IG histotypes. Those patients could be categorized for more developed follow-up with more adequate treatment such as heparin derivatives or HS mimetics that have been synthesized with reduced or absent anticoagulant activity but maintaining their binding selectivity potential towards a vast array of HS-binding proteins, many of which with pivotal roles in cancer growth and progression.

This study will be continued by in vitro experiments to test the implication of HPSE and Sulf activity in regulating endometrial cells migration, and invasion in vitro. The follow-up of

patients with endometrioid carcinoma will also be done to show correlation between aHS, HPSE and Sulf expression in endometrioid cancer and metastatic relapse.

6. Material & Methods

Tissue specimens

It is a retrospective study of 102 human cases with uterine endometrioid carcinoma Grade 1, stade pT1a and pT1b that had been treated with hysterectomy from 1998 until 2017, in the Department of Gynecology at the Geneva University Hospitals. Surgical specimens were fixed in buffered formalin, and samples were paraffin embedded and 5 µm-thick sections were obtained for each case. The cases were classified and graded following the World Health Organization criteria [214], and were staged according to the International Federation of Gynecology and Obstetrics [215]. Since we aim at finding precocious markers, only low grade cases of adenocarcinoma where taken. We took cases that were diagnosed for a period long enough to be able to do a clinical follow-up. As control group, we took 56 physiological cases with normal histology of the endometrium that underwent hysterectomy independently of cancer. They are divided into different cycle stages: 20 proliferative, 16 early secretory and20 secretory. To enrich the analysis, 14 atrophic, 7 granulo-kystic and 23 hyperplasia endometrium were also analysed. The study was approved by the local ethical committee (CER 10-155R).

Histological classification of Grade 1 cancer and patterns of myometrial invasion

The grade of an EC is based on their architecture. In grade 1 endometrioid cancer, the glandular componant is more than 95% of cancerous. Stage 1a and b refers to the depth of invasion in the myometrium, less or more than 50%.

Pattern of myometrial invasion refers to the manner in which cancer infiltrates tissue at the tumor/host interface [216]. The prognostic significance of the pattern of myometrial infiltration was evaluated. Cases were classified in 4 differents patterns of myometrial invasiom: 37 Infiltrating glands cases (IG), 36 Broad front cases (BF), 17 Microcystic, elongated, and fragmented cases (MELF) and 12 Adenomyosis like cases (AL). All cancer cases were dispatched amont these 4 categories.

Considering that neoplasia infiltrating in a widely dispersed manner are more aggressive than those growing in a bulky pushing fashion [217], we have then splitted thoses patterns into two groups according to their histological degree of aggressiveness: BF and AL as the less aggressive and IG and MELF as the most invasive and aggressive.

Localization and expression of aHS and HPSE

Histochemical analysis of aHS and HPSE were conducted on paraffin tissue sections. Consecutive histological sections were used to perform in parallel both ligand-binding of aHS and immunohistochemistry of HPSE. HPSE was detected using the monoclonal mouse anti-human HPSE antibody IgG1K Mab 130 (Chemie Brunschwig #INS-26-1-0000-21) and was labelled with a second antibody coupled to peroxidase (Envision+System HRP anti-mouse, DAKO K40019), and revealed by diaminobenzidin (DAB+). Histological sections of first

and last trimester placental villi, known to highly express HPSE, were used as positive control tissue.

aHS, on the other hand, was detected in a ligand binding assay using biotinylated and fluorescent (Alexa Fluor 488) antithrombin (AT-b) developed by us following the protocol previously described [196]. aHS was labelled with a Streptavidin-peroxydase HRP from DAKO (K5001), followed by diaminobenzidin revelation. Wild type murine uterus was used as positive control tissue. Negative controls were incubated with BSA buffer instead of AT. To ensure the specificity of aHS-AT binding a competition assay was done by co-incubation of AT-b with heparin (liquemin, Drossapharm AG). DxS was used as negative control.

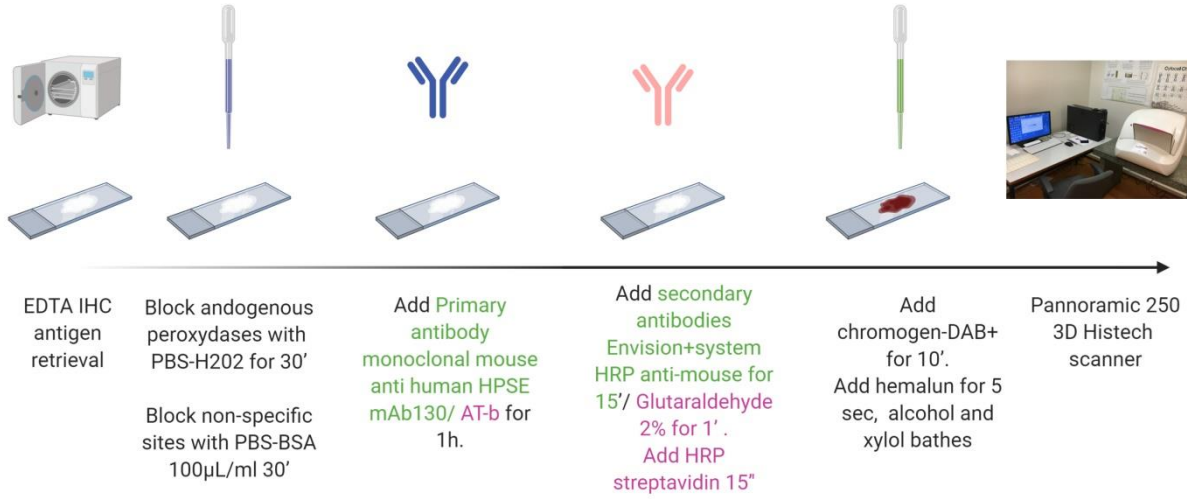

Figure 32. Schematic representing the steps for immunodetection and ligand binding of HPSE and aHS on human FFPE histological sections.

The EDTA based solution is designed to break the protein cross-links, therefore unmask the antigens and epitopes in formalin-fixed and paraffin embedded tissue. Non-specific sites of HRP and endogenous peroxydases were blocked with H2O2 and BSA buffer. Following with primary antibody/ AT-b incubation for HPSE and aHS labelling respectively. Binding of AT with endogenous aHS is fragile and need an additional glutaraldehyde fixation. Secondary antibody coupled with peroxidase is then administrated followed by DAB+ revelation.

After evaluating histological sections qualitatively, we quantified the labeling using the following formula:

(Intensity×% of glands labeled at tumor front)+ (Intensity×% of glands labeled at tumor front)+…… until reaching 100% of total glands

We first identified the control tissue marker and we assigned it the maximum intensity 3.We then evaluated the percentage of glands with this intensity in relation to the whole tumor front, *exemple 3× 40%.* We then evaluated the rest of the gland population in comparison with the control tissue marker intensity. This intensity between 0 and 3 (with 3 for intensity of the glands identical to that of the control) is then multiplied by the percentage of labeled glands, the result not exceeding 300, *exemple (3× 40%)+(2× 10%)+(1× 30%)+(0× 20%)=170.*

Determination of microvessel density (MVD)

Angiogenesis and lymphangiogenesis wer analyzed in physiological and pathological cases. Labeling of blood and lymphatic vessels were performed using the pan-endothelial CD-31 primary antibody (DAKO, M0823) and the lymphatic endothelial cells labelling was done using the anti podoplanin D2-40 primary antibody (DAKO, M3619), followed by secondary antibody and then diaminobenzidin revelation (DAB+). CD31, a member of the immunoglobulin superfamily, is a 130-kDa transmembrane glycoprotein also designated as PECAM-1 (platelet endothelial cell adhesion molecule 1). It is present on the surface of platelets, monocytes, macrophages, and neutrophils and is a constituent of the endothelial intercellular junction [218]. D2-40, is a ~38 kDa O-linked transmembrane sialoglycoprotein antibody that reacts with a fixation-resistant epitope on lymphatic endothelium [219].

The immunohistochemical study was performed on 20 proliferative cases, 16 early secretory, 20 secretory, 19 BF, 20 IG and 17 MELF cases. We determined microvessel density by counting the number of CD-31+ and D2-40+ vessels in five high power fields (400X) of each case. In physiological cases, the MVD were evaluated in three areas: in functional endometrium, basal endometrium and superficial myometrium. In tumor cases, the MVD were evaluated in intra-tumoral region and the myometrium adjacent to the tumor, the tumor microenvironment TME.

Determination of microvessel proliferation (MVP)

MVP is a measure of the number of vessels containing proliferating endothelial cells. First, Nestin positive vessels or single endothelial cells were detected using Nestin antibody (R&D, MAB1259) labelled with nitrotetrazolium blue chloride (NBT) - Alkaline phosphatase immunodetection in pink. Secondly, we assessed whether the endothelial cells had a Ki-67 positive proliferating nucleus. Ki-67 positive nuclei were detected using MIB-1 antibody (DAKO, M7240) and stained brown by DAB-Peroxidase Substrate immunodetection, and only Nestin positive endothelial cells with Ki-67 positive nuclei clearly within the endothelial cell body were recorded as proliferating endothelial cells. 19 BF cases, 20 IG, 17 MELF, 20 proliferatifs and 20 secretory cases were analyzed.

Tissue slides were scanned using a Pannoramic 250 Flash II scanner (3DHistech, Ungary) with resolution of 0.22 µm/px. The following regions were defined manually: tumor front and its physiological homolog, the superficial myometrium. For each case, the deep myometrium was used for individual normalization. Within these regions, vessels were detected based on Hue values using the HSV color space with Definiens Developer XD [Version 2.7.0. (Definiens Inc., Munich, Germany), http://www.definiens.com/]. Vessels were grouped by size and presence of lumen to focus our analysis on capillaries. Mib1+ cell numbers and Mib1+ area were quantified for each vessel based on the DAB channel intensity after applying a color deconvolution algorithm [220]. Data was summarized and exported using R [Version 3.5.1 (R Core Team (2017). R: A language and environment for statistical computing. R Foundation for Statistical]. The algorythm was created with the help of Dr. Kreutzfeldt at the Faculty of Medicine of the University of Geneva and was adjusted until optimization of detection (Figure 33). The raw data was processed by converting the Nestin+ and Mib-1+ pixel areas into a

number of object while being careful to remove duplicate Mib-1 in the same blood vessel. We then calculated the percentage of vessels with dual labelling. This percentage was then normalised to the deep myometrium value to reduce individual fluctuation. Microvessels were regarded as proliferating when they contained one or more proliferating endothelial cells.

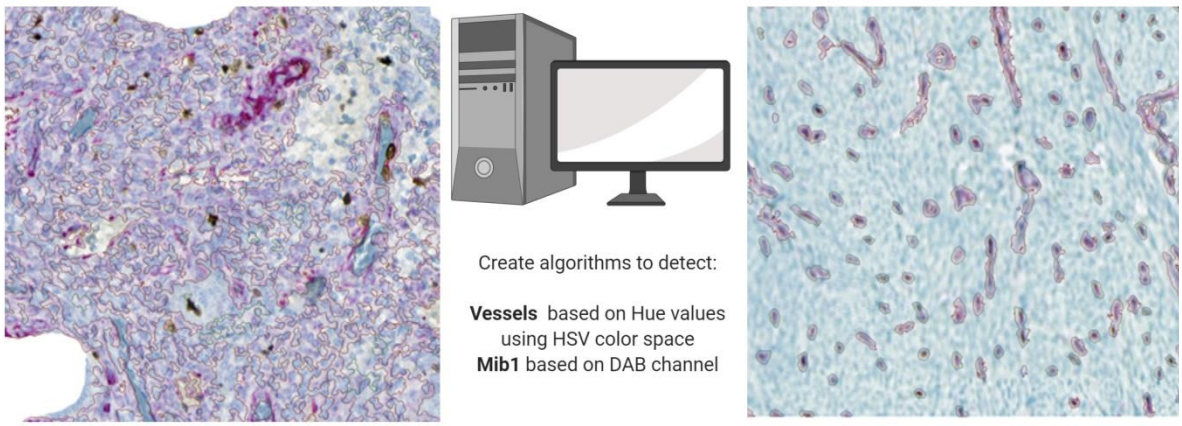

Figure 33. Illustration of algorythm optimization to detect Nestin+Mib-1+ vessels for MVP analysis.

Optimization allowed us to adjust detection to blood vessels only by removing the background detection. Left picture: before optimization example, right picture: after optimization example.

Localization and expression of SULF

IHC staining for SULF was conducted on paraffin tissue sections. We used the anti-Rana 19 polyclonal antibody generously given by Romain Vivès that target SULF2. The antibody was visualized using nitrotetrazolium blue chloride (NBT) - Alkaline phosphatase immunodetection in pink. Histological sections of first and last trimester placental villi, highly expressing SULF, were used as positive control tissue.

Clinical follow-up of cancer cases analysed with respect of the histotypes

After approval by the ethical committee, the clinical follow-up of cancer cases will be done and the patients that had relapse will be recorded. Finally, we will analyze if together the cohort study and the histological characterization of pattern of myometrial invasion have a prognostic value at early stage of the desease Grade 1 to potentially predict which patients are going to evolve into a metastatic outcome.

Statistical analysis

The statistical analysis was performed using the Prism5 program for Windows (GraphPad Prism® Software Inc., CA, USA). When comparing the two groups, the Mann-Whitney test was applied, and to compare more than two groups, the ordinary one-way ANOVA test was applied, followed by the Holm-Šídák or Tukey test. For the analyses, the quantitative variables were described by average, designed by the symbol (+) in the box, and standard deviation, while the significance level was set as $p < 0.05$.

All illustrations and graphs were created using GraphPad Prism, Pannoramic 250 3D Histech viewer, Microsoft Excel, and Adobe Illustrator.

HS and its derivatives in EC therapy: the challenge of modulating tumor cell invasion and angiogenesis

Note: *This thesis was kept confidential until August 2020, date of the patent filing of IFREMER compounds.*

1. SUMMARY

In the human uterus, aHS is present in epithelial cells of the glandular epithelium and endothelial cells basement membrane but disappears during pathological tissue remodelling occurring in invasive EC with active neo-angiogenesis. In cancer, HS catabolic enzyme HPSE is elevated and shifted to an extracellular form modulating several cancer-related functions such as GF signalling and ECM remodelling. We postulate that aHS downregulation through HPSE degradation facilitates tumoral invasion and angiogenesis. Thus the anti-tumoral activity of HPSE inhibitors was evaluated *in vitro* on Ishikawa human endometrial tumor cell line proliferation, migration, invasion and angiogenesis. Those HPSE inhibitors are customized heparin mimetic compounds designed to increase potency and binding selectivity towards HPSE and specific proteins involved in cancer. We first evaluated their anti-migration and anti-invasion effects on Ishikawa human endometrial tumor cells. Drugs treatments remarkably slowed wound closure speed with a maximum of -52.62% on a concentration 100µg/ml compared to non-treated cells. We have found that higher inhibition was attributed to compounds with high sulfation and was not mediated through AT-aHS interactions. N-acetylation of oxyheparin in glycol-split compounds did not increase the inhibitory activity. Tumour cell invasion was decreased by 87% and we observed an inhibition of -52.97% of cell proliferation. HS derivatives also inhibited tumour-induced angiogenesis by decreasing the number of endothelial branches induced by tumour conditioned media suggesting that these inhibitors neutralize angiogenic molecules released by tumour cells. AT-ligand binding assay of conditioned media revealed that sulfated glycans, in addition to their anti-HPSE activity, induce a turnover where endogenous aHSPG are released into their extracellular form. In vitro inhibition of tumorigenesis-related processes under HS derivatives supports their therapeutic potential.

2. INTRODUCTION

Endometrial adenocarcinoma is the most common malignancy of the female genital tract in developed countries [61]. Different therapeutic modalities including radiotherapy and surgery and systemic therapies such as chemotherapy and hormone therapy are used to treat

recurrent EC [221]. Nevertheless approximately 13% of all ECs recur and the prognosis for recurrent disease is poor with the median survival hardly exceeds 12 months [222]. Clinical trials evaluating chemotherapy regimens in patients with EC include combinations of doxorubicin and cisplatin, cyclophosphamide or paclitaxel and carboplatin, most of them administered in a palliative setting. These systemic treatment options are often accompanied by high toxicity. There is thus an urgent need to find modalities to develope more adequate treatment for patients with high risk of recurrence [223].

Since venous thromboembolism is a well-known cause of death in patients with cancer [9], heparin has frequently been used in the treatment of cancer-associated thromboembolism. Accordingly, increasing clinical evidences demonstrated that cancer patients treated with unfractionated and low-molecular weight heparin (LMWH) survive longer than patients treated with other anticoagulants, especially patients in the early stage of the disease [10, 134, 224, 225]. Heparin, which can be considered a highly sulfated version of HS, has been shown to possess anticancer, antiangiogenic, and antimetastatic activity [226, 227], but its anticoagulant activity and the possible side effects as bleeding and heparin-induced thrombocytopenia limit long-term treatment [134].

A promising branch then emerged and led to an increased focus on heparins in anticancer treatment. Heparin derivatives or HS mimetics are highly sulfated, structurally distinct analogues of glycosaminoglycans (GAGs) and have been engineered to have reduced or absent anticoagulant activity while maintaining their binding selectivity potential towards a vast array of HS-binding proteins, many of which with pivotal roles in cancer growth and progression [228, 229]. These heparin mimetics that inhibit HPSE enzymatic activity are being evaluated in numerous clinical trials for various types of cancer, and appear to be well tolerated and also beneficial in combination with conventional anticancer drugs, thus providing a strong rationale for applying anti-HPSE therapy in EC [134]. For more information about HS derivatives and their application as modulators of HS turnover in Mucopolysaccharidosis disorders and Cancer, I highly suggest you to read a review I co-wrote earlier this year which you can find in the appendix to this thesis.

HS is expressed on the cell surfaces of all mammalian cells where they serve as endocytic receptors and storage for macromolecules. HSPGs participate in a variety of cellular processes including cell migration, angiogenesis, proliferation and invasion. HPSE action influences the global distribution of HSPGs and thus participates in the process of tumorgenesis and spread [134].

The previous study on EC Grade 1 revealed that tumour glands are characterized by decrease of aHS and by increased HPSE suggesting a correlation between the two events. Tumor progression was related to extensive aHS downregulation with predominance in strongly invasive phenotypes and with higher blood vessels proliferation in the tumour microenvironment, conditions that allow cell invasion, angiogenesis and metastatization. Tissue remodelling, invasion and angiogenesis therefore constitute privileged targets in the development of therapeutics tools. The stroma undergoes tissue remodelling during cancer progression under the action of enzymes such as glycosyltransferases, sulfotransferases, HPSE, and SULFs that modify the glycosidic chains of the ECM [150].

As already reported in the introduction, HPSE is the only known mammalian endoglycosidase that cleaves HS chains and whose activity contributes to degradation and remodeling of ECM and thus is implicated in tissue remodeling and tumor progression [139]. HPSE cleaves the β (1,4) glycosidic linkage between GlcA and GlcNS, generating 5–10 kDa HS fragments (10–20 sugar units) and cleaves also heparin, which share a high structural similarity with HS [230]. In addition, other two extracellular enzymes with aryl sulfatase activity at neutral pH, Sulf1 and Sulf2, selectively remove 6-O-sulfate groups from glucosamine residues within HS polymers [104]. Modification of the 6-O-sulfation profiles at the heart of the S domains affects the ability of the polysaccharide to modulate the activity of a large number of GFs, morphogens and chemokines [118]. Changes within HS structure by both HPSE and Sulfs lead to massive alterations in their functional properties. Since the ECM serves as a reservoir for numerous bioactive molecules that bind to HSPGs, their cleavage orchestrate cellular responses in both normal and pathological situations.

In this study we propose to evaluate HS as therapeutic tool in the treatment of EC Grade 1. Due to the important role of HPSE in HS post-biosynthetic modification and catabolism, we focus on the possibility to use HS mimetics competing with the endogenous HS as a mean to selectively inhibit HPSE activity. This study will focus on the possibility to control HS turnover and reduce aHS degratation by acting upon HPSE in order to decrease tumor cell proliferation, invasion and tumor-induced angiogenesis. The data obtained will enable us to evaluate the therapeutic potential of HS and its derivatives in EC Grade 1 treatments.

3. Results

3.1 Analysis of HS derivatives characteristics.

3.1.1. Molecular characteristics

GAGs are the main mediators of communication (cell–cell and cell–ECM communication) in the extracellular space. Thus, they play a role in malignant transformation and tumor metastasis, and they can act as either promoters or inhibitors of the disease. Because of their high specificity, GAG sulfation patterns are strongly related to their function [13].

Glycosaminoglycans were first used as treatment. Unfractionated heparin (UFH) commercially known as Liquemin, LMWH Clexane, CS A and C together with Dermatan sulfate (DS) were supplied by Sigma (St. Louis, MO, USA). High and low MW dextran sulfate (HMW DxS and LMW DxS) was used to assess wether the effect was only dependant to the charge.

In addition, two groups of manufactured HS mimetics, with low or absent anticoagulant activity, were also analyzed in our cancer model to evaluate their anti-tumoral activity. Those drugs are obtained from heparin and from marine bacteria exopolysaccharides and are currently being tested in clinical trials as potential drugs against various cancers. They act as competitive inhibitors that resemble the endogenous HS substrate of HPSE. These series of drugs are GAG-mimetics chemically customized to be potentially suitable as bioactive agents for medical applications with potent heparin-associated functions, small molecular size and reduced anticoagulant activity for suitable patients administration without heparin’s side effects. The first group obtained from IFREMER institute are marine bacterial exopolysaccharide

derivatives that share similar structure to HS. The two tested compounds were: low-molecular weight GY785 DRS (A5-4), 36% sulfate content and oversulfated low-molecular weight GY785 DRS (A8), 45 % sulfate content. We also tested low-molecular weight "heparin-like" compounds HE800DR (A5), oversulfated HE800DRS (A5-3), and oversulfated HE800DRS (A6) which have respectively 0%, 17.8% and 30% sulfate content (Table 3). The second group, obtained from RONZONI Institute, is composed of heparin derivatives. Their size and sulfation degree have been determined and five compounds in total were tested. G5460 is pig mucosa heparin and is an analogue of liquemin both in terms of sulfation and MW. Two other compounds were obtained from G5460 by fractionation onto an AT-column and correspond to the high or low affinity fractions for antithrombin, respectively: G5460HA and G5460NA. And finally we tested glycol-split (RO) compounds that are obtained through periodate oxidation followed by borohydride reduction of uronic acids, a modification that introduces more flexibility in the molecule and disrupts the binding site for AT, causing loss of the anticoagulant activity. G9694 is an RO heparin, while G10239 is N-acetylated glycol-split heparin obtained by N-desulfation and N-acetylation of glucosamines followed by glycol-splitting.

Table 3. Glycans used.

Name	Sulfate content (%)	Molecular weight (g/mol)	Groups
UFH Liquemin	30	15000	GAGs
LMWH Clexane		4500	GAGs
HMW DxS		500000	GAGs
LMW DxS		5000	GAGs
CS AC		21600	GAGs
DS		36000	GAGs
A5	0	34000	Marine sulfated glycans - Group A
A6	30	16000	
A5_3	17.8	5100	
A8	45	15000	Marine sulfated glycans - Group B
A5_4	36	8000	
G5460	30	<16000	Ronzoni heparin derivatives
G5460 HA	>30	<16000	
G5460 NA	<30	<16000	
G9694	30	<16000	
G10239 (SST0001)	<30	16000	

Table 3. Molecular characteristics of the glycans used in the study.
GAGs, marine sulfhated glycans analogues of HS and heparin derivatives with different molecular weight, % sulfate contentand anti-thrombin affinity have been used in this exploratory study.

3.1.2. Anti-heparanase activity analysis

It is well known that heparin and HS are substrates for HPSE. UFH and LMWH as well as Ronzoni heparin derivatives are potent HPSE inhibitors and their anti-HPSE activity has already been well characterized and these compounds have been enrolled into clinical trials for cancer [134].

Since IFREMER sulfated glycans are new HS mimetics, we determined the anti-HPSE activity only on these products, in collaboration with Jin-ping Li (Uppsala, Sweden). The anti-HPSE was evaluated by measuring the signal of remaining substrate after the incubation. The concentrations required for 50% HPSE inhibition (IC_{50} value) for the glycans were ranging from 1 to 1.5 µM (Table 4) for A5_3, A5_4 and A6, so these glycans have a strong potential as HPSE inhibitors. A5, however, seems to not affect HPSE activity. Since this glycan is not sulfated, the activity is dependent of the charge of the glycan conveyed by sulfation but is not affected significantly by the glycan size, from large HMW to LMW species ranging from 16'000 to 5'100 Da.

HS derivatives	MW (g/mol)	anti HPSE IC50 (µM)	anti HPSE IC50 (µg/ml)	anti - HPSE
A5	34000	-		no
A5_3	5100	1 - 1.5	5.1 - 7.7	strong
A5_4	8000	1 - 1.5	8 - 12	strong
A6	16000	1 - 1.5	16 - 24	strong
A8	15000	10	-	medium

Table 4. Summary table of anti-HPSE activities of IFREMER HS mimetics.
Structure-activity relationships was examined. The inhibitory activity of sulfated glycans showed to be greatly dependent on their degree of sulfation, but independent of their molecular size.

3.1.3. Anti-Sulf activity analysis

To assess anti-Sulf activity, two complementary analyses were performed, in collaboration with Romain Vivès, (IBS, Grenoble, France).

We first analyzed the arylsulfatase activity of recombinant HSulf-2 using the 4MUS assay, which measures the ability of arylsulfatases to convert the non-fluorescent 4-MUS pseudo-substrate into the fluorescent 4-MU product [116]. The ability of HSulf-2 enzyme to process the 4MUS is represented by 100 % (T+). HS mimetics were first evaluated at high concentration of 10 and 100µg/ml. The Figure 34A represents the activity measured after 4h of incubation and shows significant inhibition of HSulf-2 activity by A5_3, A5_4, A6 and A8 products. A5 product, in contrast, seems to increase the arylsulfatase activity of HSulf-2. A5 seems to not target the active site but could bind to the enzyme and induce a conformational change more favorable to the activity. Anti-Sulf activity of A5_3, A5_4, A6 and A8 products was then assessed at lower concentration (Figure 34B). The analysis revealed that A5_3 and A8 exhibit an anti-sulf activity starting at 10µg/ml, while A5_4 and A6 can have an anti-Sulf activity at lower concentration, starting at 1µg/ml (Figure 34B, Table 5).

HS binding properties of HSulf-2 was next investigated by assessing 6-O-endosulfatase activity. In this assay, heparin is treated with HSulf-2, then depolymerized into disaccharides to determine its composition. The ability of HSulf-2 enzyme to process heparin is represented by the ratio of disaccharide products (IdoA,2S-GlcNS) / disaccharide substrates (IdoA,2S-GlcNS,6S). T-control represents untreated heparin and T+ represents HSulf-2 treated heparin in absence of inhibitor. A5_4 was first evaluated at high concentration of 10 and 100µg/ml and

showed complete inhibition of HSulf-2 activity, with a ratio product/substrate comparable to that of untreated heparin at 4 and 24h (Figure 34C,D). A good inhibition was observed from 1µg/ml for A5_4 compound, and to a lesser extent for A5_3 compound (Figure 34E and Table 5).

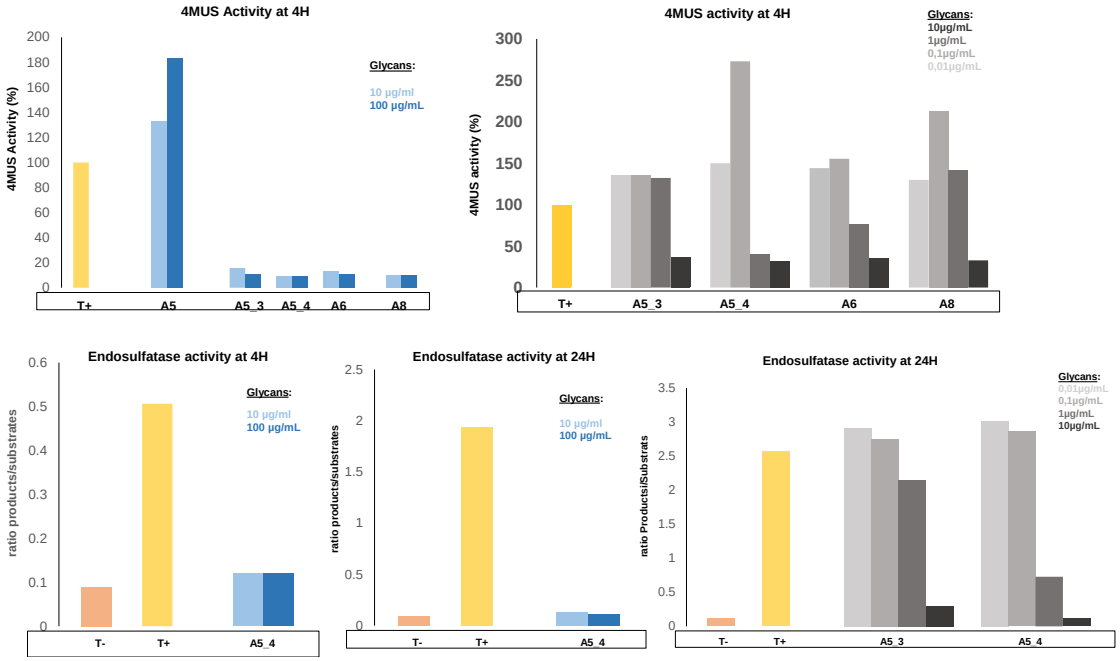

Figure 34. Anti Sulf activity analysis on IFREMER HS mimetics.

A, B: 4MUS activity measured after 4h of incubation and show a good inhibition of A5_4 and A6 at 1µg/mL, A5_3 and A8 products at 10µg/mL. Endosulfatase activity of A5_4 product measured after 4h C; and 24 D; show a good inhibition at 10 µg/mL. E: Endosulfatase activity of A5_4 and A5_3 products measured after 24h show an inhibition starting from 1 µg/mL.

These results show that in addition to HPSE, IFREMER products can also be a substrate for Sulfs and a potent inhibitor of arylsulfatase and 6-O-endosulfatase activity at from 100 to 1/10 µg/mL. As the study is mainly focused on post synthetic modification (degradation/desulfation) of aHS-mediated cancer activities, we will perform the following anti-cancer experiments with a concentration of 100 µg/mL of our products in order to inhibit HPSE and Sulfs activities [231].

Inhibitors	MW (g/mol)	Sulfate content (%)	Effect on 4MUS activity	Effect on Endosulfatase activity
A5	34 000	0	Activation	-
A5_3	5 100	17	Inhibition at 10µg/mL	Inhibition at 1µg/mL
A5_4	8 000	36	Inhibition at 1µg/mL	Inhibition at 1µg/mL
A6	16 000	30	Inhibition at 1µg/mL	-
A8	15 000	45	Inhibition at 10µg/mL	-

Table 5. Summary table of anti- arylsulfatase and 6-O-endosulfatase activity of IFREMER HS mimetics.

Except for A5 product, all IFREMER HS mimetics have been shown to be potent inhibitors of both arylsulfatase and 6-O-endosulfatase activity of Sulfs between 1 to 10 µg/mL.

3.2 Characterization of aHS and HPSE expression and production in our in vitro tumor and endothelial model cell lines.

In order to analyze the action of HPSE inhibitors on aHS turnover the cells were first selected according to their ability to express and produce aHS and HPSE. Synthesis and degradation of HS are both complex pathways involving a variety of different enzymes, so we focused our analysis on the aHS key synthetic enzyme HS-3-O-sulfotransferase-1 (*3OST1)* which is responsible for introducing the trisulfate glucosamine residue in the AT-binding domain of HS chains and is thus specific of aHS.

First, cell surface aHS and HPSE expression were analysed on Ishikawa monolayer cultured on coverslips using labelled AT binding and IHC for aHS and HPSE localization, respectively (Figure 35A). Human EC Ishikawa cell line displayed a weak positive signal for aHS and a medium signal for HPSE on the cell surface suggesting a rapid turnover of aHS and on the cell membrane. Human endothelial EAhy-926 cell line gave a medium signal for HPSE and a medium signal for aHS.

In addition, their production was analysed at the biosynthesis level by the expression of mRNA of HS-3-O- sulfotransferase-1 and of HPSE mRNA by RT-PCR. Ishikawa tumor cells displayed a very low level of 3-O-ST-1 mRNA expression of 0.053 AU and a good level of HPSE mRNA expression with 115.63 (±38.42) AU (Figure 35B). EAhy-926 endothelial cells also showed low level of 3-O-ST-1 mRNA with a value of 0.328 AU and a medium level of HPSE mRNA expression with 47.56 (±70.21) AU (Figure 35B). It is well characterized that tumor cells exhibit higher level of HPSE.

These data show that both Ishikawa and EAhy-926 cells express and produce aHSPG and HPSE thus allowing their manipulationfor our purposes.

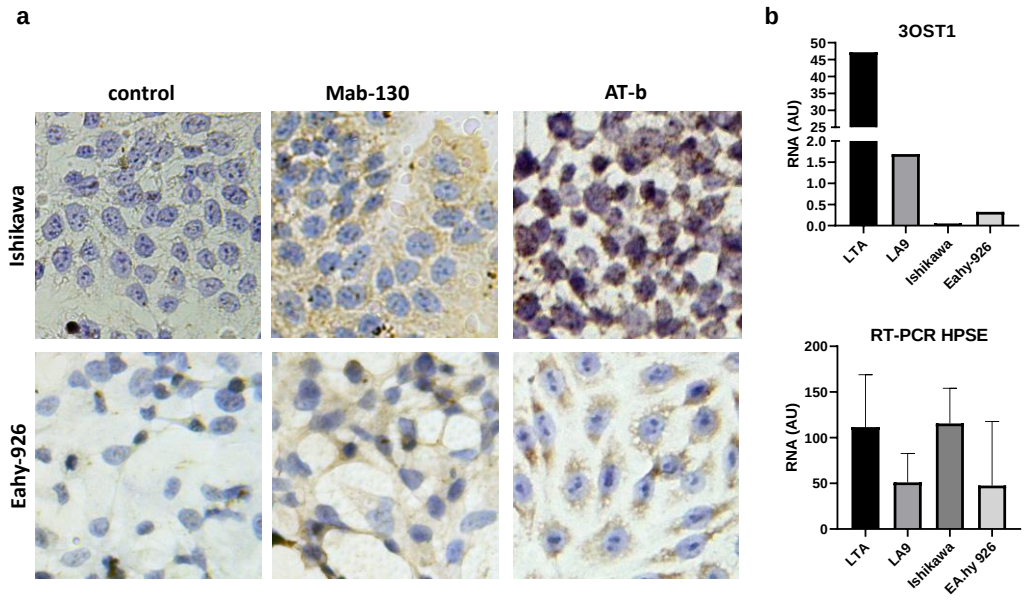

Figure 35. Characterization of in vitro model cells lines for aHS and HPSE.

A: Images showing the labelling for aHS expression (left) and the immunostaining for HPSE expression (middle) on Ishikawa and Eahy-926 monolayers mounted on coverslips. Both cell lines express HPSE and aHS. Negative controls were incubated with BSA buffer. B: Synthesis of HS-3-O- sulfotransferase-1 (top) and HPSE (bottom) was evaluated by RT-PCR. Ishikawa show a 0.053 AU level of 3-O-ST-1 mRNA and 115.63 (±38.42) AU level of HPSE mRNA. EAhy-926 show 0.328 AU level of 3-O-ST-1 mRNA and 47.56 (±70.21) AU level of HPSE mRNA. Positive LTA cells are derived from mouse 929 fibroblastic L cells and were used as positive control. LTA-related LA9 line is devoid of aHS.

3.3 Effect of treatment on aHS turnover.

Ishikawa and EAhy-926 cells were treated with HS derivatives and the effect on aHS turnover was analysed by measuring aHS release in conditioned media by ligand-binding assay. Both endothelial and endometrial tumor cell line gave strong positive signals for the soluble form of aHSPGs in culture media comparing to our positive control LTA cell line (Figure 36A). These results demonstrate that the cells release soluble forms of aHSPGs in the extracellular environment. Dot-blot with 100µg/ml UFH 100µg/ml LMWH and 100µg/ml DxS proved the specificity of our antithrombin to bind to the 3-O sulfated pentasaccharide which is a common biding site for aHSPG and heparin (Figure 36B). We then tested the effect of the inhibitor A6 from IFREMER on aHSPG release in conditioned media of Ishikawa tumor cells and human endothelial cells after 24 hours of incubation. Under 100µg/ml A6 inhibitor, the amount of extracellular aHSPG increase visibly compared to non-treated cells (Figure 36A). Compound A6 seems to induce a turnover where endogenous aHSPG are released into their extracellular form.

The possible mechanism is that HPSE inhibitors prevent cleavage of aHS from aHSPG and thus suppresse intracellular catabolism of aHS fragments. This leads to accumulation of membrane bound aHSPG and shedding of soluble form in the extracellular space by proteases.

Yang *et al*. observed that removal of HS from the cell surface using bacterial heparitinase dramatically accelerated Sdc-1 shedding, suggesting that the effects of HPSE on Sdc-1 expression by tumor cells may be due, at least in part, to enzymatic removal or reduction in the size of HS chains [232]. This suggests that, in absence of HPSE activity, cells attempt to maintain a normal level of Sdc-1 on the cell surface by increasing the rate of shedding.

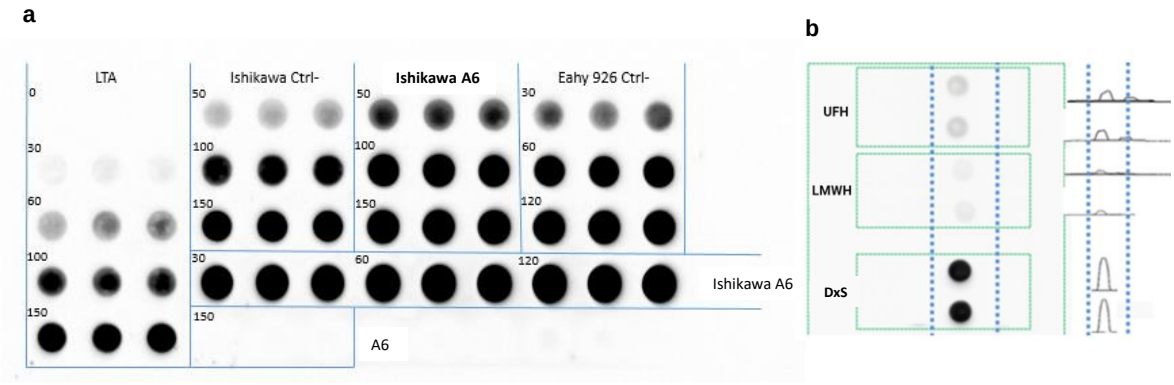

Figure 36. A6 inhibitor effect on aHSPG release on conditioned media.
A: Under 100µg/ml of A6, cells modify the turnover of aHSPG by increasing their release into the conditioned media in both Ishikawa and Eahy-926. Since nitrocellulose membranes used in the assay binds only proteoglycans and not glycosaminoglycans, the A6 inhibitor did not bind to the membrane. B: To ensure the specificity of aHSPG binding-AT a competition assay was done by co-incubation of AT-b with UFH and LMWH at a concentration of 100µg/ml that share the same AT binding site with aHS. DxS was used as negative control.

3.4 The effect of GAGs and heparin derivatives on tumorigenesis-related processes.

Tumor progression is the third and last phase in tumor development after tumor initiation and tumor promotion. This phase is first characterised by a multi-step process beginning with changes in cancer cells to undergo clonal growth or proliferation, followed by individual cell migration and invasion by which tumor cells overcome barriers of the ECM and spread into surrounding tissues. Cell proliferation, invasion, and migration were investigated in this study.

3.4.1 HS mimetics' effect on tumor cell proliferation and cell viability.

The level of cell proliferation was measured by counting the number of cells obtained after 72h compared to initial number of cells seeded on the well. A6 compound significantly decreased cell proliferation on tumor and endothelial cells. After 72h incubation, Ishikawa cells have 9.48 (±0.59) times more cells in control well while we only observe 4.43 (±0.93) times more cells in A6 treated well (Figure 37A). A6 inhibitor also decreased the final number of EAhy-926 after 72h with 2.36 (±0.12) times more cells in A6 treated well compared to 3.83 (±0.56) times more cells in control well (Figure 37A). We observe a 52.97% decrease in cell proliferation in Ishiwaka cell line and of 37.28% in EAhy-926 cell line when treated with the drug (Figure 37B). The cell proliferation response to A6 inhibitor was dose-dependent with a maximum of inhibition observed at 75µg/ml followed by a plateau (Figure 37C). A concentration of 25µg/ml of A6 gives already a very good reduction in cell proliferation with

an inhibition of 41.39% (±13.06) compared to untreated control suggesting that treatments with A6 compound could be used at low concentration, reducing possible side effects. Heparin derivatives seems to have stronger effect on tumor cells. We have seen in **3.2** that tumor cells express and produce larger amount of HPSE suggesting an important role of HPSE on their metabolism. Thus, inhibition of HPSE on tumor cells has a bigger impact on tumor metabolism including cell proliferation.

Cell toxycity was also evaluated by analysing the effect of A6 coumpond on cell viability. The number of dead cells does not increase after 72h of incubation with 100µg/ml A6. In Ishikawa cells, only 5.33% (± 0.40) of dead cell was counted under A6 treatment compared to 5.30 (±0.56) in control conditions. We also counted 6.57% (±0.35) dead cells in A6 treated *vs* 6.20% (±0.30) in non-treated EAhy-926 cells (Figure 37D). These data suggest that A6 coumpound exerted an anti-proliferative activity without a proapoptotic activity suggesting global safety for use.

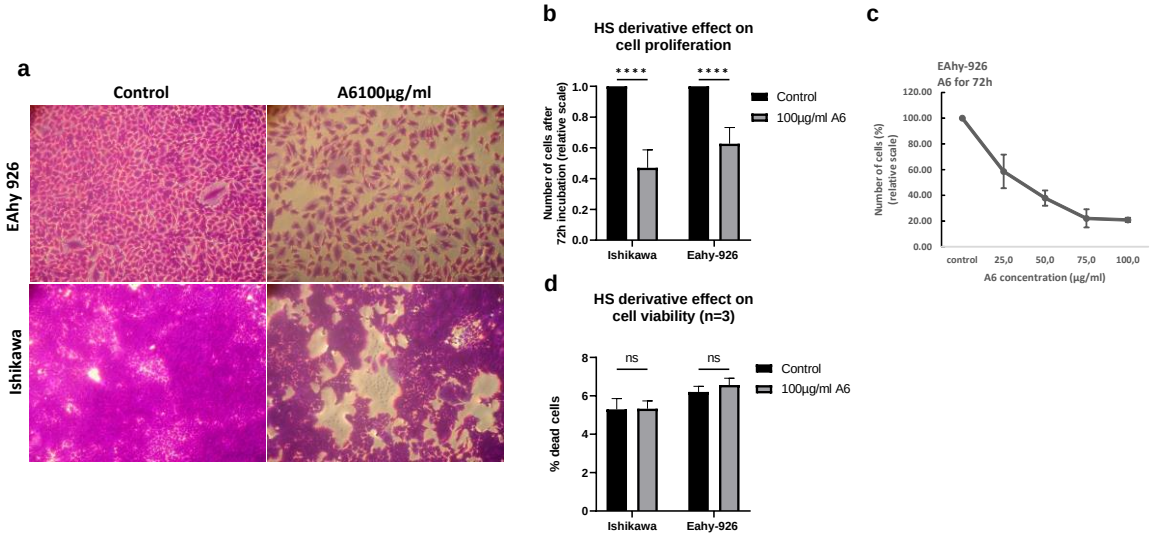

Figure 37. A6 HS mimetic effect on tumor cell proliferation and cell viability.
A: Images showing reduced number of cell on cell monolayer after 72h of A6 treatment at a concentration of 100µg/ml compared to normal proliferation profile. B: Quantification of cell proliferation under A6 100µg/ml compared to non treated cells. Ishikawa and EAhy-926 proliferation are reduced by 52.97% and 37.28% respectively. C: Cell proliferation response to A6 inhibitor was dose-dependent with a maximum of inhibition observed at 75µg/ml followed by a plateau. D: Evaluation of cell viability shows that A6 inhibitor does not increase cell death in both cell lines. ****, p-value≤0.0001.

3.4.2 The effect of HS and heparin mimetics on tumor cell migration.

A large screening of heparin, GAGs and HS derivatives was performed on migration analysis. This screening will allow us to analyze the main characteristics of sulfated GAGs that are implicated in the anti-tumoral activity.

3.4.2.1. The effect of Heparin and GAGs on cell migration analysis in 2D wound closure assay

The migratory potential of Ishikawa cell line was evaluated in 2D wound closure assay. The cells were treated with highly sulfated GAG drugs including heparin. After 20 hours, Ishikawa cells started to show visible cell migration and showed a good response to treatments. Ishikawa cell line reached 50% of gap closure in 120 hours with a cell front velocity of 3.098µm/h (±0.002).

UFH induced a slight slowdown in gap closure speed decreased by 11.62% and 18.06% with concentrations of 50µg/ml and 100µg/ml, respectively, compared to non-treated cells (Figure 38A-C). The cell front velocity was slower with 2.738µm/h (±0.219) and 2.539µm/h (±0.237) for UFH at 50µg/ml and 100µg/ml compared to the control group 3.098µm/h (±0.003) (Figure 38B). Lower concentrations of heparin did not affect gap closure speed. At 100µg/ml concentration, LMWH (Clexane) slow down the gap closure speed by 15.89% with a cell front velocity value of 2.606µm/h (±0.132) (Figure 38B).

HMW DxS gave the most effective slowdown reaching 42.93% of gap closure speed at concentration 100µg/ml with a cell front velocity of 1.768µm/h (±0.047) (Figure 38A-C). The inhibition of Ishikawa cells migration by DxS shows that it is not mediated through AT-aHS interactions, since DxS does not compete with aHS for AT-binding. However, higher concentration of HMW DxS reduced the efficacy with an inhibition of 25.53% (Figure 38B). Nearly identical migration distance curve to control were obtained for LMW DxS 5000 Da at 100µg/ml (Figure 38C). The fact that only HMW DxS inhibits cell migration, while LMW DxS has no effect underlines the charge density effect of DxS, which is highly sulfated and thus negatively charged, with about 2 negative charges per monosaccharide.

CS ABC also slowed gap closure speed at 200µg/ml by 17.82% with a cell front velocity of 2.546µm/h (±0.457) (Figure 38B). In order to determine whether this effect was attributed to CS AC or DS, both compounds were incubated independently. DS alone slowed by 18.61% compared to 2.89% for CS AC in the same 200 µg/ml concentrations with respective cell front velocity of 2.522µm/h (±0.292) and 3.009µm/h (±0.033) (Figure 38B, C). Thus, DS is responsible of the slowdown in CS ABC complex.

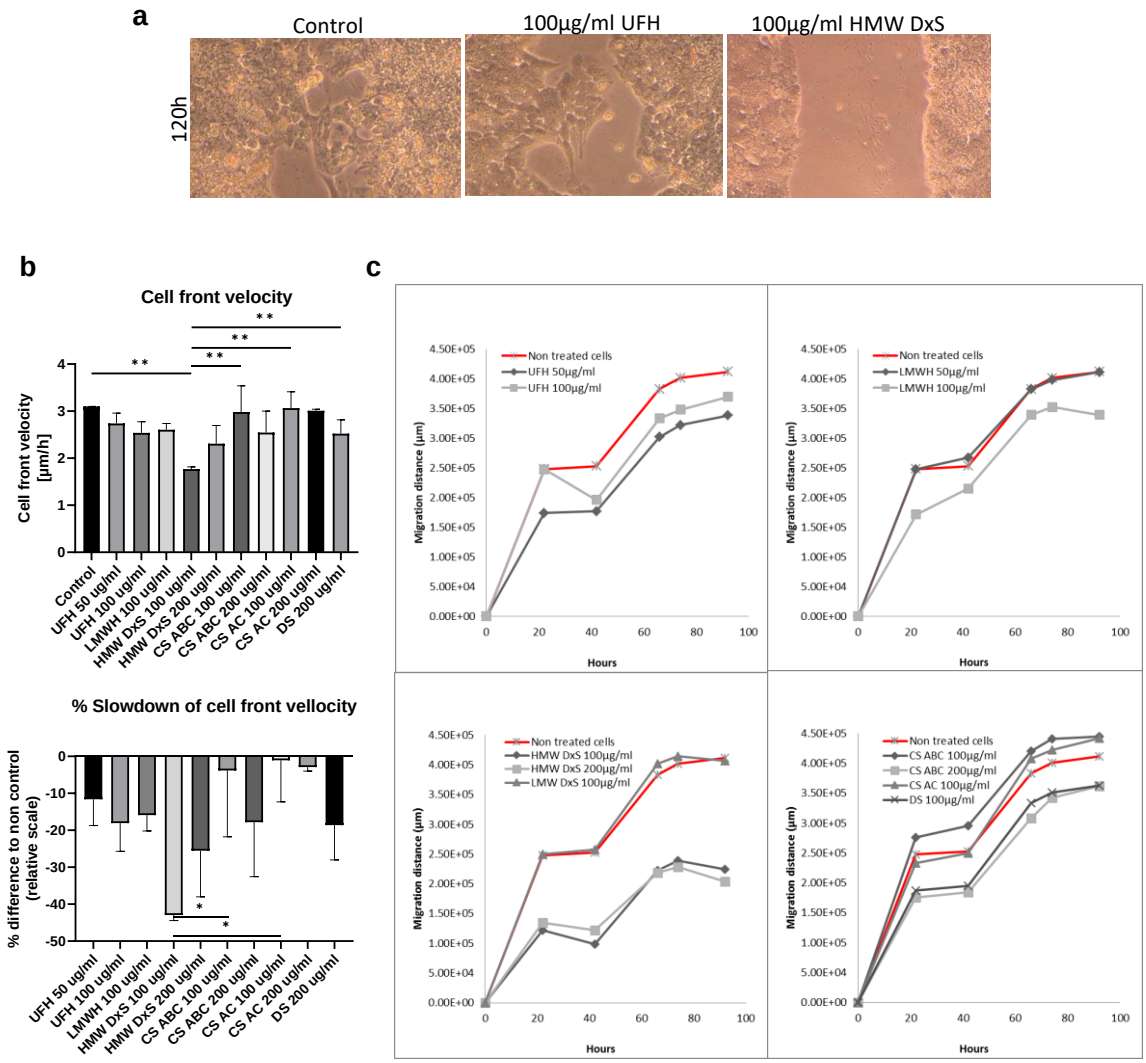

Figure 38. Heparin and GAGs effects on Ishikawa cell migration.

A: Tumor cells were scratched with a pipette tip and then treated with heparin and DxS. The cells migrated into wound surface and the average surface of migrating cells was determined by phase-contrast microscopy (magnification, x20). B: Cell front velocity in µm/hour of the Ishikawa cell line under the different treatments (top). % of slowdown from velocities of each treatment compared to control group (bottom). A mean of 4 experiments is represented. C: Migration distances of Ishikawa cells under each treatment of a representative experiment. .*, p-value≤0.05; **, p-value≤0.01.

3.4.2.2. Cell migration analysis in 2D wound closure assay: the effect of HS derivatives.

Ishikawa cells were then treated with heparin derivatives. After 6 hours, cells started to show visible cell migration and a good response to treatments. Ishikawa cell line reached 50% of gap closure in 30 hours with a cell front velocity of 7.88µm/h (±1.34). The difference in the timing compared to the previous experiment is due to shorter gap of ibidi inserts used in this second part (Figure 39A). All the inhibitors from IFREMER induced a slight slowdown in gap closure speed (Figure 39B). The most significant ones were A6 and A8 with respective slowdown 52.62% and 28.09% at a concentration 100µg/ml compared to non-treated cells, with a cell front velocity of 3.89 (±1.74) and 5.69 (±1.81) with A6 and A8 (Figure 39B,C).

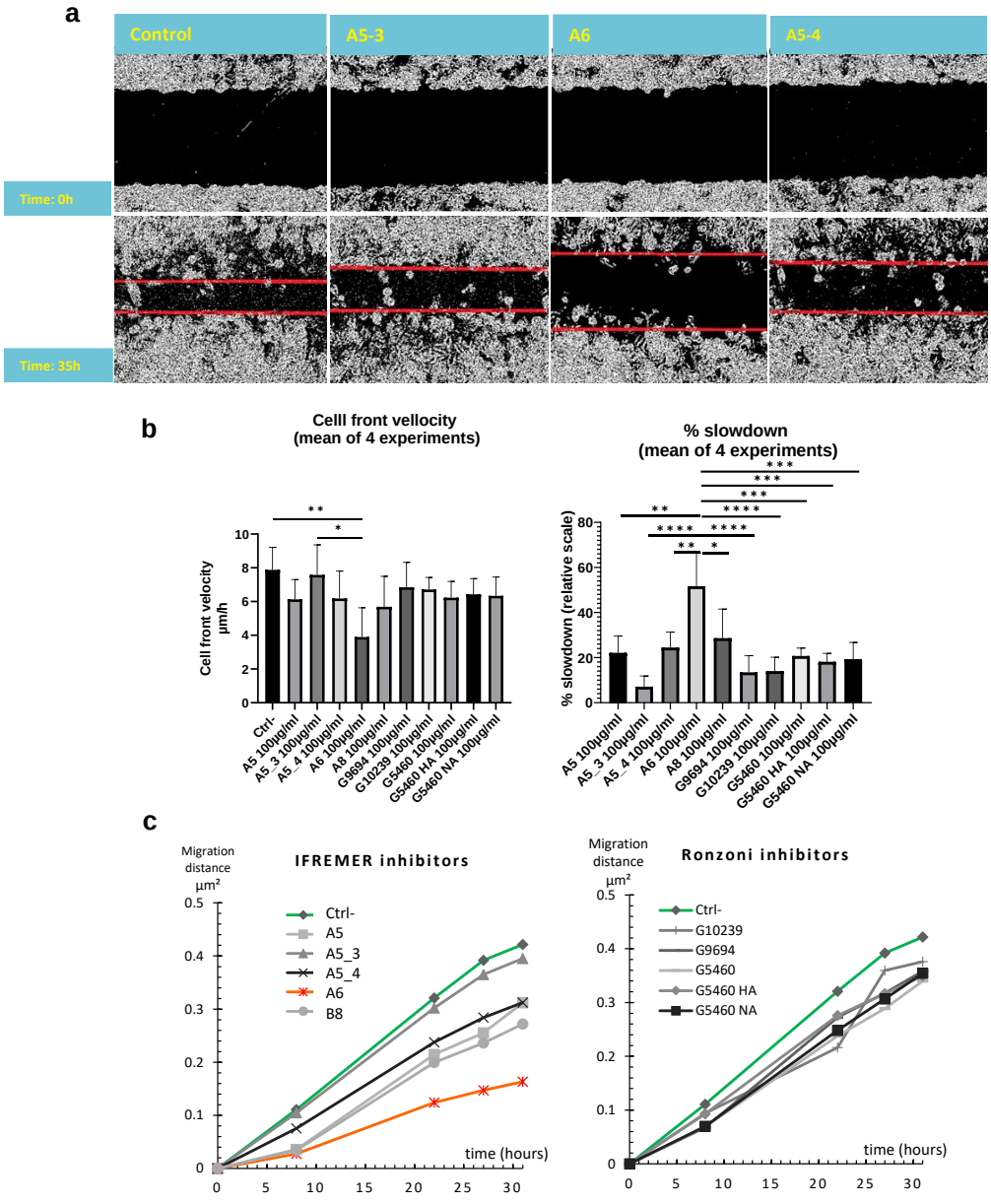

Figure 39. Heparin derivatives and HS mimetics effects on Ishikawa cell migration

A: The gap on the wound was performed by removing the ibidi insert from tumor cell monolayer and various treatments were administrated. A5_3, A5_4 and A6 inhibitors effect on gap closure after 35h was illustrated by phase-contrast microscopy (magnification, x20). B: Cell front velocity in µm/hour of the Ishikawa cell line under the different treatments (top). % of slowdown from velocities of each treatment compared to control group (bottom). A mean of 4 experiments is represented. C: Migration distances of Ishikawa cells under each treatment of a representative experiment. *, p-value≤0.05; **, p-value≤0.01; ***, p-value≤0.001; ****, p-value≤0.0001.

These two inhibitors have the particularity to be highly sulfated with a percentage of 30% for A6 and 45% for A8. The second group of HPSE inhibitors is from Ronzoni Institute. All the inhibitors from Ronzoni induced a non-significant slowdown in gap closure speed with an average of 17% compared to non-treated cells (Figure 39B). We didn't see any differences in

the wound closure speed between the different compounds (Figure 39B, C). We have found that higher inhibition was attributed to compounds with high sulfation such as UFH, HMW DxS A8 and A6 compounds. N-acetylation of glycol-split heparin did not increase the inhibitory activity and did not show a better anti-migrative activity on our tumor cells, as indeed it reduces the sulfation degree. Derivatives even surpassed control heparin and displayed a potent anti-migration activity.

3.4.3 The effect of Heparin derivatives on tumor cell invasion.

The capacity of cells to degrade an ECM-like tridimensional collagen gel and to change their shape to pass through a porous membrane was used as a measure of tumor cell invasion to test the effect of A6 HS derivative and of UFH on tumor cells invasiveness.

After 72h, 387.6 (±39.63) invasive cells/ field had migrated to the lower side of the membrane towards the FBS-rich medium in the lower compartment (Figure 40A, B). To ensure the robustness of the experimental procedure, a negative control condition where the medium with low FBS was the same in both compartments was adopted. Almost no cell invasion was measured in this condition with a mean of invaded cells/field of 5.2 (±2.28) (Figure 40C). As positive control condition, the tumour cells were placed directly on the porous membrane of Transwell without matrigel so the cells had no physical barrier to invade. A mean of invaded cells/field of 525.0 (±37.52) was counted (Figure 40C). These results show that in these conditions only 26.17% of Ishikawa cells are blocked by the matrigel barrier, and that Ishikawa tumor cells provide a good in vitro model for invasion.

Thereby, the anti-tumoral effect of UFH and A6 HS derivative was assesed. We counted a mean of invaded cells/field of 49.80 (±10.55), 90.50 (±15.50) and 110.8 (±30.06) on 100µg/ml A6, 100 and 50µg/ml UFH respectively (Figure 40B). HPSE inhibitor and GAG treatment inhibit significantly tumor cell invasion compared to controls, and lower concentration tested showed similar effect. A6 also inhibts significantly the extravasion of tumour cells inside the porous membrane on control wells, without matrigel (Figure 40C). A6 compound is a potent inhibitor of both mechanisms of cell invasion: degradation of the ECM-like collagen gel and cytoskeleton change of the structural shape of the cell for migration through the pores. Theses results suggest that preservation of HS degradation inhibits tumor cell invasion.

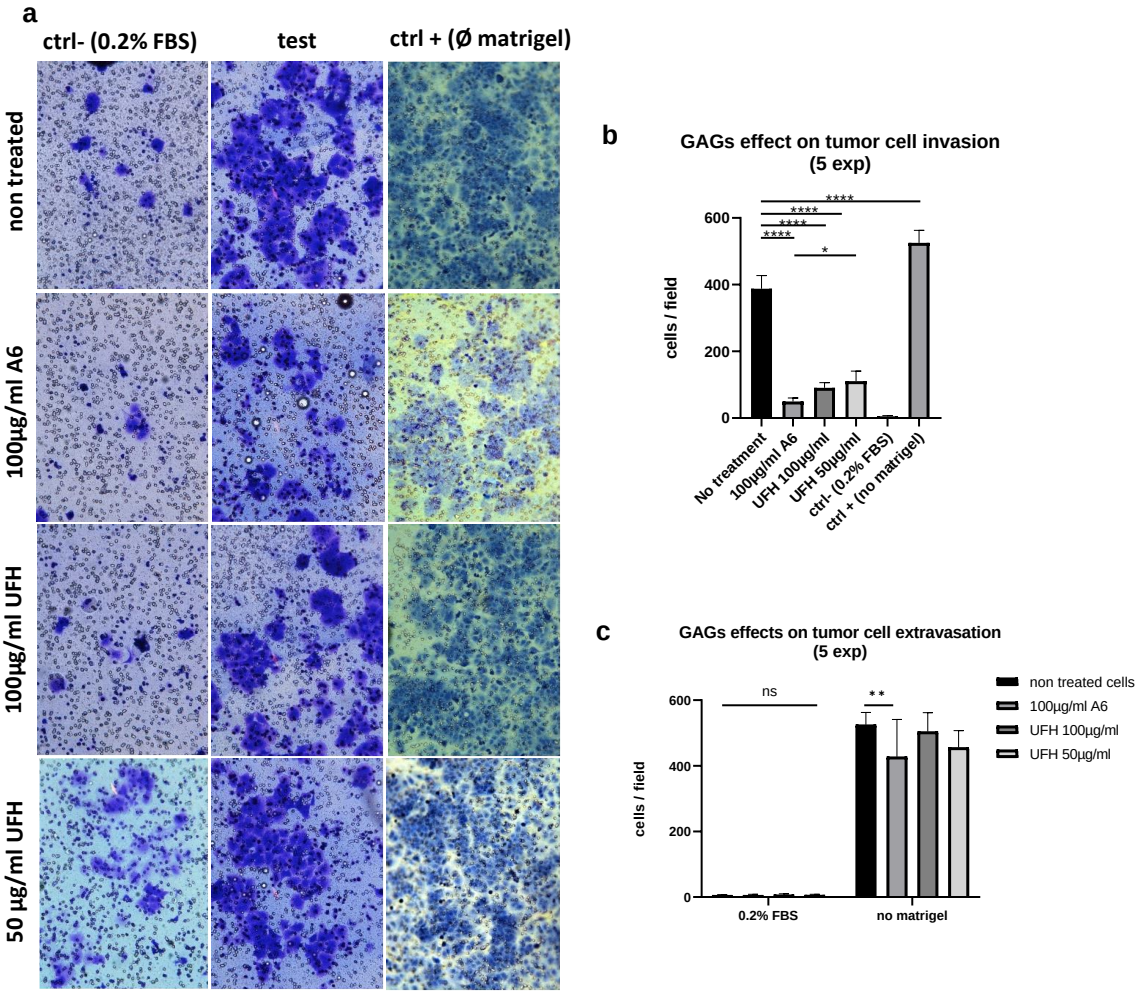

Figure 40. Heparin derivatives effects on tumor cell invasion

A: Representative images of the invasion assay in Ishikawa cells under A6 HS derivative and UFH. B: Comparisons of the cell counts of invaded cells in different treatments. C: Effect of A6 HS derivative on cell extravasation through the porous membrane without invasion of the matrigel proving both effects on both mechanisms of invasion: extravasation and degradation of the matrigel. *, p-value≤0.05; **, p-value≤0.01; ****, p-value≤0.0001.

3.5 The effect of GAGs and heparin derivatives on tumor induced angiogenesis.

3.5.1 Tumor cells effects on endothelial cell tube formation.

To evaluate the influence of tumor cells on angiogenesis, we carried out a tube formation assay on a gelled basement matrix. When cultivated on it, EAhy-926 cells form tube-like structures that originate from cells that appear elongated and that connect each other to form a cell-cell network. Angiogenesis occurs spontaneously. Supplementation with 18 ng/ml VEGF didn't increase the angiogenic score. On the contrary, we observe even less number of branches with an angiogenic score of 62.5% (±47.87) compared to 100% in control cells (Figure 41A). In Figure 41B, EAhy-926 cells were co-cultured with Ishikawa cells at the same density or were incubated with 24h conditioned media from Ishikawa cells cultured with and without a

matrigel matrix. We can see that conditioned media of tumour cells significantly increase the number of EAhy-926 branches. Indeed, we observe an increase of 56.6 % of branches when the endothelial cells are incubated with 24h Ishikawa cells conditioned media, with an angiogenic index of 156.6% (±43.51) compared to 100% when EAhy-926 cells are seeded alone (Figure 41B). However, the angiogenic index of EAhy-926 co-cultured with Ishikawa cells is much lower (16.67% ±28.87). This decrease can be justified by a space limiting factor as Ishikawa cells limit the space available for EAhy-926 to form cell-cell junctions. This result suggests that tumour cells can stimulate endothelial cell tube formation at distance without cell-cell interaction by releasing angiogenic molecules in the environment. To further analyse the origin of these angiogenic molecules, we assessed whether they could derive from degradation of the matrigel matrix or be delivered by the tumour cells themselves. We compared the effect of the conditioned media of Ishikawa cultured for 24h with and without a matrigel matrix (Figure 41B). We found that matrigel did not affect the growth of EAhy-926 branches. This result suggests that there is no accumulation of factors from the matrigel degradation. We can conclude that the activation of endothelial cells is due to a direct release by tumor cells of molecules that stimulate endothelial cell tube formation.

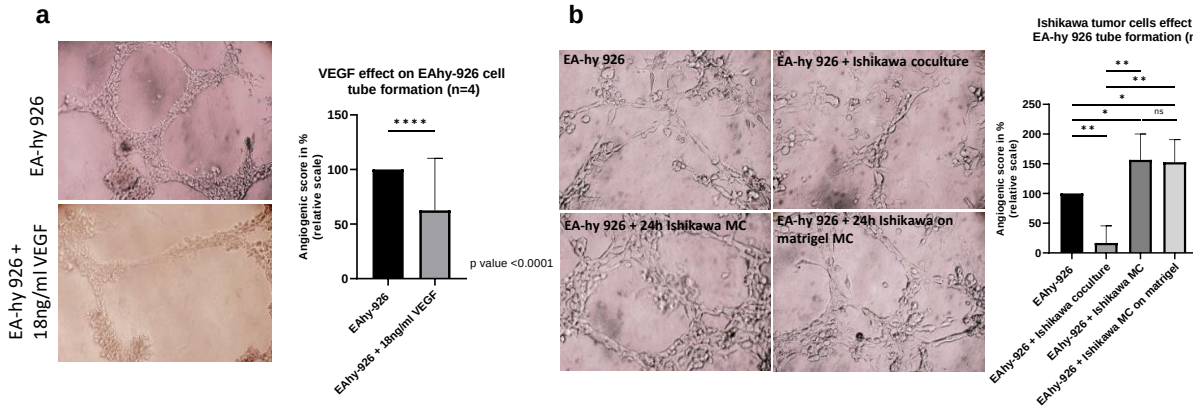

Figure 41. Tumor cells effects on endothelial cell tube formation

A: Representative images of cell tube formation and quantification of number of branches with and without VEGF supplementation. B: Ishikawa conditioned media and Ishikawa co-culture effects on endothelial cell tube formation. *, p-value≤0.05; **, p-value≤0.01; ****, p-value≤0.0001.

3.5.2 The effect of HPSE inhibitors on spontaneous endothelial cell tube formation and tumor induced angiogenesis.

We next evaluated the influence of HPSE inhibitors on tumour-induced angiogenesis by incubating EAhy-926 cells with different heparin analogues. In Figure 42A, we show that the angiogenesis induced by the MC of Ishikawa cells is significantly reduced when the MC is treated with HPSE inhibitors. We observe a mitotic index of 66.67% (±29.29), 75.67% (±25.63) and 58.66% (±8.08) when the MC of Ishikawa is treated with A6, UFH and A5-3 respectively compared to a mitotic index of 156.6% (±43.51) without treatments (Figure 42A).

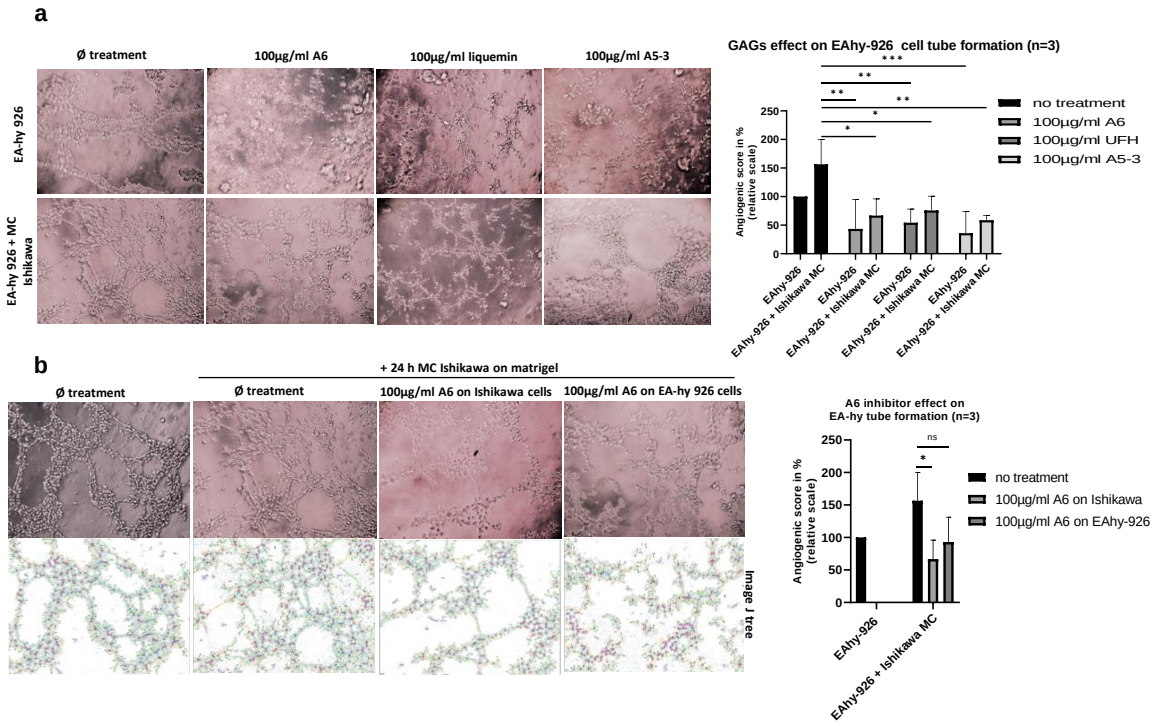

Figure 42. Effect of heparin and HPSE inhibitors on spontaneous and tumor-induced endothelial cell tube formation

A: Effect of Heparin and A6 on endothelial cell tube formation. A6 and heparin significantly reduced tumor CM-induced angiogenesis. B: A6 treatment on either Ishikawa or EAhy-926 on endothelial cell tube formation. .*, p-value≤0.05; **, p-value≤0.01; ***, p-value≤0.001.

The angiogenic score of EAhy-926 treated with 100 µg/mL UFH (liquemin), A6 and A5-3, without Ishikawa CM, is 54.33% (±23.79), 43.33% (±51.32) and 36.00% (±37.59), respectively, compared to 100% of control (Figure 42A). However, this inhibition is not statistically significant and suggests that spontaneous angiogenesis in EAhy-926 is less mediated through HPSE catabolic activity but through homeostatic processes including physiological HS-VEGF signalling. In addition, we have proven at the biosynthetic level that EAhy-926 cells produce less HPSE mRNA compared to tumor cells.

We further evaluated the action of heparin derivatives by directly treating tumour cells before collecting the CM (Figure 42B). We have found that when we incubate EAhy-926 with this 'treated' CM from Ishikawa cells, inhibition of cell tube formation is more effective. It can be explained by a possible effect of the inhibitor on HPSE production and release or it can be explained by a better inhibition of already released HPSE due to longer exposure to treatment. Further investigations should be made as today there are no evidences in litterature on the effect of HS mimetics on HPSE expression or secretion, but only on its activity. In Figure 43, we can see that A6 induces a strong decrease of HPSE expression on tumor cells but does not seems to affect HPSE expression on endothelial cells. This observation supports the fact that 24h incubation of HS mimetics on tumour cells has more impact on HPSE expression on tumor cells and thus inhibits more cell tube formation.

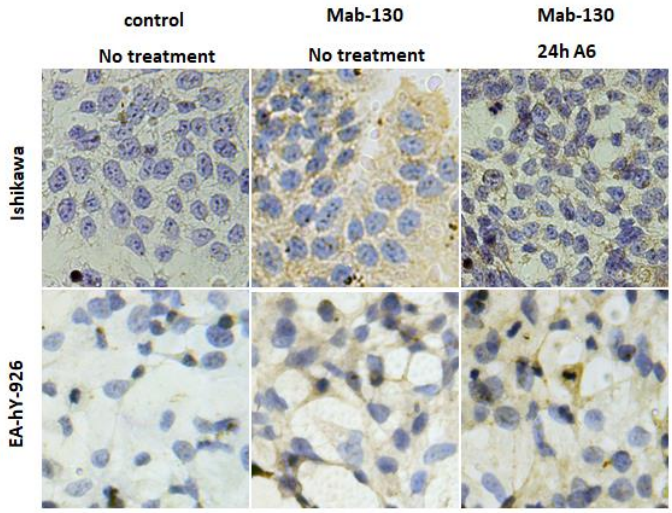

Figure 43. HPSE expression is influenced by treatment with HS mimetics.
Images showing the immunostaining for HPSE expression on Ishikawa monolayers. Interestingly, 24h of incubation with A6 induced an inhibition of HPSE expression on tumor cells. Negative controls were incubated with BSA buffer.

3.5.3 Heparin derivatives maintain cell tube structure over time.

To evaluate the stability of HS derivatives on EAhy-926 cells tube formation inhibition and to have an idea on their turnover, we have incubated EAhy-926 cells with Ishikawa MC and A6 inhibitor beyond 24h, up to 48h (Figure 44). Interestingly, the endothelial cells seeded alone giving spontaneous angiogenesis loss their branched structures. The branches which were composed of one to two layers of cells at 24h have undergone strong cell proliferation reaching a monolayer. EAhy-926 cells that were incubated with 24h Ishikawa conditioned media, however, maintained cell tubes architecture and exhibited moderate proliferation with thicker branches. This result suggests that tumour cells maintain tube formation over time. When 100µg/mL A6 is added, EAhy-926 cells exhibit the same structure of branches as 24h without increase of tube formation or cell proliferation. The HPSE inhibitor seems to freeze cell proliferation and maintains cell tube formation over time without evolution of the structure.

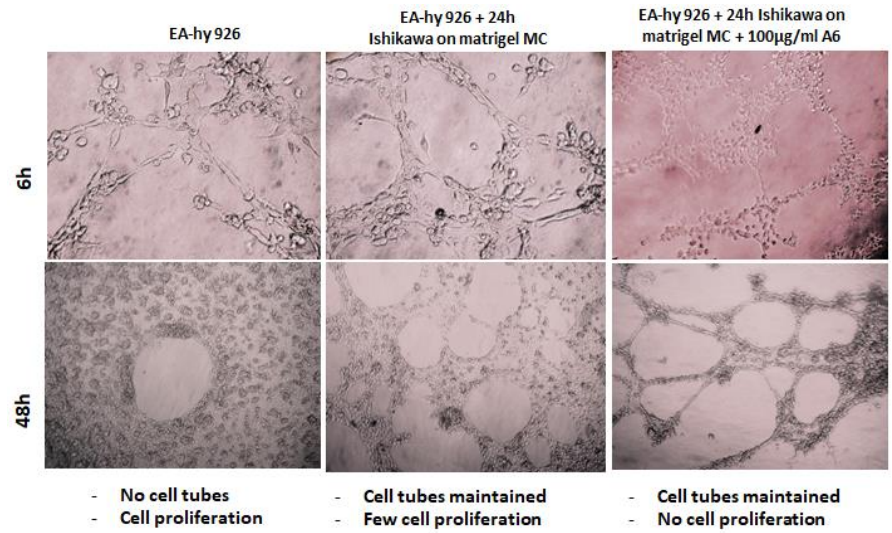

Figure 44. Effect of A6 on cell tube structure over time

Images showing the labelling endothelial cell tube structure of Eahy-926 alone, with Ishikawa CM and A6 inhibitor. Both cell lines express HPSE and aHS. Tumor conditioned media maintains cell tube formation over time with the increase of branche thickness. HPSE inhibitor seems to freeze cell proliferation and stagnate cell tube formation over time.

4. ADDITIONAL EXPERIMENTS

4.1. Verification of migration rather than proliferation.

4.1.1. The mitotic index of migrating cells.

To elucidate whether the gap reduction during the wound closure assay was due to cell proliferating in the gap we performed a BrdU incorporation assay on Ishikawa tumor cells. We observed that 16.42% (±5.32) of Ishikawa cells in the gap of the migration assay are positive for BrdU reflecting active proliferation (Figure 45A). This percentage is considered as low and not majoritary. Measurement of proliferative cells on other fields of the monolayer distant from the gap showed similar percentage of cell proliferation with 17.56 (±8.59) (Figure 45A). Cell proliferation is a process implicated in the gap closure but negligible in the measure of migration. This percentage confirms that the results measured in the wound closure assay are predominantly due to migration.

4.1.2. ɣ- and β- cytoplasmic actin expression analysis of migrating cells.

Active migration in the tumor core is driven by the actin cytoskeleton. Actins are an essential component of the cytoskeleton, with critical roles in a wide range of cellular processes, including cell migration, cell division, and the regulation of gene expression. These functions are attributed to the ability of actin to form filaments that can rapidly assemble and disassemble according to the needs of the cell. Immunohistochemistry showed that ɣ-actin is mainly organized as a meshwork in cortical and lamellipodial structures while β-actin is preferentially localized in stress fibers (Figure 45B). Actins are well known cell motility markers and hallmark of migration in wound healing, confirming that cells perform migration

through the gap and not through replication. Morphologically, cell migration involving cell polarization, lamellipodia extension, and trailing edge retraction was observed in all treatments and group control.

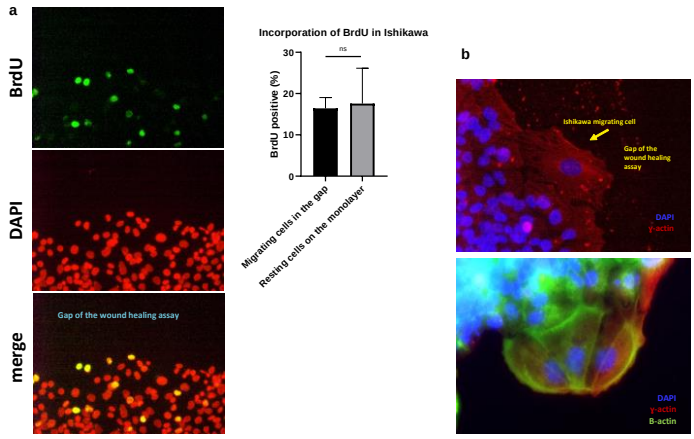

Figure 45. Verification of migration rather than proliferation

A: Evaluation of the mitotic index of migrating cells inside the gap and in the monolayer. No increase of cell proliferation was observable in the migrative cells in the gap compared to the monolayer. B: ɣ- and β-cytoplasmic actin expression on migrating cells highlight cell polarization and lamellipodia extension. Together, these analysis confirm that cells perform migration through the gap and not through replication

5. Discussion

The study of cell migration and invasion in cancer research is of particular interest as the main cause of death in cancer patients is related to metastatic progression. The ability of an EC cell to undergo migration and invasion allows it to change position within the endometrium and enter gradually in myometrium and lymphatic and blood vessels for dissemination into the circulation, and to then undergo metastatic growth in distant organs. Cancer therapeutics that are designed to target adhesion receptors or proteases have not proven to be effective in slowing tumor progression in clinical trials, this might be due to the fact that cancer cells can modify their migration mechanisms in response to different conditions [233].

To spread within the tissues, tumor cells use broad spectrum migration mechanisms that are similar to those that occur in normal, non-neoplastic cells during physiological processes such as embryonic morphogenesis, would healing and immune cell trafficking [233-235]. However, changes in the signaling pathways directing its regulation can lead to the pathological processes of tumor cell invasion and metastasis [236]. GAGs can act as a physical and biochemical barrier, creating specific microenvironments around cells [13]. The strategy of tumor cells to bypass this barrier and to induce signalling pathways activation will be to degrade TME and cell surface GAG chains in order to release bioactive molecules.

In order for cancer to spread and disseminate throughout the body, cancer cells must migrate through ECM, intravasate into blood circulation, attach to a distant site, and finally extravasate to form distant foci [237]. It has been shown on vast array of studies that HPSE is

upregulated in cancer cells and their production is shifted to an extracellular form to modulate ECM by modifying the glycosidic chains of the ECM under enzymatic degradation liberating numerous grow factors implicated in tumour spread [134]. In EC, tumour glands are characterized by increased expression of HPSE and an extensive downregulation of aHS in the cases of the most invasive glands. Those cases, characterized with an aggressive phenotype, display also a strong reduction of aHS expression in capillaries of the tumor micro-environment associated with an increasing blood proliferation index.

We hypothesised that if we could manage to reduce aHS degradation induced by HPSE, the invasion and tumoral angiogenesis will be inhibited. To inhibit HPSE activity, we used HS derivatives as mimetic substrate. HPSE will preferentially bind to those compounds instead of endogenous HS thus preserving endogenous HS.

This study aimed at screening anti-tumor lead compounds targeting HS turnover by inhibiting HPSE activity and to evaluate the cellular mechanisms of aHS regulation in tumour cell proliferation, migration, invasion and angiogenesis.

These compounds share similar structure to HS in order to maintain their binding selectivity potential towards proteins and their ability to sequestrate tumorigenic and angiogenic factors. Particularly, the chosen sulfated GAGs and heparin derivatives used are mostly able to interact with HS-bindign proteins and some show anti-HPSE activity. The biological activity of GAGs depends on several properties, such as molecular weight, monosaccharide constituents, and bonds between the disaccharide repeating units. Among these properties, negative charge, which is intrinsic to all GAGs, is paramount and is generally associated with the presence of sulfate groups, although also carboxyl groups contribute to a minor extent. A large screening of these compounds with diverse structural features including polysaccharide size, degree and pattern of sulfation, anticoagulant activity, N-acetylation of hexosamines and glycol-splitting of uronic acid was performed in comparison with standard heparin.

Heparin and HS are sulfated glycosaminoglycans that are produced by the same biosynthetic steps [238]. In vitro experimental evidence demonstrated that heparin and the HS derivatives were strongly effective drugs against tumour cell migration and slowed the gap closure speed with respective values of -18.06% and -52.62% on a concentration 100µg/ml compared to non-treated cells. Our resulted showed that the anti-migratory action of the compounds was associated with sulfation rate [239, 240]. Changes in the degree of sulfation and/or the pattern of GAGs including CSs and HSs are associated with breast [241, 242], ovarian [243, 244], colorectal [245], prostate [246, 247], and gastric [248] cancers, among others. In most cases, these changes have been proposed as cancer biomarkers [249].

Our most effective HS derivative, A6, was further selected for 3D-invasion and proliferation assay. This HPSE inhibitor displayed remarkable inhibition of tumor cell invasion. We counted a mean of 49.50 (±10.55) of invasive cells/field with 100µg/ml A6 compared to 387.6 (±39.63) invasive cells/ field in control. A6 also decreased Ishikawa tumor cell proliferation in a dose-dependent manner starting from 25µg/ml. A6 displayed a antiproliferative, antimigration and antiinvasive activities without proapoptotic activity suggesting a global safety for use. Endothelial cells tubes formation was increased by 56.6%

when incubated with 24h CM from Ishikawa cells, highlighting the fact that tumor cells stimulate endothelial cell tube formation at distance without cell-cell interaction. Indeed, in the previous study on EC, large aHS negative halo on blood vessels was seen reaching more than 400µm from tumor front. The TME of these cases was characterized by strong increase of endothelial proliferation suggesting a tumor-TME cross-talk. Inhibitor A6 significantly decreased the number of branches induced by the CM of Ishikawa cells as well as endothelial cell proliferation on branches over time, suggesting that the pro-angiogenic molecules released by tumor cells can be trapped by the drug.

Since many processes are affected, the molecular mechanism underlying these molecules is quite complex and have not been fully defined, a consequence of the pleiotropic effects diplaied by HS. Here we suggest three possible mechanisms of action. The anti-cancer potential of HS derivatives is due to their ability: (1) to inhibit HPSE activity, an indirect action in which inhibition of HS degradation will inhibit the release of pro-tumorigenic molecules; (2) to bind to free pro-tumorigenic molecules such as GFs, a more direct action; and (3) to induce a turnover in which endogenous HSPGs are released from the cells to the TME to trap free pro-tumorigenic molecules. Indeed, these mimetics are rationally designed to increase potency and binding selectivity towards specific proteins involved in disease manifestations [229].

aHS turnover was analysed in this study. We observed that under 100µg/ml A6 treatment, the amount of extracellular aHSPGs increased in the conditioned media of tumor cells. The first obligatory step in HS degradation is the cleavage in smaller fragments by the endoglycosidase HPSE. Since intracellular degradation of HS requires HPSE cleavage, in the absence of full HPSE activity, HSPG should be preferentially recycled to the cell surface where they can be shed in soluble form in the extracellular space by proteases or directly released in the extracellular compartment via exosomes thus catching pro-angiogenic molecules, such as fibroblast growth factors (FGFs) and vascular endothelial growth factor (VEGF), and inhibiting cell tube formation. It has been found that soluble HSPGs and heparin promoted differentiation in neuroblastoma and decreased proliferation through FGFR1 and ERK phosphorylation [149]. Surface and soluble Sdc-1 have opposing actions on EMT signalling.

In addition to that, HPSE released by tumor cells are trapped by the compound thus inhibiting degradation of the glycosidic chains and endogenous heparin/HS content presents on the cell surface and in the ECM. As the matrigel matrix is essentially being composed of glycoproteins, the barrier will therefore not be degraded and the cells will not be able to cross and pass through the porous membrane of the Transwell and thus inhibiting tumoral invasion. In addition, by limiting HS degradation, the HS derivatives maintain the sequestration of numerous grow factors thus inhibiting the activation of pathways implicated in mitotic activation, migration and angiogenesis. Indeed, HPSE have been shown to promote signal transduction, including Akt, STAT, Src, Erk, HGF-, IGF- and EGF-receptor signaling [131]. Moreover, HPSE regulates the transcription of many other factors spanning from proangiogenic (i.e., VEGF-A, VEGF-C, COX-2, and MMP-9), to pro-inflammatory (i.e., TNFα, IL-1, and IL-6) and mitogenic (i.e., HGF) factors [250]. A recent study showed that supersulfated low-molecular weight heparins reduce synovial sarcoma growth and metastases in vitro and in vivo by interfering with the activity of HPSE, GF/receptor axes and

proinflammatory molecules [251]. In addition, inhibition of angiogenesis by HS derivatives have been shown to be mediated through heparin which act as ligands for P-selectin, thereby blocking binding of P-selectin to its natural and tumor mucin ligands [252].

And finally, GAGs analysis revealed that in addition to HPSE inhibition by heparin/HS mimetics through specific binding, GAGs can also inhibit side effects of HPSE, by acting primarily on GFs and chemokines, without direct interaction with HPSE. Indeed, the anti-migration potential of DS suggests that GAGs treatments can potentially trap available bioactive molecules released in the conditioned media to reduce cell-cell signaling, signal transduction activation and migratory potential of tumor cells since no binding of DS with HPSE have been described.

Collectively, these results confirmed our working hypothesis that inhibition of aHS degradation through HS mimetics correlates with inhibition of tumorigenesis-related processes including tumor cell proliferation, migration, invasion and angiogenesis. HS mimetics play a protective role to prevent pathological tissue remodeling. Such molecules could be interesting as new therapeutic tool to treat, in addition to the standard of care, highly invasive EC patients that have higher risk of metastatization, had relapsed or were refractory to standard therapy .This analysis focused on evaluation of HS derivatives in our cancer model and gave ideas on the mechanisms beneath. A deeper analysis of mechanisms and underlying pathways should be investigated to complement this study.

6. Material & Methods

Cell culture

The Ishikawa human endometrial carcinoma cell line is a well-differentiated epithelial-like morphology cell line derived from primary tumor characterized by PTEN mutation without mutation in p53, a signature of early grade EC. Ishikawa cells were grown in Dulbecco's modified Eagle medium (DMEM) (Sigma-Aldrich, USA) supplemented with 10% fetal bovine serum (FBS, Gibco Life Technologies, USA) and 1% penicillin-streptomycin at 37°C and 5% CO_2.

Angiogenesis analysis was performed using the Eahy-926 human endothelial cell line. The cells were derived from the fusion of Human umbilical vessel endothelial cells (HUVECs) with the immortal human lung carcinoma cell line thioguanine-resistant clone of A549. EA.hy926 cells were grown in F12 supplemented with 10% FBS and 1% penicillin-streptomycin at 37 °C in 5% CO_2 atmosphere. EA.hy926 hybrid clones were selected in 1% supplemented HAT medium.

Anti-heparanase activity of the glycans

The anti-HPSE activity was performed by Jin-ping Li (Uppsala, Sweden) in term of a collaboration. HPSE enzymatic activity was determined using a time-resolved fluorescence energy transfer-based (TR-FRET–based) assay (Cisbio). All compounds were dissolved and diluted to different concentration using sample buffer (50 mM Tris-HCl pH 7.4, 0.15 M NaCl, 0.1% protease free BSA, 0.1% CHAPS). 3 ul of compound solution or sample buffer (as a

control) and 7 ul semi-purified HPSE solution or sample buffer (as a blank) were added into 384-well low volume microplate. After 10 min pre-incubation at 37°, an enzyme reaction was initiated by adding 5 ul Biotin-HS-Eu (K) (4.2 ng in 0.2 M Acetate buffer pH 5.5) to each well, and the plate was incubated for 30 min at 37°. To stop the enzyme reaction and detect the remaining substrate, 5 ul streptavidin-d2 (12 ng in 62.5 mM Hepes pH 7.4, 0.8 M KF, 0.1% protease free BSA, 2 mg/ml heparin) were added into each well. After 15 min incubation at RT, the HTRF signal was measured by POLARstar OMEGA reader using the following setup: excitation filter 337 nm, emission filters 620 nm and 665 nm. Each reaction was run in triplicate.

Anti-Sulf activity of the glycans analysis

The anti-sulf activity of HS mimetics was done by Romain Vivès in the term of collaboration (Univ. Grenoble Alpes, CNRS, CEA) under the following procedures:

Aryl-sulfatase assay

Arylsulfatase activity of recombinant WT and mutant HSulf-2 was assessed using the fluorigenic pseudo-substrate 4-methyl umbelliferyl sulfate (4-MUS), as described previously [253]. Briefly, 0.01 to 100µg/ml of HS mimetics were incubated with 2 µg of HSulf2-WT for 20 min, then 20mM 4-MUS was added in 50 mM Tris 10 mM $MgCl_2$, pH 7.5 for 2-4-24h at 37 °C. Reaction was monitored by fluorescence measurement (excitation 355 nm, emission 460 nm) [231].

Endosulfatase assay

25µg of digested heparin was pre-incubated with 2 µg of HSulf2-WT for 20 min then the different HS mimetics were added in 50 µl of 50 mM Tris and 2.5 mM $MgCl_2$, pH 7.5 for 4 h. The enzyme was inactivated by heating the sample at 100 °C for 5 min, then an aliquot of the digestion products (~ 1/10) was exhaustively degraded into disaccharides by incubation with heparinase I, II and III (Grampian enzymes, 10 mU each) in 100 mM sodium acetate, 0.5 mM $CaCl_2$, pH 7.1 and for 48 h at 37 °C. Detection of products (IdoA2S-GlcNS) and substrates (IdoA2S-GlcNS,6S) was performed by RPIP-HPLC as previously described [84]. Samples were injected onto a Phenomenex Luna 5 µm C18 reversed phase column (4.6 × 300 mm, Phenomenex) equilibrated at 0.5 mL/min in 1.2 mM tetra-*N*-butylammonium hydrogen sulfate (TBA) and 8.5% acetonitrile, then resolved using a multi-step NaCl gradient (0–30 mM in 1 min, 30–90 mM in 39 min, 90–228 mM in 2 min, 228 mM for 4 min, 228–300 mM in 2 min and 300 mM for 4 min) calibrated with HS disaccharide standards (Iduron). Post-column disaccharide derivatization was achieved by on-line addition of 2-cyanoacetamide (0.25%) in NaOH (0.5%) at a flow rate of 0.16 mL/min, followed by fluorescence detection (excitation 346 nm, emission 410 nm).

aHS expression analysis by Ligand-binding histochemical staining

Ishikawa cells were grown on 0.1% gelatin coated glass coverslips until reaching 70% confluence. Cells were fixed with MeOH at -20°C for 5 min. aHS was detected in a ligand binding assay using biotinylated antithrombin (AT-b) as previously described. aHS was labelled with a Streptavidin-peroxidase HRP from DAKO (K5001), followed by

diaminobenzidin revelation and counterstained with hematoxylin . Wild type murine uterus was used as positive control tissue. Negative controls were incubated with BSA buffer without AT.

HPSE expression analysis by immunohistochemistry

Ishikawa cells were grown on 0.1% gelatin coated glass coverslips until reaching 70% confluence. Cells were fixed with MeOH at -20°C for 5 min. HPSE was detected using the monoclonal mouse anti-human HPSE antibody IgG1K Mab 130 (Chemie Brunschwig #INS-26-1-0000-21) and was labelled with a second antibody coupled to peroxidase from Envision+System HRP anti-mouse (DAKO K40019), followed by diaminobenzidin revelation (DAB+). Histological sections of first and last trimester human placental villi, known to highly express HPSE, were used as positive control tissue. Negative controls were incubated with BSA buffer.

Analysis of HS3ST1 mRNA expression

To examine the expression of hs-3-O- sulfotransferase-1 (HS3ST1), key synthetic enzyme of aHS AT-binding pentasaccharide sequence, at the mRNA level, cDNA was synthesized from two µg of total RNA using the SuperScriptTM III First-Strand Synthesis System (Invitrogen, CA). The mRNA expression of HS3ST1 was analyzed using RT-PCR and quantitative real-time PCR (qRT-PCR). Quantitative real-time PCR was performed on a LightCycler® 480 Real-Time PCR System (Roche Applied Science). GAPDH was used as a reference gene, and the relative expression level was calculated using the ΔCT method (ΔCT= CT of GAPDH - CT of HS3ST1). The primers used were ALL-F (5′-AGCTTCTGCGAAAGCGG -3′) and ALL-R (5′-GCCTTGTAGTCCACATTGAGC-3′) for human HPSE; glyceraldehyde 3-phosphate dehydrogenase (GAPDH) R (5′-TCCACCACCCTGTTGCTGT-3′) and GAPDH-F (5′-ACCACAGTCCATGCCATCAC -3′) for human GAPDH. PCR conditions for HS3ST1 included an initial denaturation of 3 minutes at 94 °C followed by 34 cycles of denaturation at 94 °C, annealing for 45sec at 58 °C, and extension for 45sec at 72 °C. PCR conditions for GAPDH included an initial denaturation of 3 minutes at 94 °C followed by 24 cycles of denaturation at 94 °C, annealing for 45sec at 60 °C, and extension for 45sec at 72 °C.

HPSE RNA Isolation and Reverse Transcription

RNA was isolated with TRIzol reagent (Life Technologies, 15596-026), according to the manufacturer's instructions, and quantified by spectrophotometry. After oligo(dT)-primed reverse transcription of 500 ng of total RNA, the resulting single-stranded cDNA was amplified using Hot Start Taq polymerase and buffer (TAKARA BIO INC, RR037A). The primers used were ALL-F (5′-GTCCTGACATCGGTCAGCCT -3′) and ALL-R (5′-CACATAAAGCCAGCWGCAAA-3′) for human HPSE; glyceraldehyde 3-phosphate dehydrogenase (GAPDH) R (5′-CCATCCACAGTCTTCTGGGT-3′) and GAPDH-F (5′-ATCACCATCTTCCAGGAGCG -3′) for human GAPDH. PCR conditions included an initial denaturation of 4 minutes at 94 °C followed by 30 cycles of denaturation at 56 °C, annealing for1 minute at 60 °C, and extension for 1 minute at 56 °C. Aliquots (6 µL) of the amplification products were separated by electrophoresis through a 2% agarose gel and visualized by Sybr

green staining. The intensity of each band was quantified using ImageJ software. Only RNA samples that gave completely negative results in PCR without reverse transcriptase were used to rule out the presence of genomic DNA contamination.

Conditioned media (CM) collection

Cells are plated in t25 cell culture flask. When the cells are post-confluent, cells are washed with PBS 1X and 10 mL of DMEM low glucose (+ 100 µg/mL of acid treated BSA) were added. After 24H, conditioned media is collected. The conditioned media is centrifuged at 600 rcf for 5 minutes in order to remove cell debris.

Soluble aHSPG analysis by Ligand-binding assay

A dot blot analysis of Ishikawa tumor cells and Eahy-926 human endothelial cell conditioned media was performed to evaluate the effect of HPSE inhibitor on aHSPG release. Cells were incubated with A6 IFREMER inhibitor at a concentration of 100µg/ml for 24-hours in FBS-free media. CM was then loaded with CM (30 - 100 ul) and proteins immobilized on the nitrocellulose membranes (NC). aHSPG was detected using AT-b and was labelled with Streptavidin-peroxidase followed by ECL detection. LTA cell line was used as aHS positive control and was used for standard dilution curve. LA9 cell line was used as aHS negative control signal. To ensure the specificity of aHSPG binding-AT a competition assay was done by co-incubation of AT-b with UFH and DxS at a concentration of 100µg/ml, as competing and non-competing GAG, respectively. Since NC binds proteoglycans and not glycosaminoglycans, the HPSE inhibitors did not bind to the NC (data not shown).

Cell proliferation and viability analysis

Cells were seeded on a 24 well plate at initial concentrations of 10 x 10^6/ well and 40 x 10^6/well for Eahy-926 and Ishikawa lines respectively. The cells were incubated for 72h with 500µl of media containing or not treatments of heparin derivatives at 25-50-75 and100 ug/ml. Before counting, cell were washed with PBS and incubated 1 minute with trypsine and 0.4% trypan blue stain. Cells were counted using a haemocytometer counting chamber. Final concentrations were calculated and % of proliferation was calculated and normalized to the non-treated well. Cell viability was also calculated by measuring % of dead cells colored with Trypan blue among total number of cells. Duplicate wells were used to stain the monolayer with crystal violet to illustrate cell proliferation and snap shot images were taken using a 40× objective. The experiment was repeated 3 times.

Cell migration analysis by wound closure assay

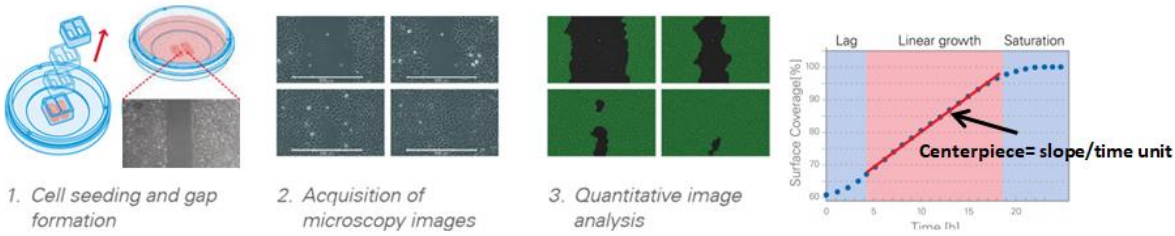

Figure 46. Steps of the wound closure assay

Cells are first seeded on the two chambers of the Ibidi insert. When reaching confluence, the insert is removed and the wound closure speed is quantified by taking snap shot images. Quantification was performed using ImageJ software by measuring the surface coverage over time. The velocity was calculated from the centrepiece.

Ishikawa tumour cells migration was assessed using Ibidi™ culture inserts (Thistle Scientific Ltd, UK) and we compared the effects of HPSE inhibitors on wound closure's speeds. Briefly, the inserts consist of two chambers separated by a 0.5mm divider, each chamber with a growth area of 0.22cm^2. The inserts were installed into 35mm tissue culture dishes using sterile tweezers. Cell suspensions were prepared at 7-9x10^5 cells/ml in medium, of which 70µl was transferred to each chamber. The cells were left to adhere and grow to confluence. The inserts where then removed leaving a 500 µm diameter gap between each chamber. The cells were then exposed to fresh treatment and/or suplemented media and decreasing wound size over time were measured by taking Snap shot images with an inverted microscope. The measurement of decreasing wound size over time was performed using Image-J software. For each time, we measured the migration distance *[cell covered area at T0 – cell covered area at T]* in µm and the percentage of slowdown relative to the non-treated control *[100 - (%Treatment TimeT * 100 / %Ctrl- TimeT]* and the percentage of cell-covered area at different time points according to 100% for hole observation area covered, were calculated. The cell-covered area, which is given for each analysed picture, is an absolute value that is dependent on the observation area, magnification and width of the gap. Thus, it must be normalized for comparison with other experiments. To this end, we evaluated the center piece approximation which is the slope of the linear growth phase *[% coverage/time unit]* that will give us the characteristic increase of the cell-covered area. We converted the center piece approximation into a normalized value which is the cell front velocity in µm/h *[(total area of microscopic picture in µm2 * center piece approximation in %/h)/2* height of the picture in µm]*. A total of 4 experiences was performed.

Determination of mitotic index of migrating cells

In order to discriminate whether reduction of wound closure is due to migration of cells or to proliferation, we evaluated the mitotic index of cells in the gap during the wound healing by performing a 5-bromo-2'-deoxyuridine (BrdU) incorporation analysis. We first proceeded to a migration assay as usual on a 6 wells plate. At 48h of migration, cells were serum deprived with 0.2% BSA 24h to synchronize the cell cylce before BrdU incorporation. The cells were

then incubated during 18h at 37°C in complete medium containing 0.01M of BrdU generously given by Marie-Luce Bochaton-Piallat. This synthetic nucleoside which is an analogue of thymidine is incorporated in newly synthesized DNA of replicating cells (during the S phase of the cell cycle) activated by serum. 18 hours after incorporation and before any other new cell replication (occurring in 35.14 ±2.68h approximatively) the cells were then fixed with MetOH. DNA was hydrolyzed with 1M HCL and then was neutralized with 0.1M BORAX solution. BrdU detection was finaly done by immunofluorescence using the monoclonal mouse anti BrdU Clone Bu20a (1/5) (DAKO, M0744) and the goat anti-mouse Alexa Fluor 488 antibody (Mol. Prob). Only proliferating cells expose the incorporated BrdU to the antibody and are labeled. We quantified the proliferation by calculating the mitotic index (percentage of BrdU labeled cells compared to total DAPI labelled cells) on 10 fields (approximatively 986 cells evaluated) and a total of 3 experiences was performed.

Cytoplasmic actin isoforms labelling

To further support the phenotype of migration of cells, we labelled actin filaments and focal adhesion in Ishikawa to analyse ɣ- and β-cytoplasmic actin expression of cells in the gap of the wound closure assay. We first proceeded to a migration assay as usual on a 6 wells plate using Ibidi inserts. At 48h of migration the cells were sequentially fixed with PFA 1% for 30 min at room temperature and permeabilized with cold Methanol for 3 min. Cytoplasmic ɣ-actin was detected with monoclonal mouse anti ɣ-cyto 2A3 (IgG2b) 1/100 and labeled with anti-mouse IgG2b Rhod 1/50. β-actin was detected with monoclonal mouse anti β-cyto (IgG1) 1/100 and labeled with anti-mouse IgG1 Alexa 488 1/50. These antibodies were generously given by Marie-Luce Bochaton-Piallat. A total of 3 experiences was performed.

Cell invasion analysis by 3D collagen gel invasion and Transwell assay

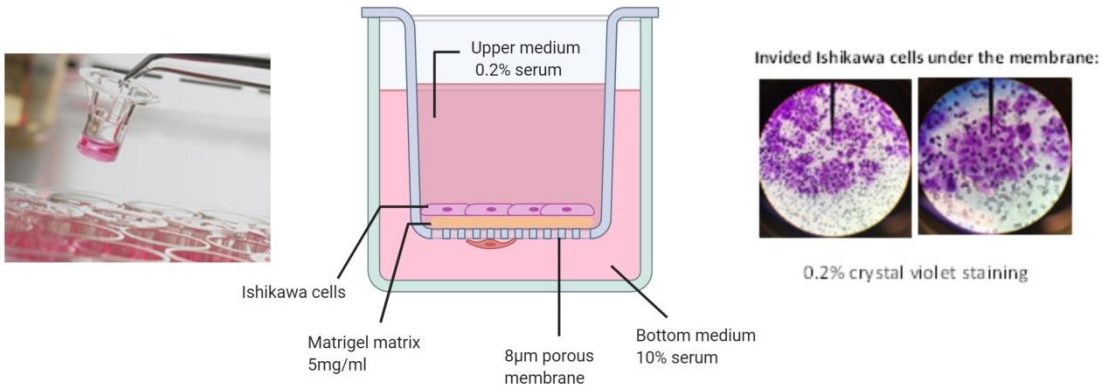

Figure 47. Schematic diagram of the Transwell.
Transwell invasion schematic with serum gradient conditions. Cells are seeded on a 5 mg/ml collagen gel and allowed to invade through the matrix and pass through 8 µm pores. Invaded cells are stained with 0.2% crystal violet.

Transwell ThincertTM 8 µm-pore 12-well cell culture inserts (Greiner Bio-One GmbH, Frickenhausen, Germany, Cat. No. 662160) were placed into the wells of a 24-well cell culture

plate. 70µl of Corning matrigel basement membrane matrix (Cat. No. 354234) at a concentration of 5mg/ml diluted in an ice-cold serum free medium was incorporated on the surface of the Transwell insert giving a gel thickness of at least 70µm (2-3 cell diameters). The plate was placed in an incubator at 37°C for 60 min to allow gelling and then was placed at 4°C to cool overnight. Cell cultures were prepared with DMEM containing 10 % FBS at standard culture conditions. For this assay, the cells were harvested and resuspended in the DMEM medium with 0.2 % BSA. 200 µl of the cell suspensions were added on the upper chamber (5.10^4 cells/well). The upper medium was then supplemented with the different treatments. Then, 500µl of the culture 10% FBS DMEM medium were added to the lower part of the arrangement of each well, where they could diffuse, forming a serum concentration gradient to attract cell from the upper chamber. The cells were incubated at standard conditions for 72 h and quantifications were made. The medium in each well was replaced after 48h and at 72h, the media in the cell inserts were removed, and the residual ECM gel in the upper chamber was also pipetted off. Cells in the lower part of the membrane was fixed with 5% Glutaraldehyde 10 min at room temperature by putting the fixative in the lower chamber. After that, the fixative was removed and the non-invasive cells on the top of the membrane were removed with dampened cotton bud 2 times. The invasive cells were then stained with 0.2% crystal violet and 2% ethanol for 20 min. The insert was then washed 3 times with PBS until the water was clear and the membrane was detached from the insert using a scalpel and mounted on slide and viewed on inverted microscope. Experiments were performed in triplicate and quantified by averaging the number of stained cells per 20x field of view counting 5 fields per chamber. Mean number of cells invading through the membrane x 100/mean number of cells migrating through the control membrane.

Analysis of cell angiogenesis by cell tube formation assay

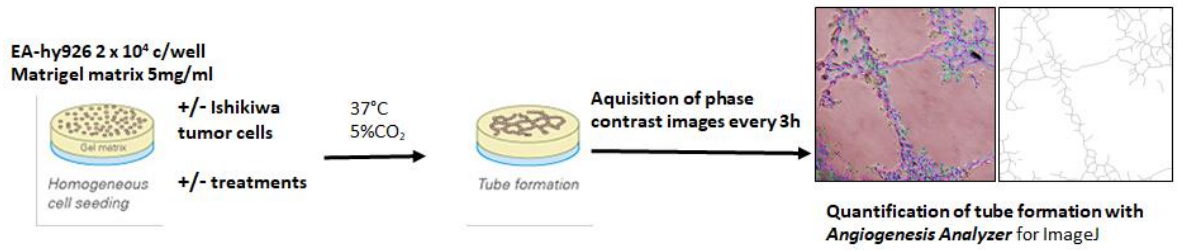

Figure 48. Steps of the cell tube formation assay

Endothelial cells are seeded on a 5mg/ml matrigel. Initially, cobblestones-like cells aggregate to cell clusters from which cells are sprouting out. Second: In those clusters cornerstone cells are formed which function as anchorage for the spindle-shaped cells. Third: Latter cells from adjacent clusters are guided chemotactically via an ATP gradient and join together to tubes. Quantification of tubes was performed using ImageJ software to detect number of branches.

A Matrigel tube-formation assay was performed to assess in vitro angiogenesis. EA-hy926 cells were seeded at 2×10^4 cells/well on a 48 well plate precoated with 200µl GF-reduced Matrigel (BD, San Jose, CA, USA) at a concentration of 5mg/ml per well. Cells were incubated with 500µl control DMEM medium. EA-hy926 cells were incubated together with Ishikawa cells at the same cell density, in coculture, or with 24h Ishikawa CM done one day before the

experiment. Test compounds with LMWH and HPSE inhibitors at concentration of 100 µg/ml were added to the medium. Aquisition of phase contrast images was taken at 0h and every 3h on inverted microscope. Five fields were counted for each well (original magnification, ×20). The mean number of branches was quantified by Angiogenesis Analyzer for ImageJ. The result was normalized to 100% for control EAhy-926 cells seeded alone without medium complementation.

Statistical analysis

Experimental data were analyzed by using Prism5 program for Windows (GraphPad Prism® Software Inc., CA, USA). When comparing the two groups, the Mann-Whitney test was applied, and to compare more than two groups, the ordinary one-way ANOVA test was applied, followed by the Holm-Šídák or Tukey test. Values are presented as mean±SEM. $p<0.05$ was considered significant.

All illustrations and graphs were created using ImageJ Fiji, Graphpad Prism and Adobe Illustrator.

Laser capture microdissection and RNA-Seq analysis: high sensitivity approaches to explore biosynthetic pathways implicated in aHSPG downregulation and tumor-microenvironment crosstalk in Endometrioid Carcinoma Grade 1 cases

Note: *This analysis was performed under collaboration with Lou Romanens and Sana Intidhar Labidi-Galy that gave us optimized LCM and RNA extraction procedures for FFPE tissues; and Petros Tsantoulis and Prasad Chaskar for the bioinformatical analysis of raw data. Data shown in this thesis result from a preliminary analysis. Some questions are still unanswered. Further investigations will be done downstream to fully investigate genes expressions.*

1. SUMMARY

While progression from normal endometrial epithelium to invasive cancer is driven by molecular alterations, tumor cells and cells in the TME are co-dependent and co-evolve. Indeed, we have shown that tumor progression was related to aHS downregulation on glands and the TME with predominance in strongly invasive phenotypes MELF, conditions allowing cell invasion and angiogenesis. These MELF tumor cases displayed a large halo of aHS negative capillaries around the tumor with the biggest index of endothelial cell proliferation. We have seen that tumor cells induce endothelial cell tube formation by releasing pro-angiogenic molecules into the ECM, thus the released signal activates distant host cells. The purpose of this study is to understand how tumor glands downregulate aHS on blood vessels of the TME across such a long distance. Few human studies to date have focused on TME. Here, we performed gene expression profiling of laser capture microdissected MELF invasive endometrial epithelial tissue and compared it to medium and less invasive IG and BF endometrial epithelial tissues, each with its immediately surrounding stroma constituting the TME. Whereas tumor epitheliums were similar in gene expression space, stroma adjacent to the tumor was significantly different in the subtypes. A stromal gene signature reflecting HS-related signalling activation and immune-related pathways was upregulated in high compared to low invasive cases. These preliminary data suggest that the microenvironment may influence EC initiation, and metastatic progression involving active implication of extracellular HPSE and Sulfatases in HS mediated pathways.

2. INTRODUCTION

As a reminder, the endometrium consists of the glandular epithelium and supporting stroma. This connective stroma is comprised of fibroblasts, myofibroblasts, smooth muscle cells, vascular endothelial cells, nerve cells, and inflammatory cells. While EC arises from the epithelial component of the gland, the surrounding stroma is increasingly recognized as an important contributor in the process of carcinogenesis and a driver of cancer progression [254, 255]. The pattern of myometrial invasion in EC varies considerably from widely scattered glands with little or no stromal response to invasive glands and cell nests, often associated with a fibromyxoid stromal reaction (desmoplasia) and/or a lymphocytic infiltrate. Numerous modifications appears accompagniying glandular invasion. At the tumoral comportment level, a glandular proliferation manifests followed by an EMT of tumor cells in MELF. At the TME level, the ECM undergoes morphological and functional remodelling in the presence of cancer cells and a visible desmoplastic reaction takes place, characterized by the pervasive growth of dense fibrous tissue around the tumor with collagen bundles and strong vasculogenesis, as previously seen. When the stromal compartment becomes reactive, normal fibroblasts are replaced by cancer-associated fibroblasts that play an important role for the TME [256] and whose increase begins around in situ lesions and evolves during endometrial tumorigenesis, being inversely proportional to tumor differentiation [257]. Signaling factors from the microenvironment influence epithelial cells to acquire properties such as increased motility, proliferation or migratory and invasive behavior [258].

The bidirectional signaling between epithelial cells and stromal constituents during normal endometrial homeostasis is disrupted early in tumorigenesis [259]. It is well established that tumor initiation and spread are complex mechanisms involving numerous interactions between tumor cells and the surrounding stroma [260]. Due to their binding properties to numerous GFs and chemokines implicated in initiation of numerous signaling pathways, heparan sulfate (HS) plays important regulatory roles in stromal-epithelial interactions in this tumor-TME crosstalk during endometrial tumorigenesis. We have explicited earlier in the introduction how the tumor influences the TME breakdown and how in return the TME influences tumor proliferation, spread and distant angiogenesis through enzymatic modifications of HS glycosidic chains and protease activity of MMPs. These assumptions are supported by the results shown in chapter 1 and chapter 2. Indeed, we have previously found that the tumor progression is related to decreased aHS expression and to the increase of the HS post-synthetic modification enzymes HPSE and Sulfs, capable of modifying the glycosidic chains of HS and to perturbe ligand-sequestering as more soluble ligands are rendered available for pathways activations. In turn, soluble cytokines and chemokines influence the interaction between the epithelial and stromal compartments during EC progression. Furthermore, aHS downregulation and vessel proliferation was more relevant in the most invasive phenotype: MELF, supporting a strong relashionship between aHS integrity and the invasion/angiogenesis processes. These MELF cases displayed the largest halo of negative aHS on TME capillaries reaching 1751µm in MELF together with the biggest index of endothelial cell proliferation. This tumor-TME cross talk was also highlighted in the second chapter where tumor cells could induce in vitro cell tube formation by releasing angiogenic molecules in their conditioned media thus sending signals

to distanced host cells. Understanding how tumor glands downregulate aHS expression on blood vessels of the TME at such long distance could be very informative in cancer research.

Most human studies have focused on the mutational landscapes in tumors in an attempt to predict biologic and clinical behavior of human EC [261, 262]. In addition, epigenetic and transcriptional epithelial signatures are associated with the degree of differentiation and are an important adjunct in predicting aggressive and indolent tumor behavior [254]. While these contribute to additional independent prognostic information, they could be further improved by knowledge of the contribution of stromal elements. Such analysis could highlight the differences of MELF pattern of invasion and could support the molecular characteristics we have noticed in the first chapter and thus confirm the necessity to reclassify MELF cases with high aHS decrease as potential risk factor for recurrent EC.

Here, we hypothesize that progression of BF mild invasive EC to most invasive IG and metastatic-like MELF patterns is driven by molecular alterations in both epithelium and stroma, and that changes in the microenvironment can potentially contribute to tumor initiation, maintenance and progression as it was seen in chapter 1 by progressive from the microenvironment influence epithelial cells to acquire properties such as increased motility, proliferation or migratory and invasive behavior [258].

Laser capture microdissection LCM has facilitated the isolation and study of specific cellular populations of both tumor glands and adjacent TME including blood vessels. This labor-intensive technology, however, limits large-scale studies. We had thus limited our study to BF, IG and MELF cases with distinct aHS expression to hilight differences according to the degree on invasion. To date, no such analysis was done on EC grade 1, thus this analysis constitute an interesting starting point to characterize more this cancer and to better understand the pathways implicated in aHS downregulation and tumor invasion and angiogenesis in EC.

3. RESULTS

3.1. Quality control of samples.

3.1.1. Experimental design

We performed gene expression profiling of laser capture microdissected tissue specimens from 29 low-grade (10 BF, 9 IG and 10 MELF) radical hysterectomy cases. For each case, we took 2 regions of interest: tumoral glands (Tumor), and each with its adjacent stroma TME (Figure 49). As complement to the first retrospective study, we took the cases from the first cohort study after aHS expression analysis to select the cases with the main characteristics. MELF cases with largest aHS distances in the TME were selected. Since long formaldehyde fixation used in FFPE blocs is critical for RNA integrity, we first performed quality control of the samples.

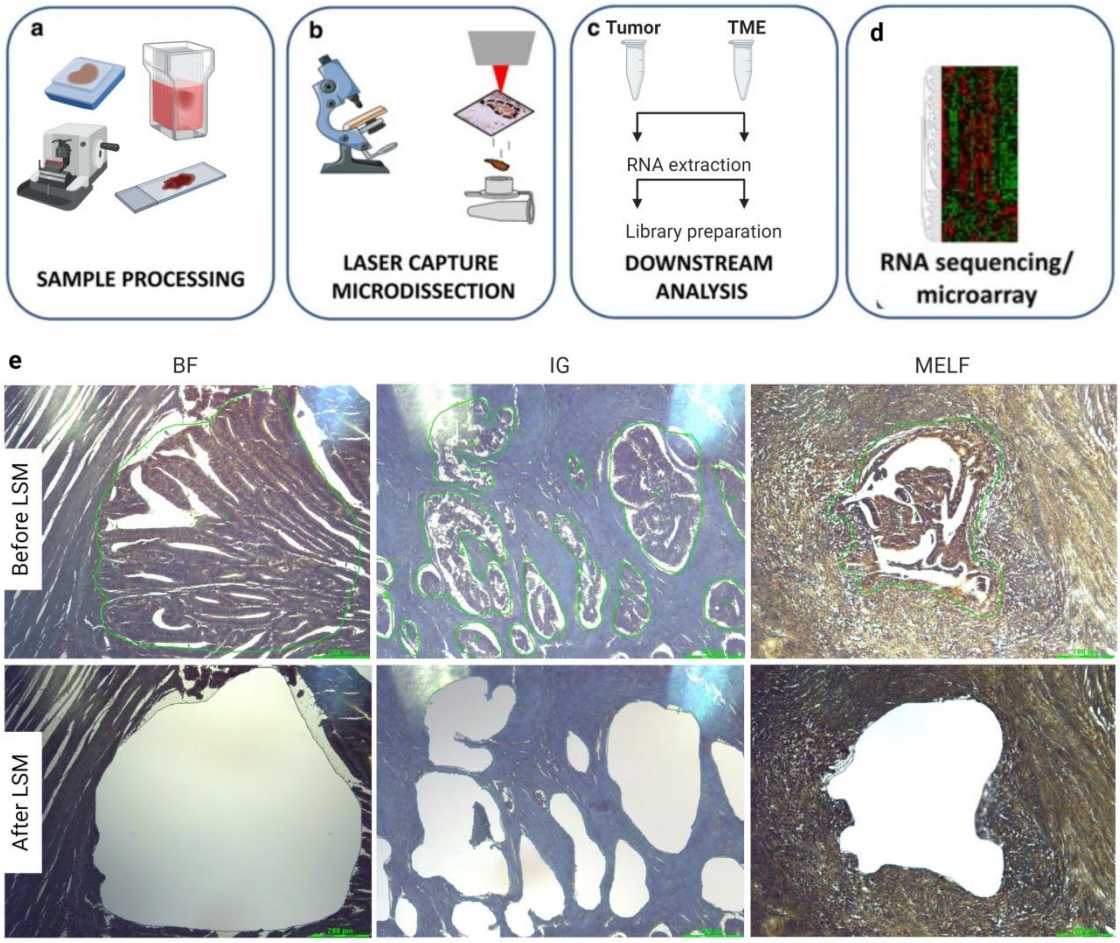

Figure 49. Laser capture microdissection LCM procedure

A: Sample processing; fresh tissue is preserved, sectioned and stained prior to LCM. B LCM; selected area is visualized under microscope, excised by laser and collected in the tube's cap. C: Downstream analysis; RNA is extracted from the area selected and used for quality control analysis. D: Applications; transcriptomic proteomic profiling is performed. E: Example of microdissection of BF, IG and MELF epithelial tumor areas of FFPE tissue sections from patients. Tumor area before and after microdissection. Adapted from [263].

1.1.1. Quality control of extracted RNA

The samples were selected according to their quality number. Only samples with a DV200 over 30% were taken. Between these samples, only samples that have suffisant amount of RNA remaining after quality control in order to perform RNA Seq (100 ng) and RT-PCR control (40 ng additional) were taken (Table 6). The total RNA normalised for 20 mm^2 of surface microdissected was calculated to evaluate the density of cell population on each subtype of myometrial invasion (Figure 50A). As expected, total amount of RNA in tumor glands is twice bigger compared to the value of TME. It can be explained by the fact that tumor glands have dense epithelial cells clustered as result of active tumor proliferation. The TME however is composed of stromal cells mixed with myometrial cells and component of the ECM. This compartment is more relaxed with larger and fewer cells per area. Identical amount of RNA was recorded between the subtypes giving an overview of good manipulation.

We then evaluated the quality control according to the age of the FFPE bloc. Interestingly, contrary to the predictions of specialists, no correlation of the age of FFPE bloc with DV_{200} value was seen in TME. Blocks dated back to 1998 gave good 46% DV_{200} (Figure 50B). Only a trend toward a decrease of DV_{200} in older blocks was observable in the tumor. This result removes the limitation barrier of retrospective studies on FFPE blocks on RNA-Seq.

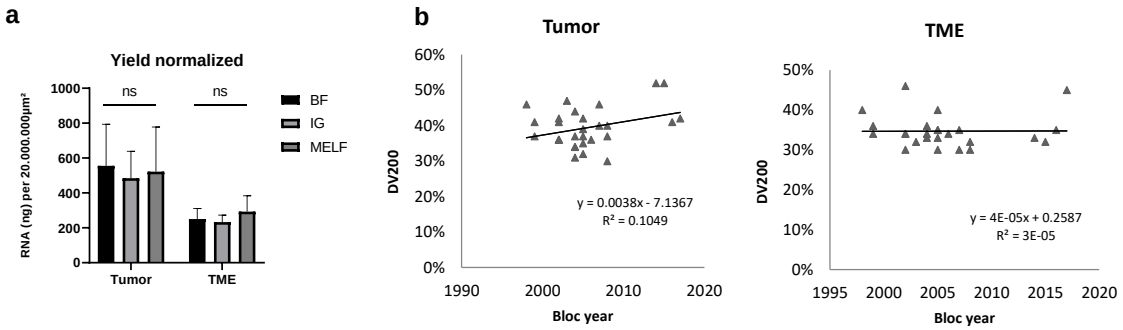

Figure 50. Quality control of extracted RNA

A: The yield /dissected surface was normalized and compared between the subtypes of myometrial invasion.
B: DV_{200} value was evaluated on each area individually accoarding to the age of the FFPE bloc.

1.1. Exploratory data analysis.

Tumor zone contains exclusively tumor epithelial cells. The TME is composed of a mixture of cells (smooth muscle cells, endothelial cells and inflammatory cells) and fibrotic connective tissue (fibroblast, collagen, HSPGs). The Principal Component Analysis (PCA) clearly separated tumor cells and TME which reflects the quality of microdissection (Figure 51A). We already observed a tendency of gene expression in MELF TME suggesting a particular morphological and functional characteristics. These results suggest that IG and BF samples are more similar to each other in the tumor as well as TME, while MELF exhibit a distinct profile. PCA showed that MELF samples were placed distinctly to the two other BF and IG on the primary PCA axis, indicating that gene expression profiles of BF and IG are more similar than MELF (Figure 51A). The distribution of tumor and TME samples according to PCA was in agreement with the dendrogram and the heat map generated based on correlation distances between samples (Figure 51B).

n° case	Type of myometrial invasion	Bloc age	Cell type	Dissected surface (µm²)	RNA ng/µl	DV_{200}	RIN	Yield (ng) remaining	Quantity for RNA-Seq (ng)
1	BF	17	tumor	13 310 951	36.4	47%	2.2	473.2	100
			TME	14 015 835	16.1	32%	2.4	193.2	100
2	BF	15	tumor	20 947 592	16.9	32%	2.3	219.7	100
			TME	18 243 256	10.7	33%	2.4	128.4	100
3	BF	16	tumor	21 721 059	33	44%	2.1	429	100
			TME	21 454 965	15.2	33%	2.5	197.6	100
4	BF	12	tumor	16 706 860	29.4	30%	2.3	382.2	100
5	BF	18	tumor	24 279 653	71.8	41%	2.2	933.4	100
			TME	19 088 013	15	34%	2.3	195	100
6	BF	18	tumor	23 987 107	67.8	42%	2.3	813.6	100
			TME	21 583 740	24.8	46%	2.1	322.4	100
7	BF	13	tumor	26 704 727	32.9	40%	2.2	427.7	100
			TME	25 000 042	17.3	30%	2.3	207.6	100
8	BF	16	tumor	27 489 018	27.1	37%	2.3	352.3	100
			TME	25 060 058	22.9	36%	2.2	297.7	100
9	BF	13	tumor	27 444 680	38.2	46%	2.2	496.6	100
			TME	24 416 062	17	35%	2.3	221	100
10	BF	15	tumor	20 618 116	47.2	39%	2.2	613.6	100
			TME	23 000 000	18.9	30%	2.3	245.7	100
1	IG	16	tumor	20 011 686	31.8	34%	2.3	413.4	100
2	IG	16	tumor	20 435 593	18.2	34%	2.3	236.6	100
			TME	20 398 056	11.6	34%	2.3	150.8	100
3	IG	15	tumor	21 461 551	36	42%	2.2	468	100
			TME	21 003 776	15.9	40%	2.2	206.7	100
4	IG	18	tumor	26 354 268	26.5	36%	2.3	344.5	100
			TME	23 930 654	16.3	30%	2.4	211.9	100
5	IG	12	tumor	26 704 727	64.6	40%	2.1	839.8	100
			TME	25 000 042	21	30%	2.3	273	100
6	IG	15	tumor	26 444 649	53.6	35%	2.4	643.2	100
			TME	26 336 824	24.3	35%	2.3	315.9	100
7	IG	15	tumor	26 000 000	49.9	37%	2.2	648.7	100
			TME	26 000 000	23.1	35%	2.2	300.3	100
8	IG	16	tumor	28 056 804	32.1	31%	2.3	417.3	100
9	IG	18	tumor	23 126 407	43.3	36%	2.2	562.9	100
1	MELF	14	tumor	20 000 000	69.3	36%	2.2	900.9	100
			TME	23 030 927	23	34%	2.2	299	100
2	MELF	12	tumor	28 000 000	58	37%	2.2	754	100
			TME	23 000 000	37	32%	2.4	481	100
3	MELF	6	tumor	28 000 000	72.9	52%	2.2	874.8	100
			TME	26 045 838	21.3	33%	2.4	276.9	100
4	MELF	5	tumor	28 000 000	22.7	52%	2.3	295.1	100
			TME	28 000 000	16.9	32%	2.3	202.8	100
5	MELF	21	tumor	25 000 000	19.3	41%	2.2	250.9	100
			TME	25 000 000	14.9	34%	2.3	193.7	100
6	MELF	4	tumor	26 000 000	32.5	41%	2.2	422.5	100
			TME	25 000 042	30	35%	2.2	390	100
7	MELF	18	tumor	26 336 824	55.6	36%	2.2	722.8	100
			TME	26 336 824	31	34%	2.3	403	100
8	MELF	22	tumor	26 800 000	44	46%	2.2	572	100
			TME	28 000 000	24.9	40%	2.2	323.7	100
9	MELF	21	tumor	29 822 971	31.3	37%	2.3	406.9	100
			TME	27 852 165	28.8	36%	2.3	374.4	100
10	MELF	3	tumor	30 000 000	49.2	42%	2.1	639.6	100
			TME	30 000 000	24.8	45%	2.1	322.4	100

Table 6. Summary table of samples used for LCM and RNA evaluation

For each case, and each sample, yield RNA was quantified as well as fragment size analysis represented by DV_{200} and RIN values. The input quantities of RNA for Sequencing were adjusted to the DV_{200} values.

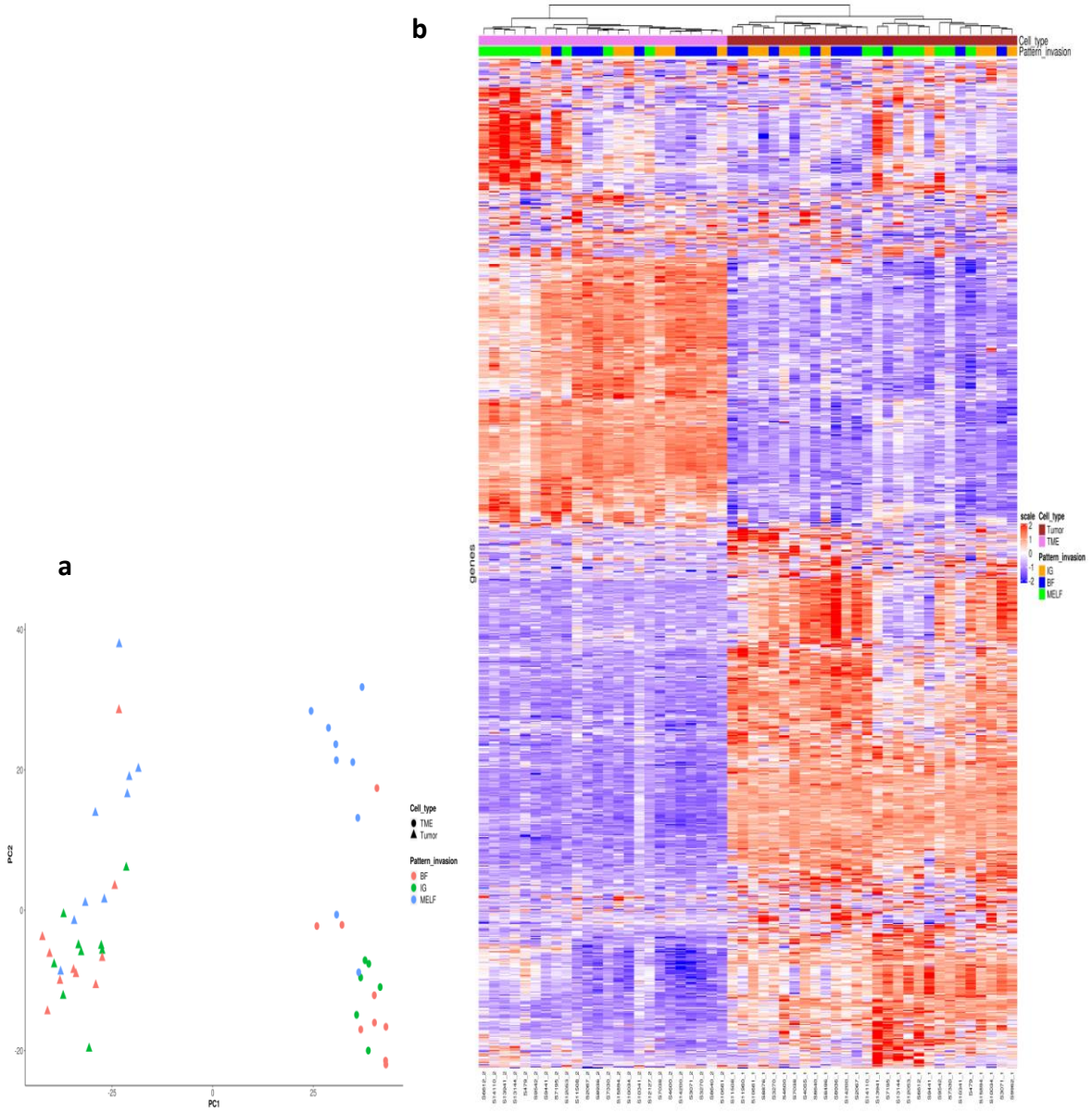

Figure 51. Correlation between heat map and Principal Component Analysis
A: Principle Component Analysis two-dimensional scatter plot (tumor and TME) of normalized expression data obtained from BF (red) IG (green) and MELF (red). B: Heatmap depicting differential gene expression in tumor and TME. Samples were clustered accoarding to the similarities in gene expression. A cluster is visible for MELF in the TME.

1.2. Differential expression analysis

1.2.1. Differences between tumor and TME compartments across progression

As expected from our experimental design, the major share of variability in gene expression was explained by differences between epithelial and stromal tissue compartments (Figure 52). We first analyzed the differences between tumor and TME on each pattern of myometrial

invasion. Some genes as well as pathways were shared across the BF tumor- TME, IG tumor-TME and MELF tumor-TME comparisons. Biological processes commonly upregulated in the epithelium, and which were maintained through “progression” to invasive tumors, included glutathion signalling and glucose metabolic regulation, metabolism of nucleotides, DNA replication pathways and regulation of mitotic cell cycle. Common processes upregulated in stroma were mostly muscle development (myogenesis) as well as changes in ECM organisation, platelet activation signaling and collagen formation. Interestingly, most cancer-related pathways upregulated in all patterns were concentrated in the TME.

Among processes upregulated in all BF TME components compared to tumor, we find TGFβ signaling pathway, JAK-STAT signaling pathway, PI3K-AKT activation and PI3K cascade, FGFR signaling pathway, PDGF and MAPK signaling (Figure 52A). Among processes upregulated in all IG TME components compared to tumor, we find PDGF signaling and integrin pathways (Figure 52B). Among processes upregulated in all MELF TME components compared to tumor, we find Toll-like receptor pathways, immune system pathways, VEGF signaling pathway, MAPK signaling, DPGF and FGFR signaling pathway, cytokines signaling in immune system and chemokine signaling. Numerous genes were also upregulated in MELF TME compared to tumor, including STAT4 Signal Transducer and Activator of Transcription, AKT oncoprotein, FGFR 1 and 4, TGF Prostaglandin receptor and TGFBR mutant transforming GF receptor (Figure 52C). These results interestingly suggest that in early grade, oncogenic genes and pathways are mostly upregulated in the TME. The TME compartment is thus an active player in the initiation and progression of the tumor. All these pathways are known to be related to HS as shown in the introduction and participate to cell proliferation (FGFR, STAT, MAPK, AKT), cell transformation (JAK-STAT), cell survival (AKT oncoprotein), cell migration (MAPK) and angiogenesis (VEGF and platelet activation signaling).

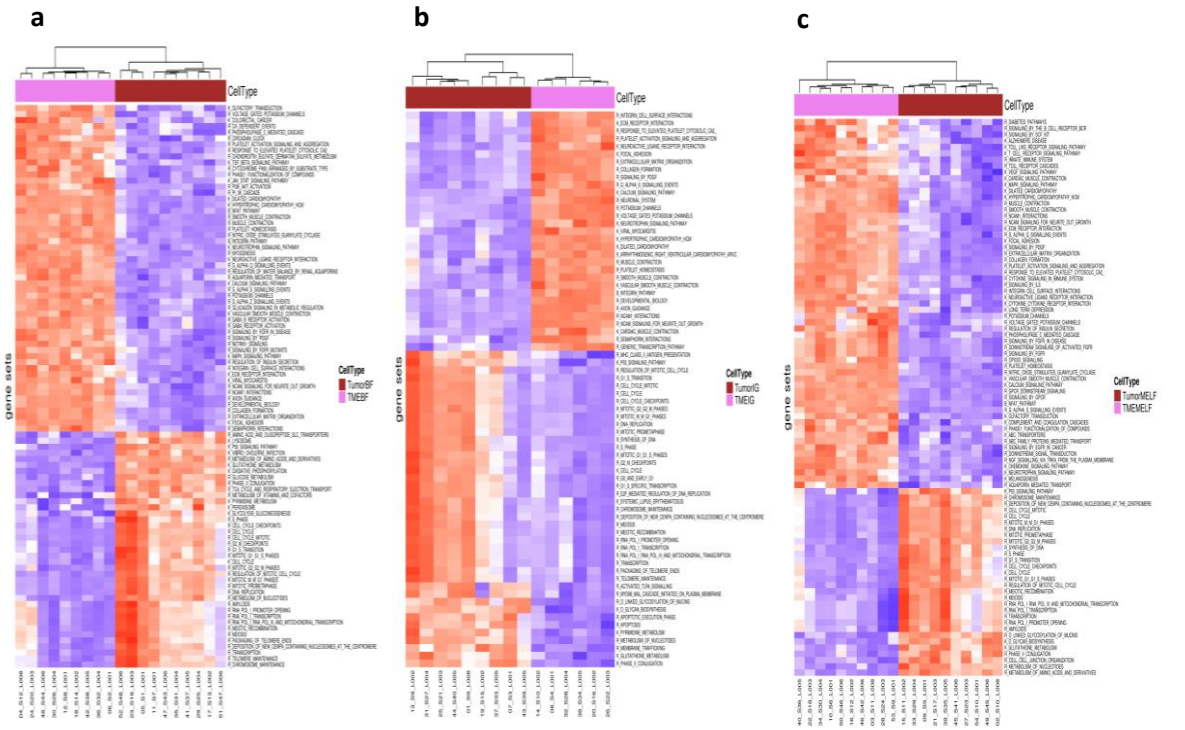

Figure 52. Heat maps of pathways upregulated in tumor and TME compartments in each myometrial invasion subtypes.

Pathways upregulated across the BF tumor-TME, IG tumor-TME and MELF tumor-TME comparisons. Most oncogenic pathways were upregulated in the TME of each subtype. Upon these pathways we find TGFβ, JAK-STAT, FGFR and MAPK signaling activation in BF, PDGF and CAM signaling activation in IG; and VEGF, MAPK, EGFR, FGFR, STAT4, AKT and CAM in MELF.

1.1.1. Differences between the patterns of myometrial invasion in the tumor compartment

We then analyzed the differences between each pattern of myometrial invasion across the tumor BF-IG, tumor BF-MELF and tumor IG-MELF comparisons (Figure 53). Few genes were shown to be upregulated in IG compared to BF. Among these genes we observed Notch4 (NOTCH4). Notch4 expression was shown to be associated with tumor migration and invasion and aggressive clinic pathological features. MELF pattern presented the most important amount of upregulated genes. One on the most interesting gene for our problematic was the Sulfatase 1 (SULF1) which is implicated in post-synthetic modification of HS chains. The level of MMPs is also elevated with a sharp upregulation in MMP 7 and MMP9. MMPs are known to be released into the ECM and participate to the shedding of membrane bound HSPGs and HSPGs from the matrix to remodel the TME and participate to activation of HS-related signaling observed in the previous figure. These results confirm that tumor cells induce functional readjustments to release enzymes capable to modify the glycosidics chains in the TME to allow tumor propagation.

1.1.2. Differences between the patterns of myometrial invasion in the TME compartment

We finally analyzed the differences in TME between each pattern of myometrial invasion across the TME BF-IG, TME BF-MELF and TME IG-MELF comparisons (Figure 53). When comparing MELF pattern to the less invasive BF pattern, we observe numerous genes activations. Among these genes, we can see MMP9 and MMP2. Sulfotransferase SULT2B1 was seen to be upregulated in MELF TME compared to BF as well as SULF1 highlighting the importance of sulfate group modifications in tumor progression. Notch4, MMP9 and MMP12 were also upregulated in MELF compared to IG pattern. SULF-1 is particularly upregulated in MELF cases while SULF-2 is seen among all the patterns of myometrial invasion suggesting a pro-invasive and cellular transforming function of SULF-2. Interestingly, HPSE was seen to be upregulated in the TME and not in tumor cells. VGFA and FGF2 were also upregulated in the matrix compartment by tumor stromal cells and capillaries. This result suggests that stromal cells seems to be activated in the TME where they upregulate pro-oncogenic genes supplementing action of tumor cells. Collectively these results hightlight the strong complementarity of TME and the tumor in cancer initiation and progression.

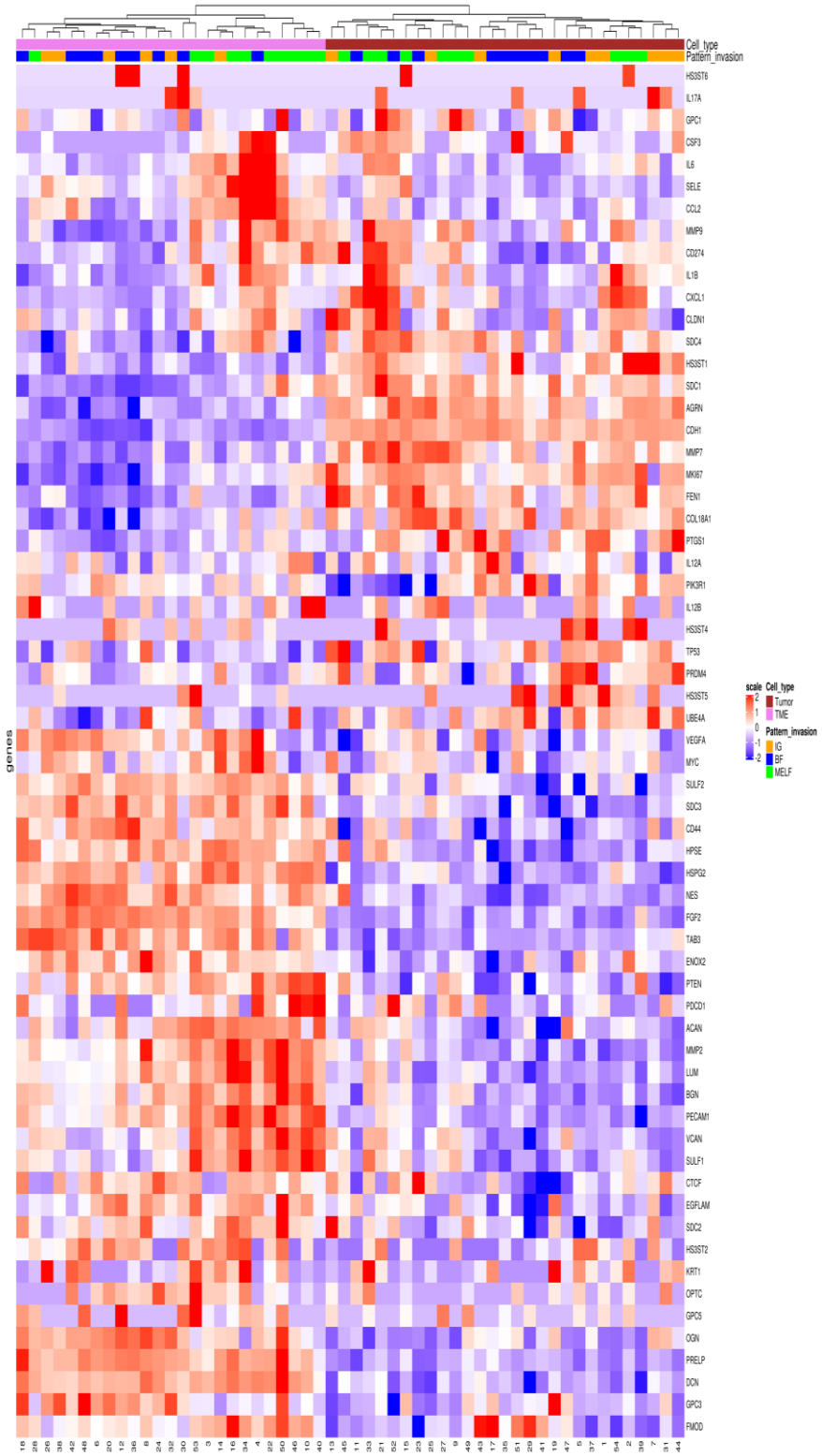

Figure 53. Heat map of genes upregulated in pattern of myometrial invasion

Genes upregulated across the tumor-tumor and TME-TME between patterns comparisons. The most oncogenic genes upregulated in MELF tumor compared to less invasive patterns are: NOTCH4, SULF1, MMP9 and MMP7. The most oncogenic genes upregulated in MELF TME compared to less invasive patterns are: SULFs, MMP9, MMP2, MMP12, VGFA and FGF2. SULF-1 is particularly upregulated in MELF cases while SULF-2 is seen among all the patterns of myometrial invasion

4. DISCUSSION

This analysis is still undergoing which prevents us from answering all the questions asked. However, preliminary results gave interesting outputs. Numerous genes associated in HS modification and degradation were upregulated in the most invasive pattern MELF compared to BF. In turn, HS modifications are thought to enhance signaling pathways implicated in tumor progression by releasing bio-available GFs and chemokines. We observed that stromal and to a lesser extent epithelial gene expression, obtained from BF areas differs significantly from that of MELF. The most characterized pathway implicated with HS signaling is FGFR-PI3K-AKT/PKB that is involved in cell proliferation and survival. MELF was also seen to upregulate MAPK signaling which results in upregulation of MMPS that in turn initiate tumor migration through shedding of core proteins in the ECM. These pathways are important in a variety of biological processes and are commonly altered in cancer. In addition platelet activation was shown to be upregulated in cancer by activation by thrombin of PAR-1. aHS and heparin are known to suppress platelet activation through AT-heparin/aHS mediated thrombin inhibition. Their anticoagulant activity was shown to be potentially associated with antitumorigenic effects as heparin-treated platelets released less VEGF[160]. We have seen that in our tumor cases, aHS was strongly downregulated in both tumor and TME. Alteration of aHS distribution in cancer is therefore also involved in VEGF pathway activation.

The two known human sulfatases, Sulf1 and Sulf2, are released as soluble enzymes that can cleave the 6-O sulfate on glucosamine in HS chains. Despite mechanistic similarities, the SULFs have opposing roles in carcinogenesis, which is best demonstrated in hepatocellular carcinoma [264]: Sulf1 suppresses FGF2-mediated tumor cell proliferation and invasion, whereas Sulf2 enhances these processes to promote disease progression [265]. Sulf1 is down-regulated in breast, pancreatic, ovarian, and head and neck cancers, where it functions to suppress tumor cell proliferation and invasion by inhibiting the co-receptor function of HSPGs [266]. Conversely, in our study we found that Sulf1 is particularly upregulated in invasive MELF cases with strongest aHS downregulation while Sulf2 is seen among all the patterns of myometrial invasion. Consistent with our result, a study published in 2017 stated that Sulf1 overexpression indicates poor prognosis in urothelial carcinoma of the urinary bladder and upper tract and thus underlined its role in promoting tumor progression [267]. Sulf2 has additional roles in the pathogenesis of non-small-cell lung cancer, pancreatic cancer, and glioblastoma despite unaltered expression levels [268, 269]. In addition, Sulf2 was shown to regulate PDGFRα signaling in malignant glioma [269]. These results demonstrate the critical importance of HS desulfation in the GF signaling in cancer cells.

The traditional consensus is that tumorigenesis is caused by mutations exclusive to epithelial cells that promote increased growth and invasive capacity, eventually resulting in metastasis. However we have seen in this analysis that the microenvironment within which the cancer cells reside plays a pivotal role in cancer initiation and progression. Furthermore, altered microenvironment may even precede genetic alterations in epithelial cells. Our results show that changes in the microenvironment are important contributors to tumor initiation and may affect progression. The major modifications observable between poorly invasive and invasive EC is principally seen on the TME.

One of the major questions was to investigate if MELF cases should be re-evaluated as grade 1 EC or should be classified into a high-risk prognosis class in result to the characterization made in chapter 1 showing major decrease of aHS along with increased tissue remodeling in both tumor and TME compartments and endothelial cell proliferation. FIGO grade is one of the strongest clinical predictors of EC progression and outcomes. An mRNA signature associated with FIGO grade improves risk stratification. In this analysis we found that MELF pattern have particular gene signatures in the tumor and TME compared to less invasive patterns. However, identical signaling pathways were shown to be upregulated in BF and MELF patterns. We identified only two signaling pathway differentially expressed between MELF and BF in the TME, VEGF and cytokine signaling in immune system. These pathways were previously shown to be associated with angiogenesis and it is known that cytokines regulate and mediate immunity and inflammation [270]. It is also known that circulating leucocytes such as neutrophils, which are released in the endometrial stroma when cells become activated, express VEGF and thus participate in VEGF pathway activation [197]. Furthermore, it has been demonstrated that HS modulates neutrophils and that in turn the activity of neutrophils is influenced by the sulfation pattern of HS [271]. This result explains the explosion in microvessel proliferation observed in MELF TME compared to BF and IG in the first chapter. However, this preliminary analysis does not allow us yet to answer the question of aHS-distances stated in chapter 1. Further differential genes expression will be investigated.

To conclude, MELF pattern expose particular oncogene signature in both tumor and TME cells and upregulate HPSE, Sulfs and MMPs that in turn will induce enzymatic remodeling of HSPGs in the TME leading to activation of HS-related oncogenic pathways. VEGF angiogenesis pathway is particularly upregulated in MELF pattern and mostly activated oncogenic pathways are found in the TME. Together these results highlight the importance of TME in tumor-stroma crosstalk.

5. Material and Methods

Tissue specimens

A total of 29 EC Grade 1 patients who underwent hysterectomy were enrolled in this study. The cases were taken from the preliminary immunohistochemical analysis of the 102 cohort study of the chapter 1. From the 29 cases, we have 10 BF cases, 9 IG cases and 10 MELF cases. For each case two samples was harvested, one from the epithelial glandular tumor and one from the TME adjacent to the tumor front. A total of 54 samples were analyzed.

Tissue processing for LCM

FFPE tissue LCM sections were cut at 8 µm. Bench, microtome and accessories were cleaned with RNAse ZAP (inVITROGEN, AM9780, AM9782). The steel frames PET Membrane Glass Slides (Applied Biosystems™ 20398) were coated with 300µl Poly-lysine overnight in a slide holder to let dry. The slides were then put under UV for 30min. DEPC treated water was used for the microtome HM 360 (ThermoFisher Scientific), the blade was cleaned with RNase away™ (Ambion). The tissue was mounted on steel Slides and mounted

tissue sections were left to dry for 30 min at room temperature. To visualize the areas of interest, tissue sections were stained with Hematoxylin according to Labidy-Galy Laboratory protocol. The staining protocol is composed of 2 min deparaffination with xylene, successive rehydratation from 100-95-75% ethanol 1 min each, and 2 min DEPC water, 1 min Hematoxylin and successive wash on DEPC water and dehydration with a final 1 min Xylene bath. To allow for proper excision performance, slides were completely air dried before microdissection. For every tissue sample that underwent LCM, a second 4µm tissue slide was stained with conventional Hematoxylin–Eosin staining and were scanned using Pannoramic 250 Flash III scanner (3D Histech, Budapest, Hungary) for validation of tissue morphology in case of uncertainty using the adapted hematoxylin stain.

Laser-capture microdissection

Before microdissection, identification of tumor glands characteristics of each pattern and their stroma was performed in supervision of a pathologist (Jean-Cristophe Tille). For Microdissection the Leica LMD7000 and Leica Laser Microdissection software were used. Laser parameters were set as follows: laser power of 39 mW, a wavelength of 349 nm, pulse frequency of 664 Hz and pulse energy of 120 µJ. Two areas were analyzed, tumor glands at the tumor front and the superficial myometrium adjacent to the tumor front to analyze tumor-TME crosstalk. Highly enriched populations of tumor glands with histological characteristics of myometrial invasion types were identified and isolated as well as the superficial myometrium adjacent to those glands. A mean of 20'000'000 µm2 of micro dissected tissue were taken per area and per case. Excised tissues were put on 0.6 ml micro centrifuge tubes suitable for the LCM device (Axygen REF MCT-060-C). The tubes were directly given for total RNA purification right after microdissection.

Isolation protocol for RNA from FFPE tissue sections

Extraction of total RNA was performed immediately after microdissection using the RNeasy® FFPE kit from Qiagen (REF 73504) according to the manufacturer's protocol with following adjustments. Microdissected cells were lysed by incubation with 10µl proteinase K and 150 µl PKD buffer (Qiagen, Hilden, Germany) at 56°C and while stirring at 400 rpm for 3h. Samples were treated with DNase I and RNA was eluted from the spin columns using 15 µl of RNAse-free water. The eluate was aliquoted before analysis and stored at −80 °C.

To reduce sample degradation, the bench and instruments required for all laboratory procedures described above were cleaned using RNAzap (Sigma-Aldrich, Missouri, USA) to minimize surrounding RNase enzyme.

RNA quantification and fragment size analysis

RNA abundance and quality was analyzed in the Genomics Platform of iGE3. Total RNA was quantified using Qubit™ RNA HS Assay Kit and Qubit® Fluorometer (Thermo Fisher Scientific, MA, USA). For RNA fragment size analysis, 5ng of each sample was run on an RNA 6000 Pico chip on the 2100 Bioanalyzer (Agilent, CA, USA) using Eukaryote total RNA Pico assay (Agilent, CA, USA). This analysis is critical for sample discrimination as processing and storing of FFPE tissues request formaldehyde fixation which gives fragmented and

degraded RNA. The RNA integrity number RIN is measured as well as the DV200 value (the percentage of fragments >200 nucleotides).

Library preparation and exome-capture RNA Sequencing

The library preparation and the Sequencing was performed in the The Genomics Platform of iGE3 and the University of Geneva. Multiplex paired-end exome-capture RNA-sequencing was performed on microdissected samples. Libraries were prepared using TruSeq RNA Exome® kit (Illumina Inc, CA, USA) according to manufacturer's protocols. The input quantities of RNA were adjusted to the DV200 values following supplier's protocol (Illumina Inc, No. 470-2014-001). For a DV200 between 30 to 50 %, samples are normalized with an input quantities of RNA of 100ng to perform RNA-Sequencing. Each library was paired-end sequenced (2 × 100 bp) in duplicate in two different flow cell lanes (50 Million reads per library in total) using the TruSeq SBS Kit v3-HS on a HiSeq2000 platform.

Data processing

Raw data processing was performed in collaboration with the bioinformatician Prasad Chaskar under the supervision of Petros Tsantoulis in the HUG. Quality control was performed on raw sequencing data using the FastQC tool [272]. Paired-end reads were aligned to the human reference transcriptome Homo_sapiens.GRCh38.cdna.all.fa.gz (release 94, obtained from ftp://ftp.ensembl.org/pub/release-94/fasta/homo_sapiens/cdna/) using Salmon v0.11.4 [273]. Salmon uses a quasi-mapping approach for the fast quantification of transcripts expression. For mapping, the --gcBias flag was used, which accounts for fragment-level GC biases (under-representation of some sub-sequences of the transcriptome) present in RNA-seq data. R Bioconductor (R version 3.6.2 and Bioconductor version 3.10) packages tximport (version 1.14.0) and DESeq2 (version 1.26.0) were used [274, 275] to summarize the transcript-level and gene-level estimates and for further down-stream analyses [276].

The dataset was filtered by discarding genes that had very low expression (gene abundance count < 10, across all samples). Variance stabilization transformation was performed using the VST function [277, 278] implemented into the DESeq2 package. To visualize the sample to sample variation, PCA was performed on the top 500 most variable genes using the built-in R function prcomp(), and the principal components obtained were visualized using ggplot2 [279]. For hierarchical clustering, the top 1000 variable genes were selected from transformed data matrix and estimated the sample-to-sample Pearson correlation distances using cor() function. Hierarchical clustering was performed with a complete linkage method using hclust() R function. A heat map was plotted using the Heatmap() function from the ComplexHeatmap R package [280].

Gene expression analysis

Differential expression analysis was performed using DESeq function from the DEseq2 R package [274] on gene-level abundance estimates from Salmon. DESeq function estimates size factors, dispersion values for each gene, fits a negative binomial model and performs hypothesis testing using the Wald test. DESeq2 performs multiple test corrections on the p-values obtained from the Wald test using Benjamini-Hochberg adjustment method. Adjusted

p-value (FDR < 0.05) and log fold change (lfcThreshold = 0.58, which corresponds to a fold change of 1.5) were used to identify differentially expressed genes between tumor cells and TME samples.

Functional analysis

Pathway annotation was performed with Gene set variant analysis (GSVA) by using KEGG, Biocarta and Reactome gene sets from the C2 collection of the MSigDB v6.2 (c2BroadSets) [281, 282]. GSVA analysis was performed on the variance stabilized expression value matrix of 1776 differentially expressed genes (adjusted p-value<0.05 and FoldChange ≥ 1.5, i.e. log2FC>0.58). Limma was used for the generalized linear model fitting on GSVA output in order to identify enriched pathways between BF, IG and MELF as well as between Tumor and TME. Benjamini-Hochberg adjustment for FDR was applied.

General Discussion

Tumorigenesis is a multi-step process. It is widely accepted that the progression of EC depends on a sequential accumulation of mutations within glandular epithelial cells. These mutations constitute an independent process that induces a metabolic reprogramming to support and enable rapid proliferation, continuous growth, survival in harsh conditions, invasion, metastasis, and resistance to cancer treatments [283]. In addition, tumor glands imperatively need the involvement of stroma cells to progress and involve complex interconnected processes. The differentiation process can reverse and tumor cells dedifferentiate to enable them to invade the host tissue by active locomotion, [284, 285], proteolytic degradation of the ECM [286] and spread by active angiogenesis. Invasion and angiogenesis are cooperative and complementary processes requiring bidirectional communication between cells and their microenvironment [287].

What drives the progression of cancer?

Because GAGs are the main mediators of communication (cell–cell and cell–ECM communication) in the intercellular space, they play a major role in malignant transformation and tumor spread [13]. Several hallmarks of cancer, such as sustained growth signaling, suppression of apoptosis, deregulated metabolism, immune evasion and angiogenesis are enhanced through pathological alterations of normal physiological processes implicating HS [288].

The work presented here sheds new light on aHS implication in physiological and pathological tissue remodeling in endometrium and documents a novel and unprecedented role of post-synthetic enzymatic modifications leading to aberrant expression of aHS in invasion and angiogenesis as potential early marker of aggressive EC. Next, the pioneering results from transcriptomic profiling of myometrial invasion subtypes, described in parallel of the immunohistochemical analysis, show new insights of gene profiling and activated pathways implicated in aHS remodeling according to the degree of invasion. Furthermore, this work reports the anti-tumorigenic potential of new customized HS mimetics in vitro, which will provide new therapeutic insights in adjuvant treatments of EC. Even if tumor and TME are profoundly interconnected, we will discuss the two topics separately based on experimental results either directed on the tumor itself to investigate tumor invasion or on the TME to investigate tumor angiogenesis.

1. aHS SUPPRESSION ENHANCES TUMOR INVASION IN EC GRADE 1

Our initial investigations on aHS and HPSE expression during estrus cycle highlighted the implication of aHS in physiological tissue remodeling occurring in the endometrium. In normal endometrial glands, in the functional zone, aHS and HPSE vary in parallel during the estrous cycle, with maximum expression in the proliferative phase and decrease in secretory. The repression peaks in the receptive endometrium during the implantation window. In the stable basal zone aHS is high and HPSE is low throughout the cycle limiting local tissue remodeling (Figure 22). Time and local limitations of aHS repression as well as low level of HPSE contains the overshoot of endometrium remodeling. Increasing expression of HPSE in the latent

precancer hyperplasia, reaches its maximum in the established cancer (Figure 29). In the same way, aHS is decreased in tumor glands compared to the healthy glands. In this work we have demonstrated that the invasive and pre-metastatic MELF glands exert extensive aHS suppression (Figure 23).

A major consequence of HPSE upregulation in cancer is a robust up-regulation of GF expression and increased shedding of Sdc-1 [289]. Here we found that MELF epithelial cells overexpress MMP9, MMP7 and HPSE that together participate in aHS degradation and Sdc1 shedding to the ECM where additional extracellular HPSE and Sulfs process further proteoglycan by enzymatic modifications on aHS chains (Figure 53). Sdc shedding was often described as enhancer of cancer progression by reducing cell-to-cell contacts and increasing the acquisition of a fibroblast-like morphology, which are both associated with cancer metastasis [288, 290]. Thus, various components of the HS signaling pathway coordinate to promote carcinogenesis. However, we observed that the release of aHSPGs in the extracellular medium was beneficial to limit in vitro tumor cell invasion in our model, suggesting that depending on the presence of HPSE activity, soluble aHSPG can have opposite functions (Figure 36, 40). When processed by a combination of degrading enzymes, aHS loses its selective binding towards ligands while intact aHSPG could at the opposite act as trap, sequestering soluble mediators such as GFs. This assessment is supported by a study where soluble HSPGs has been shown to block hepatocellular carcinoma growth by blocking WNT signaling and MAP kinase and AKT pathways [291]. Taken together, these studies and our results presented in this work underpin that aHS and aHSPGs can exert either pro- or anticancer functions depending upon the context [288].

Additionally, MELF TME is histologically characterized by strong desmoplasia with activated myofibroblast. MELF TME cells were shown to overexpress HPSE, SULF-1, SULF-2, MMP9, MMP2 and MMP12 (Figure 53). Stromal cells activated by the neighboring tumor also participate in aHSPG remodeling. Cancer-associated myofibroblasts have been proven to contribute to ECM remodeling and foster cancer cell invasion by producing MMPs, such as MMP-1-3, MMP-7, MMP-9 and MMP13-14 [292, 293]. Tumor and stromal cells act in cohesion to degrade aHS chains and the protein core of cell surface and ECM proteoglycans and participate to the disruption of the matrix priming the TME for cancer cell migration and invasion. Although loss of Sdc-1 correlates well with the gain of cancerous characteristics in a wide range of cancers [294].

Furthermore, ligand binding by HS chains depends on its pattern of sulfation. SULF-1 is particularly upregulated in MELF cases while SULF-2 is seen among all the patterns of myometrial invasion (Figure 53). In addition to enzymatic cleavage of aHS chains, extracellular removal of 6-O-sulfate groups by the endosulfatases Sulf1 and Sulf2 modulate multiple signaling pathways including the augmentation of Wnt/ß-catenin signaling [295].

Upregulation of aHSPG post-biosynthetic modifying genes by invasive tumor cells and activated TME cells will in turn induce enzymatic remodeling of HSPGs in the TME leading to desequestration of bioactive molecules from aHS chains and activation of HS-related oncogenic pathways. Among processes upregulated in all MELF we find cell proliferation (FGFR, STAT, MAPK, AKT), cell transformation (JAK-STAT), cell survival (AKT

oncoprotein) and cell migration (MAPK) (Figure 52). Transcriptomic analysis further revealed that FGF2 is upregulated in the TME of the most invasive pattern where we believe that soluble aHS enhances FGF2 binding to cells resulting by the upregulation of pathways described before.

Contrary to the expression of HS, the decrease of Sdc has been the subject of several but controversial studies in EC. The loss of Sdc-1 in EC cells has been demonstrated to be accompanied by a decrease in the activation of Erk and Akt and a concomitant decrease in the phosphorylation of PTEN and PDK1, which are known as negative and positive regulators of AKT activation, respectively [294]. Another study demonstrated that epithelial Sdc-1 expression and basement membrane expression of HS was significantly lower in advanced stage, high grade, and deep myometrial invasion while stromal Sdc-1 expression was significantly higher in high-grade tumors [296, 297].

To sum-up, HSPGs are the principal modulators of these pathways due to their binding potential toward numerous GFs, cytokines, chemokines and morphogens needed for specific receptor activation. HPSE expression upregulates protease activity and participate in the shedding and degradation of aHS chains in EC. In addition, Sulfs activity further reduces the binding potential of aHS leading to the activation of signaling pathways of invasion. aHS deletion has been demonstrated to be proportional to the degree of myometrial invasion.

This prompted us to assess in vitro, the effect of aHS degradation inhibition on human endometrial tumor cell invasion. HS mimetics with potent anti-HPSE and anti-Sulfs activities were used in this analysis. We have demonstrated that high MW HS mimetics with high sulfation degree inhibited significantly the different steps of tumor invasion including: cellular migration, degradation of the ECM-like collagen matrix and extravasation (Figure 39, 40).

Together, our results confirm that enzymatic degradation of aHS is an important player of EC invasion and treatment with HS mimetics rescues endogenous aHS and inhibits tumor invasion.

2. aHS DELETION ENHANCES TUMOR ANGIOGENESIS IN EC GRADE 1

In a similar methodology, we explored a second and not least important parameter: tumor angiogenesis. The new vessels not only help to meet the growing metabolic demands of the tumor by supplying additional nutrients, but also provide potential routes for tumor dissemination and metastasis, therefore strongly correlating to invasion [298]. Angiogenesis is the result of the combined activity of the TME and signaling molecules both implicating HS network [299]. Our analysis revealed brand new lights on aHS expression in vessels of the TME in EC. For the first time, a black negative halo for aHS has been observed around the tumor raising exciting questions about their function (Figure 26), especially since the extent of this inhibition reaches interesting distances of several hundred micrometers from the mother tumor. How is it possible?

EC Grade 1 cases with the most extensive downregulation of aHS in capillaries of the TME have been interestingly found to be the ones with the strongest aHS diminishing on glands of the tumor front and the highest degree of myometrial invasion (Figure 26, 27). This

downregulation was attributed only to pathological tissue remodeling since the labeling was strongly present without fluctuation in capillaries of endometrial stroma during the menstrual cycle (Figure 26). These aHS positive capillaries also exhibited constant proliferating index while negative capillaries in the TME showed intensive proliferation by increasing the MVP by 2- and 6- fold in less and more invasive myometrial patterns respectively (Figure 25). aHS expression on capillaries is thus a marker of integrity and its deletion coincides with endothelial cell proliferation and increase of angiogenesis.

Transcriptomic analyses revealed that, in addition to cell proliferation, pathways involved in angiogenesis and GF production- including the FGF2, platelet activation and VEGFA pathways, were amongst the most upregulated pathways in MELF cases in comparison with the less invasive cases (Figure 53). It has been demonstrated that platelet factor 4 has a high affinity for vascular aHS and its binding inhibits both FGF2 signaling and platelet activation [160, 300]. MELF TME is characterized by a strong inflammatory reaction recruiting platelets and neutrophils containing VEGF granules. Thus, in the absence of aHS in TME vessels, platelets become activated and release together with neutrophils VEGF and GFs initiating downstream pathways. The anti-inflammatory role of aHS is also crutial in this process. It have been demonstrated that aHS inhibits leucocytes-endothelial interactions [301], and the downregulation of aHS in MELF TME could help promote leucocyte recruitment into the TME.

In addition, we have demonstrated that tumor cells release pro-angiogenic molecules capable of enhancing in vitro angiogenesis, while incubation with HPSE inhibitors restores normal angiogenesis (Figure 41, 42). Two possible mechanisms underlies: HS mimetics could either neutralize HPSE inhibiting aHS degradation on endothelial cells or could neutralize released growth factors such as FGF2 or VEGF implicated in angiogenesis pathway activation on endothelial cells.

3. aHS AS DIAGNOSTIC AND PROGNOSTIC TOOL IN EC GRADE 1

To this date, the diagnosis of EC is mainly based on histological features by analyzing the extent of myometrial/other tissues invasion and the aspect of tumor cells by measuring the degree of differentiation. However, this diagnosis has a grey zone as a significant number of tumors show overlapping clinical, morphologic, and molecular features between Grade 1 and 2. A tumor classified with good prognosis could evolve rapidly into a more aggressive pattern and escape the first treatment, which subsequently gives risk to recurrence without being able to detect this subset early enough to adapt treatments.

MELF have been shown to exhibit morphological and molecular characteristics of invasive features. Epithelial tumor cells appear less differentiated with mesenchymal transformation and strong stromal reaction. However, no clinical evidences could demonstrate that this pattern of invasion is associated with increasing disease recurrence. Combination of markers in addition to histology should thus be used to better target within population.

The implication of aHS in the establishment of protective barriers has remained largely undocumented up to date, in part due to the preponderant attention focused on HPSE and Sdc-1 in cancer.

Previous investigations from our group had demonstrated that the anticoagulant form of HS is essential for the control of proteolytic activities at ovulation in granulosa cells and is involved in the control of inflammatory events occurring during tissue remodeling in hormone-responsive tissues [187].

The present work has provided more evidence that aHS expression in tumor institutes a barrier that contains the overtake of signaling implicated in tumor progression, thereby restraining pathological tissue remodeling in endometrial glands and their stroma.

The diminishing of aHS on endometrial epithelial cells was shown to be correlated with the invasive potential of tumor glands. And aHS decrease on capillaries was shown to correlate with endothelial cell proliferation and desmoplasia of the TME. Sdc-1 and HPSE expression are the main glycobiologic approaches analyzed and associated with potential prognosis in cancer [302-305]. However in the case of EC Grade1, HPSE expression alone was not able to distinguish within the invasion patterns. Our results show the potential of detecting aHS expression as a marker that could be used to discriminate within cancer population among cases with higher invasive and angiogenic features, quickly and with a simple binding assay.

4. aHS AS THERAPEUTIC TOOL IN EC GRADE 1

The data reported here for aHS derivatives could have important implications for the refinement or improvement of currently used adjuvant therapies in EC. Our results have indicated that pharmacologic inhibition of HPSE and Sulfs activities in human endometrial tumor cells restores different biological dynamic activities including: cell proliferation, cell migration and tumor induced angiogenesis in vitro. Screening for drug response of GAGs and aHS-like derivatives indicates that their activity is strongly dependent of the sulfation pattern; such polysaccharides could thus be useful for developing new delivery systems for conventional chemotherapeutic agents, even if their mechanism of action is not yet known. Preliminary results have indicated a broad action and could potentially affect multiple targets. Several possible mechanisms could be responsible for this positive interaction.

A plausible explanation is that aHS derivatives play as substrate for HPSE and Sulfs reducing degradation of endogenous aHS (Table 3, 4). It has been suggested in the literature that HPSE recognizes the same glycosaminoglycan sequence of heparin/HS than the heparin interacting protein (HIP). Because HIP was shown to compete with AT for binding to HS glycosaminoglycans [306], it appears that HPSE may cleave the chain either within or adjacent to the pentasaccharide. This finding is supported by studies that show that HPSE, purified from platelets or hepatoma cells, can cleave an octasaccharide that contains the highly sulfated AT-binding sequence [307, 308]. By binding to heparin/HS derivatives, the antithrombin-binding domain of endogenous aHS is preserved and could maintain normal level of expression.

Heparin derivatives and HS mimetics can affect tumor biological behavior by exerting pleiotropic effects through a context-specific mechanism of action based not only on HPSE

inhibition, but also on the counteraction of HSPG functions [228]. We suppose that HS derivatives also act as nets trapping released bioactive molecules in the extracellular component and thus inhibiting downstream signaling activation. Those HPSE inhibitors are designed to have increased binding selectivity towards specific proteins involved in cancer. Our results support this assumption as conditioned media treated with HS derivatives blocks stimulation of angiogenesis induced by tumor cells conditioned media (Figure 41). This mechanism is also supported by the observation that also treated EAhy-926 cells alone decreased the angiogenesis index, potentially by neutralizing GFs involved in cell-cell interaction and needed for the formation of cells junctions and tubes (Figure 42). Additionally, almost the totality of GAGs and glycans inhibited cell migration via their Sulfation degree (Figure 38).

A less apparent but not trivial implication of these HS derivatives is that the endogenous replenishment of the intracellular aHSPGs reservoir is likely to be externalized giving more extracellular availability (Figure 36). Indeed, the mere blockade of intracellular HPSE degradation in the lysosomes denuded the tumor endometrial cells of tumor functions by reducing cancer related mechanisms (proliferation, migration, invasion and angiogenesis). Intact released aHSPGs could supplement HS derivatives to neutralize GFs. Blockade acts on two distinct mechanisms, such that their combination provides a markedly superior anti-tumor response.

5. PERSPECTIVES

The present study relates the anti-tumor activities of aHS on human EC cells. Mechanisms underlying this effect are still not well understood and are likely context-dependent. These satisfactory results leave an open door to a multitude of applications and rise the interest of understanding the mechanisms to better target their actions.

The transcriptomic profiling gave light to genes and pathways potentially implicated in the process. Secondly, it would be necessary to analyze in vitro the response of inhibitors on these pathways by measuring each players. In addition, the sequestration of soluble bioactive molecules could be demonstrated by showing the formation of aHS/GFs complexes.

In addition to morphological and molecular analysis of aHS negative MELF glands, a clinical follow-up of the patients should be proceeded to evaluate concretely their implication in disease recurrence. The low percentage of EC Grade 1 patients relapsing limits our analysis. In order to prove a correlation of central recurrence in low stage-low grade MELF (+) aHS (-) EC patients, more cases should be enrolled in the study.

Changes into clinical practice could only be made if a univariate analysis could prove a direct correlation of clinicopathologic association and prognostic value with aHS decrease. However, the results presented here rise the interest to investigate more in details this approach.

References

1. Lee, W.L., et al., *Hormone therapy for patients with advanced or recurrent endometrial cancer.* J Chin Med Assoc, 2014. **77**(5): p. 221-6.
2. Aghajanian, C., et al., *Phase II trial of bevacizumab in recurrent or persistent endometrial cancer: a Gynecologic Oncology Group study.* J Clin Oncol, 2011. **29**(16): p. 2259-65.
3. Vivès, R.R., *Héparanes sulfate : Structure, fonctions, régulation*, in *Sciences du Vivant*. 2011, Université de Grenoble: Grenoble. p. 148.
4. Wardrop, D. and D. Keeling, *The story of the discovery of heparin and warfarin.* Br J Haematol, 2008. **141**(6): p. 757-63.
5. Yanagishita, M., *A brief history of proteoglycans.* Experientia, 1993. **49**(5): p. 366-8.
6. Irving M. Shapiro, M.V.R., *The Intervertebral Disc: Molecular and Structural Studies of the Disc in Health and Disease*. 2013: Springer Science & Business Media.
7. Petitou, M., B. Casu, and U. Lindahl, *1976-1983, a critical period in the history of heparin: the discovery of the antithrombin binding site.* Biochimie, 2003. **85**(1-2): p. 83-9.
8. Jaques, L.B., J. Mahadoo, and J.F. Riley, *The mast cell/heparin paradox.* Lancet, 1977. **1**(8008): p. 411-3.
9. Voigtlaender, M. and F. Langer, *Low-Molecular-Weight Heparin in Cancer Patients: Overview and Indications.* Hamostaseologie, 2019. **39**(1): p. 67-75.
10. Smorenburg, S.M., et al., *The effects of unfractionated heparin on survival in patients with malignancy--a systematic review.* Thromb Haemost, 1999. **82**(6): p. 1600-4.
11. Kakkar, A.K., *Thrombosis and cancer.* Hematol J, 2004. **5 Suppl 3**: p. S20-3.
12. Afratis, N., et al., *Glycosaminoglycans: key players in cancer cell biology and treatment.* FEBS J, 2012. **279**(7): p. 1177-97.
13. Soares da Costa, D., R.L. Reis, and I. Pashkuleva, *Sulfation of Glycosaminoglycans and Its Implications in Human Health and Disorders.* Annu Rev Biomed Eng, 2017. **19**: p. 1-26.
14. Henderson, B.E. and H.S. Feigelson, *Hormonal carcinogenesis.* Carcinogenesis, 2000. **21**(3): p. 427-33.
15. Harrison, R.J., *Human reproductive system*, in *Encyclopædia Britannica*. 2020, Encyclopædia Britannica, inc.
16. *The endometrium-specific proteome*.
17. Yu, N.Y., et al., *Complementing tissue characterization by integrating transcriptome profiling from the Human Protein Atlas and from the FANTOM5 consortium.* Nucleic Acids Res, 2015. **43**(14): p. 6787-98.
18. Curry, T.E., Jr. and K.G. Osteen, *Cyclic changes in the matrix metalloproteinase system in the ovary and uterus.* Biol Reprod, 2001. **64**(5): p. 1285-96.
19. Gellersen, B. and J.J. Brosens, *Cyclic decidualization of the human endometrium in reproductive health and failure.* Endocr Rev, 2014. **35**(6): p. 851-905.
20. Zieba, A., et al., *The Human Endometrium-Specific Proteome Defined by Transcriptomics and Antibody-Based Profiling.* OMICS, 2015. **19**(11): p. 659-68.
21. Deroo, B.J., et al., *Estradiol regulates the thioredoxin antioxidant system in the mouse uterus.* Endocrinology, 2004. **145**(12): p. 5485-92.
22. Lai, C.Y., et al., *Identification of UAP1L1 as a critical factor for protein O-GlcNAcylation and cell proliferation in human hepatoma cells.* Oncogene, 2019. **38**(3): p. 317-331.
23. Denis, C.J. and A.M. Lambeir, *The potential of carboxypeptidase M as a therapeutic target in cancer.* Expert Opin Ther Targets, 2013. **17**(3): p. 265-79.
24. Han, G., et al., *NUSAP1 gene silencing inhibits cell proliferation, migration and invasion through inhibiting DNMT1 gene expression in human colorectal cancer.* Exp Cell Res, 2018. **367**(2): p. 216-221.

25. Liu, H., et al., *SLC9A3R1 stimulates autophagy via BECN1 stabilization in breast cancer cells.* Autophagy, 2015. **11**(12): p. 2323-34.
26. Kamarainen, M., et al., *Progesterone-associated endometrial protein--a constitutive marker of human erythroid precursors.* Blood, 1994. **84**(2): p. 467-73.
27. Wang, P., L. Zhu, and X. Zhang, *The role of placental protein 14 in the pathogenesis of endometriosis.* Reprod Sci, 2013. **20**(12): p. 1465-70.
28. Wang, L.F., et al., *Expression of HOXA11 gene in human endometrium.* Am J Obstet Gynecol, 2004. **191**(3): p. 767-72.
29. Ford, C.E., et al., *The Wnt gatekeeper SFRP4 modulates EMT, cell migration and downstream Wnt signalling in serous ovarian cancer cells.* PLoS One, 2013. **8**(1): p. e54362.
30. Maas, J.W., et al., *Endometrial angiogenesis throughout the human menstrual cycle.* Hum Reprod, 2001. **16**(8): p. 1557-61.
31. Gordon, J.D., et al., *Angiogenesis in the human female reproductive tract.* Obstet Gynecol Surv, 1995. **50**(9): p. 688-97.
32. Findlay, J.K., *Angiogenesis in reproductive tissues.* J Endocrinol, 1986. **111**(3): p. 357-66.
33. Gargett, C.E. and P.A. Rogers, *Human endometrial angiogenesis.* Reproduction, 2001. **121**(2): p. 181-6.
34. Folkman, J. and Y. Shing, *Angiogenesis.* J Biol Chem, 1992. **267**(16): p. 10931-4.
35. Jain, R.K., et al., *Quantitative angiogenesis assays: progress and problems.* Nat Med, 1997. **3**(11): p. 1203-8.
36. Risau, W., *Mechanisms of angiogenesis.* Nature, 1997. **386**(6626): p. 671-4.
37. Hanahan, D. and J. Folkman, *Patterns and emerging mechanisms of the angiogenic switch during tumorigenesis.* Cell, 1996. **86**(3): p. 353-64.
38. Gambino, L.S., et al., *Angiogenesis occurs by vessel elongation in proliferative phase human endometrium.* Hum Reprod, 2002. **17**(5): p. 1199-206.
39. Burri, P.H. and V. Djonov, *Intussusceptive angiogenesis--the alternative to capillary sprouting.* Mol Aspects Med, 2002. **23**(6S): p. S1-27.
40. Girling, J.E. and P.A. Rogers, *Recent advances in endometrial angiogenesis research.* Angiogenesis, 2005. **8**(2): p. 89-99.
41. Rogers, P.A., *Structure and function of endometrial blood vessels.* Hum Reprod Update, 1996. **2**(1): p. 57-62.
42. Pellerin, G.P. and M.A. Finan, *Endometrial cancer in women 45 years of age or younger: a clinicopathological analysis.* Am J Obstet Gynecol, 2005. **193**(5): p. 1640-4.
43. Karadeniz, Z., et al., *Inhibition of midkine by metformin can contribute to its anticancer effects in malignancies: A proposal mechanism of action of metformin in context of endometrial cancer prevention and therapy.* Med Hypotheses, 2020. **134**: p. 109420.
44. Corzo, C., et al., *Updates on Conservative Management of Endometrial Cancer.* J Minim Invasive Gynecol, 2018. **25**(2): p. 308-313.
45. Shafiee, M.N., et al., *Preventing endometrial cancer risk in polycystic ovarian syndrome (PCOS) women: could metformin help?* Gynecol Oncol, 2014. **132**(1): p. 248-53.
46. Vale, C.L., et al., *Chemotherapy for advanced, recurrent or metastatic endometrial carcinoma.* Cochrane Database Syst Rev, 2012(8): p. CD003915.
47. Park, L.S., et al., *Time trends in cancer incidence in persons living with HIV/AIDS in the antiretroviral therapy era: 1997-2012.* AIDS, 2016. **30**(11): p. 1795-806.
48. Jemth, P., et al., *Biosynthetic oligosaccharide libraries for identification of protein-binding heparan sulfate motifs. Exploring the structural diversity by screening for fibroblast growth factor (FGF)1 and FGF2 binding.* J Biol Chem, 2002. **277**(34): p. 30567-73.
49. Stewart, C.J. and L. Little, *Immunophenotypic features of MELF pattern invasion in endometrial adenocarcinoma: evidence for epithelial-mesenchymal transition.* Histopathology, 2009. **55**(1): p. 91-101.

50. Euscher, E., et al., *The pattern of myometrial invasion as a predictor of lymph node metastasis or extrauterine disease in low-grade endometrial carcinoma.* Am J Surg Pathol, 2013. **37**(11): p. 1728-36.
51. Stewart, C.J., et al., *MELF pattern invasion in endometrial carcinoma: association with low grade, myoinvasive endometrioid tumours, focal mucinous differentiation and vascular invasion.* Pathology, 2009. **41**(5): p. 454-9.
52. Sivalingam, V.N., et al., *Metformin in reproductive health, pregnancy and gynaecological cancer: established and emerging indications.* Hum Reprod Update, 2014. **20**(6): p. 853-68.
53. Ma, J., N. Ledbetter, and L. Glenn, *Testing women with endometrial cancer for lynch syndrome: should we test all?* J Adv Pract Oncol, 2013. **4**(5): p. 322-30.
54. Group, S.G.O.C.P.E.C.W., et al., *Endometrial cancer: a review and current management strategies: part I.* Gynecol Oncol, 2014. **134**(2): p. 385-92.
55. Wallbillich, J.J., et al., *High Glucose-Mediated STAT3 Activation in Endometrial Cancer Is Inhibited by Metformin: Therapeutic Implications for Endometrial Cancer.* PLoS One, 2017. **12**(1): p. e0170318.
56. Chiu, H.C., et al., *Epithelial to Mesenchymal Transition and Cell Biology of Molecular Regulation in Endometrial Carcinogenesis.* J Clin Med, 2019. **8**(4).
57. Ghosh, S., M. Basu, and S.S. Roy, *ETS-1 protein regulates vascular endothelial growth factor-induced matrix metalloproteinase-9 and matrix metalloproteinase-13 expression in human ovarian carcinoma cell line SKOV-3.* J Biol Chem, 2012. **287**(18): p. 15001-15.
58. Bray, F., et al., *Endometrial cancer incidence trends in Europe: underlying determinants and prospects for prevention.* Cancer Epidemiol Biomarkers Prev, 2005. **14**(5): p. 1132-42.
59. Benedet, J.L., *Progress in gynecologic cancer detection and treatment.* Int J Gynaecol Obstet, 2000. **70**(1): p. 135-47.
60. Edey, K.A., S. Rundle, and M. Hickey, *Hormone replacement therapy for women previously treated for endometrial cancer.* Cochrane Database Syst Rev, 2018. **5**: p. CD008830.
61. Huijgens, A.N. and H.J. Mertens, *Factors predicting recurrent endometrial cancer.* Facts Views Vis Obgyn, 2013. **5**(3): p. 179-86.
62. Odagiri, T., et al., *Multivariate survival analysis of the patients with recurrent endometrial cancer.* J Gynecol Oncol, 2011. **22**(1): p. 3-8.
63. Sorbe, B., C. Juresta, and C. Ahlin, *Natural history of recurrences in endometrial carcinoma.* Oncol Lett, 2014. **8**(4): p. 1800-1806.
64. Roma, A.A., et al., *Risk factor analysis of recurrence in low-grade endometrial adenocarcinoma.* Hum Pathol, 2015. **46**(10): p. 1529-39.
65. Prodromidou, A., et al., *MELF pattern of myometrial invasion and role in possible endometrial cancer diagnostic pathway: A systematic review of the literature.* Eur J Obstet Gynecol Reprod Biol, 2018. **230**: p. 147-152.
66. Kihara, A., et al., *Clinicopathologic Association and Prognostic Value of Microcystic, Elongated, and Fragmented (MELF) Pattern in Endometrial Endometrioid Carcinoma.* Am J Surg Pathol, 2017. **41**(7): p. 896-905.
67. Joehlin-Price, A.S., et al., *The Microcystic, Elongated, and Fragmented (MELF) Pattern of Invasion: A Single Institution Report of 464 Consecutive FIGO Grade 1 Endometrial Endometrioid Adenocarcinomas.* Am J Surg Pathol, 2017. **41**(1): p. 49-55.
68. Singh, N., et al., *Pathologic Prognostic Factors in Endometrial Carcinoma (Other Than Tumor Type and Grade).* Int J Gynecol Pathol, 2019. **38 Suppl 1**: p. S93-S113.
69. Lee, W.L., et al., *Hormone therapy for younger patients with endometrial cancer.* Taiwan J Obstet Gynecol, 2012. **51**(4): p. 495-505.
70. Fanning, J., *Treatment for early endometrial cancer. Cost-effectiveness analysis.* J Reprod Med, 1999. **44**(8): p. 719-23.
71. Reinbolt, R.E. and J.L. Hays, *The Role of PARP Inhibitors in the Treatment of Gynecologic Malignancies.* Front Oncol, 2013. **3**: p. 237.

72. Del Barco, S., et al., *Metformin: multi-faceted protection against cancer.* Oncotarget, 2011. **2**(12): p. 896-917.
73. Petchsila, K., et al., *Effect of Metformin For Decreasing Proliferative Marker in Women with Endometrial Cancer: A Randomized Double-blind Placebo-Controlled Trial.* Asian Pac J Cancer Prev, 2020. **21**(3): p. 733-741.
74. Pabona, J.M.P., et al., *Metformin Promotes Anti-tumor Biomarkers in Human Endometrial Cancer Cells.* Reprod Sci, 2020. **27**(1): p. 267-277.
75. Hu, M., et al., *Alterations of endometrial epithelial-mesenchymal transition and MAPK signaling components in women with PCOS are partially modulated by metformin in vitro.* Mol Hum Reprod, 2020.
76. Oza, A.M., et al., *Phase II study of temsirolimus in women with recurrent or metastatic endometrial cancer: a trial of the NCIC Clinical Trials Group.* J Clin Oncol, 2011. **29**(24): p. 3278-85.
77. Colombo, N., et al., *Ridaforolimus as a single agent in advanced endometrial cancer: results of a single-arm, phase 2 trial.* Br J Cancer, 2013. **108**(5): p. 1021-6.
78. Marchetti, C., et al., *Ixabepilone for the treatment of endometrial cancer.* Expert Opin Investig Drugs, 2016. **25**(5): p. 613-8.
79. Gingis-Velitski, S., et al., *Heparanase uptake is mediated by cell membrane heparan sulfate proteoglycans.* J Biol Chem, 2004. **279**(42): p. 44084-92.
80. Carey, D.J., *N-syndecan: structure and function of a transmembrane heparan sulfate proteoglycan.* Perspect Dev Neurobiol, 1996. **3**(4): p. 331-46.
81. Yurt, R.W., R.W. Leid, Jr., and K.F. Austen, *Native heparin from rat peritoneal mast cells.* J Biol Chem, 1977. **252**(2): p. 518-21.
82. Sarrazin, S., W.C. Lamanna, and J.D. Esko, *Heparan sulfate proteoglycans.* Cold Spring Harb Perspect Biol, 2011. **3**(7).
83. Casale, J. and J.S. Crane, *Biochemistry, Glycosaminoglycans*, in *StatPearls*. 2020: Treasure Island (FL).
84. Henriet, E., et al., *A jasmonic acid derivative improves skin healing and induces changes in proteoglycan expression and glycosaminoglycan structure.* Biochim Biophys Acta Gen Subj, 2017. **1861**(9): p. 2250-2260.
85. Ghiselli, G., *Drug-Mediated Regulation of Glycosaminoglycan Biosynthesis.* Med Res Rev, 2017. **37**(5): p. 1051-1094.
86. Williams, R.V.S.a.S.J., *Carbohydrates: The Essential Molecules of Life*. 2009.
87. Slevin, M., et al., *Hyaluronan-mediated angiogenesis in vascular disease: uncovering RHAMM and CD44 receptor signaling pathways.* Matrix Biol, 2007. **26**(1): p. 58-68.
88. Mikami, T. and H. Kitagawa, *Biosynthesis and function of chondroitin sulfate.* Biochim Biophys Acta, 2013. **1830**(10): p. 4719-33.
89. Trowbridge, J.M. and R.L. Gallo, *Dermatan sulfate: new functions from an old glycosaminoglycan.* Glycobiology, 2002. **12**(9): p. 117R-25R.
90. Caterson, B. and J. Melrose, *Keratan sulfate, a complex glycosaminoglycan with unique functional capability.* Glycobiology, 2018. **28**(4): p. 182-206.
91. Ajit Varki, E.E., Richard D Cummings, Jeffrey D Esko, Pamela Stanley, Gerald W Hart, Markus Aebi, Alan G Darvill, Taroh Kinoshita, Nicolle H Packer, James H Prestegard, Ronald L Schnaar, and Peter H Seeberger, *Essentials of Glycobiology*. 2017.
92. Veraldi, N., et al., *Structural Features of Heparan Sulfate from Multiple Osteochondromas and Chondrosarcomas.* Molecules, 2018. **23**(12).
93. Liu, J. and L.C. Pedersen, *Anticoagulant heparan sulfate: structural specificity and biosynthesis.* Appl Microbiol Biotechnol, 2007. **74**(2): p. 263-72.
94. Capila, I. and R.J. Linhardt, *Heparin-protein interactions.* Angew Chem Int Ed Engl, 2002. **41**(3): p. 391-412.
95. Weitz, J.I., *Heparan sulfate: antithrombotic or not?* J Clin Invest, 2003. **111**(7): p. 952-4.

96. Prydz, K. and K.T. Dalen, *Synthesis and sorting of proteoglycans.* J Cell Sci, 2000. **113 Pt 2**: p. 193-205.
97. Zhang, L., G. David, and J.D. Esko, *Repetitive Ser-Gly sequences enhance heparan sulfate assembly in proteoglycans.* J Biol Chem, 1995. **270**(45): p. 27127-35.
98. Kreuger, J. and L. Kjellen, *Heparan sulfate biosynthesis: regulation and variability.* J Histochem Cytochem, 2012. **60**(12): p. 898-907.
99. Esko, J.D. and U. Lindahl, *Molecular diversity of heparan sulfate.* J Clin Invest, 2001. **108**(2): p. 169-73.
100. Kreuger, J., et al., *Role of heparan sulfate domain organization in endostatin inhibition of endothelial cell function.* EMBO J, 2002. **21**(23): p. 6303-11.
101. Robinson, C.J., et al., *VEGF165-binding sites within heparan sulfate encompass two highly sulfated domains and can be liberated by K5 lyase.* J Biol Chem, 2006. **281**(3): p. 1731-40.
102. Spillmann, D., D. Witt, and U. Lindahl, *Defining the interleukin-8-binding domain of heparan sulfate.* J Biol Chem, 1998. **273**(25): p. 15487-93.
103. Lortat-Jacob, H., J.E. Turnbull, and J.A. Grimaud, *Molecular organization of the interferon gamma-binding domain in heparan sulphate.* Biochem J, 1995. **310 (Pt 2)**: p. 497-505.
104. Forsberg, E., et al., *Abnormal mast cells in mice deficient in a heparin-synthesizing enzyme.* Nature, 1999. **400**(6746): p. 773-6.
105. Li, J., et al., *Biosynthesis of heparin/heparan sulfate. cDNA cloning and expression of D-glucuronyl C5-epimerase from bovine lung.* J Biol Chem, 1997. **272**(44): p. 28158-63.
106. Lindahl, B., L. Eriksson, and U. Lindahl, *Structure of heparan sulphate from human brain, with special regard to Alzheimer's disease.* Biochem J, 1995. **306 (Pt 1)**: p. 177-84.
107. Fedarko, N.S. and H.E. Conrad, *A unique heparan sulfate in the nuclei of hepatocytes: structural changes with the growth state of the cells.* J Cell Biol, 1986. **102**(2): p. 587-99.
108. Jemth, P., et al., *Oligosaccharide library-based assessment of heparan sulfate 6-O-sulfotransferase substrate specificity.* J Biol Chem, 2003. **278**(27): p. 24371-6.
109. Petitou, M., *[From heparin to synthetic antithrombotic oligosaccharides].* Bull Acad Natl Med, 2003. **187**(1): p. 47-56; discussion 56-7.
110. Shukla, D., et al., *A novel role for 3-O-sulfated heparan sulfate in herpes simplex virus 1 entry.* Cell, 1999. **99**(1): p. 13-22.
111. Hu, Y.P., et al., *Divergent synthesis of 48 heparan sulfate-based disaccharides and probing the specific sugar-fibroblast growth factor-1 interaction.* J Am Chem Soc, 2012. **134**(51): p. 20722-7.
112. Gotte, M., et al., *Role of syndecan-1 in leukocyte-endothelial interactions in the ocular vasculature.* Invest Ophthalmol Vis Sci, 2002. **43**(4): p. 1135-41.
113. Grobe, K., et al., *Cerebral hypoplasia and craniofacial defects in mice lacking heparan sulfate Ndst1 gene function.* Development, 2005. **132**(16): p. 3777-86.
114. Westphal, V., et al., *Reduced heparan sulfate accumulation in enterocytes contributes to protein-losing enteropathy in a congenital disorder of glycosylation.* Am J Pathol, 2000. **157**(6): p. 1917-25.
115. Kalus, I., et al., *Differential involvement of the extracellular 6-O-endosulfatases Sulf1 and Sulf2 in brain development and neuronal and behavioural plasticity.* J Cell Mol Med, 2009. **13**(11-12): p. 4505-21.
116. Morimoto-Tomita, M., et al., *Cloning and characterization of two extracellular heparin-degrading endosulfatases in mice and humans.* J Biol Chem, 2002. **277**(51): p. 49175-85.
117. Ai, X., et al., *QSulf1 remodels the 6-O sulfation states of cell surface heparan sulfate proteoglycans to promote Wnt signaling.* J Cell Biol, 2003. **162**(2): p. 341-51.
118. Uchimura, K., et al., *HSulf-2, an extracellular endoglucosamine-6-sulfatase, selectively mobilizes heparin-bound growth factors and chemokines: effects on VEGF, FGF-1, and SDF-1.* BMC Biochem, 2006. **7**: p. 2.

119. Fuller, M., et al., *A defect in exodegradative pathways provides insight into endodegradation of heparan and dermatan sulfates.* Glycobiology, 2006. **16**(4): p. 318-25.
120. Zetser, A., et al., *Processing and activation of latent heparanase occurs in lysosomes.* J Cell Sci, 2004. **117**(Pt 11): p. 2249-58.
121. Secchi, M.F., et al., *Recent data concerning heparanase: focus on fibrosis, inflammation and cancer.* Biomol Concepts, 2015. **6**(5-6): p. 415-21.
122. Knelson, E.H., J.C. Nee, and G.C. Blobe, *Heparan sulfate signaling in cancer.* Trends Biochem Sci, 2014. **39**(6): p. 277-88.
123. Lindahl, U. and J.P. Li, *Interactions between heparan sulfate and proteins-design and functional implications.* Int Rev Cell Mol Biol, 2009. **276**: p. 105-59.
124. Xu, D. and J.D. Esko, *Demystifying heparan sulfate-protein interactions.* Annu Rev Biochem, 2014. **83**: p. 129-57.
125. Liang, O.D., et al., *Identification of novel heparin-binding domains of vitronectin.* FEBS Lett, 1997. **407**(2): p. 169-72.
126. Filmus, J., M. Capurro, and J. Rast, *Glypicans.* Genome Biol, 2008. **9**(5): p. 224.
127. Thunberg, L., G. Backstrom, and U. Lindahl, *Further characterization of the antithrombin-binding sequence in heparin.* Carbohydr Res, 1982. **100**: p. 393-410.
128. Ashikari-Hada, S., et al., *Characterization of growth factor-binding structures in heparin/heparan sulfate using an octasaccharide library.* J Biol Chem, 2004. **279**(13): p. 12346-54.
129. Ornitz, D.M., *FGFs, heparan sulfate and FGFRs: complex interactions essential for development.* Bioessays, 2000. **22**(2): p. 108-12.
130. Proudfoot, A.E.I., et al., *Glycosaminoglycan Interactions with Chemokines Add Complexity to a Complex System.* Pharmaceuticals (Basel), 2017. **10**(3).
131. Celie, J.W., et al., *Subendothelial heparan sulfate proteoglycans become major L-selectin and monocyte chemoattractant protein-1 ligands upon renal ischemia/reperfusion.* Am J Pathol, 2007. **170**(6): p. 1865-78.
132. Armistead, J.S., et al., *A role for heparan sulfate proteoglycans in Plasmodium falciparum sporozoite invasion of anopheline mosquito salivary glands.* Biochem J, 2011. **438**(3): p. 475-83.
133. Poulain, F.E. and H.J. Yost, *Heparan sulfate proteoglycans: a sugar code for vertebrate development?* Development, 2015. **142**(20): p. 3456-67.
134. Veraldi, N., N. Zouggari, and A. de Agostini, *The Challenge of Modulating Heparan Sulfate Turnover by Multitarget Heparin Derivatives.* Molecules, 2020. **25**(2).
135. Wang, Y., Y. Xia, and Z. Lu, *Metabolic features of cancer cells.* Cancer Commun (Lond), 2018. **38**(1): p. 65.
136. Romero-Garcia, S., et al., *Tumor cell metabolism: an integral view.* Cancer Biol Ther, 2011. **12**(11): p. 939-48.
137. Mohan, C.D., et al., *Targeting Heparanase in Cancer: Inhibition by Synthetic, Chemically Modified, and Natural Compounds.* iScience, 2019. **15**: p. 360-390.
138. Kelly, T., et al., *High heparanase activity in multiple myeloma is associated with elevated microvessel density.* Cancer Res, 2003. **63**(24): p. 8749-56.
139. Masola, V., et al., *Heparanase: A Multitasking Protein Involved in Extracellular Matrix (ECM) Remodeling and Intracellular Events.* Cells, 2018. **7**(12).
140. Xie, Z.J., et al., *Heparanase expression, degradation of basement membrane and low degree of infiltration by immunocytes correlate with invasion and progression of human gastric cancer.* World J Gastroenterol, 2008. **14**(24): p. 3812-8.
141. Purushothaman, A., et al., *Heparanase stimulation of protease expression implicates it as a master regulator of the aggressive tumor phenotype in myeloma.* J Biol Chem, 2008. **283**(47): p. 32628-36.

142. Blich, M., et al., *Macrophage activation by heparanase is mediated by TLR-2 and TLR-4 and associates with plaque progression.* Arterioscler Thromb Vasc Biol, 2013. **33**(2): p. e56-65.
143. Zcharia, E., et al., *Newly generated heparanase knock-out mice unravel co-regulation of heparanase and matrix metalloproteinases.* PLoS One, 2009. **4**(4): p. e5181.
144. Hull, E.E., M.R. Montgomery, and K.J. Leyva, *Epigenetic Regulation of the Biosynthesis & Enzymatic Modification of Heparan Sulfate Proteoglycans: Implications for Tumorigenesis and Cancer Biomarkers.* Int J Mol Sci, 2017. **18**(7).
145. Theocharis, A.D. and N.K. Karamanos, *Proteoglycans remodeling in cancer: Underlying molecular mechanisms.* Matrix Biol, 2019. **75-76**: p. 220-259.
146. Huang, G., et al., *alpha3 Chains of type V collagen regulate breast tumour growth via glypican-1.* Nat Commun, 2017. **8**: p. 14351.
147. Baba, F., et al., *Syndecan-1 and syndecan-4 are overexpressed in an estrogen receptor-negative, highly proliferative breast carcinoma subtype.* Breast Cancer Res Treat, 2006. **98**(1): p. 91-8.
148. Maeda, T., J. Desouky, and A. Friedl, *Syndecan-1 expression by stromal fibroblasts promotes breast carcinoma growth in vivo and stimulates tumor angiogenesis.* Oncogene, 2006. **25**(9): p. 1408-12.
149. Knelson, E.H., et al., *Stromal heparan sulfate differentiates neuroblasts to suppress neuroblastoma growth.* J Clin Invest, 2014. **124**(7): p. 3016-31.
150. Lanzi, C., N. Zaffaroni, and G. Cassinelli, *Targeting Heparan Sulfate Proteoglycans and their Modifying Enzymes to Enhance Anticancer Chemotherapy Efficacy and Overcome Drug Resistance.* Curr Med Chem, 2017. **24**(26): p. 2860-2886.
151. Whitelock, J.M. and R.V. Iozzo, *Heparan sulfate: a complex polymer charged with biological activity.* Chem Rev, 2005. **105**(7): p. 2745-64.
152. Harris, N.C., et al., *The propeptides of VEGF-D determine heparin binding, receptor heterodimerization, and effects on tumor biology.* J Biol Chem, 2013. **288**(12): p. 8176-86.
153. van Wijk, X.M. and T.H. van Kuppevelt, *Heparan sulfate in angiogenesis: a target for therapy.* Angiogenesis, 2014. **17**(3): p. 443-62.
154. Lei, J., A. Jiang, and D. Pei, *Identification and characterization of a new splicing variant of vascular endothelial growth factor: VEGF183.* Biochim Biophys Acta, 1998. **1443**(3): p. 400-6.
155. Gitay-Goren, H., et al., *The binding of vascular endothelial growth factor to its receptors is dependent on cell surface-associated heparin-like molecules.* J Biol Chem, 1992. **267**(9): p. 6093-8.
156. Xu, D., et al., *Heparan sulfate regulates VEGF165- and VEGF121-mediated vascular hyperpermeability.* J Biol Chem, 2011. **286**(1): p. 737-45.
157. Soker, S., et al., *VEGF165 mediates formation of complexes containing VEGFR-2 and neuropilin-1 that enhance VEGF165-receptor binding.* J Cell Biochem, 2002. **85**(2): p. 357-68.
158. Korf-Klingebiel, M., et al., *Heparan Sulfate-Editing Extracellular Sulfatases Enhance VEGF Bioavailability for Ischemic Heart Repair.* Circ Res, 2019. **125**(9): p. 787-801.
159. Vicente, C.M., et al., *Enhanced tumorigenic potential of colorectal cancer cells by extracellular sulfatases.* Mol Cancer Res, 2015. **13**(3): p. 510-23.
160. Battinelli, E.M., et al., *Anticoagulation inhibits tumor cell-mediated release of platelet angiogenic proteins and diminishes platelet angiogenic response.* Blood, 2014. **123**(1): p. 101-12.
161. Roghani, M., et al., *Heparin increases the affinity of basic fibroblast growth factor for its receptor but is not required for binding.* J Biol Chem, 1994. **269**(6): p. 3976-84.
162. Sharma, B., et al., *Antisense targeting of perlecan blocks tumor growth and angiogenesis in vivo.* J Clin Invest, 1998. **102**(8): p. 1599-608.
163. Vlodavsky, I., et al., *Significance of heparanase in cancer and inflammation.* Cancer Microenviron, 2012. **5**(2): p. 115-32.

164. Elgundi, Z., et al., *Cancer Metastasis: The Role of the Extracellular Matrix and the Heparan Sulfate Proteoglycan Perlecan.* Front Oncol, 2019. **9**: p. 1482.
165. Doweck, I., et al., *Heparanase localization and expression by head and neck cancer: correlation with tumor progression and patient survival.* Neoplasia, 2006. **8**(12): p. 1055-61.
166. Weissmann, M., et al., *Heparanase-neutralizing antibodies attenuate lymphoma tumor growth and metastasis.* Proc Natl Acad Sci U S A, 2016. **113**(3): p. 704-9.
167. Zhao, S. and Z. Wang, *Changes in heparan sulfate sulfotransferases and cell-surface heparan sulfate during SKM-1 cells granulocytic differentiation and A549 cells epithelial-mesenchymal transition.* Glycoconj J, 2020. **37**(2): p. 151-164.
168. Vicente, C.M., et al., *SULF2 overexpression positively regulates tumorigenicity of human prostate cancer cells.* J Exp Clin Cancer Res, 2015. **34**: p. 25.
169. Mythreye, K. and G.C. Blobe, *Proteoglycan signaling co-receptors: roles in cell adhesion, migration and invasion.* Cell Signal, 2009. **21**(11): p. 1548-58.
170. Inki, P., et al., *Immunohistochemical localization of syndecan-1 in normal and pathological human uterine cervix.* J Pathol, 1994. **172**(4): p. 349-55.
171. Inki, P. and M. Jalkanen, *The role of syndecan-1 in malignancies.* Ann Med, 1996. **28**(1): p. 63-7.
172. Kirkbride, K.C., B.N. Ray, and G.C. Blobe, *Cell-surface co-receptors: emerging roles in signaling and human disease.* Trends Biochem Sci, 2005. **30**(11): p. 611-21.
173. Mennerich, D., et al., *Shift of syndecan-1 expression from epithelial to stromal cells during progression of solid tumours.* Eur J Cancer, 2004. **40**(9): p. 1373-82.
174. Chakraborty, S., et al., *Hepatocyte growth factor is an attractive target for the treatment of pulmonary fibrosis.* Expert Opin Investig Drugs, 2013. **22**(4): p. 499-515.
175. Jackson, D.G., et al., *Proteoglycan forms of the lymphocyte homing receptor CD44 are alternatively spliced variants containing the v3 exon.* J Cell Biol, 1995. **128**(4): p. 673-85.
176. Orian-Rousseau, V., et al., *CD44 is required for two consecutive steps in HGF/c-Met signaling.* Genes Dev, 2002. **16**(23): p. 3074-86.
177. Uterine, C.R.U.K. *Cancer incidence trends over time*. 2018; Available from: https://www.cancerresearchuk.org/health-professional/cancer-statistics/statistics-by-cancer-type/uterine-cancer/incidence#heading-Two.
178. CRUK. *Uterine cancer incidence by age*. 2019 [cited 2019 Accessed 30th Jul 2019]; Available from: https://www.cancerresearchuk.org/health-professional/cancer-statistics/statistics-by-cancer-type/uterine-cancer/incidence#heading-One.
179. Lax, S.F., *Pathology of Endometrial Carcinoma.* Adv Exp Med Biol, 2017. **943**: p. 75-96.
180. Quick, C.M., et al., *Low-grade, low-stage endometrioid endometrial adenocarcinoma: a clinicopathologic analysis of 324 cases focusing on frequency and pattern of myoinvasion.* Int J Gynecol Pathol, 2012. **31**(4): p. 337-43.
181. Townsend, M.H., et al., *Potential new biomarkers for endometrial cancer.* Cancer Cell Int, 2019. **19**: p. 19.
182. Poltavets, V., et al., *The Role of the Extracellular Matrix and Its Molecular and Cellular Regulators in Cancer Cell Plasticity.* Front Oncol, 2018. **8**: p. 431.
183. Bielenberg, D.R. and B.R. Zetter, *The Contribution of Angiogenesis to the Process of Metastasis.* Cancer J, 2015. **21**(4): p. 267-73.
184. Agostini, A.I.d., et al., *Role of Anticoagulant Heparan Sulfate in Mammalian Reproduction*. Chemistry and Biology of Heparin and Heparan Sulfate. 2005.
185. Smits, N.C., et al., *HS3ST1 genotype regulates antithrombin's inflammomodulatory tone and associates with atherosclerosis.* Matrix Biol, 2017. **63**: p. 69-90.
186. de Agostini, A.I., et al., *Human follicular fluid heparan sulfate contains abundant 3-O-sulfated chains with anticoagulant activity.* J Biol Chem, 2008. **283**(42): p. 28115-24.
187. de Agostini, A., *An unexpected role for anticoagulant heparan sulfate proteoglycans in reproduction.* Swiss Med Wkly, 2006. **136**(37-38): p. 583-90.

188. de Agostini, A.I., et al., *Localization of anticoagulantly active heparan sulfate proteoglycans in vascular endothelium: antithrombin binding on cultured endothelial cells and perfused rat aorta.* J Cell Biol, 1990. **111**(3): p. 1293-304.
189. Princivalle, M., et al., *Anticoagulant heparan sulfate proteoglycans expression in the rat ovary peaks in preovulatory granulosa cells.* Glycobiology, 2001. **11**(3): p. 183-94.
190. Kaltenbach, D.D., et al., *Sulfotransferase and Heparanase: Remodeling Engines in Promoting Virus Infection and Disease Development.* Front Pharmacol, 2018. **9**: p. 1315.
191. Hammond, E., et al., *The Role of Heparanase and Sulfatases in the Modification of Heparan Sulfate Proteoglycans within the Tumor Microenvironment and Opportunities for Novel Cancer Therapeutics.* Front Oncol, 2014. **4**: p. 195.
192. Bame, K.J., *Heparanases: endoglycosidases that degrade heparan sulfate proteoglycans.* Glycobiology, 2001. **11**(6): p. 91R-98R.
193. Nasser, N.J., *Heparanase involvement in physiology and disease.* Cell Mol Life Sci, 2008. **65**(11): p. 1706-15.
194. Folkman, J., *Tumor angiogenesis: therapeutic implications.* N Engl J Med, 1971. **285**(21): p. 1182-6.
195. Torry, D.S., et al., *Vascular endothelial growth factor expression in cycling human endometrium.* Fertil Steril, 1996. **66**(1): p. 72-80.
196. Girardin, E.P., et al., *Synthesis of anticoagulantly active heparan sulfate proteoglycans by glomerular epithelial cells involves multiple 3-O-sulfotransferase isoforms and a limiting precursor pool.* J Biol Chem, 2005. **280**(45): p. 38059-70.
197. Webb, N.J., et al., *Activated human neutrophils express vascular endothelial growth factor (VEGF).* Cytokine, 1998. **10**(4): p. 254-7.
198. Subbarayan, K. and B. Seliger, *Tumor-dependent Effects of Proteoglycans and Various Glycosaminoglycan Synthesizing Enzymes and Sulfotransferases on Patients' Outcome.* Curr Cancer Drug Targets, 2019. **19**(3): p. 210-221.
199. Barkeer, S., et al., *Novel role of O-glycosyltransferases GALNT3 and B3GNT3 in the self-renewal of pancreatic cancer stem cells.* BMC Cancer, 2018. **18**(1): p. 1157.
200. Kundu, S., et al., *Heparanase Promotes Glioma Progression and Is Inversely Correlated with Patient Survival.* Mol Cancer Res, 2016. **14**(12): p. 1243-1253.
201. Gutter-Kapon, L., et al., *Heparanase is required for activation and function of macrophages.* Proc Natl Acad Sci U S A, 2016. **113**(48): p. E7808-E7817.
202. Pinho, S.S. and C.A. Reis, *Glycosylation in cancer: mechanisms and clinical implications.* Nat Rev Cancer, 2015. **15**(9): p. 540-55.
203. Liu, X., et al., *Heparanase Promotes Tumor Growth and Liver Metastasis of Colorectal Cancer Cells by Activating the p38/MMP1 Axis.* Front Oncol, 2019. **9**: p. 216.
204. Kruger, K., et al., *Microvessel proliferation by co-expression of endothelial nestin and Ki-67 is associated with a basal-like phenotype and aggressive features in breast cancer.* Breast, 2013. **22**(3): p. 282-8.
205. Jerdan, J.A., R.G. Michels, and B.M. Glaser, *Extracellular matrix of newly forming vessels--an immunohistochemical study.* Microvasc Res, 1991. **42**(3): p. 255-65.
206. Marchand, M., et al., *Extracellular matrix scaffolding in angiogenesis and capillary homeostasis.* Semin Cell Dev Biol, 2019. **89**: p. 147-156.
207. Gubbiotti, M.A., T. Neill, and R.V. Iozzo, *A current view of perlecan in physiology and pathology: A mosaic of functions.* Matrix Biol, 2017. **57-58**: p. 285-298.
208. Pozzi, A., P.D. Yurchenco, and R.V. Iozzo, *The nature and biology of basement membranes.* Matrix Biol, 2017. **57-58**: p. 1-11.
209. Manikowski, D., et al., *Soluble Heparin and Heparan Sulfate Glycosaminoglycans Interfere with Sonic Hedgehog Solubilization and Receptor Binding.* Molecules, 2019. **24**(8).

210. Farrugia, B.L., et al., *The Role of Heparan Sulfate in Inflammation, and the Development of Biomimetics as Anti-Inflammatory Strategies.* J Histochem Cytochem, 2018. **66**(4): p. 321-336.
211. Topfedaisi Ozkan, N., et al., *Factors associated with survival after relapse in patients with low-risk endometrial cancer treated with surgery alone.* J Gynecol Oncol, 2017. **28**(5): p. e65.
212. Pavlakis, K., et al., *MELF invasion in endometrial cancer as a risk factor for lymph node metastasis.* Histopathology, 2011. **58**(6): p. 966-73.
213. Dogan Altunpulluk, M., et al., *The association of the microcystic, elongated and fragmented (MELF) invasion pattern in endometrial carcinomas with deep myometrial invasion, lymphovascular space invasion and lymph node metastasis.* J Obstet Gynaecol, 2015. **35**(4): p. 397-402.
214. Lu, Z. and J. Chen, *[Introduction of WHO classification of tumours of female reproductive organs, fourth edition].* Zhonghua Bing Li Xue Za Zhi, 2014. **43**(10): p. 649-50.
215. Amant, F., et al., *Cancer of the corpus uteri.* Int J Gynaecol Obstet, 2018. **143 Suppl 2**: p. 37-50.
216. Kurman, R., *Blaustein's Pathology of the Female Genital Tract*. Blaustein's Pathology of the Female Genital Tract 7th ed. 2019 Edition, ed. R.J. Kurman, L.H. Ellenson, and B.M. Ronnett. 2019: Springer; 7th ed. 2019 edition (September 6, 2019). 1525.
217. Saman, W., *Chapter-13 Oral Cancer*. Oral Medicine & Pathology: A Guide to Diagnosis and Management. 2014.
218. Pusztaszeri, M.P., W. Seelentag, and F.T. Bosman, *Immunohistochemical expression of endothelial markers CD31, CD34, von Willebrand factor, and Fli-1 in normal human tissues.* J Histochem Cytochem, 2006. **54**(4): p. 385-95.
219. Kahn, H.J., D. Bailey, and A. Marks, *Monoclonal antibody D2-40, a new marker of lymphatic endothelium, reacts with Kaposi's sarcoma and a subset of angiosarcomas.* Mod Pathol, 2002. **15**(4): p. 434-40.
220. Ruifrok, A.C. and D.A. Johnston, *Quantification of histochemical staining by color deconvolution.* Anal Quant Cytol Histol, 2001. **23**(4): p. 291-9.
221. Dinkic, C., et al., *Influence of Paclitaxel and Heparin on Vitality, Proliferation and Cytokine Production of Endometrial Cancer Cells.* Geburtshilfe Frauenheilkd, 2017. **77**(10): p. 1104-1110.
222. Fung-Kee-Fung, M., et al., *Follow-up after primary therapy for endometrial cancer: a systematic review.* Gynecol Oncol, 2006. **101**(3): p. 520-9.
223. Bestvina, C.M. and G.F. Fleming, *Chemotherapy for Endometrial Cancer in Adjuvant and Advanced Disease Settings.* Oncologist, 2016. **21**(10): p. 1250-1259.
224. Kuderer, N.M., T.L. Ortel, and C.W. Francis, *Impact of venous thromboembolism and anticoagulation on cancer and cancer survival.* J Clin Oncol, 2009. **27**(29): p. 4902-11.
225. Garcia-Escobar, I., et al., *Pleiotropic effects of heparins: does anticoagulant treatment increase survival in cancer patients?* Clin Transl Oncol, 2018. **20**(9): p. 1097-1108.
226. Borsig, L., *Heparin as an inhibitor of cancer progression.* Prog Mol Biol Transl Sci, 2010. **93**: p. 335-49.
227. Bobek, V. and J. Kovarik, *Antitumor and antimetastatic effect of warfarin and heparins.* Biomed Pharmacother, 2004. **58**(4): p. 213-9.
228. Lanzi, C. and G. Cassinelli, *Heparan Sulfate Mimetics in Cancer Therapy: The Challenge to Define Structural Determinants and the Relevance of Targets for Optimal Activity.* Molecules, 2018. **23**(11).
229. Mohamed, S. and D.R. Coombe, *Heparin Mimetics: Their Therapeutic Potential.* Pharmaceuticals (Basel), 2017. **10**(4).
230. Coombe, D.R. and N.S. Gandhi, *Heparanase: A Challenging Cancer Drug Target.* Front Oncol, 2019. **9**: p. 1316.

231. Seffouh, A., et al., *Expression and purification of recombinant extracellular sulfatase HSulf-2 allows deciphering of enzyme sub-domain coordinated role for the binding and 6-O-desulfation of heparan sulfate.* Cell Mol Life Sci, 2019. **76**(9): p. 1807-1819.
232. Yang, Y., et al., *Heparanase enhances syndecan-1 shedding: a novel mechanism for stimulation of tumor growth and metastasis.* J Biol Chem, 2007. **282**(18): p. 13326-33.
233. Friedl, P. and K. Wolf, *Tumour-cell invasion and migration: diversity and escape mechanisms.* Nat Rev Cancer, 2003. **3**(5): p. 362-74.
234. Justus, C.R., et al., *In vitro cell migration and invasion assays.* J Vis Exp, 2014(88).
235. Bozzuto, G., P. Ruggieri, and A. Molinari, *Molecular aspects of tumor cell migration and invasion.* Ann Ist Super Sanita, 2010. **46**(1): p. 66-80.
236. Jiang, W.G., et al., *Tissue invasion and metastasis: Molecular, biological and clinical perspectives.* Semin Cancer Biol, 2015. **35 Suppl**: p. S244-S275.
237. van Zijl, F., G. Krupitza, and W. Mikulits, *Initial steps of metastasis: cell invasion and endothelial transmigration.* Mutat Res, 2011. **728**(1-2): p. 23-34.
238. Naimy, H., N. Leymarie, and J. Zaia, *Screening for anticoagulant heparan sulfate octasaccharides and fine structure characterization using tandem mass spectrometry.* Biochemistry, 2010. **49**(17): p. 3743-52.
239. Gama, C.I., et al., *Sulfation patterns of glycosaminoglycans encode molecular recognition and activity.* Nat Chem Biol, 2006. **2**(9): p. 467-73.
240. Habuchi, H., O. Habuchi, and K. Kimata, *Sulfation pattern in glycosaminoglycan: does it have a code?* Glycoconj J, 2004. **21**(1-2): p. 47-52.
241. Fernandez-Vega, I., et al., *Specific genes involved in synthesis and editing of heparan sulfate proteoglycans show altered expression patterns in breast cancer.* BMC Cancer, 2013. **13**: p. 24.
242. Cooney, C.A., et al., *Chondroitin sulfates play a major role in breast cancer metastasis: a role for CSPG4 and CHST11 gene expression in forming surface P-selectin ligands in aggressive breast cancer cells.* Breast Cancer Res, 2011. **13**(3): p. R58.
243. Backen, A.C., et al., *Heparan sulphate synthetic and editing enzymes in ovarian cancer.* Br J Cancer, 2007. **96**(10): p. 1544-8.
244. Vallen, M.J., et al., *Highly sulfated chondroitin sulfates, a novel class of prognostic biomarkers in ovarian cancer tissue.* Gynecol Oncol, 2012. **127**(1): p. 202-9.
245. Kalathas, D., et al., *Alterations of glycosaminoglycan disaccharide content and composition in colorectal cancer: structural and expressional studies.* Oncol Rep, 2009. **22**(2): p. 369-75.
246. Ricciardelli, C., et al., *Elevated stromal chondroitin sulfate glycosaminoglycan predicts progression in early-stage prostate cancer.* Clin Cancer Res, 1997. **3**(6): p. 983-92.
247. Ricciardelli, C., et al., *Prostatic chondroitin sulfate is increased in patients with metastatic disease but does not predict survival outcome.* Prostate, 2009. **69**(7): p. 761-9.
248. Theocharis, A.D., et al., *Altered content composition and structure of glycosaminoglycans and proteoglycans in gastric carcinoma.* Int J Biochem Cell Biol, 2003. **35**(3): p. 376-90.
249. Sakko, A.J., et al., *Immunohistochemical level of unsulfated chondroitin disaccharides in the cancer stroma is an independent predictor of prostate cancer relapse.* Cancer Epidemiol Biomarkers Prev, 2008. **17**(9): p. 2488-97.
250. Hu, J., et al., *Heparanase and vascular endothelial growth factor expression is increased in hypoxia-induced retinal neovascularization.* Invest Ophthalmol Vis Sci, 2012. **53**(11): p. 6810-7.
251. Cassinelli, G., et al., *Supersulfated low-molecular weight heparin synergizes with IGF1R/IR inhibitor to suppress synovial sarcoma growth and metastases.* Cancer Lett, 2018. **415**: p. 187-197.
252. Ludwig, R.J., et al., *Endothelial P-selectin as a target of heparin action in experimental melanoma lung metastasis.* Cancer Res, 2004. **64**(8): p. 2743-50.

253. Frese, M.A., et al., *Characterization of the human sulfatase Sulf1 and its high affinity heparin/heparan sulfate interaction domain.* J Biol Chem, 2009. **284**(41): p. 28033-44.
254. Tyekucheva, S., et al., *Stromal and epithelial transcriptional map of initiation progression and metastatic potential of human prostate cancer.* Nat Commun, 2017. **8**(1): p. 420.
255. Spaw, M., S. Anant, and S.M. Thomas, *Stromal contributions to the carcinogenic process.* Mol Carcinog, 2017. **56**(4): p. 1199-1213.
256. Liu, T., et al., *Cancer-Associated Fibroblasts Build and Secure the Tumor Microenvironment.* Front Cell Dev Biol, 2019. **7**: p. 60.
257. Yoshida, G.J., et al., *Activated Fibroblast Program Orchestrates Tumor Initiation and Progression; Molecular Mechanisms and the Associated Therapeutic Strategies.* Int J Mol Sci, 2019. **20**(9).
258. Talbot, L.J., S.D. Bhattacharya, and P.C. Kuo, *Epithelial-mesenchymal transition, the tumor microenvironment, and metastatic behavior of epithelial malignancies.* Int J Biochem Mol Biol, 2012. **3**(2): p. 117-36.
259. Sahoo, S.S., et al., *The Emerging Role of the Microenvironment in Endometrial Cancer.* Cancers (Basel), 2018. **10**(11).
260. Valkenburg, K.C., A.E. de Groot, and K.J. Pienta, *Targeting the tumour stroma to improve cancer therapy.* Nat Rev Clin Oncol, 2018. **15**(6): p. 366-381.
261. Hong, B., M. Le Gallo, and D.W. Bell, *The mutational landscape of endometrial cancer.* Curr Opin Genet Dev, 2015. **30**: p. 25-31.
262. Li, J., et al., *Whole-Genome DNA Methylation Profiling Identifies Epigenetic Signatures of Uterine Carcinosarcoma.* Neoplasia, 2017. **19**(2): p. 100-111.
263. Aguilar-Bravo, B. and P. Sancho-Bru, *Laser capture microdissection: techniques and applications in liver diseases.* Hepatol Int, 2019. **13**(2): p. 138-147.
264. Lai, J.P., et al., *Heparin-degrading sulfatases in hepatocellular carcinoma: roles in pathogenesis and therapy targets.* Future Oncol, 2008. **4**(6): p. 803-14.
265. Lai, J.P., et al., *Sulfatase 2 up-regulates glypican 3, promotes fibroblast growth factor signaling, and decreases survival in hepatocellular carcinoma.* Hepatology, 2008. **47**(4): p. 1211-22.
266. Lai, J.P., et al., *The tumor suppressor function of human sulfatase 1 (SULF1) in carcinogenesis.* J Gastrointest Cancer, 2008. **39**(1-4): p. 149-58.
267. Lee, H.Y., et al., *Sulfatase-1 overexpression indicates poor prognosis in urothelial carcinoma of the urinary bladder and upper tract.* Oncotarget, 2017. **8**(29): p. 47216-47229.
268. Rosen, S.D. and H. Lemjabbar-Alaoui, *Sulf-2: an extracellular modulator of cell signaling and a cancer target candidate.* Expert Opin Ther Targets, 2010. **14**(9): p. 935-49.
269. Phillips, J.J., et al., *Heparan sulfate sulfatase SULF2 regulates PDGFRalpha signaling and growth in human and mouse malignant glioma.* J Clin Invest, 2012. **122**(3): p. 911-22.
270. Oberholzer, A., C. Oberholzer, and L.L. Moldawer, *Cytokine signaling--regulation of the immune response in normal and critically ill states.* Crit Care Med, 2000. **28**(4 Suppl): p. N3-12.
271. Xu, D., et al., *Heparan Sulfate Modulates Neutrophil and Endothelial Function in Antibacterial Innate Immunity.* Infect Immun, 2015. **83**(9): p. 3648-56.
272. S, A. *FastQC: a quality control tool for high throughput sequence data 2010*. Available from: http://www.bioinformatics.babraham.ac.uk/projects/fastqc/.
273. Patro, R., et al., *Salmon provides fast and bias-aware quantification of transcript expression.* Nat Methods, 2017. **14**(4): p. 417-419.
274. Love, M.I., W. Huber, and S. Anders, *Moderated estimation of fold change and dispersion for RNA-seq data with DESeq2.* Genome Biol, 2014. **15**(12): p. 550.
275. Soneson, C., M.I. Love, and M.D. Robinson, *Differential analyses for RNA-seq: transcript-level estimates improve gene-level inferences.* F1000Res, 2015. **4**: p. 1521.

276. Soneson, C. and M.D. Robinson, *Towards unified quality verification of synthetic count data with countsimQC.* Bioinformatics, 2018. **34**(4): p. 691-692.
277. Bourgon, R., R. Gentleman, and W. Huber, *Independent filtering increases detection power for high-throughput experiments.* Proc Natl Acad Sci U S A, 2010. **107**(21): p. 9546-51.
278. Anders, S. and W. Huber, *Differential expression analysis for sequence count data.* Genome Biol, 2010. **11**(10): p. R106.
279. Wickham, H., *ggplot2: Elegant Graphics for Data Analysis*. 2016, New York: Springer-Verlag
280. Gu, Z., R. Eils, and M. Schlesner, *Complex heatmaps reveal patterns and correlations in multidimensional genomic data.* Bioinformatics, 2016. **32**(18): p. 2847-9.
281. Subramanian, A., et al., *Gene set enrichment analysis: a knowledge-based approach for interpreting genome-wide expression profiles.* Proc Natl Acad Sci U S A, 2005. **102**(43): p. 15545-50.
282. Mootha, V.K., et al., *PGC-1alpha-responsive genes involved in oxidative phosphorylation are coordinately downregulated in human diabetes.* Nat Genet, 2003. **34**(3): p. 267-73.
283. Phan, L.M., S.C. Yeung, and M.H. Lee, *Cancer metabolic reprogramming: importance, main features, and potentials for precise targeted anti-cancer therapies.* Cancer Biol Med, 2014. **11**(1): p. 1-19.
284. Gabbert, H., et al., *Tumor dedifferentiation: an important step in tumor invasion.* Clin Exp Metastasis, 1985. **3**(4): p. 257-79.
285. Jogi, A., et al., *Cancer cell differentiation heterogeneity and aggressive behavior in solid tumors.* Ups J Med Sci, 2012. **117**(2): p. 217-24.
286. Liotta, L.A., *Adhere, Degrade, and Move: The Three-Step Model of Invasion.* Cancer Res, 2016. **76**(11): p. 3115-7.
287. Quail, D.F. and J.A. Joyce, *Microenvironmental regulation of tumor progression and metastasis.* Nat Med, 2013. **19**(11): p. 1423-37.
288. Nagarajan, A., P. Malvi, and N. Wajapeyee, *Heparan Sulfate and Heparan Sulfate Proteoglycans in Cancer Initiation and Progression.* Front Endocrinol (Lausanne), 2018. **9**: p. 483.
289. Ramani, V.C., et al., *The heparanase/syndecan-1 axis in cancer: mechanisms and therapies.* FEBS J, 2013. **280**(10): p. 2294-306.
290. Jang, B., et al., *Syndecan-2 enhances E-cadherin shedding and fibroblast-like morphological changes by inducing MMP-7 expression in colon cancer cells.* Biochem Biophys Res Commun, 2016. **477**(1): p. 47-53.
291. Zittermann, S.I., et al., *Soluble glypican 3 inhibits the growth of hepatocellular carcinoma in vitro and in vivo.* Int J Cancer, 2010. **126**(6): p. 1291-301.
292. Lu, P., et al., *Extracellular matrix degradation and remodeling in development and disease.* Cold Spring Harb Perspect Biol, 2011. **3**(12).
293. Garalla, H.M., et al., *Matrix metalloproteinase (MMP)-7 in Barrett's esophagus and esophageal adenocarcinoma: expression, metabolism, and functional significance.* Physiol Rep, 2018. **6**(10): p. e13683.
294. Choi, D.S., et al., *Syndecan-1, a key regulator of cell viability in endometrial cancer.* Int J Cancer, 2007. **121**(4): p. 741-50.
295. Maltseva, I., et al., *The SULFs, extracellular sulfatases for heparan sulfate, promote the migration of corneal epithelial cells during wound repair.* PLoS One, 2013. **8**(8): p. e69642.
296. Hasengaowa, et al., *Prognostic significance of syndecan-1 expression in human endometrial cancer.* Ann Oncol, 2005. **16**(7): p. 1109-15.
297. Hasengaowa, et al., *Loss of basement membrane heparan sulfate expression is associated with tumor progression in endometrial cancer.* Eur J Gynaecol Oncol, 2005. **26**(4): p. 403-6.
298. Hanahan, D. and R.A. Weinberg, *The hallmarks of cancer.* Cell, 2000. **100**(1): p. 57-70.
299. Chen, Y., et al., *Human tumor cells induce angiogenesis through positive feedback between CD147 and insulin-like growth factor-I.* PLoS One, 2012. **7**(7): p. e40965.

300. Lord, M.S., et al., *Platelet Factor 4 Binds to Vascular Proteoglycans and Controls Both Growth Factor Activities and Platelet Activation.* J Biol Chem, 2017. **292**(10): p. 4054-4063.
301. Shworak, N.C.S.a.N.W., *Novel Role of Anticoagulant Heparan Sulfate in Antithrombin Anti-inflammatory Signaling.* Arteriosclerosis, Thrombosis, and Vascular Biology, 2018. **Vol. 32**.
302. Juuti, A., et al., *Syndecan-1 expression--a novel prognostic marker in pancreatic cancer.* Oncology, 2005. **68**(2-3): p. 97-106.
303. Seidel, C., et al., *Serum syndecan-1: a new independent prognostic marker in multiple myeloma.* Blood, 2000. **95**(2): p. 388-92.
304. Vlodavsky, I., et al., *Heparanase: From basic research to therapeutic applications in cancer and inflammation.* Drug Resist Updat, 2016. **29**: p. 54-75.
305. Shafat, I., et al., *Heparanase levels are elevated in the plasma of pediatric cancer patients and correlate with response to anticancer treatment.* Neoplasia, 2007. **9**(11): p. 909-16.
306. Liu, S., et al., *A heparin-binding synthetic peptide of heparin/heparan sulfate-interacting protein modulates blood coagulation activities.* Proc Natl Acad Sci U S A, 1997. **94**(5): p. 1739-44.
307. Thunberg, L., et al., *Enzymatic depolymerization of heparin-related polysaccharides. Substrate specificities of mouse mastocytoma and human platelet endo-beta-D-glucuronidases.* J Biol Chem, 1982. **257**(17): p. 10278-82.
308. Pikas, D.S., et al., *Substrate specificity of heparanases from human hepatoma and platelets.* J Biol Chem, 1998. **273**(30): p. 18770-7.

Paper in published format

molecules

MDPI

Review

The Challenge of Modulating Heparan Sulfate Turnover by Multitarget Heparin Derivatives

Noemi Veraldi [1], Nawel Zouggari [2] and Ariane de Agostini [3,*]

1 Division of Clinical Pathology, Department of Diagnostics, Geneva University Hospitals, 1211 Geneva 14, Switzerland; noemi.veraldi@gmail.com
2 Department of Biochemistry, Faculty of Science and Department of Pathology and Immunology, School of Medicine, University of Geneva, 1211 Geneva 14, Switzerland; nawel.zouggari@unige.ch
3 Department of Pathology and Immunology, School of Medicine, University of Geneva and Division of Clinical Pathology, Department of Diagnostics, Geneva University Hospitals, 1211 Geneva 14, Switzerland
* Correspondence: ariane.deagostini@unige.ch; Tel.: +41-223794661

Academic Editors: Giangiacomo Torri, Jawed Fareed and Job Harenberg
Received: 5 December 2019; Accepted: 14 January 2020; Published: 17 January 2020

check for updates

Abstract: This review comes as a part of the special issue "Emerging frontiers in GAGs and mimetics". Our interest is in the manipulation of heparan sulfate (HS) turnover by employing HS mimetics/heparin derivatives that exert pleiotropic effects and are interesting for interfering at multiple levels with pathways in which HS is implicated. Due to the important role of heparanase in HS post-biosynthetic modification and catabolism, we focus on the possibility to target heparanase, at both extracellular and intracellular levels, a strategy that can be applied to many conditions, from inflammation to cancer and neurodegeneration.

Keywords: heparan sulfate; heparin derivatives; neurodegenerative disorders; heparanase; cancer; mucopolysaccharidosis

1. Introduction

1.1. HS Turnover and the Role of Heparanase

Heparan sulfate (HS) is an anionic polysaccharide belonging to the glycosaminoglycan family that assembles as disaccharide building blocks of glucuronic acid (GlcA) linked α1-4 to N-acetyl-glucosamine (GlcNAc) and undergoes extensive modification through the action of at least four families of sulfotransferases and one epimerase. The sulfation of HS is carefully regulated in the ER-Golgi pathway where the first modification is introduced by N-deacetylase/N-sulfotransferase (NDST) enzymes and plays a key role in determining the subsequent modifications, dictating the position of the sulfated domains. Epimerization of some GlcA residues into iduronic acid (IdoA) can occur and it is followed by 2-O-sulfation of some iduronic acid residues, catalyzed by heparan sulfate 2-O-sulfotransferase (HS2ST), which can also act on some GlcA units. Next, on selected glucosamine residues sulfate groups are introduced by HS6ST1-3 transferases in the 6-O position and, finally, the relatively rare 3-O-sulfation is catalyzed by HS3ST1-6 [1]. Not only the length, but also the pattern of sulfation of HS is specific to the tissue and the moment of expression, and may be dynamically remodeled. For instance, high levels of 3-O-sulfated glucosamine were found in HS from follicular fluid, where nearly 50% of total HS is endowed with anticoagulant activity [2] and participates in the anticoagulant state of preovulatory follicular fluid. HS chains are usually attached to a core protein to form proteoglycans (HSPGs) that can be expressed on the cell membrane (syndecans and glypicans), or released in the extracellular matrix (ECM) where they constitute major structural molecules (agrin, perlecan, and type XVIII collagen) or be present in secretory vesicles [3].

HS is expressed on the cell surfaces of all mammalian cells where HSPGs participate in a variety of cellular processes and their functions depend on both HS and the protein core; for example, they serve as endocytic receptors and storage for macromolecules, such as lipid, growth factors, and morphogens [3,4], as modulators of cell mobility [5], and can participate in transportation of solutes between vessels and ECM (for review, see [6]). Also, heparan sulfate accounts for 60–90% of the total amount of the glycocalyx synthesized by endothelial cells [7] and whose anticoagulant and overall charge are very important for the repulsion of negatively charged molecules, including albumin, leukocytes, red blood cells, and platelets. Thus, the network of interactions of HS regulates fundamental biochemical and developmental processes and has been called the "HS-interactome" [8]. The last step of HS biosynthesis which is 6-O-desulfation by endosulfatases (SULF1 and SULF2), takes place on the cell surface and results in release of growth factors and cytokines immobilized on HSPGs and regulation of the effects of signal transduction [9,10]. In fact, the removal of sulfate groups from HS causes the release of HSPG-sequestered ligands that can act back on the cells and, indeed, overexpression of SULFs has been reported in a wide range of human tumors [11,12].

HSPGs expressed on the cell surface can be subjected to limited proteolysis and release in the medium or can be internalized by endocytosis and degraded by a multi-step process terminating in the lysosomes. The best characterized degradation pathway is that of ovarian granulosa cells in which two pathways have been described [13]. HSPGs anchored to the membrane by glycosylphosphatidylinositol (GPI) are quickly transported to lysosomes after endocytosis. Instead, HSPGs with transmembrane protein domains are first treated in prelysosomal compartments for removal of the protein core and partial degradation of HS chains. Secondly, HS chains are completely degraded in lysosomes. Differently, HSPGs in cultured rat hepatocytes have been shown to be long recycled back to the plasma membrane or to be associated with intracellular compartments before being degraded in lysosomes with no preliminary processing in early endosomes [14]. At the moment it is not clear if differences in HSPGs endocytosis reported in literature could be justified by the cellular context and the type of extracellular ligand.

The only known mammalian endoglycosidase able to cleave HS is heparanase (HPSE), which is secreted as a latent 65-kDa enzyme, which rapidly binds to HSPGs and the complex is then internalized by endocytosis [15]. Heparanase uptake is a prerequisite for the delivery to lysosomes where it is activated by cathepsin L and cuts HS at a limited number of sites, specifically the β-(1,4) glycosidic linkage between GlcA and GlcNS, producing fragments that are 10–20 saccharide units in length and still able to interact with protein ligands [16,17]. Also, a second HPSE protein named heparanase-2, without enzymatic activity, has been discovered and can compete for the substrate thus inhibiting HPSE activity but, its role in healthy tissues is broadly unknown [18]. Upon heparanase action, another nine exo-enzymes are responsible for the rapid and complete degradation of HS fragments: five sulfatases, three glycosidases, and an integral membrane enzyme required for the transfer of acetyl groups [19]. The process is influenced by the structure of the to-be-degraded HS: in CHO mutant cells, HS bearing reduced 2-O-sulfation was less cleaved by intracellular heparanase thus allowing recycling of unprocessed proteoglycans. In fact, higher amounts of extracellular HS chains were detected and accounted for the missing intermediate and small fragments observed inside the cells [20]. It has also been shown that heparanase drives fusion of lysosomes with autophagosomes thus controlling the basal levels of autophagy and contributing to maintain homeostasis [21] (Figure 1). Although numerous studies have accumulated regarding HS turnover especially in the last years, there is still debate on certain aspects which remain unclear. For example, the exact location and moment of activation of heparanase, whether in late endosomes or lysosomes, is still not precisely defined, together with the mechanism of HSPGs trafficking. We can speculate that a certain number of possibilities are available rather than a single linear mechanism, all converging to a final aim which is the reaction of the cell to different types of stimuli.

Synthesis and degradation of HS are both complex pathways involving a variety of different enzymes, spatially and temporarily tuned to produce heterogeneous chains with different sulfation

degree but tissue-specific expression of ligand-binding sequences. The overall pattern of HS modification appears relatively constant within a specific cell type or organ; therefore, the control of HS biosynthesis must be strictly regulated [22]. Not unexpectedly, altered levels of HSPGs or altered expression of genes coding for HS biosynthetic enzymes have been associated with the development of many diseases [23–29].

Today, all genes responsible for HS biosynthesis have been cloned and identified, which helps investigate the possible association of these genes with several pathologies. Also, mouse models in which different genes important for HS biosynthesis have been knocked out have helped understanding that genetic ablation of biosynthetic enzymes does not strictly correlate with a predicted phenotype in vivo [30,31], probably due to the existence of compensation mechanisms and to functional redundancy between gene family members involved in HSPG biosynthesis and redundancy in HS sequence–activity relationships. For example, ablation of the gene EXT1 in mice, which codes for a polymerase involved in the elongation of HS chains, resulted in loss of HS, disruption of gastrulation, and embryonic lethality before E8.5 [32]. In other cases, the outcome of a gene knockout may be complex as several enzymes occur in isoforms [22]. Mice that lack 3-O-sulfotransferase-1 (3-OST-1) do not show a procoagulant phenotype, although the 3-O-sulfate group is essential for the interaction of vascular HS with antithrombin [26]. Nevertheless, the other existing 3-OST isoforms have distinct substrate preferences, and may therefore regulate different biologic properties of HS [33,34]; therefore, the final phenotype is not explained by their compensatory activity. Actually, all experimental data accumulated cannot be summarized by a simple scheme.

1.2. The Use of HS Mimetics

Due to the pleiotropic effects that HS can exert and to the fact that HSPGs are ubiquitous, the idea of interfering with HS turnover can either be seen as the intriguing possibility to obtain multiple effects or the limiting fear that non-specificity would impact undesired pathways. According to most of the observations reported to date, only certain interactions rely on specific oligosaccharide sequences [35,36], whereas many others rely on a certain type of sulfation or negative charge density [37,38]. Nevertheless, the interest in HS-protein interactions is continuously growing also thanks to advance in analytical techniques and chemical synthesis of oligosaccharides with precise structures which bring light on the structural requirements for HS activity [39,40].

It is well known that heparin, which can be considered a highly sulfated version of heparan sulfate, has been used clinically for more than half a century as anticoagulant drug and has been shown to possess a number of beneficial effects in other diseases than thrombosis [41]. Prolonged administration of heparin can cause adverse effects, mostly related to bleeding [42], but also an immunological reaction, heparin-induced thrombocytopenia [43–45]. Other side effects are clinically irrelevant, despite the possible interactions that can be established following heparin diffusion into tissues, suggesting that they may be absorbed by the network of proteins with which heparin and heparan sulfate interact. These considerations support investigation on the use of heparin as a starting material to generate derivatives or HS mimetics as therapeutic agents to interfere with pathways in which HS is involved as a means of intervening in biochemical processes for medical purposes.

A plethora of different compounds both of GAG and not-GAG nature have been synthesized, the potential use of which has been comprehensively and recently reviewed [46–48]. A body of evidence indicates that the altered expression or activity of heparanase determines a profound impact on tumor behavior; indeed, heparin analogs able to inhibit heparanase have been developed to primarily target cancer and some proved very active and have been tested in clinical trials [49].

This review will focus on the possibility to control HS turnover by acting upon heparanase, at both extracellular and intracellular levels, a strategy that can be applied to many conditions, from inflammation to cancer and neurodegeneration. Many papers on HPSE have been written, and it is not our purpose to review exhaustively the biological literature on heparanase and the use of heparin derivatives, which has been undertaken successfully elsewhere [46,47,49].

Heparanase has a role intracellularly where it is involved in the catabolism of HS but it is also present extracellularly. On one hand, heparanase is overexpressed in many tumors and the active form of the enzyme is released extracellularly, therefore, explaining the rational of employing HPSE inhibitors to block tumor progression. On the other hand, in different conditions such as mucopolysaccharidosis, and, in particular, Sanfilippo syndrome, which is a neurodegenerative lysosomal storage disease, the use of HPSE inhibitors may impact HPSE action and influence the global distribution of HSPGs.

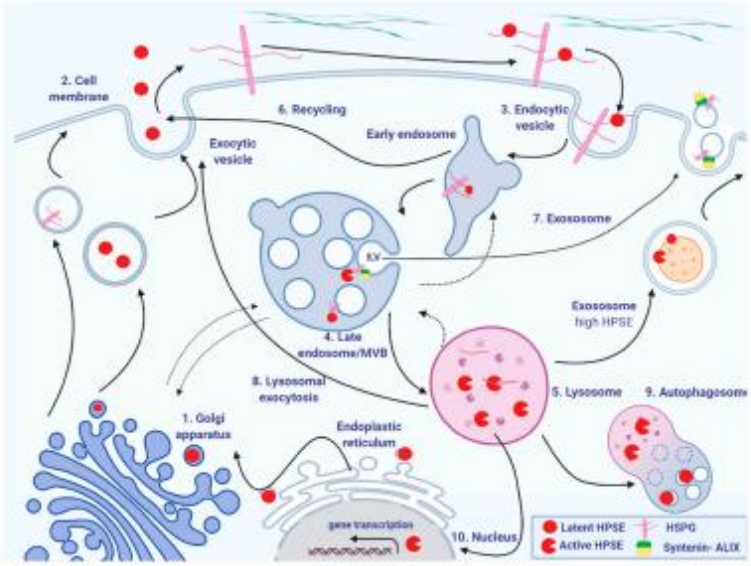

Figure 1. Schematic model of heparan sulfate proteoglycans and heparanase trafficking. (1) In the Golgi apparatus HS chains are polymerized and preHPSE is processed to produce proHPSE by the elimination of the N-terminal signal peptide. (2) The newly biosynthesized HSPGs are then shifted to the cell membrane where they can interact with the proHPSE and (3) the complex is rapidly internalized by endocytosis and then (4) accumulated in the late endosome. (5) Upon fusion of the late endosome with lysosome, proHPSE is activated and cleaves HS chains that are completely degraded by lysosomal hydrolases. (6) HPSE and HSPGs can be recycled to the cell surface from endosomes. It appears that active HPSE pursues other paths in the cells. (7) Trimming of HS from syndecans by active HPSE present in late endosomes leads to formation of the syndecan-syntenin-ALIX complex [50]. Intraluminal vesicles (ILV) are then formed by the invagination of endosomal membranes, resulting in the formation of multivesicular bodies (MVBs). MVBs release ILVs as exosomes upon fusion with the cell membrane and deliver their cargo to recipient cells. In the presence of high levels of HPSE, the enzyme can be found on the surface of exosomes and modulates tumor microenvironment. (8) Lysosomal exocytosis has been observed in malignant cells. (9) HPSE also regulates autophagy by driving fusion of lysosomes with autophagosomes which degrade macromolecules into monomeric units. (10) Perinuclear lysosomal HPSE can also translocate into the nucleus and regulate gene transcription and cell differentiation.

2. HS in Neurodegenerative Disorders

2.1. Different Involvement of HS in Neurodegenerative Disorders

Convergent phenotypes have been observed among the major pathologies affecting the brain. Neurodegenerative diseases are characterized by progressive accumulation of specific protein aggregates in the brain, e.g., amyloid-β (Aβ) in Alzheimer's disease (AD), α-synuclein in Parkinson's disease (PD) [51], and proteins with expanded polyglutamine (polyQ) in Huntington's disease (HD) [52].

According to the concept of "seeding", soluble proteins with nonnative conformations could assemble to form long unbranched structures called amyloid fibrils, able to trigger further incorporation of monomers into the fibrils. Regardless of the nature of the amyloid protein, HS has been found in all extracellular amyloid deposits [53,54], and HSPGs have been shown to be present at all stages of the degeneration process: neuron, intracellular and extracellular neurofibrillary tangles (NFTs). These fibrillary aggregates are formed by hyperphosphorylated forms of the microtubule-associated protein tau and have been detected in many neurodegenerative disorders, including AD [53,55–59]. Membrane-associated HS participates in the uptake and internalization of tau seeds [54], and concomitant hyperphosphorylation of tau was observed in neuroblastoma cultures [60], justifying the possible association with tau neurons. Moreover, cell surface HS directly binds fibrillar Aβ [61] and mediates its stabilization, internalization and deposition [62,63]. Evidence for HS participation in the development of amyloid disorders was also confirmed by overexpression of heparanase which resulted in inhibition of HS–amyloid interactions [64,65]. Accumulation of HS was also observed in neuronal nuclei in AD brain and it ultimately ended in altered protein expression and neuronal dysfunction [66]. Interestingly, HS may play distinct and partly contradictory roles in Aβ aggregation and deposit. In fact, binding of HS to the enzyme β-secretase (BACE1), involved in the liberation of Aβ peptide from the amyloid precursor protein (APP), prevents proteolytic cleavage and therefore the formation of Aβ peptide [67]. A comprehensive review has been recently written on HS and tauopathies [68].

HS mediates the fibril uptake of tau and α-synuclein but not Hungtington fibrils, suggesting that the mechanism depends on cell type and on certain type of sulfation of HS but not on specific sequences [69]. Castillo et al. showed that removal of O-sulfates led to a significant loss of heparin-enhanced Aβ fibrillization [70], whereas later Zhang et al. observed the presence of 6-O-sulfated glucosamine residues within the HS sequence interacting with Aβ [71], and recently 6-O sulfation was identified as a major determinant of tau binding in vitro [72]. Finally, the central role of 3-O-sulfation in tau abnormal phosphorylation was recently discovered by inhibiting the HS3ST2 enzyme in zebrafish, which resulted in arrest of tauopathy and animal functional recovery [60].

APP and Aβ are degraded (or recycled) in part by an endosomal–lysosomal pathway [73–75], and lysosomes are responsible for degradation of internalized aggregates in both neurons and in glial cells [76]. Efficient clearance of extracellular protein aggregates would prevent their transfer between cells, whereas compromised lysosomal efficiency may impair the degradation of many molecules normally processed within these organelles. Indeed, deficiency of lysosomal hydrolases is associated with the development of many human diseases, referred to as lysosomal storage disorders, which are often characterized by neurodegeneration [77]. Particularly, shortage or lack of specific lysosomal GAG-degrading enzymes impairs the autophagosome–lysosome fusion and leads to accumulation of GAGs; these diseases are called mucopolysaccharidoses (MPS) and many subtypes have been identified depending on the type of GAG and the specific enzyme affected. MPS III, called also Sanfilippo syndrome, is caused by deficiency of the lysosomal enzyme N-sulfoglucosamine sulfohydrolase (SGSH), resulting in incomplete degradation of HS and dramatic effects on the central nervous system with devastating consequences. Undegraded HS can affect cell functions not only due to its storage into lysosomes, but also when present outside the cell; probably, failure to degrade GAGs in MPS results in secretion and deposition in the ECM, as dysregulation of the ECM has been identified in several case reports [78,79]. Increased levels of protein markers associated with AD and PD have been detected in the brains of MPSIII mice: deposition of hyperphosphorylated tau and tau kinase, lysozyme, amyloid-β and amyloid precursor protein are all evident [80]. Moreover, α-synuclein aggregation and accumulation with neurons were observed both in MPSIII patients [81,82] and in MPSIIIA mice [83,84].

2.2. *The Use of HS Derivatives in Neurodegenerative Disorders*

Therapeutic approaches that target the central nervous system (CNS) are challenging due to the presence of the blood–brain barrier (BBB), which in healthy brain impedes most compounds from transiting from the blood to the brain. BBB permeability is influenced by molecular weight, charge, lipid

solubility, surface activity, and relative size of the molecule [85]. If active compounds are small enough or lipid soluble they can pass the BBB by passive diffusion, alternatively they may be actively uptaken by receptors, transporters or carriers expressed by the cells of the BBB (endothelial cells, pericytes, astrocytes and neurons). The components of the BBB continuously adapt in response to various physiological changes in the brain and the integrity of the BBB is compromised in many pathological conditions including PD, AD, and MPS [81,86,87]. As a consequence, cytokines and immune cells could enter the CNS, activate glial cells, and cause alterations in the extracellular environment with consequent inflammation and damage [88,89].

A body of evidence supports targeting of HS-protein interactions in tauopathies as a therapeutic strategy. As already mentioned, studies on amyloidosis showed that overexpression of heparanase resulted in disruption of the HS–amyloid interactions, suggesting a potential strategy to interfere with the formation of fibrils. Indeed, administration of exogenous GAGs could competitively inhibit the harmful processes mediated by endogenous GAGs [90] and, in fact, heparin disaccharides were shown in vitro to pass the BBB and to efficiently decrease Aβ deposition [91], whereas chemically synthesized heparin-like oligosaccharides up to decasaccharides proved able to reduce the uptake of tau oligomers limiting their infectivity [92]. Neuroparin, a mixture of oligosaccharides with average MW of 2.1 kDa obtained by gamma irradiation of heparin, crosses the blood–brain barrier and was reported to attenuate the abnormal tau immunoreactivity in rat hippocampus and to have neuroprotective effects in several animal models of AD [93,94]. These compounds were small enough to cross the BBB and indeed an important consideration for therapeutic purposes is the extent of bioavailability of the administered GAG in the CNS. Nevertheless, in inflammatory conditions and highly damaged tissues, it is probable that increased permeability of the BBB would allow the entrance of compounds that would normally be rejected.

2.3. The Possible Use of HS Derivatives in MPS III

In MPS III disease, neurodegeneration is a consequence of HS accumulation in lysosomes [95]. To date, no treatments have shown promise in modifying the progression of this exceptionally rare, but ultimately lethal, disease. A review has been recently published summarizing treatment approaches for the brain in MPS [96]; therefore, only a brief summary on possible therapies will be treated in this paragraph, with a final focus on the use of heparin derivatives.

The promising Enzyme Replacement Therapy (ERT), which works for MPS I, MPS II, MPS IVA, and MPS VI, is more difficult in MPS III, where it should cross the blood–brain barrier. The approach is based on systemic delivery of recombinant lysosomal hydrolases which are internalized through mannose-6-phosphate receptors [97–99]. Intravenously delivered enzyme has been shown not to cross the BBB in an adequate amount to prevent progression of neurological manifestations [100]. Gene therapy as a treatment for MPS can potentially provide a stable and continuous source of enzyme in combination with immunosuppression to prevent an immune response against the vector. Indeed, intracerebral injection of the vector AAVrh10-hMPS3A in four children with MPS IIIA and of the vector ABO-102 in six MPS IIIA patients showed good tolerability and evidence of decreased neurocognitive decline [101]. Fusion of the recombinant enzyme to a monoclonal antibody against the human insulin receptor has been shown by Boado and coworkers to facilitate the uptake in the brain by exploiting the transport mechanisms already present in the BBB [102,103]. Another strategy called substrate reduction therapy (SRT), aims to inhibit the early stage of the lysosomal degradation pathway, reducing GAGs synthesis [104]; however, results of a 6-month clinical trial with miglustat—an imminosugar used in the treatment of type I Gaucher disease—showed no improvement of cognition or behavior in MPS III patients [105]. Another approach under investigation is chaperone therapy, with the aim of partially restore the missing enzymatic activity. In fact, 10% activity is considered sufficient to prevent lysosomal GAG storage in MPS patients [106]. Lastly, also hematopoietic stem cells transplantation (HSCT) which consist in delivery of donor stem cells producing the deficient lysosomal enzyme, has been extensively studied over the past decades with variable results [107].

HS in MPS patients is not only accumulated in lysosomes, but seems to be redistributed to different cellular and extracellular localizations [108,109]. De Pasquale et al. recently published an innovative approach called substrate-masking technology based on sequestering of extracellular excess HS (and/or DS) with consequent restoring of the natural equilibrium. Treatment of primary fibroblasts from MPS IIIA- and MPS IIIB-patients with the protein NK1 resulted in decreased GAGs accumulation and restoration of FGF2 signaling [110].

As already suggested [111], targeting HPSE in lysosomes may be an interesting way to affect autophagy either by employing HPSE inhibitors, whose ability to cross the BBB is nevertheless still unclear, or by decreasing the lysosomal content of HPSE. For example, treatment with the inhibitor PG545 was shown to decrease autophagy and promote accumulation of HPSE extracellularly while reducing its level in the lysosomes [112]. Our strategy is to employ HPSE inhibitors as a mean to affect HS turnover, based on the idea that uncleaved HS chains may fuel recycling of HSPGs and lead to a lower amount of HS degraded in lysosomes. We have tested several HPSE inhibitors on primary fibroblast from KO MPS-IIIA and spontaneously mutated MPS-IIIA mouse models [113]. Indeed, treatment with these compounds could affect HS turnover, leading to decreased HSPGs production.

3. HS in Cancer

3.1. Expression of HSPGs in Tumorigenesis

Heparan sulfate and HSPGs are expressed on all eukaryotic cells, including cancerous cells and stromal cells surrounding the tumor and play an important role in tumor–stroma cross-talk, and thus in cancer development, transformation, growth, and metastasis. Therefore, alteration of the normal expression levels of HSPGs has often been described in tumors. Several HSPGs have been shown to be upregulated in many cancers [114]; for example, increasing expression level of Agrin in hepatocellular carcinoma [115] and of glypican-1 in pancreas carcinoma was detected and associated with poor prognosis [116]. Levels of glypican-1 and syndecan-2 are also increased in colorectal cancer [117]. Syndecan-1 has been demonstrated to regulate $\alpha v\beta 3$ and $\alpha v\beta 5$ integrin activation during angiogenesis and tumorigenesis on mammary carcinoma cells [118], whereas shedding of syndecan-2 has an antiangiogenic effect on the endothelium [119]. Moreover, breast cancer was found to upregulate glypican-1 [120] and syndecan-4 [121] and to downregulate glypican-3 [122], whereas low expression of glypican-3 promotes tumor proliferation and metastasis [123]. Contrarily, glypican-3 was found to be overexpressed in approximately 70% to 80% of hepatocellular carcinomas [124] and high glypican-5 expression levels in non-small cell lung cancer were associated with poor differentiation, vascular invasion, regional lymph node metastasis, and a higher TNM stage (TNM classification of malignant tumors) [125]. In addition, glypican-2 is upregulated in neuroblastoma and associated with poor overall survival [117].

In general, remodeling of HSPGs through enzymatic modification of HS chains is associated with malignant transformation of cells and can potentially serve as molecular biomarker to aid in the diagnosis and prognosis of cancer [114,126]. Also, alteration of glycosylation affects cellular adhesion and is associated with oncogenic transformation and metastasis [114]. Indeed, altered HSPGs glycosylation has been described in lung and brain cancer [127].

3.2. Tumor–Stroma Cross-talk

Tumor stroma is composed of the ECM including proteoglycans, fibronectin, collagen, cytokines, and growth factors. As the tumor evolves, the stroma undergoes tissue remodeling under the action of enzymes able to modify the glycosidic chains of the ECM, i.e., glycosyltransferases, sulfotransferases, sulfatases, and heparanase [128]. The presence and amount of these GAG-related enzymes help to identify high-risk patients and to develop personalized therapeutics [129]. Indeed, Barkeer and collaborators demonstrated that elevated O-glycosyltransferases GALNT3 and B3GNT3 expression regulates cancer stem cell markers in pancreatic cancer and their knockdown leads to decreased

clonogenicity and migratory capacity [130]. Increased heparanase expression is also often described to promote an aggressive tumor behavior via multiple mechanisms [71,83]. It has been demonstrated that tumors are more aggressive when developed in transgenic mice overexpressing heparanase (Hpa-Tg and MMTV-heparanase), whereas smaller tumors develop in Hpa-KO mice [95,120].

HPSE functions inside the cell to promote autophagy and tumor growth by driving fusion of lysosomes with autophagosomes thus controlling the basal levels of autophagy [111]. Heparanase is an important player not only in maintaining homeostasis, as a postsynthetic modification enzyme for HS structure but also for its non-enzymatic and HS-independent effects which may contribute to tumor aggressiveness [131,132]. Therefore, heparanase orchestrates cellular responses in both normal and pathologic conditions. HSPGs bind to numerous bioactive molecules, i.e., growth factors, cytokines, chemokines, enzymes, which are stored in the ECM and can be released upon cleavage by extracellular heparanase. This strategy is adopted by tumor cells to ensure rapid tissue response as a fast-acting mechanism independent from *de novo* protein synthesis that meets their needs to promote tumor growth, angiogenesis, peripheral immune tolerance and formation of a metastatic niche. Briefly, tumor cells can change the nature of the microenvironment and vice versa the microenvironment can affect how a tumor grows and spreads [133].

Heparanase promotes signal transduction, including Akt, STAT, Src, Erk, HGF-, IGF- and EGF-receptor signaling [131]. Moreover, HPSE regulates the transcription of many other factors spanning from proangiogenic (i.e., VEGF-A, VEGF-C, COX-2, and MMP-9), to pro-thrombotic (i.e., tissue factor), proinflammatory (i.e., TNFα, IL-1, and IL-6), profibrotic (i.e., TGFβ), mitogenic (i.e., HGF), and osteolyic (RANKL) [133–135]. In summary, more and more functions of HPSE are being discovered, thus confirming its importance also in normal cell processes and the need of controlling its action and expression. The presence of heparanase was reported in Langerhans cells [136], where its function still has to be elucidated, and in astrocytes in mice after ischemia, where it can participate in the repair process [137]. Interestingly, increased expression of heparanase was found in placentas with preeclampsia [138,139], where it would enhance the increase of VEGF release and it would influence the invasion of trophoblast, similarly to the invasion of cancer cells [140].

While heparanase upregulation by tumor cells is well documented, not enough attention has been given to the protumorigenic function of heparanase expressed by non-tumor cells residing in the tumor microenvironment. In fact, heparanase released from platelets, neutrophils and mast cells upon degranulation participates in ECM degradation, facilitating diapedesis and extravasation of inflammatory cells [141–145]. HPSE release can therefore be a strategy used by metastatic tumor cells to invade blood and lymphatic vessels. Moreover, HPSE was discovered to mediate TLR activation at the cell membrane, followed by Erk/p38/JNK activation therefore regulating cytokine expression by macrophages, their activation and function in tumorigenesis and cross-talk with the tumor microenvironment [146].

Tumor cells are able to influence the responses of surrounding healthy cells as demonstrated by experiments in which healthy lymphocytes were co-cultured with sera from breast cancer patients or media from MCF-7 cells. Increased expression of HPSE and secretion of exosomes was indeed observed, thus revealing the importance of cross-talk [147,148]. Exosomes serve as mediators for intercellular communication through the delivery of proteins, factors and HS chains, important for signaling processes. Heparanase overexpression dramatically increases exosome secretion in human cancer cells of myeloma, lymphoblastoid, and breast cancer [149].

It has been recently discovered that chemotherapy upregulates heparanase expression in myeloma surviving cells and induces secretion of chemoexosomes with heparanase loaded on surface [150]. These tumor chemoexosomes can remodel extracellular matrix by degrading ECM heparan sulfate and/or by transferring their heparanase cargo to cells where HS degradation will induce signal activation [150], resulting in enhanced secretion of an important myeloma growth factor, TNF-α, by macrophages. Additionally, heparanase stimulates the expression of MMP-9 via ERK signaling, promoting shedding of syndecan-1 proteoglycan (CD138) from the myeloma cell surface [150]. Shed

syndecan-1 ectodomain was shown to capture VEGF and form a complex that activates integrin and VEGF receptors on adjacent endothelial cells thereby stimulating tumor angiogenesis [151].

3.3. Heparanase Targeting by Heparin and Its Derivatives in Cancer Therapy

As venous thromboembolism is a well-known cause of death in patients with cancer [152], heparin has been frequently used in the treatment of cancer-associated thromboembolism. Accordingly, accumulation of clinical evidence shows that cancer patients treated with unfractionated and low-molecular weight heparin (LMWH) survive longer than patients treated with other anticoagulants, especially patients in the early stage of the disease [153–157]. Heparin has been showned to possess anticancer, antiangiogenic, and antimetastatic activity [158,159], including inhibition of heparanase, blocking of P- and L-selectin-mediated cell adhesion, and inhibition of angiogenesis, but its anticoagulant activity and the possible side effects as bleeding and heparin-induced thrombocytopenia limit long-term treatment. As already mentioned, heparin derivatives or HS mimetics have been synthesized with reduced or absent anticoagulant activity but maintaining their binding selectivity potential towards a vast array of HS-binding proteins, many of which with pivotal roles in cancer growth and progression [46].

Nowadays the interest of researchers in oncology is not only limited to tumor cells but especially on tumor microenvironment. Information gathered on the two topics is so vast that they appear as two different specialized areas of research that are, on the contrary, profoundly interconnected. The separation into the following sections is based on experimental observations either directed on the tumor itself or on the components of the tumor microenvironment.

3.3.1. Targeting the Tumor

Numerous clinical association studies have consistently demonstrated that upregulation of heparanase expression correlates with increased tumor size, tumor angiogenesis, enhanced metastasis, and poor prognosis [160,161]. In contrast, knockdown of heparanase or treatments of tumor-bearing mice with heparanase-inhibiting compounds markedly attenuate tumor progression [162–164], further underscoring the potential of anti-heparanase therapy for multiple types of cancer.

Extensive research was done on targeting HS-degrading activity of heparanase [49,128,165,166]. The heparanase inhibitory effects of non-anticoagulant heparin have been described by Bar-Ner et al., suggesting that heparanase inhibition was dependent on polysaccharide size, degree and pattern of sulfation, and N-substitution of hexosamines [167].

Some supersulfated low-molecular weight heparins (ssLMWH) have been synthesized with low anticoagulant activity despite the high degree of sulfation and were shown to reduce synovial sarcoma growth and metastases in vitro and in vivo by interfering with the activity of heparanase, growth factor/receptor axes and proinflammatory molecules (e.g., leucocyte elastase and cathepsin G) [168]. Another compound, SSLMW-19, a key factor in the regulation of iron metabolism, and also involved in carcinogenesis and metastasis, was shown to rapidly and strongly inhibit the expression of hepcidin in vitro and in vivo [169].

Glycol-splitting of unsubstituted uronic acids obtained by periodate oxidation and borohydride reduction has been applied to a variety of heparin derivatives and increased the flexibility of the molecules for a better interaction and inhibition of heparanase or growth factors. M402 (Necuparanib) is a glycol-split LMWH with reduced anticoagulant activity [170] that was found to reduce tumor burden in vivo in KPFMC pancreatic cancer mice model at a dose of 40 mg/kg/day and reduce AsPC-1 pancreatic cancer cell line proliferation and invasion in vitro in a 3D-culture model [171]. Boothello et al. synthesized a non-saccharide compound, G2.2, which is structurally homogeneous and easy to obtain by chemical synthesis, as a mimetic of an HS hexasaccharide active on cancer stem cells. This HS mimetic reduced in a dose-dependent manner the growth of colon subcutaneous xenografts in mice and delayed the growth when added to oxaliplatin and 5-fluorouracil, which are the most frequently used chemotherapy treatment for colon cancer [172]. Also, polysaccharides from

different sources are potentially able to interfere with tumorigenesis. For example, an oversulfated heparin-like polysaccharide from marine origin was recently evaluated for its ability to reduce cancer cell characteristics on human endometrioid cancer cell line in vitro. This compound effectively reduces the ability of tumor cells to initiate migration by inducing 51.6% of slowdown and induces 87% of inhibition of tumor cell invasion on Transwell compared to non-treated cells (unpublished data). It also inhibits endometrial tumor cell proliferation and is well tolerated at concentrations of 100, 75, 50, and 25µg/mL (unpublished data). A sulfated oligosaccharide mimetic of heparan sulfate, PI-88, was used to inhibit HS effector functions and heparanase activity. PI-88 reduced tumor volume by 66–70% in RIP1-Tag2 mice model of pancreatic islet cell carcinogenesis [173]. Joyce and collaborators also noticed decreased tumor cell proliferation, increased apoptosis and impaired angiogenesis associated with reduction of VEGF-A and its receptor VEGF-R2 on the tumor endothelium [173].

3.3.2. Targeting the Tumor Microenvironment

Impact of heparanase on tumor progression is related to its function in mediating tumor-host cross-talk, priming the tumor microenvironment to better support tumor seeding and growth [174]. Targeting of heparanase in the tumor microenvironment is a promising strategy to restrain tumor growth and dissemination. Indeed, a study showed the effect of heparanase-neutralizing antibodies to attenuate the growth of lymphoma cells that do not express heparanase, implying that targeting microenvironment may be sufficient [175].

Heparin derivatives and HS mimetics can also affect invasion and metastatic tumor behavior by counteracting HSPGs functions.. Yoshitomi et al. observed reduced tumor growth dissemination on several murine metastatic models by employing a glycol-split weak anticoagulant heparin [176].

Another strategy to contain metastatic progression could be targeting the angiogenic pathway. A low-molecular-weight glycol-split heparin (ST2184), generated by nitrous acid depolymerization of an undersulfated glycol-split heparin derivative (ST1514), was shown to act as VEGF antagonist by exploiting binding to VEGF165 while preventing receptor engagement [177]. This molecule inhibited neovascularization in the chick embryo chorioallantoic membrane, metastatic dissemination to the lung in the B16-BL6 mouse model of melanoma and significantly reduced angiogenesis of human MeVo melanoma xenografts [46,177]. Naggi and coworkers developed a 100% N-acetylated and 25% glycol split heparin, known as SST0001 (Roneparstat) [178], which is a potent heparanase inhibitor that is also able to suppress angiogenesis and to downregulate HGF, VEGF, and the expression of ECM-remodeling proteins (Matrix metalloproteinase 9, pentraxin, and urokinase-type plasminogen activator) [179]. Also, in combination with dexamethasone it was able to inhibit myeloma tumor growth in vivo through dual targeting of the tumor and its microenvironment via the heparanase/syndecan-1 axis [180].

We previously mentioned that M402 heparin mimetic effectively targeted pancreatic tumor cells. Interestingly, MacDonald et al. observed that M402 also targeted the stromal compartment. On a co-culture of pancreatic tumor cells and stellate cells that mimics epithelial–stromal interactions, treatment of M402 significantly decreased the invasive behavior in a dose-dependent manner, whereas in vivo it extended survival and reduced metastasis by reducing the protein levels of matrix metalloprotease 1 and by increasing the tissue inhibitor of metalloproteinase 3 (TIMP3) [171]. Karoli et al. demonstrated that carbohydrate-based HS-mimicking compounds, PI-88 and analogues, inhibit heparanase and compete with growth factors (FGF-1, FGF-2, and VEGF) for binding to HS, and therefore impact anti-angiogenic and anti-metastatic activity [48,181]. Another octasaccharide-based heparin mimetic synthesized by Dollé and coworkers was characterized in vitro for its binding affinities and towards VEGF-A, FGF-2, PDGF-β, and SDF1-α using the BIAcore technology and for the potential inhibition in an heparanase activity assay [182]. This novel molecule could thus potentially inhibit angiogenesis by interfering with components of the extracellular matrix. Lim and collaborators developed saccharide-free polyproline-based GAG mimetics (PGMs) that recapitulate key GAG structural features, notably the sized repeating units, periodicity, and helicity. GAG activities were also maintained, indeed PGMs effectively inhibited chondroitin sulfate-E binding to P-selectin which

is implicated in metastasis, thrombosis and inflammation and successfully attenuate hematogenous metastasis in vivo in mice model as effectively as heparin and tinzaparin without any adverse effects on mice model, suggesting its safe use in vivo [183].

3.4. Clinical Considerations

Over the last 30 years of active research, there has been an explosion of information about the molecular biology of cancer. The challenge remains to translate this information into advances in patient care to convert new molecular information into drug therapy. According to all these studies, high levels of heparanase could be used as predictive and prognostic molecular marker for cancer. In a study published in 2016, high level of HPSE in the melanoma metastases predicted poor prognosis in patients stage IVc [184]. However, HPSE expression in the primary tumor does not always reflect metastatic output. This is the case in breast cancer patients, where the primary lesion stained positive for heparanase in some cases while the metastasis stained negative, and vice versa [185]. In addition, we observed high HPSE expression in all primary lesions from endometrioid cancer grade 1 patients despite different patterns and degree of invasions.

A number of preclinical and clinical studies have suggested that heparin and LMWH treatment in addition to conventional treatment significantly improves overall survival in cancer patients with advanced stage cancer but increasing the risk for bleeding complications [186,187]. Regarding the use of heparanase inhibitors to block tumor progression and their weak anticoagulant activity, Muparfostat PI-88 was the first heparanase inhibitor tested in early stage clinical trials in cancer patients in 2011. PI-88 was administered both alone and together with docetaxel to cancer patients in two Phase 1 studies validating their tolerance and safety for the patients [135,136]. PI-88 was also the first to enter clinical trials reaching phase III, where it was administered as an adjuvant therapy for hepatitis virus related hepatocellular carcinoma (HV-HCC) after its surgical resection. PI-88 prolonged the disease-free survival in the microvascular invasion subgroup (40% of the trial population) and exhibited anti-inflammatory properties [137]. Liao et al. demonstrated that heparanase was upregulated in both postsurgical plasma of HCC patients and in orthotopic mouse model induced after hepatectomy [137]. Upregulation of HPSE enhanced the sensitivity of HCC cells to PI-88 and thus the inhibitory effect of PI-88 on cell proliferation and migration. Likewise, Ramani et al. also showed that heparanase is upregulated in response to chemotherapy in myeloma patients and the surviving cells acquire drug resistance due to heparanase-mediated ERK signaling [138].

SST0001 heparin mimetic effectively inhibited myeloma growth in vivo, even when confronted with an aggressively growing tumor within human bone [180]. An open-label, multicenter, phase I, first-in-human study was designed to assess the safety and tolerability profile of Roneparstat in patients with relapsed/refractory multiple myeloma, and was well tolerated by patients exposed to the drug at dose levels of 200 and 400 mg/day without any clinically relevant toxicities [188]. Consequently, Roneparstat was found to be highly effective and overcome initial chemoresistance when used in combination with chemotherapeutic agents against established and aggressive myeloma tumors growing within bone or to treat brain metastatic breast cancer [189,190].

Analysis of plasma samples of patients with metastatic pancreatic cancer enrolled in a phase I/II study show that treatment with necuparanib in addition to the standard of care significantly increased TIMP3 plasma protein levels confirming the in vivo and in vitro studies on pancreatic cancer models [171].

PG545 has been selected over the PG500 series of heparan sulfate mimetics for the ability to inhibit both angiogenesis and heparanase activity and was selected as the lead clinical candidate for oncology [191]. Eight years after, PG545 was then evaluated on a Phase I study in patients with advanced solid malignancies that had relapsed or was refractory to standard therapy, and showed a disease control up to 24 weeks in 38% of evaluable subjects with increases in innate immune cell activation, plasma IFNγ, TNFα, IP-10, and MCP-1 [192].

These heparin mimetics that inhibit heparanase enzymatic activity are being evaluated in numerous clinical trials for various types of cancer, and appear to be well tolerated and also beneficial in combination with conventional anticancer drugs, thus providing a strong rationale for applying anti-heparanase therapy. Another strategy uses heparanase-neutralizing monoclonal antibodies to target the interaction of heparanase with HS and has been tested in pre-clinical studies for various types of cancer, including myeloma, pancreatic carcinoma, and hepatocellular carcinoma [175]. These heparanase-neutralizing mAbs profoundly attenuated myeloma and lymphoma tumor growth and dissemination of tumor xenografts produced by human lymphoma cells in preclinical models [175].

Although clinical trials focus on cancer patients, the same heparanase inhibitors are likely to be applied in other applications as chronic inflammation, sepsis, autoimmune diabetes, diabetic nephropathy, bone osteolysis, pancreatitis, viral infection, acute kidney injury, thrombosis, and atherosclerosis, as well as various rare diseases like mucopolysaccharidosis. Additional opportunities for development of anti-heparanase therapeutics include monoclonal antibodies and the use of the recently published crystal structure of heparanase for identification of small inhibitory molecules [81].

4. Conclusions

We gathered existing data around the idea of interfering with HS turnover by affecting heparanase and, indeed, the literature does support this working hypothesis. It is hoped that the review will promote discussion regarding the concrete possibility to therapeutically use HS mimetics/heparin derivatives which are able to act on existing pathways and to modulate them. We are confident that new discoveries will help clarify the aspects of HS turnover which are still foggy.

Author Contributions: Conceptualization, writing—original preparation, review and editing, N.V. and N.Z.; supervision, A.d.A. All authors have read and agreed to the published version of the manuscript.

Funding: This research received no external funding.

Acknowledgments: We thank Antonella Bisio and MD Jean-Christophe Tille for critical reading of the manuscript.

Conflicts of Interest: The authors declare no conflicts of interest.

References

1. Esko, J.D.; Selleck, S.B. Order out of chaos: Assembly of ligand binding sites in heparan sulfate. *Annu. Rev. Biochem.* **2002**, *71*, 435–471. [CrossRef] [PubMed]
2. de Agostini, A.I.; Dong, J.C.; de Vantery Arrighi, C.; Ramus, M.A.; Dentand-Quadri, I.; Thalmann, S.; Ventura, P.; Ibecheole, V.; Monge, F.; Fischer, A.M.; et al. Human follicular fluid heparan sulfate contains abundant 3-o-sulfated chains with anticoagulant activity. *J. Biol. Chem.* **2008**, *283*, 28115–28124. [CrossRef] [PubMed]
3. Sarrazin, S.; Lamanna, W.C.; Esko, J.D. Heparan sulfate proteoglycans. *Cold Spring Harb. Perspect. Biol.* **2011**, *3*, a004952. [CrossRef] [PubMed]
4. Christianson, H.C.; Belting, M. Heparan sulfate proteoglycan as a cell-surface endocytosis receptor. *Matrix Biol.* **2014**, *35*, 51–55. [CrossRef]
5. Asplund, A.; Ostergren-Lunden, G.; Camejo, G.; Stillemark-Billton, P.; Bondjers, G. Hypoxia increases macrophage motility, possibly by decreasing the heparan sulfate proteoglycan biosynthesis. *J. Leukoc. Biol.* **2009**, *86*, 381–388. [CrossRef]
6. Bishop, J.R.; Schuksz, M.; Esko, J.D. Heparan sulphate proteoglycans fine-tune mammalian physiology. *Nature* **2007**, *446*, 1030–1037. [CrossRef]
7. Reitsma, S.; Slaaf, D.W.; Vink, H.; van Zandvoort, M.A.; Oude Egbrink, M.G. The endothelial glycocalyx: Composition, functions, and visualization. *Pflugers Arch.* **2007**, *454*, 345–359. [CrossRef]
8. Ori, A.; Free, P.; Courty, J.; Wilkinson, M.C.; Fernig, D.G. Identification of heparin-binding sites in proteins by selective labeling. *Mol. Cell. Proteom.* **2009**, *8*, 2256–2265. [CrossRef]
9. Uchimura, K.; Morimoto-Tomita, M.; Bistrup, A.; Li, J.; Lyon, M.; Gallagher, J.; Werb, Z.; Rosen, S.D. Hsulf-2, an extracellular endoglucosamine-6-sulfatase, selectively mobilizes heparin-bound growth factors and chemokines: Effects on vegf, fgf-1, and sdf-1. *BMC Biochem.* **2006**, *7*, 2. [CrossRef]

10. Dhoot, G.K.; Gustafsson, M.K.; Ai, X.; Sun, W.; Standiford, D.M.; Emerson, C.P., Jr. Regulation of wnt signaling and embryo patterning by an extracellular sulfatase. *Science* **2001**, *293*, 1663–1666. [CrossRef]
11. Lemjabbar-Alaoui, H.; van Zante, A.; Singer, M.S.; Xue, Q.; Wang, Y.Q.; Tsay, D.; He, B.; Jablons, D.M.; Rosen, S.D. Sulf-2, a heparan sulfate endosulfatase, promotes human lung carcinogenesis. *Oncogene* **2010**, *29*, 635–646. [CrossRef] [PubMed]
12. Tatrai, P.; Egedi, K.; Somoracz, A.; van Kuppevelt, T.H.; Ten Dam, G.; Lyon, M.; Deakin, J.A.; Kiss, A.; Schaff, Z.; Kovalszky, I. Quantitative and qualitative alterations of heparan sulfate in fibrogenic liver diseases and hepatocellular cancer. *J. Histochem. Cytochem.* **2010**, *58*, 429–441. [CrossRef] [PubMed]
13. Yanagishita, M. Glycosylphosphatidylinositol-anchored and core protein-intercalated heparan sulfate proteoglycans in rat ovarian granulosa cells have distinct secretory, endocytotic, and intracellular degradative pathways. *J. Biol. Chem.* **1992**, *267*, 9505–9511. [PubMed]
14. Egeberg, M.; Kjeken, R.; Kolset, S.O.; Berg, T.; Prydz, K. Internalization and stepwise degradation of heparan sulfate proteoglycans in rat hepatocytes. *Biochim. Biophys. Acta* **2001**, *1541*, 135–149. [CrossRef]
15. Gingis-Velitski, S.; Zetser, A.; Kaplan, V.; Ben-Zaken, O.; Cohen, E.; Levy-Adam, F.; Bashenko, Y.; Flugelman, M.Y.; Vlodavsky, I.; Ilan, N. Heparanase uptake is mediated by cell membrane heparan sulfate proteoglycans. *J. Biol. Chem.* **2004**, *279*, 44084–44092. [CrossRef]
16. Zetser, A.; Levy-Adam, F.; Kaplan, V.; Gingis-Velitski, S.; Bashenko, Y.; Schubert, S.; Flugelman, M.Y.; Vlodavsky, I.; Ilan, N. Processing and activation of latent heparanase occurs in lysosomes. *J. Cell. Sci.* **2004**, *117*, 2249–2258. [CrossRef]
17. Secchi, M.F.; Masola, V.; Zaza, G.; Lupo, A.; Gambaro, G.; Onisto, M. Recent data concerning heparanase: Focus on fibrosis, inflammation and cancer. *Biomol. Concepts* **2015**, *6*, 415–421. [CrossRef]
18. Levy-Adam, F.; Feld, S.; Cohen-Kaplan, V.; Shteingauz, A.; Gross, M.; Arvatz, G.; Naroditsky, I.; Ilan, N.; Doweck, I.; Vlodavsky, I. Heparanase 2 interacts with heparan sulfate with high affinity and inhibits heparanase activity. *J. Biol. Chem.* **2010**, *285*, 28010–28019. [CrossRef]
19. Hopwood, J.J. Enzymes that Degrade Heparin and Heparan Sulfate. In *Heparin, Chemical and Biological Properties, Clinical Applications*; Lane, D.A., Lindahl, U., Eds.; CRC Press Inc.: Boca Raton, FL, USA, 1989; pp. 191–228.
20. Bai, X.; Bame, K.J.; Habuchi, H.; Kimata, K.; Esko, J.D. Turnover of heparan sulfate depends on 2-o-sulfation of uronic acids. *J. Biol. Chem.* **1997**, *272*, 23172–23179. [CrossRef]
21. Shteingauz, A.; Boyango, I.; Naroditsky, I.; Hammond, E.; Gruber, M.; Doweck, I.; Ilan, N.; Vlodavsky, I. Heparanase enhances tumor growth and chemoresistance by promoting autophagy. *Cancer Res.* **2015**, *75*, 3946–3957. [CrossRef]
22. Esko, J.D.; Lindahl, U. Molecular diversity of heparan sulfate. *J. Clin. Investig.* **2001**, *108*, 169–173. [CrossRef] [PubMed]
23. Gotte, M.; Joussen, A.M.; Klein, C.; Andre, P.; Wagner, D.D.; Hinkes, M.T.; Kirchhof, B.; Adamis, A.P.; Bernfield, M. Role of syndecan-1 in leukocyte-endothelial interactions in the ocular vasculature. *Invest Ophthalmol. Vis. Sci.* **2002**, *43*, 1135–1141. [PubMed]
24. Xu, J.; Park, P.W.; Kheradmand, F.; Corry, D.B. Endogenous attenuation of allergic lung inflammation by syndecan-1. *J. Immunol.* **2005**, *174*, 5758–5765. [CrossRef] [PubMed]
25. Grobe, K.; Inatani, M.; Pallerla, S.R.; Castagnola, J.; Yamaguchi, Y.; Esko, J.D. Cerebral hypoplasia and craniofacial defects in mice lacking heparan sulfate ndst1 gene function. *Development* **2005**, *132*, 3777–3786. [CrossRef]
26. HajMohammadi, S.; Enjyoji, K.; Princivalle, M.; Christi, P.; Lech, M.; Beeler, D.; Rayburn, H.; Schwartz, J.J.; Barzegar, S.; de Agostini, A.I.; et al. Normal levels of anticoagulant heparan sulfate are not essential for normal hemostasis. *J. Clin. Investig.* **2003**, *111*, 989–999. [CrossRef]
27. Westphal, V.; Murch, S.; Kim, S.; Srikrishna, G.; Winchester, B.; Day, R.; Freeze, H.H. Reduced heparan sulfate accumulation in enterocytes contributes to protein-losing enteropathy in a congenital disorder of glycosylation. *Am. J. Pathol.* **2000**, *157*, 1917–1925. [CrossRef]
28. Morita, H.; Yoshimura, A.; Inui, K.; Ideura, T.; Watanabe, H.; Wang, L.; Soininen, R.; Tryggvason, K. Heparan sulfate of perlecan is involved in glomerular filtration. *J. Am. Soc. Nephrol.* **2005**, *16*, 1703–1710. [CrossRef]
29. Arikawa-Hirasawa, E.; Watanabe, H.; Takami, H.; Hassell, J.R.; Yamada, Y. Perlecan is essential for cartilage and cephalic development. *Nat. Genet.* **1999**, *23*, 354–358. [CrossRef]

30. Bullock, S.L.; Fletcher, J.M.; Beddington, R.S.; Wilson, V.A. Renal agenesis in mice homozygous for a gene trap mutation in the gene encoding heparan sulfate 2-sulfotransferase. *Genes Dev.* **1998**, *12*, 1894–1906. [CrossRef]
31. Li, J.P.; Gong, F.; Hagner-McWhirter, A.; Forsberg, E.; Abrink, M.; Kisilevsky, R.; Zhang, X.; Lindahl, U. Targeted disruption of a murine glucuronyl c5-epimerase gene results in heparan sulfate lacking l-iduronic acid and in neonatal lethality. *J. Biol. Chem.* **2003**, *278*, 28363–28366. [CrossRef]
32. Lin, X.; Wei, G.; Shi, Z.; Dryer, L.; Esko, J.D.; Wells, D.E.; Matzuk, M.M. Disruption of gastrulation and heparan sulfate biosynthesis in ext1-deficient mice. *Dev. Biol.* **2000**, *224*, 299–311. [CrossRef] [PubMed]
33. Shworak, N.W.; Liu, J.; Petros, L.M.; Zhang, L.; Kobayashi, M.; Copeland, N.G.; Jenkins, N.A.; Rosenberg, R.D. Multiple isoforms of heparan sulfate d-glucosaminyl 3-o-sulfotransferase. Isolation, characterization, and expression of human cdnas and identification of distinct genomic loci. *J. Biol. Chem.* **1999**, *274*, 5170–5184. [CrossRef] [PubMed]
34. Shukla, D.; Liu, J.; Blaiklock, P.; Shworak, N.W.; Bai, X.; Esko, J.D.; Cohen, G.H.; Eisenberg, R.J.; Rosenberg, R.D.; Spear, P.G. A novel role for 3-o-sulfated heparan sulfate in herpes simplex virus 1 entry. *Cell* **1999**, *99*, 13–22. [CrossRef]
35. Thunberg, L.; Backstrom, G.; Lindahl, U. Further characterization of the antithrombin-binding sequence in heparin. *Carbohydr. Res.* **1982**, *100*, 393–410. [CrossRef]
36. de Paz, J.L.; Moseman, E.A.; Noti, C.; Polito, L.; von Andrian, U.H.; Seeberger, P.H. Profiling heparin-chemokine interactions using synthetic tools. *ACS Chem. Biol.* **2007**, *2*, 735–744. [CrossRef]
37. Ashikari-Hada, S.; Habuchi, H.; Kariya, Y.; Itoh, N.; Reddi, A.H.; Kimata, K. Characterization of growth factor-binding structures in heparin/heparan sulfate using an octasaccharide library. *J. Biol. Chem.* **2004**, *279*, 12346–12354. [CrossRef]
38. Lindahl, U.; Li, J.P. Interactions between heparan sulfate and proteins-design and functional implications. *Int. Rev. Cell. Mol. Biol.* **2009**, *276*, 105–159.
39. Zhang, X.; Pagadala, V.; Jester, H.M.; Lim, A.M.; Pham, T.Q.; Goulas, A.M.P.; Liu, J.; Linhardt, R.J. Chemoenzymatic synthesis of heparan sulfate and heparin oligosaccharides and nmr analysis: Paving the way to a diverse library for glycobiologists. *Chem. Sci.* **2017**, *8*, 7932–7940. [CrossRef]
40. Yates, E.A.; Rudd, T.R. Recent innovations in the structural analysis of heparin. *Int. J. Cardiol.* **2016**, *212*, S5–S9. [CrossRef]
41. Ludwig, R.J. Therapeutic use of heparin beyond anticoagulation. *Curr. Drug Discov. Technol.* **2009**, *6*, 281–289. [CrossRef]
42. Alban, S. Adverse effects of heparin. *Handb. Exp. Pharmacol.* **2012**, *207*, 211–263.
43. Warkentin, T.E.; Sheppard, J.A.; Horsewood, P.; Simpson, P.J.; Moore, J.C.; Kelton, J.G. Impact of the patient population on the risk for heparin-induced thrombocytopenia. *Blood* **2000**, *96*, 1703–1708. [CrossRef] [PubMed]
44. Andreescu, A.C.; Possidente, C.; Hsieh, M.; Cushman, M. Evaluation of a pharmacy-based surveillance program for heparin-induced thrombocytopenia. *Pharmacotherapy* **2000**, *20*, 974–980. [CrossRef] [PubMed]
45. Jang, I.K.; Hursting, M.J. When heparins promote thrombosis: Review of heparin-induced thrombocytopenia. *Circulation* **2005**, *111*, 2671–2683. [CrossRef] [PubMed]
46. Lanzi, C.; Cassinelli, G. Heparan sulfate mimetics in cancer therapy: The challenge to define structural determinants and the relevance of targets for optimal activity. *Molecules* **2018**, *23*, 2915. [CrossRef] [PubMed]
47. Mohamed, S.; Coombe, D.R. Heparin mimetics: Their therapeutic potential. *Pharmaceuticals (Basel)* **2017**, *10*, 78. [CrossRef] [PubMed]
48. Morla, S. Glycosaminoglycans and glycosaminoglycan mimetics in cancer and inflammation. *Int. J. Mol. Sci.* **2019**, *20*, 1963. [CrossRef]
49. Cassinelli, G.; Zaffaroni, N.; Lanzi, C. The heparanase/heparan sulfate proteoglycan axis: A potential new therapeutic target in sarcomas. *Cancer Lett.* **2016**, *382*, 245–254. [CrossRef]
50. Friand, V.; David, G.; Zimmermann, P. Syntenin and syndecan in the biogenesis of exosomes. *Biol. Cell.* **2015**, *107*, 331–341. [CrossRef]
51. Selkoe, D.J. Cell biology of protein misfolding: The examples of alzheimer's and parkinson's diseases. *Nat. Cell. Biol.* **2004**, *6*, 1054–1061. [CrossRef]
52. Ross, C.A.; Poirier, M.A. Protein aggregation and neurodegenerative disease. *Nat. Med.* **2004**, *10*, S10–S17. [CrossRef] [PubMed]

53. Goedert, M.; Spillantini, M.G.; Davies, S.W. Filamentous nerve cell inclusions in neurodegenerative diseases. *Curr. Opin. Neurobiol.* **1998**, *8*, 619–632. [CrossRef]
54. Holmes, B.B.; DeVos, S.L.; Kfoury, N.; Li, M.; Jacks, R.; Yanamandra, K.; Ouidja, M.O.; Brodsky, F.M.; Marasa, J.; Bagchi, D.P.; et al. Heparan sulfate proteoglycans mediate internalization and propagation of specific proteopathic seeds. *Proc. Natl. Acad. Sci. USA* **2013**, *110*, E3138–E3147. [CrossRef] [PubMed]
55. Grundke-Iqbal, I.; Iqbal, K.; Quinlan, M.; Tung, Y.C.; Zaidi, M.S.; Wisniewski, H.M. Microtubule-associated protein tau. A component of alzheimer paired helical filaments. *J. Biol. Chem.* **1986**, *261*, 6084–6089.
56. Grundke-Iqbal, I.; Iqbal, K.; Tung, Y.C.; Quinlan, M.; Wisniewski, H.M.; Binder, L.I. Abnormal phosphorylation of the microtubule-associated protein tau (tau) in alzheimer cytoskeletal pathology. *Proc. Natl. Acad. Sci. USA* **1986**, *83*, 4913–4917. [CrossRef] [PubMed]
57. Nieto, A.; Correas, I.; Montejo de Garcini, E.; Avila, J. A modified form of microtubule-associated tau protein is the main component of paired helical filaments. *Biochem. Biophys. Res. Commun.* **1988**, *154*, 660–667. [CrossRef]
58. Perez, M.; Valpuesta, J.M.; Medina, M.; Montejo de Garcini, E.; Avila, J. Polymerization of tau into filaments in the presence of heparin: The minimal sequence required for tau-tau interaction. *J. Neurochem.* **1996**, *67*, 1183–1190. [CrossRef]
59. Wood, J.G.; Mirra, S.S.; Pollock, N.J.; Binder, L.I. Neurofibrillary tangles of alzheimer disease share antigenic determinants with the axonal microtubule-associated protein tau (tau). *Proc. Natl. Acad. Sci. USA* **1986**, *83*, 4040–4043. [CrossRef]
60. Sepulveda-Diaz, J.E.; Alavi Naini, S.M.; Huynh, M.B.; Ouidja, M.O.; Yanicostas, C.; Chantepie, S.; Villares, J.; Lamari, F.; Jospin, E.; van Kuppevelt, T.H.; et al. Hs3st2 expression is critical for the abnormal phosphorylation of tau in alzheimer's disease-related tau pathology. *Brain* **2015**, *138*, 1339–1354. [CrossRef]
61. Gupta-Bansal, R.; Frederickson, R.C.; Brunden, K.R. Proteoglycan-mediated inhibition of a beta proteolysis. A potential cause of senile plaque accumulation. *J. Biol. Chem.* **1995**, *270*, 18666–18671. [CrossRef]
62. Sandwall, E.; O'Callaghan, P.; Zhang, X.; Lindahl, U.; Lannfelt, L.; Li, J.P. Heparan sulfate mediates amyloid-beta internalization and cytotoxicity. *Glycobiology* **2010**, *20*, 533–541. [CrossRef] [PubMed]
63. Ancsin, J.B. Amyloidogenesis: Historical and modern observations point to heparan sulfate proteoglycans as a major culprit. *Amyloid* **2003**, *10*, 67–79. [CrossRef] [PubMed]
64. Zcharia, E.; Metzger, S.; Chajek-Shaul, T.; Aingorn, H.; Elkin, M.; Friedmann, Y.; Weinstein, T.; Li, J.P.; Lindahl, U.; Vlodavsky, I. Transgenic expression of mammalian heparanase uncovers physiological functions of heparan sulfate in tissue morphogenesis, vascularization, and feeding behavior. *FASEB J.* **2004**, *18*, 252–263. [CrossRef] [PubMed]
65. Li, J.P.; Galvis, M.L.; Gong, F.; Zhang, X.; Zcharia, E.; Metzger, S.; Vlodavsky, I.; Kisilevsky, R.; Lindahl, U. In vivo fragmentation of heparan sulfate by heparanase overexpression renders mice resistant to amyloid protein a amyloidosis. *Proc. Natl. Acad. Sci. USA* **2005**, *102*, 6473–6477. [CrossRef]
66. Su, J.H.; Cummings, B.J.; Cotman, C.W. Localization of heparan sulfate glycosaminoglycan and proteoglycan core protein in aged brain and alzheimer's disease. *Neuroscience* **1992**, *51*, 801–813. [CrossRef]
67. Scholefield, Z.; Yates, E.A.; Wayne, G.; Amour, A.; McDowell, W.; Turnbull, J.E. Heparan sulfate regulates amyloid precursor protein processing by bace1, the alzheimer's beta-secretase. *J. Cell. Biol.* **2003**, *163*, 97–107. [CrossRef]
68. Alavi Naini, S.M.; Soussi-Yanicostas, N. Heparan sulfate as a therapeutic target in tauopathies: Insights from zebrafish. *Front. Cell. Dev. Biol.* **2018**, *6*, 163. [CrossRef]
69. Ihse, E.; Yamakado, H.; van Wijk, X.M.; Lawrence, R.; Esko, J.D.; Masliah, E. Cellular internalization of alpha-synuclein aggregates by cell surface heparan sulfate depends on aggregate conformation and cell type. *Sci. Rep.* **2017**, *7*, 9008. [CrossRef]
70. Castillo, G.M.; Lukito, W.; Wight, T.N.; Snow, A.D. The sulfate moieties of glycosaminoglycans are critical for the enhancement of beta-amyloid protein fibril formation. *J. Neurochem.* **1999**, *72*, 1681–1687. [CrossRef]
71. Zhang, G.L.; Zhang, X.; Wang, X.M.; Li, J.P. Towards understanding the roles of heparan sulfate proteoglycans in alzheimer's disease. *Biomed. Res. Int.* **2014**, *2014*, 516028. [CrossRef]
72. Zhao, J.; Huvent, I.; Lippens, G.; Eliezer, D.; Zhang, A.; Li, Q.; Tessier, P.; Linhardt, R.J.; Zhang, F.; Wang, C. Glycan determinants of heparin-tau interaction. *Biophys. J.* **2017**, *112*, 921–932. [CrossRef] [PubMed]
73. Koo, E.H.; Squazzo, S.L. Evidence that production and release of amyloid beta-protein involves the endocytic pathway. *J. Biol. Chem.* **1994**, *269*, 17386–17389. [PubMed]

74. Koo, E.H.; Squazzo, S.L.; Selkoe, D.J.; Koo, C.H. Trafficking of cell-surface amyloid beta-protein precursor. I. Secretion, endocytosis and recycling as detected by labeled monoclonal antibody. *J. Cell. Sci.* **1996**, *109*, 991–998. [PubMed]
75. Yamazaki, T.; Koo, E.H.; Selkoe, D.J. Trafficking of cell-surface amyloid beta-protein precursor. Ii. Endocytosis, recycling and lysosomal targeting detected by immunolocalization. *J. Cell. Sci.* **1996**, *109*, 999–1008.
76. Lee, H.J.; Suk, J.E.; Bae, E.J.; Lee, J.H.; Paik, S.R.; Lee, S.J. Assembly-dependent endocytosis and clearance of extracellular alpha-synuclein. *Int. J. Biochem. Cell. Biol.* **2008**, *40*, 1835–1849. [CrossRef]
77. Futerman, A.H.; van Meer, G. The cell biology of lysosomal storage disorders. *Nat. Rev. Mol. Cell. Biol.* **2004**, *5*, 554–565. [CrossRef]
78. Heppner, J.M.; Zaucke, F.; Clarke, L.A. Extracellular matrix disruption is an early event in the pathogenesis of skeletal disease in mucopolysaccharidosis i. *Mol. Genet. Metab.* **2015**, *114*, 146–155. [CrossRef]
79. Young, R.D.; Liskova, P.; Pinali, C.; Palka, B.P.; Palos, M.; Jirsova, K.; Hrdlickova, E.; Tesarova, M.; Elleder, M.; Zeman, J.; et al. Large proteoglycan complexes and disturbed collagen architecture in the corneal extracellular matrix of mucopolysaccharidosis type vii (sly syndrome). *Invest. Ophthalmol. Vis. Sci.* **2011**, *52*, 6720–6728. [CrossRef]
80. Ohmi, K.; Kudo, L.C.; Ryazantsev, S.; Zhao, H.Z.; Karsten, S.L.; Neufeld, E.F. Sanfilippo syndrome type b, a lysosomal storage disease, is also a tauopathy. *Proc. Natl. Acad. Sci. USA* **2009**, *106*, 8332–8337. [CrossRef]
81. Hamano, K.; Hayashi, M.; Shioda, K.; Fukatsu, R.; Mizutani, S. Mechanisms of neurodegeneration in mucopolysaccharidoses ii and iiib: Analysis of human brain tissue. *Acta Neuropathol.* **2008**, *115*, 547–559. [CrossRef]
82. Winder-Rhodes, S.E.; Garcia-Reitbock, P.; Ban, M.; Evans, J.R.; Jacques, T.S.; Kemppinen, A.; Foltynie, T.; Williams-Gray, C.H.; Chinnery, P.F.; Hudson, G.; et al. Genetic and pathological links between parkinson's disease and the lysosomal disorder sanfilippo syndrome. *Mov. Disord.* **2012**, *27*, 312–315. [CrossRef]
83. Beard, H.; Hassiotis, S.; Gai, W.P.; Parkinson-Lawrence, E.; Hopwood, J.J.; Hemsley, K.M. Axonal dystrophy in the brain of mice with sanfilippo syndrome. *Exp. Neurol.* **2017**, *295*, 243–255. [CrossRef] [PubMed]
84. Parker, H.; Bigger, B.W. The role of innate immunity in mucopolysaccharide diseases. *J. Neurochem.* **2019**, *148*, 639–651. [CrossRef] [PubMed]
85. Goyal, D.; Shuaib, S.; Mann, S.; Goyal, B. Rationally designed peptides and peptidomimetics as inhibitors of amyloid-beta (abeta) aggregation: Potential therapeutics of alzheimer's disease. *ACS Comb. Sci.* **2017**, *19*, 55–80. [CrossRef] [PubMed]
86. Valstar, M.J.; Marchal, J.P.; Grootenhuis, M.; Colland, V.; Wijburg, F.A. Cognitive development in patients with mucopolysaccharidosis type iii (sanfilippo syndrome). *Orphanet. J. Rare Dis.* **2011**, *6*, 43. [CrossRef] [PubMed]
87. Bartels, A.L.; Willemsen, A.T.; Kortekaas, R.; de Jong, B.M.; de Vries, R.; de Klerk, O.; van Oostrom, J.C.; Portman, A.; Leenders, K.L. Decreased blood-brain barrier p-glycoprotein function in the progression of parkinson's disease, psp and msa. *J. Neural Transm. (Vienna)* **2008**, *115*, 1001–1009. [CrossRef] [PubMed]
88. Baeten, K.M.; Akassoglou, K. Extracellular matrix and matrix receptors in blood-brain barrier formation and stroke. *Dev. Neurobiol.* **2011**, *71*, 1018–1039. [CrossRef] [PubMed]
89. Kelleher, R.J.; Soiza, R.L. Evidence of endothelial dysfunction in the development of alzheimer's disease: Is alzheimer's a vascular disorder? *Am. J. Cardiovasc. Dis.* **2013**, *3*, 197–226.
90. Wang, P.; Ding, K. Proteoglycans and glycosaminoglycans in misfolded proteins formation in alzheimer's disease. *Protein Pept. Lett.* **2014**, *21*, 1048–1056. [CrossRef]
91. Leveugle, B.; Ding, W.; Laurence, F.; Dehouck, M.P.; Scanameo, A.; Cecchelli, R.; Fillit, H. Heparin oligosaccharides that pass the blood-brain barrier inhibit beta-amyloid precursor protein secretion and heparin binding to beta-amyloid peptide. *J. Neurochem.* **1998**, *70*, 736–744. [CrossRef]
92. Wang, P.; Lo Cascio, F.; Gao, J.; Kayed, R.; Huang, X. Binding and neurotoxicity mitigation of toxic tau oligomers by synthetic heparin like oligosaccharides. *Chem. Commun. (Camb.)* **2018**, *54*, 10120–10123. [CrossRef] [PubMed]
93. Dudas, B.; Cornelli, U.; Lee, J.M.; Hejna, M.J.; Walzer, M.; Lorens, S.A.; Mervis, R.F.; Fareed, J.; Hanin, I. Oral and subcutaneous administration of the glycosaminoglycan c3 attenuates abeta(25-35)-induced abnormal tau protein immunoreactivity in rat brain. *Neurobiol. Aging* **2002**, *23*, 97–104. [CrossRef]

94. Dudas, B.; Rose, M.; Cornelli, U.; Pavlovich, A.; Hanin, I. Neuroprotective properties of glycosaminoglycans: Potential treatment for neurodegenerative disorders. *Neurodegener. Dis.* **2008**, *5*, 200–205. [CrossRef] [PubMed]
95. Dwyer, C.A.; Scudder, S.L.; Lin, Y.; Dozier, L.E.; Phan, D.; Allen, N.J.; Patrick, G.N.; Esko, J.D. Neurodevelopmental changes in excitatory synaptic structure and function in the cerebral cortex of sanfilippo syndrome iiia mice. *Sci. Rep.* **2017**, *7*, 46576. [CrossRef] [PubMed]
96. Scarpa, M.; Orchard, P.J.; Schulz, A.; Dickson, P.I.; Haskins, M.E.; Escolar, M.L.; Giugliani, R. Treatment of brain disease in the mucopolysaccharidoses. *Mol. Genet. Metab.* **2017**, *122S*, 25–34. [CrossRef] [PubMed]
97. Neufeld, E.F. Enzyme replacement therapy—A brief history. In *Fabry Disease: Perspectives from 5 Years of Fos*; Mehta, A., Beck, M., Sunder-Plassmann, G., Eds.; Oxford PharmaGenesis: Oxford, UK, 2006.
98. Kakkis, E.D. Enzyme replacement therapy for the mucopolysaccharide storage disorders. *Expert Opin. Investig. Drugs* **2002**, *11*, 675–685. [CrossRef]
99. Desnick, R.J. Enzyme replacement and enhancement therapies for lysosomal diseases. *J. Inherit. Metab. Dis.* **2004**, *27*, 385–410. [CrossRef]
100. Begley, D.J.; Pontikis, C.C.; Scarpa, M. Lysosomal storage diseases and the blood-brain barrier. *Curr. Pharm. Des.* **2008**, *14*, 1566–1580. [CrossRef]
101. Tardieu, M.; Zerah, M.; Husson, B.; de Bournonville, S.; Deiva, K.; Adamsbaum, C.; Vincent, F.; Hocquemiller, M.; Broissand, C.; Furlan, V.; et al. Intracerebral administration of adeno-associated viral vector serotype rh.10 carrying human sgsh and sumf1 cdnas in children with mucopolysaccharidosis type iiia disease: Results of a phase i/ii trial. *Hum. Gene Ther.* **2014**, *25*, 506–516. [CrossRef]
102. Boado, R.J.; Hui, E.K.; Lu, J.Z.; Pardridge, W.M. Glycemic control and chronic dosing of rhesus monkeys with a fusion protein of iduronidase and a monoclonal antibody against the human insulin receptor. *Drug Metab Dispos* **2012**, *40*, 2021–2025. [CrossRef]
103. Boado, R.J.; Lu, J.Z.; Hui, E.K.; Pardridge, W.M. Insulin receptor antibody-sulfamidase fusion protein penetrates the primate blood-brain barrier and reduces glycosoaminoglycans in sanfilippo type a cells. *Mol. Pharm.* **2014**, *11*, 2928–2934. [CrossRef] [PubMed]
104. Scarpa, M.; Bellettato, C.M.; Lampe, C.; Begley, D.J. Neuronopathic lysosomal storage disorders: Approaches to treat the central nervous system. *Best Pract. Res. Clin. Endocrinol. Metab.* **2015**, *29*, 159–171. [CrossRef] [PubMed]
105. Guffon, N.; Bin-Dorel, S.; Decullier, E.; Paillet, C.; Guitton, J.; Fouilhoux, A. Evaluation of miglustat treatment in patients with type iii mucopolysaccharidosis: A randomized, double-blind, placebo-controlled study. *J. Pediatr.* **2011**, *159*, 838–844.e831. [CrossRef] [PubMed]
106. Schueler, U.H.; Kolter, T.; Kaneski, C.R.; Zirzow, G.C.; Sandhoff, K.; Brady, R.O. Correlation between enzyme activity and substrate storage in a cell culture model system for gaucher disease. *J. Inherit. Metab. Dis.* **2004**, *27*, 649–658. [CrossRef] [PubMed]
107. Krivit, W.; Sung, J.H.; Shapiro, E.G.; Lockman, L.A. Microglia: The effector cell for reconstitution of the central nervous system following bone marrow transplantation for lysosomal and peroxisomal storage diseases. *Cell Transplant.* **1995**, *4*, 385–392. [CrossRef]
108. Pan, C.; Nelson, M.S.; Reyes, M.; Koodie, L.; Brazil, J.J.; Stephenson, E.J.; Zhao, R.C.; Peters, C.; Selleck, S.B.; Stringer, S.E.; et al. Functional abnormalities of heparan sulfate in mucopolysaccharidosis-i are associated with defective biologic activity of fgf-2 on human multipotent progenitor cells. *Blood* **2005**, *106*, 1956–1964. [CrossRef]
109. Holley, R.J.; Deligny, A.; Wei, W.; Watson, H.A.; Ninonuevo, M.R.; Dagalv, A.; Leary, J.A.; Bigger, B.W.; Kjellen, L.; Merry, C.L. Mucopolysaccharidosis type i, unique structure of accumulated heparan sulfate and increased n-sulfotransferase activity in mice lacking alpha-l-iduronidase. *J. Biol. Chem.* **2011**, *286*, 37515–37524. [CrossRef]
110. De Pasquale, V.; Sarogni, P.; Pistorio, V.; Cerulo, G.; Paladino, S.; Pavone, L.M. Targeting heparan sulfate proteoglycans as a novel therapeutic strategy for mucopolysaccharidoses. *Mol. Ther. Methods Clin. Dev.* **2018**, *10*, 8–16. [CrossRef]
111. Ilan, N.; Shteingauz, A.; Vlodavsky, I. Function from within: Autophagy induction by hpse/heparanase–new possibilities for intervention. *Autophagy* **2015**, *11*, 2387–2389. [CrossRef]
112. Weissmann, M.; Bhattacharya, U.; Feld, S.; Hammond, E.; Ilan, N.; Vlodavsky, I. The heparanase inhibitor pg545 is a potent anti-lymphoma drug: Mode of action. *Matrix Biol.* **2019**, *77*, 58–72. [CrossRef]

113. Lau, A.A.; King, B.M.; Thorsen, C.L.; Hassiotis, S.; Beard, H.; Trim, P.J.; Whyte, L.S.; Tamang, S.J.; Duplock, S.K.; Snel, M.F.; et al. A novel conditional sgsh knockout mouse model recapitulates phenotypic and neuropathic deficits of sanfilippo syndrome. *J. Inherit. Metab. Dis.* **2017**, *40*, 715–724. [CrossRef] [PubMed]
114. Hull, E.E.; Montgomery, M.R.; Leyva, K.J. Epigenetic regulation of the biosynthesis & enzymatic modification of heparan sulfate proteoglycans: Implications for tumorigenesis and cancer biomarkers. *Int. J. Mol. Sci.* **2017**, *18*, 1361.
115. Zhang, Q.J.; Wan, L.; Xu, H.F. High expression of agrin is associated with tumor progression and poor prognosis in hepatocellular carcinoma. *Math. Biosci. Eng.* **2019**, *16*, 7375–7383. [CrossRef] [PubMed]
116. Melo, S.A.; Luecke, L.B.; Kahlert, C.; Fernandez, A.F.; Gammon, S.T.; Kaye, J.; LeBleu, V.S.; Mittendorf, E.A.; Weitz, J.; Rahbari, N.; et al. Glypican-1 identifies cancer exosomes and detects early pancreatic cancer. *Nature* **2015**, *523*, 177–182. [CrossRef] [PubMed]
117. Theocharis, A.D.; Karamanos, N.K. Proteoglycans remodeling in cancer: Underlying molecular mechanisms. *Matrix Biol.* **2019**, *75–76*, 220–259. [CrossRef]
118. Beauvais, D.M.; Ell, B.J.; McWhorter, A.R.; Rapraeger, A.C. Syndecan-1 regulates alphavbeta3 and alphavbeta5 integrin activation during angiogenesis and is blocked by synstatin, a novel peptide inhibitor. *J. Exp. Med.* **2009**, *206*, 691–705. [CrossRef]
119. De Rossi, G.; Evans, A.R.; Kay, E.; Woodfin, A.; McKay, T.R.; Nourshargh, S.; Whiteford, J.R. Shed syndecan-2 inhibits angiogenesis. *J. Cell. Sci.* **2014**, *127*, 4788–4799. [CrossRef]
120. Huang, G.; Ge, G.; Izzi, V.; Greenspan, D.S. Alpha3 chains of type v collagen regulate breast tumour growth via glypican-1. *Nat. Commun.* **2017**, *8*, 14351. [CrossRef]
121. Baba, F.; Swartz, K.; van Buren, R.; Eickhoff, J.; Zhang, Y.; Wolberg, W.; Friedl, A. Syndecan-1 and syndecan-4 are overexpressed in an estrogen receptor-negative, highly proliferative breast carcinoma subtype. *Breast Cancer Res. Treat.* **2006**, *98*, 91–98. [CrossRef]
122. Xiang, Y.Y.; Ladeda, V.; Filmus, J. Glypican-3 expression is silenced in human breast cancer. *Oncogene* **2001**, *20*, 7408–7412. [CrossRef]
123. Han, S.; Ma, X.; Zhao, Y.; Zhao, H.; Batista, A.; Zhou, S.; Zhou, X.; Yang, Y.; Wang, T.; Bi, J.; et al. Identification of glypican-3 as a potential metastasis suppressor gene in gastric cancer. *Oncotarget* **2016**, *7*, 44406–44416. [CrossRef] [PubMed]
124. Moek, K.L.; Fehrmann, R.S.N.; van der Vegt, B.; de Vries, E.G.E.; de Groot, D.J.A. Glypican 3 overexpression across a broad spectrum of tumor types discovered with functional genomic mrna profiling of a large cancer database. *Am. J. Pathol.* **2018**, *188*, 1973–1981. [CrossRef] [PubMed]
125. Li, Y.; Miao, L.; Cai, H.; Ding, J.; Xiao, Y.; Yang, J.; Zhang, D. The overexpression of glypican-5 promotes cancer cell migration and is associated with shorter overall survival in non-small cell lung cancer. *Oncol. Lett.* **2013**, *6*, 1565–1572. [CrossRef] [PubMed]
126. Pinho, S.S.; Reis, C.A. Glycosylation in cancer: Mechanisms and clinical implications. *Nat. Rev. Cancer* **2015**, *15*, 540–555. [CrossRef] [PubMed]
127. Lemjabbar-Alaoui, H.; McKinney, A.; Yang, Y.W.; Tran, V.M.; Phillips, J.J. Glycosylation alterations in lung and brain cancer. *Adv. Cancer Res.* **2015**, *126*, 305–344.
128. Lanzi, C.; Zaffaroni, N.; Cassinelli, G. Targeting heparan sulfate proteoglycans and their modifying enzymes to enhance anticancer chemotherapy efficacy and overcome drug resistance. *Curr. Med. Chem.* **2017**, *24*, 2860–2886. [CrossRef]
129. Subbarayan, K.; Seliger, B. Tumor-dependent effects of proteoglycans and various glycosaminoglycan synthesizing enzymes and sulfotransferases on patients' outcome. *Curr. Cancer Drug Targets* **2019**, *19*, 210–221. [CrossRef]
130. Barkeer, S.; Chugh, S.; Karmakar, S.; Kaushik, G.; Rauth, S.; Rachagani, S.; Batra, S.K.; Ponnusamy, M.P. Novel role of o-glycosyltransferases galnt3 and b3gnt3 in the self-renewal of pancreatic cancer stem cells. *BMC Cancer* **2018**, *18*, 1157. [CrossRef]
131. Fux, L.; Ilan, N.; Sanderson, R.D.; Vlodavsky, I. Heparanase: Busy at the cell surface. *Trends Biochem. Sci.* **2009**, *34*, 511–519. [CrossRef]
132. Nadir, Y.; Brenner, B. Heparanase multiple effects in cancer. *Thromb Res.* **2014**, *133*, S90–S94. [CrossRef]
133. Vlodavsky, I.; Gross-Cohen, M.; Weissmann, M.; Ilan, N.; Sanderson, R.D. Opposing functions of heparanase-1 and heparanase-2 in cancer progression. *Trends Biochem. Sci.* **2018**, *43*, 18–31. [CrossRef] [PubMed]

134. Vlodavsky, I.; Singh, P.; Boyango, I.; Gutter-Kapon, L.; Elkin, M.; Sanderson, R.D.; Ilan, N. Heparanase: From basic research to therapeutic applications in cancer and inflammation. *Drug Resist. Updat.* **2016**, *29*, 54–75. [CrossRef] [PubMed]
135. He, Y.Q.; Sutcliffe, E.L.; Bunting, K.L.; Li, J.; Goodall, K.J.; Poon, I.K.; Hulett, M.D.; Freeman, C.; Zafar, A.; McInnes, R.L.; et al. The endoglycosidase heparanase enters the nucleus of t lymphocytes and modulates h3 methylation at actively transcribed genes via the interplay with key chromatin modifying enzymes. *Transcription* **2012**, *3*, 130–145. [CrossRef] [PubMed]
136. Dvir, R.; Vlodavsky, I.; Ilan, N.; Bitan, M.; Issacov, J.; Elhasid, R. Heparanase expression in langerhans cell histiocytosis. *Pediatr. Blood Cancer* **2014**, *61*, 1883–1885. [CrossRef]
137. Li, J.; Li, J.P.; Zhang, X.; Lu, Z.; Yu, S.P.; Wei, L. Expression of heparanase in vascular cells and astrocytes of the mouse brain after focal cerebral ischemia. *Brain Res.* **2012**, *1433*, 137–144. [CrossRef]
138. Ginath, S.; Lurie, S.; Golan, A.; Amsterdam, A.; Sandbank, J.; Sadan, O.; Kovo, M. The expression of heparanase in normal and preeclamptic placentas. *J. Matern. Fetal Neonatal Med.* **2015**, *28*, 1589–1593. [CrossRef]
139. Wang, Y.Y.; Zhou, R.; Zhou, B.; Wang, T.; Zhang, L.; Luo, D. Overexpression of heparanase is associated with preeclampsia by inhibiting invasion of trophocytes. *Int. J. Clin. Exp. Med.* **2015**, *8*, 18107–18114.
140. Sela, S.; Natanson-Yaron, S.; Zcharia, E.; Vlodavsky, I.; Yagel, S.; Keshet, E. Local retention versus systemic release of soluble vegf receptor-1 are mediated by heparin-binding and regulated by heparanase. *Circ. Res.* **2011**, *108*, 1063–1070. [CrossRef]
141. Ihrcke, N.S.; Parker, W.; Reissner, K.J.; Platt, J.L. Regulation of platelet heparanase during inflammation: Role of ph and proteinases. *J. Cell. Physiol.* **1998**, *175*, 255–267. [CrossRef]
142. Bashkin, P.; Razin, E.; Eldor, A.; Vlodavsky, I. Degranulating mast cells secrete an endoglycosidase that degrades heparan sulfate in subendothelial extracellular matrix. *Blood* **1990**, *75*, 2204–2212. [CrossRef]
143. Vlodavsky, I.; Eldor, A.; Haimovitz-Friedman, A.; Matzner, Y.; Ishai-Michaeli, R.; Lider, O.; Naparstek, Y.; Cohen, I.R.; Fuks, Z. Expression of heparanase by platelets and circulating cells of the immune system: Possible involvement in diapedesis and extravasation. *Invasion Metastasis* **1992**, *12*, 112–127. [PubMed]
144. Farrugia, B.L.; Lord, M.S.; Melrose, J.; Whitelock, J.M. The role of heparan sulfate in inflammation, and the development of biomimetics as anti-inflammatory strategies. *J. Histochem. Cytochem.* **2018**, *66*, 321–336. [CrossRef]
145. Sasaki, N.; Higashi, N.; Taka, T.; Nakajima, M.; Irimura, T. Cell surface localization of heparanase on macrophages regulates degradation of extracellular matrix heparan sulfate. *J. Immunol.* **2004**, *172*, 3830–3835. [CrossRef] [PubMed]
146. Gutter-Kapon, L.; Alishekevitz, D.; Shaked, Y.; Li, J.P.; Aronheim, A.; Ilan, N.; Vlodavsky, I. Heparanase is required for activation and function of macrophages. *Proc. Natl. Acad. Sci. USA* **2016**, *113*, E7808–E7817. [CrossRef] [PubMed]
147. Theodoro, T.R.; de Matos, L.L.; Sant Anna, A.V.; Fonseca, F.L.; Semedo, P.; Martins, L.C.; Nader, H.B.; Del Giglio, A.; da Silva Pinhal, M.A. Heparanase expression in circulating lymphocytes of breast cancer patients depends on the presence of the primary tumor and/or systemic metastasis. *Neoplasia* **2007**, *9*, 504–510. [CrossRef] [PubMed]
148. Theodoro, T.R.; Matos, L.L.; Cavalheiro, R.P.; Justo, G.Z.; Nader, H.B.; Pinhal, M.A.S. Crosstalk between tumor cells and lymphocytes modulates heparanase expression. *J. Transl. Med.* **2019**, *17*, 103. [CrossRef]
149. Thompson, C.A.; Purushothaman, A.; Ramani, V.C.; Vlodavsky, I.; Sanderson, R.D. Heparanase regulates secretion, composition, and function of tumor cell-derived exosomes. *J. Biol. Chem.* **2013**, *288*, 10093–10099. [CrossRef]
150. Bandari, S.K.; Purushothaman, A.; Ramani, V.C.; Brinkley, G.J.; Chandrashekar, D.S.; Varambally, S.; Mobley, J.A.; Zhang, Y.; Brown, E.E.; Vlodavsky, I.; et al. Chemotherapy induces secretion of exosomes loaded with heparanase that degrades extracellular matrix and impacts tumor and host cell behavior. *Matrix Biol.* **2018**, *65*, 104–118. [CrossRef]
151. Purushothaman, A.; Uyama, T.; Kobayashi, F.; Yamada, S.; Sugahara, K.; Rapraeger, A.C.; Sanderson, R.D. Heparanase-enhanced shedding of syndecan-1 by myeloma cells promotes endothelial invasion and angiogenesis. *Blood* **2010**, *115*, 2449–2457. [CrossRef]

152. Voigtlaender, M.; Langer, F. Low-molecular-weight heparin in cancer patients: Overview and indications. *Hamostaseologie* **2019**, *39*, 67–75. [CrossRef]
153. Smorenburg, S.M.; Hettiarachchi, R.J.; Vink, R.; Buller, H.R. The effects of unfractionated heparin on survival in patients with malignancy–a systematic review. *Thromb. Haemost.* **1999**, *82*, 1600–1604. [PubMed]
154. Kakkar, A.K. Thrombosis and cancer. *Hematol. J.* **2004**, *5*, S20–S23. [CrossRef] [PubMed]
155. Kuderer, N.M.; Ortel, T.L.; Francis, C.W. Impact of venous thromboembolism and anticoagulation on cancer and cancer survival. *J. Clin. Oncol.* **2009**, *27*, 4902–4911. [CrossRef] [PubMed]
156. Lyman, G.H.; Bohlke, K.; Khorana, A.A.; Kuderer, N.M.; Lee, A.Y.; Arcelus, J.I.; Balaban, E.P.; Clarke, J.M.; Flowers, C.R.; Francis, C.W.; et al. Venous thromboembolism prophylaxis and treatment in patients with cancer: American society of clinical oncology clinical practice guideline update 2014. *J. Clin. Oncol.* **2015**, *33*, 654–656. [CrossRef]
157. Garcia-Escobar, I.; Beato-Zambrano, C.; Munoz Langa, J.; Brozos Vazquez, E.; Obispo Portero, B.; Gutierrez-Abad, D.; Munoz Martin, A.J.; Cancer and Thrombosis Working Group of the Spanish Society of Medical Oncology (SEOM). Pleiotropic effects of heparins: Does anticoagulant treatment increase survival in cancer patients? *Clin. Transl. Oncol.* **2018**, *20*, 1097–1108. [CrossRef]
158. Borsig, L. Heparin as an inhibitor of cancer progression. *Prog. Mol. Biol. Transl. Sci.* **2010**, *93*, 335–349.
159. Bobek, V.; Kovarik, J. Antitumor and antimetastatic effect of warfarin and heparins. *Biomed. Pharmacother.* **2004**, *58*, 213–219. [CrossRef]
160. Ilan, N.; Elkin, M.; Vlodavsky, I. Regulation, function and clinical significance of heparanase in cancer metastasis and angiogenesis. *Int. J. Biochem. Cell. Biol.* **2006**, *38*, 2018–2039. [CrossRef]
161. Vreys, V.; David, G. Mammalian heparanase: What is the message? *J. Cell. Mol. Med.* **2007**, *11*, 427–452. [CrossRef]
162. Vlodavsky, I.; Ilan, N.; Naggi, A.; Casu, B. Heparanase: Structure, biological functions, and inhibition by heparin-derived mimetics of heparan sulfate. *Curr. Pharm. Des.* **2007**, *13*, 2057–2073. [CrossRef]
163. Hammond, E.; Khurana, A.; Shridhar, V.; Dredge, K. The role of heparanase and sulfatases in the modification of heparan sulfate proteoglycans within the tumor microenvironment and opportunities for novel cancer therapeutics. *Front. Oncol.* **2014**, *4*, 195. [CrossRef] [PubMed]
164. Vlodavsky, I.; Beckhove, P.; Lerner, I.; Pisano, C.; Meirovitz, A.; Ilan, N.; Elkin, M. Significance of heparanase in cancer and inflammation. *Cancer Microenviron.* **2012**, *5*, 115–132. [CrossRef] [PubMed]
165. Jia, L.; Ma, S. Recent advances in the discovery of heparanase inhibitors as anti-cancer agents. *Eur. J. Med. Chem.* **2016**, *121*, 209–220. [CrossRef] [PubMed]
166. Pisano, C.; Vlodavsky, I.; Ilan, N.; Zunino, F. The potential of heparanase as a therapeutic target in cancer. *Biochem. Pharmacol.* **2014**, *89*, 12–19. [CrossRef] [PubMed]
167. Bar-Ner, M.; Eldor, A.; Wasserman, L.; Matzner, Y.; Cohen, I.R.; Fuks, Z.; Vlodavsky, I. Inhibition of heparanase-mediated degradation of extracellular matrix heparan sulfate by non-anticoagulant heparin species. *Blood* **1987**, *70*, 551–557. [CrossRef] [PubMed]
168. Cassinelli, G.; Dal Bo, L.; Favini, E.; Cominetti, D.; Pozzi, S.; Tortoreto, M.; De Cesare, M.; Lecis, D.; Scanziani, E.; Minoli, L.; et al. Supersulfated low-molecular weight heparin synergizes with igf1r/ir inhibitor to suppress synovial sarcoma growth and metastases. *Cancer Lett.* **2018**, *415*, 187–197. [CrossRef]
169. Poli, M.; Asperti, M.; Ruzzenenti, P.; Mandelli, L.; Campostrini, N.; Martini, G.; Di Somma, M.; Maccarinelli, F.; Girelli, D.; Naggi, A.; et al. Oversulfated heparins with low anticoagulant activity are strong and fast inhibitors of hepcidin expression in vitro and in vivo. *Biochem. Pharmacol.* **2014**, *92*, 467–475. [CrossRef]
170. Mohan, C.D.; Hari, S.; Preetham, H.D.; Rangappa, S.; Barash, U.; Ilan, N.; Nayak, S.C.; Gupta, V.K.; Basappa, B.; Vlodavsky, I.; et al. Targeting heparanase in cancer: Inhibition by synthetic, chemically modified, and natural compounds. *iScience* **2019**, *15*, 360–390. [CrossRef]
171. MacDonald, A.; Priess, M.; Curran, J.; Guess, J.; Farutin, V.; Oosterom, I.; Chu, C.L.; Cochran, E.; Zhang, L.; Getchell, K.; et al. Necuparanib, a multitargeting heparan sulfate mimetic, targets tumor and stromal compartments in pancreatic cancer. *Mol. Cancer Ther.* **2019**, *18*, 245–256. [CrossRef]
172. Boothello, R.S.; Patel, N.J.; Sharon, C.; Abdelfadiel, E.I.; Morla, S.; Brophy, D.F.; Lippman, H.R.; Desai, U.R.; Patel, B.B. A unique nonsaccharide mimetic of heparin hexasaccharide inhibits colon cancer stem cells via p38 map kinase activation. *Mol. Cancer Ther.* **2019**, *18*, 51–61. [CrossRef]

173. Joyce, J.A.; Freeman, C.; Meyer-Morse, N.; Parish, C.R.; Hanahan, D. A functional heparan sulfate mimetic implicates both heparanase and heparan sulfate in tumor angiogenesis and invasion in a mouse model of multistage cancer. *Oncogene* **2005**, *24*, 4037–4051. [CrossRef] [PubMed]
174. Arvatz, G.; Weissmann, M.; Ilan, N.; Vlodavsky, I. Heparanase and cancer progression: New directions, new promises. *Hum. Vaccin. Immunother.* **2016**, *12*, 2253–2256. [CrossRef] [PubMed]
175. Weissmann, M.; Arvatz, G.; Horowitz, N.; Feld, S.; Naroditsky, I.; Zhang, Y.; Ng, M.; Hammond, E.; Nevo, E.; Vlodavsky, I.; et al. Heparanase-neutralizing antibodies attenuate lymphoma tumor growth and metastasis. *Proc. Natl. Acad. Sci. USA* **2016**, *113*, 704–709. [CrossRef] [PubMed]
176. Yoshitomi, Y.; Nakanishi, H.; Kusano, Y.; Munesue, S.; Oguri, K.; Tatematsu, M.; Yamashina, I.; Okayama, M. Inhibition of experimental lung metastases of lewis lung carcinoma cells by chemically modified heparin with reduced anticoagulant activity. *Cancer Lett.* **2004**, *207*, 165–174. [CrossRef]
177. Pisano, C.; Aulicino, C.; Vesci, L.; Casu, B.; Naggi, A.; Torri, G.; Ribatti, D.; Belleri, M.; Rusnati, M.; Presta, M. Undersulfated, low-molecular-weight glycol-split heparin as an antiangiogenic vegf antagonist. *Glycobiology* **2005**, *15*, 1C–6C. [CrossRef]
178. Naggi, A.; Casu, B.; Perez, M.; Torri, G.; Cassinelli, G.; Penco, S.; Pisano, C.; Giannini, G.; Ishai-Michaeli, R.; Vlodavsky, I. Modulation of the heparanase-inhibiting activity of heparin through selective desulfation, graded n-acetylation, and glycol splitting. *J. Biol. Chem.* **2005**, *280*, 12103–12113. [CrossRef]
179. Cassinelli, G.; Lanzi, C.; Tortoreto, M.; Cominetti, D.; Petrangolini, G.; Favini, E.; Zaffaroni, N.; Pisano, C.; Penco, S.; Vlodavsky, I.; et al. Antitumor efficacy of the heparanase inhibitor sst0001 alone and in combination with antiangiogenic agents in the treatment of human pediatric sarcoma models. *Biochem. Pharmacol.* **2013**, *85*, 1424–1432. [CrossRef]
180. Ritchie, J.P.; Ramani, V.C.; Ren, Y.; Naggi, A.; Torri, G.; Casu, B.; Penco, S.; Pisano, C.; Carminati, P.; Tortoreto, M.; et al. Sst0001, a chemically modified heparin, inhibits myeloma growth and angiogenesis via disruption of the heparanase/syndecan-1 axis. *Clin. Cancer Res.* **2011**, *17*, 1382–1393. [CrossRef]
181. Karoli, T.; Liu, L.; Fairweather, J.K.; Hammond, E.; Li, C.P.; Cochran, S.; Bergefall, K.; Trybala, E.; Addison, R.S.; Ferro, V. Synthesis, biological activity, and preliminary pharmacokinetic evaluation of analogues of a phosphosulfomannan angiogenesis inhibitor (pi-88). *J. Med. Chem.* **2005**, *48*, 8229–8236. [CrossRef]
182. Kuhnast, B.; El Hadri, A.; Boisgard, R.; Hinnen, F.; Richard, S.; Caravano, A.; Nancy-Portebois, V.; Petitou, M.; Tavitian, B.; Dolle, F. Synthesis, radiolabeling with fluorine-18 and preliminary in vivo evaluation of a heparan sulphate mimetic as potent angiogenesis and heparanase inhibitor for cancer applications. *Org. Biomol. Chem.* **2016**, *14*, 1915–1920. [CrossRef]
183. Lim, T.C.; Cai, S.; Huber, R.G.; Bond, P.J.; Siew Chia, P.X.; Khou, S.L.; Gao, S.; Lee, S.S.; Lee, S.G. Facile saccharide-free mimetics that recapitulate key features of glycosaminoglycan sulfation patterns. *Chem. Sci.* **2018**, *9*, 7940–7947. [CrossRef] [PubMed]
184. Vornicova, O.; Boyango, I.; Feld, S.; Naroditsky, I.; Kazarin, O.; Zohar, Y.; Tiram, Y.; Ilan, N.; Ben-Izhak, O.; Vlodavsky, I.; et al. The prognostic significance of heparanase expression in metastatic melanoma. *Oncotarget* **2016**, *7*, 74678–74685. [CrossRef] [PubMed]
185. Vornicova, O.; Naroditsky, I.; Boyango, I.; Shachar, S.S.; Mashiach, T.; Ilan, N.; Vlodavsky, I.; Bar-Sela, G. Prognostic significance of heparanase expression in primary and metastatic breast carcinoma. *Oncotarget* **2018**, *9*, 6238–6244. [CrossRef] [PubMed]
186. Lazo-Langner, A.; Goss, G.D.; Spaans, J.N.; Rodger, M.A. The effect of low-molecular-weight heparin on cancer survival. A systematic review and meta-analysis of randomized trials. *J. Thromb. Haemost.* **2007**, *5*, 729–737. [CrossRef] [PubMed]
187. Kuderer, N.M.; Khorana, A.A.; Lyman, G.H.; Francis, C.W. A meta-analysis and systematic review of the efficacy and safety of anticoagulants as cancer treatment: Impact on survival and bleeding complications. *Cancer* **2007**, *110*, 1149–1161. [CrossRef]
188. Galli, M.; Chatterjee, M.; Grasso, M.; Specchia, G.; Magen, H.; Einsele, H.; Celeghini, I.; Barbieri, P.; Paoletti, D.; Pace, S.; et al. Phase i study of the heparanase inhibitor roneparstat: An innovative approach for ultiple myeloma therapy. *Haematologica* **2018**, *103*, e469–e472. [CrossRef]
189. Vande Broek, I.; Vanderkerken, K.; Van Camp, B.; Van Riet, I. Extravasation and homing mechanisms in multiple myeloma. *Clin. Exp. Metastasis* **2008**, *25*, 325–334. [CrossRef]
190. Ramani, V.C.; Zhan, F.; He, J.; Barbieri, P.; Noseda, A.; Tricot, G.; Sanderson, R.D. Targeting heparanase overcomes chemoresistance and diminishes relapse in myeloma. *Oncotarget* **2016**, *7*, 1598–1607. [CrossRef]

191. Dredge, K.; Hammond, E.; Davis, K.; Li, C.P.; Liu, L.; Johnstone, K.; Handley, P.; Wimmer, N.; Gonda, T.J.; Gautam, A.; et al. The pg500 series: Novel heparan sulfate mimetics as potent angiogenesis and heparanase inhibitors for cancer therapy. *Invest. New Drugs* **2010**, *28*, 276–283. [CrossRef]
192. Dredge, K.; Brennan, T.V.; Hammond, E.; Lickliter, J.D.; Lin, L.; Bampton, D.; Handley, P.; Lankesheer, F.; Morrish, G.; Yang, Y.; et al. A phase i study of the novel immunomodulatory agent pg545 (pixatimod) in subjects with advanced solid tumours. *Br. J. Cancer* **2018**, *118*, 1035–1041. [CrossRef]

“If we knew what we were doing it would not be called research, would it?”

Albert Einstein